

https://dspace.org/

Aspects Of Ferromanganese Production In The Submerged-arc Furnace

Koursaris, A

2015-05-18
http://hdl.handle.net/10539/17789

Downloaded from a DSpace repository. https://dspace.org/

ASPECTS OF FERROMANGANESE PRODUCTION IN THE SUBMERGED-ARC FURNACE.

by

A. KOURSARIS

A thesis submitted to the Faculty of Engineering in fulfilment of the requirements for the degree of Doctor of Philosophy

University of the Witwatersrand
Johannesburg

February 1980.

UNDERTAKING

I hereby certify that this is my own work, except for the chemical analyses which were carried out by the National Institute for Metallurgy and the excavation and sampling of furnace M10 which was carried out by a team of technicians and scientists from the National Institute for Metallurgy. This team, of which I was a member, was assisted by workmen at Meyerton.

This thesis has not been submitted for the degree of Doctor of Philosophy at any other University.

A. Koursaris

TO

PHAEDRA, MICHAEL and ADAM

ABSTRACT

A variation of the stationary charge in controlled environment (SCICE) technique was used for the first time to investigate the influence of two reducing agents on the rate and mechanisms of reduction of Mamatwan manganese ore, the resistivity of the charge and the processes that take place in submerged-arc furnaces for the production of high-carbon ferromanganese.

The excavation of a 75 MV A submerged-arc furnace for the production of high-carbon ferromanganese, the taking of samples and the examination of these samples was carried out for the first time in an attempt to study the processes taking place in industrial furnaces and to assess the extent to which the SCICE technique reproduced the conditions in industrial units.

It was shown that the use of Delmas coal or Iscor coke did not affect the rate or mechanisms of reduction of Mamatwan ore to a significant extent. The physical and chemical changes that take place in Mamatwan ore at temperatures between 1200 and 1600°C, under oxidizing or reducing conditions, were investigated and it was shown that reduction of manganous oxide occurred mainly from the slag.

The resistivity of mixtures of ore and coal was significantly higher than that of mixtures of ore and coke for temperatures of less than 1100°C. At higher temperatures the resistivities of the two types of mixture were the same.

The processes that took place in the SCICE charges were shown to be very similar to those that take place in industrial furnaces between stockline level and the level of the electrode tip.

ACKNOWLEDGEMENTS

Sincere appreciation is extended to :

Drs. C W P Finn, J B See and D I Ossin for supervising the work.

Dr. N A Barcza for supervising the excavation of furnace M10

The management of the Metalloys plant of Samancor at Meyerton who supplied the materials for this study and for their co-operation with regard to the excavation and sampling of furnace M10.

The National Institute for Metallurgy, Johannesburg, for financial assistance and for permission to submit this work for higher degree.

The Ferro Alloy Producers Association for financial support.

PREFACE

The recent develcpments in the ferromanganese industry of South Africa have necessitated further research into the reduction behaviour of Mamatwan manganese ore when contacted with different reducing agents. The Mamatwan orebody is of a relatively low grade but is in plentiful supply and is therefore of basic importance to ferromanganese producers.

The lower inherent resistance of large, modern submerged-arc furnaces and the increasing scarcity and cost of metallurgical coke have forced ferroalloy producers to look at alternative reducing agents. The suitability of a reducing agent for use in a submerged-arc furnace is assessed mainly from the resistivity of the reducing agent, its ability to give stable furnace operation and its reactivity.

A limited amount of work has been carried out on the rates and mechanisms of reduction of Mamatwan ore and on the mineralogical changes that take place when the ore is heated at relatively low temperatures in oxidising and reducing atmospheres.

The aims of this work were to investigate the reactions in, and the resistivity of, charges of Mamatwan ore and two carbonaceous reducing agents under conditions similar to those that obtain in the hotter regions of a submerged-arc furnace. The applicability of the experimental method used, to the study of the processes taking place in an industrial furnace was assessed by the examination of samples taken from one such furnace.

The author was a bursar of the National Institute for Metallurgy while conducting this work.

The excavation and sampling of furnace M10 was carried out by a team of scientists and technicians of which the author was a member. This team was assisted by a team of workers of the Metalloys plant of Samancor at Meyerton.

CONTENTS

1.0 INTRODUCTION

1.1	Production of Ferromanganese in South Africa	2
1.2	Reduction of Manganese Oxides	5
1.2.1	Reduction of the Higher Oxides	5
1.2.2	Reduction of Manganous Oxide	7
1.2.3	Reduction of Manganous Oxide from Slags	11
1.3	The Mechanism of Reduction of Metal Oxides	14
1.4	Previous Research Relating to the Metallurgical Applications of Mamatwan Manganese Ore	19
1.5	Electrical and Thermal Aspects of Submerged-arc Furnace Operation	20
1.6	The Electrical Properties of Carbonaceous Reducing Agents	23
1.7	The Electrical Properties of Ores	26
1.8	The Electrical Properties of Furnace Burdens	30
1.9	The Distribution of Zones in Submerged-arc Furnaces	34
1.10	Conclusions	39

2.0 EXPERIMENTAL

2.1	Choice of Experimental Technique	42
2.1.1	Critical Appraisal of the Experimental Technique	44
2.2	Materials and the Preparation of SCICE Charges	47
2.3	Apparatus and Procedure	50
2.3.1	SCICE Experiments	50
2.3.2	Additional Experiments	57
2.3.3	Sampling and Examination of Reacted SCICE Charges	59
2.3.4	Microanalysis by the Energy Dispersive System (EDS)	59

3.0 RESULTS

3.1	The Mineralogy of the Ore	66
3.2	Observations During the Heating of SCICE Charges	73
3.3	Macro-examination of the Reacted SCICE Charges	75
3.4	Microscopic Examination of the Reacted SCICE Charges	77
3.4.1	General Microscopic Examination of the Phases in Particles of Partially Reduced Ore	77
3.4.2	Examination of the Metallic Component	85
3.5	The Distribution of Elements in the Phases of Partially Reduced Ore	96
3.5.1	X-ray Microanalysis of Reacted SCICE Charges	99
3.5.2	X-ray Diffraction Analysis	104
3.5.3	Mass Losses and Alloy and Slag Compositions	108
3.6	Results of Additional Experiments	113
3.6.1	Ore Heated in Air	113
3.6.2	Ore Heated in Carbon Monoxide	116
3.6.3	Ore Heated in Graphite Crucible	121

4.0 DISCUSSION

4.1	Some Practical Considerations on the use of Mamatwan Ore in Submerged-Arc Furnaces	131
4.2	Reduction of Higher Oxides to Manganous Oxide	134
4.3	Reactions to Form the Slag	141
4.4	Reactions to Form the Alloy	143
4.4.1	Nucleation of Metal	143
4.4.2	Growth of Metallic Nuclei	145
4.4.3	Formation of the Alloy Layer	148
4.5	The Influence of Reducing Agent on the Reduction Process	151
4.6	Conclusions	153

5.0 THE RESISTIVITY OF MIXTURES OF MAMATWAN ORE AND COKE OR COAL

5.1	Materials, Apparatus and Procedure	154
5.1.1	Determination of Resistance	154
5.1.2	Variation in Volume Fractions of Components	157
5.2	Results and Discussion	158
5.2.1	Effect of Temperature on Resistivity of Individual Charge Components	158
5.2.2	Volume Changes During Heating of Charges	166
5.2.3	Resistivities of Charges of Ore and Reducing Agents	167
5.3	Resistivity Measurements and Furnace Resistance	180
5.4	Conclusions	182

6.0 EXAMINATION OF FURNACE SAMPLES

6.1	General	184
6.2	Sampling Procedure and Sample Identification	185
6.3	Appraisal of the Furnace Excavation	189
6.4	The Internal Structure of Furnace M10	191
6.5	Processing of Furnace Samples	198
6.6	Examination of Samples from Face CE_1W_1	201
6.6.1	Visual Examination	201
6.6.2	Microscopic Examination	207
6.6.3	X-ray Diffraction Analysis	212
6.6.3.1	Analysis of the Non-metallic Constituent	212
6.6.3.2	Analysis of the Alloy	212
6.7	The Chemical Composition of Alloys	219
6.8	X-ray Microanalysis of Metal, Slag and Oxide	224
6.9	Examination of Samples from Face CE_2W_2	226
6.9.1	Visual Examination	226
6.9.2	Microscopic Examination	231
6.9.3	X-ray Diffraction Analysis	234
6.9.4	The Chemical Composition of Alloys	234
6.9.5	X-ray Microanalysis of Metal, Slag and Oxide	237

7.0 DISCUSSION

7.1 Some Practical Aspects of Submerged-arc Furnace Operation 240

7.1.1 Burden Movement and Distribution of Zones in Furnace M10 240

7.1.2 Decrepitation and Segregation of Burden Components 244

7.2 Reduction of the Ore in the Submerged-arc Furnace 247

7.3 Temperature Gradients in Submerged-arc Furnaces 252

7.4 The Carbon Content of Alloy Samples from Furnace M10 255

7.5 Conclusions 257

8.0 SUMMARY OF CONCLUSIONS 259

APPENDICES 261

A.1 Determination of Percentage Metallization 262

A.2 Determination of Cell Constant of the SCICE Apparatus 266

A.3 Furnace Parameters and Feed Material Data 286

LIST OF TABLES

2.1	Proximate and ash analyses of the reducing agents	48
2.2	The chemical composition of Mamatwan ore	49
2.3	Details of the SCICE experiments	51
3.1(a)	The integrated relative intensity of the more abundant phases in Mamatwan ore in relation to the strongest peak of each sample	69
3.1(b)	The integrated relative intensity of the more abundant phases in Mamatwan ore in relation to the strongest peak of each phase	71
3.2	Qualitative X-ray diffraction analysis of Mamatwan ore	72
3.3	EDS analyses of the more abundant minerals in Mamatwan ore.	74
3.4	Summary of the examination of charges of ore and coke reacted under different SCICE conditions.	80
3.5	The composition of different phases or components in metallic particles as obtained by X-ray microanalysis	89
3.6	The hardness of the metallic component formed under SCICE conditions	92
3.7	The distribution of elements in the alloy, the oxide and the slag that formed by reacting Mamatwan ore with Delmas coal or Iscor coke under various experimental conditions	100
3.8	Effect of experimental conditions on the mass of various charges.	109
3.9	The composition of alloys and slags formed under different experimental conditions.	112
3.10	Comparison of X-ray diffraction data for manganous oxide from different sources.	126
3.11	The lattice parameter and crystal structure of some oxides	128
6.1	Summary of the visual examination of the coarse fraction of samples from face C E_1W_1	203
6.2	The phases in the partially reacted ore samples from face C E_1W_1	214
6.3	The phases in selected constituents of some samples from face C E_1W_1	215
6.4	The phases in the metallic component of samples from face C E_1W_1	217

6.5	The chemical composition of the metallic constituent from samples in plane CE_1W_1	220
6.6	The distribution of elements in the oxide, the slag and the alloy in samples from face CE_1W_1	225
6.7	Summary of the visual examination of samples from face CE_2W_2	230
6.8	The proportions of fine material and reducing agent in the coarse fraction of samples from face CE_2W_2	232
6.9	The phases in samples from face CE_2W_2	233
6.10	Phases in the different constituents of samples from plane CE_2W_2	235
6.11	The chemical composition of alloys in samples from face CE_2W_2	236
6.12	The distribution of elements in the oxide, the slag and the alloy in samples from face CE_2W_2	238
7.1	Summary of the main reactions that occurred at different levels in the furnace	248
A2.1	The resistivity of a charge of ore of size range 2,83 - 12,7 mm	275
A2.2	The resistivity of a charge of coal of size range 2,83 - 6,35	276
A2.3	The resistivity of a charge of coke of size range 2,83 - 6,35 mm	277
A2.4	The resistivity of a coke-ore mixture	278
A2.5	The resistivity of a coke-ore mixture	279
A2.6	The resistivity of a coke-ore mixture	280
A2.7	The resistivity of a coal-ore mixture	281
A2.8	The resistivity of a coal-ore mixture	282
A2.9	The resistivity of a coal-ore mixture	283
A2.10	The variations in resistivity of different SCICE charges at constant temperature	284
A3.1	Values of some parameters of Furnace M10	287
A3.2	Raw material type and quantity charged to Furnace M10	288
A3.3	The size analyses of the raw materials fed to Furnace M10 over the period 10 to 20 September 1977	288

LIST OF FIGURES

1.1	Plot of cumulative installed furnace capacity against time	4
1.2	Plots of log P_{CO}/P_{CO_2} against temperature for two reactions	10
1.3	Free energy changes against temperature for the reduction of MnO	12
1.4	Scheme for the reduction of preheated Mamatwan manganese ore	17
1.5	Single-phase circuit representing the electrical network of a submerged-arc furnace	20
1.6	The influence of carbonization temperature on the resistivity of coal	25
1.7	Resistivity as a function of temperature for iron ores or materials containing iron oxides	29
1.8	The influence of char particle size on the resistivity of mixtures of char and quartz, for various particle sizes of quartz	31
1.9	The influence of volume fraction of chromite ore on the resistance of a mixture of ore and char	33
1.10	Principal pattern of the metallurgical structure of the interior of an electric pig-iron furnace	38
1.11	Cross section of an experimental two-phase ferrochromium furnace	38
1.12	The basic structure of a submerged-arc furnace for the production of high-carbon ferromanganese	40
2.1	a) The zones near the electrode of a submerged-arc furnace and b) probable heating curves for an element of furnace burden descending near the electrode The heating conditions for the SCICE charges are superimposed for comparison	45
2.2	Schematic section of the SCICE apparatus	53
2.3	Temperatures recorded by the inner and outer thermocouples during the heating of a charge of ore and coke	55
2.4	Cooling curves for charges of ore and coal after heating to 1600°C and cooling and after heating to 1400°C and maintaining that temperature for 2 hours	56

2.5	Temperature gradients in a charge of alumina bubbles	58
3.1	Micrograph of Mamatwan ore showing a fine aggregate of metallic (bright) and gangue (grey) minerals. Gangue in the form of a vein and as an oolite is apparent. Porosity appears black	67
3.2	Partially reduced ore particles (O) in the slag (S) formed by heating ore and coke to 1600°C and holding that temperature for 1 hour	76
3.3	Sinter and loose particles in a charge of ore and coal that was heated to 1400°C and held at that temperature for 4 hours	78
3.4	Sinter and some loose particles in a charge of ore and coal that was heated to 1600°C and cooled	78
3.5	Slag and alloy formed by heating ore and coal to 1600°C and holding that temperature for 1 hour	79
3.6	Slag and alloy formed by heating ore and coal to 1600°C and holding that temperature for 2 hours	79
3.7	Metallic particles (bright), grains of oxide (light grey), slag (dark grey) and pores (black) in an ore particle that was heated with coke to 1300°C and cooled	81
3.8	Beads of alloy on the surface of an ore particle that was heated with coke to 1400°C and cooled. The surface was covered with a film of dendritic slag	82
3.9	Interfaces between partially reduced ore and slag and coke and slag. Note the fine oxide grains in the slag	84
3.10	A particle of ore breaking up in the slag matrix formed by reacting ore and coke at 1600°C for 1 hour. Note the metallic particles in the interior of some oxide grains	84
3.11	Elongated grains of impure manganous oxide (A) and particles of graphite (B) in a matrix of slag (C) formed by reacting ore and coke at 1600°C for 2 hours	86
3.12	The reaction rim (A) that formed round grains of oxide (B) by heating ore and coke to 1400°C and cooling. Slag (C) and metallic particles (D) are indicated	86

3.13	Spreading of the reaction rim towards the centre of oxide grains from a charge of ore and coke that was heated to 1600°C and cooled	87
3.14	Grains of troostite delineated by a bright network of carbide precipitate in an alloy bead formed by heating ore and coke to 1300°C and cooling	91
3.15	Grains of a solid solution (light grey) and nodules of troostite (dark grey) surrounded by a thick network of carbide in an alloy bead formed by heating ore and coke to 1300°C and cooling	91
3.16	Dendrites of primary austenite (dark) in a eutectic of austenite and carbide in an alloy bead formed by heating ore and coke to 1300°C and cooling	94
3.17	Eutectic structure of austenite (dark) and carbide (bright) in an alloy bead formed by heating ore and coke to 1300°C and cooling	94
3.18	Alloy beads with eutectic structure formed by reacting ore and coke at 1400°C for 4 hours. Carbide appears bright, austenite dark grey and pores appear black	95
3.19	Grains of primary carbide surrounded by a two-phase constituent in an alloy bead formed by reacting ore and coke at 1400°C for 4 hours	95
3.20	Laths of primary carbide (bright) and an interstitial two-phase constituent in alloy beads formed by heating ore and coke to 1500°C and cooling	97
3.21	A section from the alloy formed by reacting ore and coke at 1600°C for 1 hour, showing porosity, cracks and fine lines of uncertain nature	97
3.22	Differential staining in the alloy of Figure 3.21	98
3.23	The distribution of elements in an ore particle that was partially reduced by heating with coke to 1500°C and cooling	
	a) Grains of oxide and metallic particles surrounded by a network of slag in the partially reduced ore particle	
	b) Calcium Kα X-ray-distribution map	
	c) Iron Kα X-ray-distribution map	
	d) Manganese Kα X-ray-distribution map	
	e) Silicon Kα X-ray-distribution map	103

3.24	Comparison between the diffractograms obtained from charges of a) ore and coke and b) ore and coal after reaction at 1600°C for 1 hour	105
3.25	Comparison between the diffractograms of the alloy formed with coal after 2 hours at 1600°C (a), and with coke after 4 hours at 1400°C (b)	107
3.26	Plots of mass loss against holding time at temperature for mixtures of ore with coal or coke	110
3.27	Plot of mass loss against reaction temperature for mixtures of ore and coke	111
3.28	Variation of manganese and iron in the alloy with reaction temperature	114
3.29	Variation in manganese content of the alloy with time at temperature	114
3.30	Cuboidal grains of impure hausmannite in a matrix of slag formed by heating Mamatwan ore at 1300°C for 4 hours in air	115
3.31	EDS analyses of the oxide formed by the heating of ore at 1300°C in air	117
3.32	EDS analyses of the slag formed by the heating of ore at 1300°C in air	117
3.33	The structure of an ore particle that was partially reduced at 1200°C in carbon monoxide. Metallic particles (bright), rounded grains of impure manganous oxide (light grey), a slag matrix (darker grey) and porosity (black) are apparent	119
3.34	Rounded grains of oxide and metallic particles in a slag matrix formed by heating ore at 1450°C for 6 hours in carbon monoxide	119
3.35	Dendrites and rounded grains of impure manganous oxide in the slag matrix near the wall of the alumina crucible. Metallic particles appear bright and grains of a complex mixture of manganous, aluminium and magnesium oxides appear dark grey	120
3.36	The structure of a grain of oxide after reaction at 1450°C for 6 hours in carbon monoxide	120
3.37	Section of sinter formed by heating a 6kg charge of ore in a graphite crucible	123

3.38	Precipitation of a calcium-manganese ferrite on the periphery and in the interior of grains of oxide in a matrix of slag	123
3.39	Precipitation of fine grains of oxide (light grey) in a slag matrix (dark grey)	124
3.40	Comparison of the diffraction patterns of the slag from the metallised and non-metallised regions	130
4.1	The 600°C isotherm of the Fe-Mn-C system	147
5.1	Circuit for the measurement of charge resistance	156
5.2	The effect of temperature on the resistivity of Mamatwan ore, Iscor coke and Delmas coal	159
5.3	Arrhenius plots of the resistivity of Mamatwan ore, Iscor coke and Delmas coal	161
5.4	Temperature differences between the inner and outer thermocouples during the heating of Delmas coal	163
5.5	Volume changes with increasing temperature for various charges	164
5.6	The influence of temperature on the resistivity of mixtures of ore and coke	168
5.7	Variations in resistivity with time at temperature for mixtures of ore and coke	173
5.8	The influence of temperature on the resistivity of mixtures of ore and coal	175
5.9	Variations in the resistivity of mixtures of ore and coal with time at 1300°C	176
5.10	Arrhenius plots for mixtures of ore and coke and ore and coal	177
5.11	A comparison of the resistivities of mixtures of ore and coke and ore and coal for different particle sizes of the reducing agent	179
6.1	Section of furnace M10 in plan showing the position of the electrodes, the furnace diameter at roof and hearth levels and the planned sampling localities	187
6.2	Vertical section through the furnace along radius CE_1W_1 (Figure 6.1) showing the planned positions for sampling	188
6.3	The distribution of zones in the vertical section AA of Figure 6.1	192
6.4	The appearance of zones in the vicinity of electrode No. 1	193

3.38	Precipitation of a calcium-manganese ferrite on the periphery and in the interior of grains of oxide in a matrix of slag	123
3.39	Precipitation of fine grains of oxide (light grey) in a slag matrix (dark grey)	124
3.40	Comparison of the diffraction patterns of the slag from the metallised and non-metallised regions	130
4.1	The 600°C isotherm of the Fe-Mn-C system	147
5.1	Circuit for the measurement of charge resistance	156
5.2	The effect of temperature on the resistivity of Mamatwan ore, Iscor coke and Delmas coal	159
5.3	Arrhenius plots of the resistivity of Mamatwan ore, Iscor coke and Delmas coal	161
5.4	Temperature differences between the inner and outer thermocouples during the heating of Delmas coal	163
5.5	Volume changes with increasing temperature for various charges	164
5.6	The influence of temperature on the resistivity of mixtures of ore and coke	168
5.7	Variations in resistivity with time at temperature for mixtures of ore and coke	173
5.8	The influence of temperature on the resistivity of mixtures of ore and coal	175
5.9	Variations in the resistivity of mixtures of ore and coal with time at 1300°C	176
5.10	Arrhenius plots for mixtures of ore and coke and ore and coal	177
5.11	A comparison of the resistivities of mixtures of ore and coke and ore and coal for different particle sizes of the reducing agent	179
6.1	Section of furnace M10 in plan showing the position of the electrodes, the furnace diameter at roof and hearth levels and the planned sampling localities	187
6.2	Vertical section through the furnace along radius CE_1W_1 (Figure 6.1) showing the planned positions for sampling	188
6.3	The distribution of zones in the vertical section AA of Figure 6.1	192
6.4	The appearance of zones in the vicinity of electrode No. 1	193

6.5	The diffuse boundary between zones 1 and 2 (Figure 6.3) made apparent due to segregation of reducing agents. Note the penetration of the furnace shell	193
6.6	The 'coke bed' directly underneath the electrode and the coke-enriched zone at some distance from the electrode tip	195
6.7	A close-up view of zone 8 (Figure 6.3) showing lumps of reducing agent embedded in the slag	195
6.8	The variable consistency of zone 9	197
6.9	The "finger-like" appearance of the tip of electrode No. 1	197
6.10	The appearance of the partially dead zone in the central region of the furnace. Lumps of reducing agent are embedded in the slag and alloy appears at the interface between slag and reducing agent	199
6.11	Scheme for the processing of furnace samples	200
6.12	Vertical section through plane CE,W, (Figure 6.1). Closed circles indicate samples that were taken. Open circles indicate samples that were not taken	202
6.13	Powdery slag in sample 1/E/0	204
6.14	Lumps of slag with associated alloy in sample 1/F/0	204
6.15	Sinter from sample 1/C/1 showing the distribution of metallic particles	206
6.16	Sinter from sample 1/D/1 showing partially reduced ore (dark grey), slag (light grey), alloy, and the positions of particles of reducing agent (C)	206
6.17	Fine material in sample 1/B/2 generated by the oxidation of reducing agents and decrepitation of ore lumps	208
6.18	Segregation of reducing agents and excessive decrepitation of the burden in sample 1/C/3	208
6.19	The porous structure of partially reduced ore from sample 1/B/1	210
6.20	An ore particle from sample 1/C/1 showing MnO particles (light grey) and metallic particles (bright) in a matrix of slag. Pores appear black	210
6.21	Metallic nuclei and grains of MnO in a matrix of slag. An alloy globule of eutectic composition adheres to the surface of the ore particle from sample 1/D/1	211

6.22	Coarse grains of MnO surrounded by a film of slag in sample 1/E/1	211
6.23	Grains of MnO and metallic particles in a matrix of slag from sample 1/F/1	213
6.24	Thick flakes of graphite in the alloy from sample 1/F/1	213
6.25	Variations in the X-ray patterns of the alloy with increasing carbon content	218
6.26	The composition of the alloy in samples from position 1 between the electrode and the furnace wall	221
6.27	The composition of alloys at level E and at various distances from the centre of the furnace hearth	222
6.28	The composition of alloys at level F and at various distances from the centre of the furnace hearth	223
6.29	A microanalysis traverse from the centre of a grain of MnO across the slag to a neighbouring oxide grain	227
6.30	The variation in the composition of alloy globules with increasing size	228
6.31	The location of samples that were successfully taken (full circles) in plane CE_2W_2 (Figure 6.1)	229
6.32	Grains of a solid solution of MnO and MgO (dark grey) with adhering metallic particles (light grey) in a matrix of slag	239
7.1	The area occupied by partially or completely stagnant burden (shaded) at stockline level	241
7.2	Horizontal section through furnace M1O showing the diameter of the furnace at roof and floor levels and the extent of the reaction zone around the three electrodes	243
7.3	The phase transformations of silica as a function of temperature	253
7.4	The solubility of carbon in alloys of iron and manganese	256
A2.1	Apparatus for the determination of the cell constant of the SCICE system	267
A2.2	The influence of temperature on the resistance of the system	269
A2.3	The influence of the depth of the solution on the resistance of the system	270
A2.4	Variation in resistance with distance of the electrode from the cell bottom	273

6.22	Coarse grains of MnO surrounded by a film of slag in sample 1/E/1	211
6.23	Grains of MnO and metallic particles in a matrix of slag from sample 1/F/1	213
6.24	Thick flakes of graphite in the alloy from sample 1/F/1	213
6.25	Variations in the X-ray patterns of the alloy with increasing carbon content	218
6.26	The composition of the alloy in samples from position 1 between the electrode and the furnace wall	221
6.27	The composition of alloys at level E and at various distances from the centre of the furnace hearth	222
6.28	The composition of alloys at level F and at various distances from the centre of the furnace hearth	223
6.29	A microanalysis traverse from the centre of a grain of MnO across the slag to a neighbouring oxide grain	227
6.30	The variation in the composition of alloy globules with increasing size	228
6.31	The location of samples that were successfully taken (full circles) in plane CE_2W_2 (Figure 6.1)	229
6.32	Grains of a solid solution of MnO and MgO (dark grey) with adhering metallic particles (light grey) in a matrix of slag	239
7.1	The area occupied by partially or completely stagnant burden (shaded) at stockline level	241
7.2	Horizontal section through furnace M1O showing the diameter of the furnace at roof and floor levels and the extent of the reaction zone around the three electrodes	243
7.3	The phase transformations of silica as a function of temperature	253
7.4	The solubility of carbon in alloys of iron and manganese	256
A2.1	Apparatus for the determination of the cell constant of the SCICE system	267
A2.2	The influence of temperature on the resistance of the system	269
A2.3	The influence of the depth of the solution on the resistance of the system	270
A2.4	Variation in resistance with distance of the electrode from the cell bottom	273

CHAPTER 1

1.0 INTRODUCTION

The Republic of South Africa possesses vast reserves of manganese ores and coal and is one of the major ferro-manganese producers in the world. The industry had its beginning in Newcastle, Natal in 1937 when ferromanganese was produced in the No.1 Blast Furnace. Since then, enormous developments have taken place in terms of production capacity and methods. The major tool for the production of the alloy today is the submerged-arc electric furnace. The shape, size and rating of the electric furnace have changed drastically since its introduction in South Africa in 1942. Recent furnaces installed have ratings between 48 and 84 MVA while the total installed capacity for ferromanganese production is estimated to be over 300 MVA.

The first electric furnace used in this country was rectangular with 3 electrodes in line and a rating of 3 MVA. Modern furnaces are cylindrical with 3 electrodes at the vertices of an equilateral triangle and have power ratings of up to 84 MVA. Developments since 1973 show that the emphasis is on units with ratings of 48 MVA or higher owing to the lower unit production costs incurred when operating in these units. The increases in furnace size however, were attended by increased technical difficulties which were aggravated further by material quality. The larger furnaces have an inherent low resistance and power factor [1] and are very sensitive to raw material quality. The scarcity of coking coals and the desire to increase the resistance of the furnace has led ferromanganese producers to look at alternative reducing agents.

In spite of the importance of the ferromanganese industry little research [2, 3] has been carried out in the production of ferromanganese alloys. Areas considered to be of

fundamental importance include the beneficiation of manganese ores, the influence of reducing agents on the reduction process and on burden resistance and the reduction and smelting processes which occur in industrial furnaces. The work that has been carried out has dealt with the gaseous reduction of lumpy ore at low temperatures [1] and with the reduction of finely ground ore with solid reducing agents at relatively low temperatures [2].

This work examines the influence of the two reducing agents, Iscor coke and Delmas coal on the reactions and the resistivity of an element of furnace burden as the latter descends in the furnace bowl. The experimental technique, the mass of the charge, and the particle size of the reactants used, were such that the experimental conditions were not completely arbitrary. The ore used was Mamatwan manganese ore which is in plentiful supply in South Africa and constitutes about 70 per cent of the total ore charged to industrial furnaces in South Africa.

The processes that take place in a 75 MVA furnace were evaluated by examining samples taken during the excavation of one such furnace.

The extent to which the experimental technique can reproduce the conditions experienced in industrial furnaces was assessed from a comparison between the laboratory results and the results obtained from the furnace samples.

1.1 Production of Ferromanganese in South Africa

The total reserves of manganese ores in South Africa amount to some 3000 million tonnes [4].

The most important orebodies are the Mamatwan and Hotazel of which the Mamatwan orebody is by far the bigger. The Mamatwan ore is of a lower grade compared with Hotazel and with high grade ores of other nations [5, 6]. Comparative figures have been given by Featherstone [7] and are indicated below:-

Element	Hotazel	Mamatwan
	Mass per cent	
Mn	51,4	39,4
Fe	10,3	4,2
Mn:Fe	4,99	9,38

The major manganese mineral in these ores is braunite ($3Mn_2O_3.MnSiO_3$) while the gangue occurs mainly as calcite ($CaCO_3$) and dolomite [8] ($CaMg(CO_3)_2$).

The Mamatwan ore has found extensive application in the production of high-carbon ferromanganese in spite of its low grade and its apparent unsuitability [7] for use in the electric furnace. This ore is generally blended with other ores to give the desired furnace characteristics and constitutes 60 to 70 percent of the total ore charged to the electric furnace in South Africa.

Some authors [7, 9] consider that the high CaO and MgO content of South African ores makes them suitable as self-fluxing burden for the low shaft blast furnace and there has been speculation [10] that the use of the blast furnace will increase in the future. However, blast furnace smelting of ferromanganese is attended by serious disadvantages such as a high coke rate and high manganese losses in the off-gases. The electric furnace offers advantages such as lower labour costs [9], greater flexibility in its ability to produce different grades of alloys and to operate with low quality reducing agents [11].

The developments in electric furnace smelting of ferromanganese alloys can be followed from Figure 1.1 which shows a plot of the cumulative installed furnace capacity against time. It can be seen that the installed capacity more than doubled between 1973 and 1979. The trend indicates that for the foreseeable future the electric furnace will remain the major tool for the production of ferromanganese alloys in South Africa.

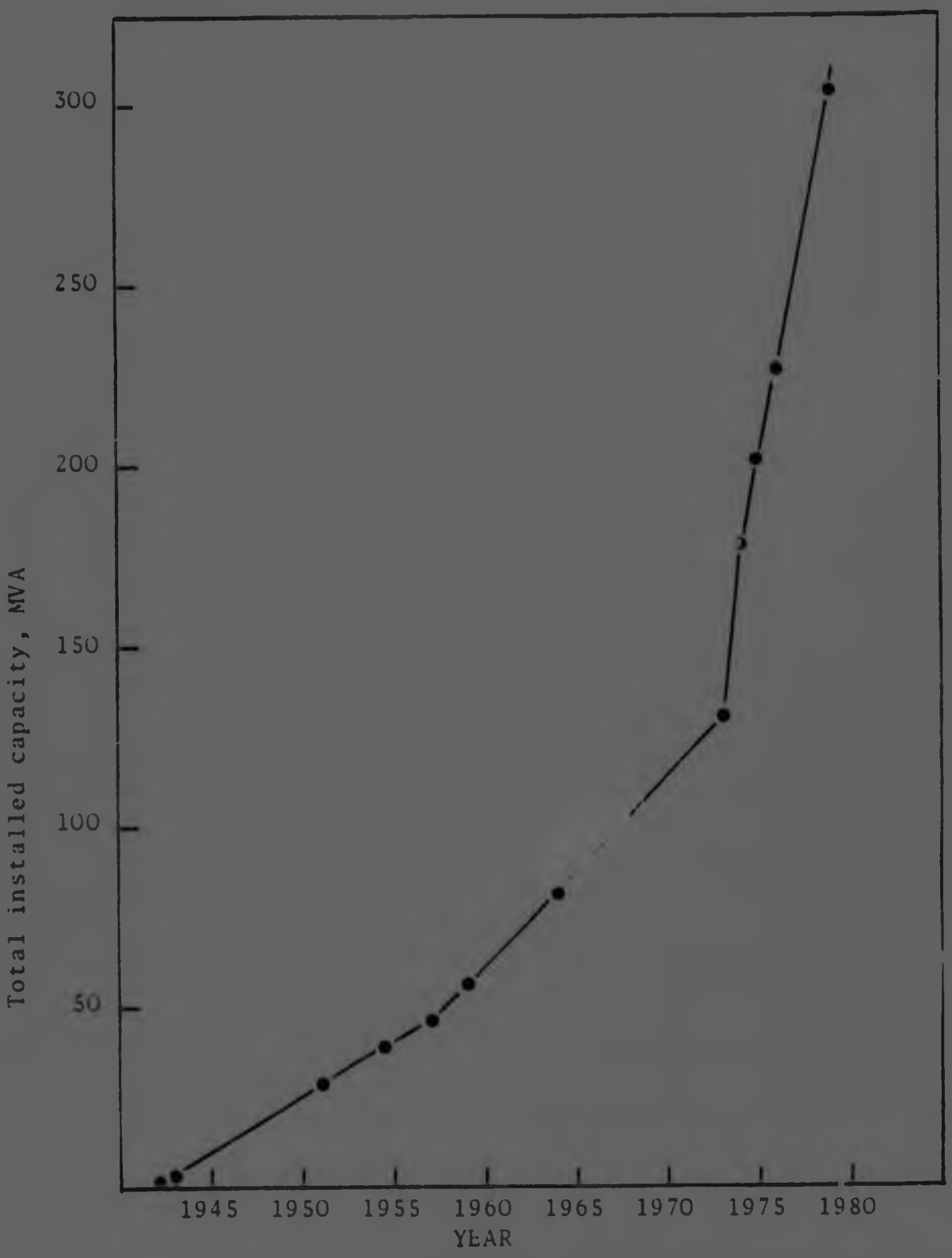


Figure 1.1 Plot of cumulative installed furnace capacity in South Africa as a function of time. (refs. 12 - 15).

1.2 Reduction of Manganese Oxides

1.2.1 Reduction of the Higher Oxides

Manganese can exist as the oxides MnO_2, Mn_2O_3, Mn_3O_4 and MnO.

The higher oxides of manganese are thermally unstable and dissociate upon heating according to the following reactions:

$$2MnO_2 = Mn_2O_3 + O_2 \quad . \quad . \quad . \quad 1.1$$

$$3Mn_2O_3 = 2Mn_3O_4 + O_2 \quad . \quad . \quad . \quad 1.2$$

$$Mn_3O_4 = 3MnO + O_2 \quad . \quad . \quad . \quad 1.3$$

The temperature of dissociation depends on the partial pressure of oxygen in the system and equilibria for one or all three of the above reactions have been given by previous investigators [16-21].

From the data of Malinin et al [19] and Hahn et al [18] the following scheme can be derived for the dissociation of the higher oxides when heated in air (P_{O2} = 21, 28kPa).

$$MnO_2 \xrightarrow{520^{\circ}C} Mn_2O_3 \xrightarrow{875^{\circ}C} Mn_3O_4 \xrightarrow{1600^{\circ}C} MnO$$

The oxide MnO is thermally stable and does not dissociate in practice. The equilibrium partial pressure of oxygen at 2000K for the reaction

$$MnO = Mn + \tfrac{1}{2}O_2 \quad . \quad . \quad . \quad . \quad 1.4$$

may be calculated to be $5{,}76 \times 10^{-13}$kPa.

The temperatures for the dissociation of the higher oxides, as given by different authors vary considerably and Hahn et al [18] have attributed these variations to the extreme difficulties in attaining equilibrium in the Mn-O system. Grimsley [5] compiled a list of dissociation temperatures for the higher oxides but did not differentiate between data obtained from pure oxides and those obtained from minerals. Dressel and Kenworthy[22] have shown that dissociation temperatures

can vary significantly for small variations in the chemical composition of the minerals.

The gaseous reduction of the higher oxides of manganese has been studied by numerous investigators [2, 3, 22-28]. The conclusion that can be drawn from these studies is that the reduction of the higher oxides by carbon monoxide or hydrogen proceeds very rapidly and at low temperatures. Therefore, in a submerged-arc furnace the higher oxides will be reduced to MnO in the upper regions of the furnace.

The reduction of Mn_3O_4 by CO may be expressed as:

$$Mn_3O_4 + CO = 3MnO + CO_2 \quad . \quad . \quad 1.5$$

$$\Delta G^{o}_{1.5}\ kJmol^{-1} = -59,9 - 0,04T\ (298\text{-}1517K)^{*}$$

If it is assumed that the activities of MnO and Mn_3O_4 are equal to 1 then the equilibrium constant for reaction 1.5 will be given by:

$$K_{1.5} = \frac{P_{CO_2}}{P_{CO}} \quad . \quad . \quad . \quad . \quad . \quad 1.6$$

and

$$\log K_{1.5} = \frac{\Delta G^{o}_{T}}{-19,147T} \quad . \quad . \quad . \quad . \quad 1.7$$

therefore

$$K_{1.5} = 3,87 \times 10^{12} \text{ at } 25^{o}C$$
$$= 1,4 \times 10^{4} \text{ at } 1244^{o}C$$

---

*Thermodynamic data were taken from Kubachewski, Evans and Alcock (reference 140).

Tnese values of $K_{1.5}$ indicate that Mn_3O_4 can be reduced at temperatures between 25 and 1244°C in gaseous atmospheres that contain very low concentrations of carbon monoxide. This assumes that tne gaseous phase contains CO and CO_2 only.

According to Tol'togusov [29] and Coetzee [30] the gaseous phase in a furnace for ferromanganese contains about 70 per cent CO and Pilter [23] has shown that the higher oxides will be reduced to MnO very rapidly in mixtures of CO and CO_2 containing as little as 10 per cent CO. Thus in the submerged-arc furnace there will be a very strong tendency for the reduction of Mn_3O_4 by CO to occur between 25 and 1244°C. The reduction of MnO_2 and Mn_2O_3 by CO will tend to proceed with an even greater ease under the same conditions.

The above considerations lead to the conclusion that the thermal dissociation of the higher manganese oxides is not of significant practical importance to the ferro-alloy industry. Even if pre-reduction of an ore were considered it would by far be better to carry out such a process in an atmosphere containing some carbon monoxide. It appears, however, that pre-reduction of the ore would not be beneficial because the reduction of Mn_2O_3 and Mn_3O_4 by carbon monoxide is exothermic and the heat generated pre-heats the burden in the upper regions of the furnace [29]. Thus a saving in energy may be realised.

The reduction of Mn_2O_3 and Mn_3O_4 by solid carbon is thermodynamically more favourable than by CO for temperatures greater than about 720°C [3]. In a ferromanganese furnace however reduction will probably occur by CO since the kinetics of gaseous reduction are much more favourable.

1.2.2. Reduction of Manganous Oxide

The theory of the gaseous reduction of oxides has been dealt with by several authors [23, 31, 32], a very good treatment being given recently by Rankin [31] in a study of the reduction of chromite in the solid state. Similar considerations can be applied to manganous oxide.

Manganous oxide is very stable and it is generally held [2,3,22,23,25,33] that its reduction by carbon monoxide does not occur due to the high partial pressures of carbon monoxide required.

The reduction of manganous oxide by carbon monoxide may be represented by the following reactions.

$$Mn + \tfrac{1}{2}O_2 = MnO \quad . \quad . \quad . \quad . \quad . \quad 1.8$$

$$\Delta G^{o}_{1.8} Jmol^{-1} = -384719 + 72,8T \ (298\text{-}1500K)$$
$$= -399154 + 82,4T \ (1500\text{-}2050K)$$

$$CO_2 = CO + \tfrac{1}{2}O_2 \quad . \quad . \quad . \quad . \quad . \quad 1.9$$

$$\Delta G^{o}_{1.9} Jmol^{-1} = 282420 - 86,8T \ (298\text{-}2000K)$$

$$(1.8+1.9)\ Mn+CO_2 = MnO+CO \quad . \quad . \quad . \quad 1.10$$

$$\Delta G^{o}_{1.10} Jmol^{-1} = -102299 - 14,0T \ (298\text{-}1500K)$$
$$= -116734 - 4,4T \ (1500\text{-}2000K)$$

The equilibrium constant, K, for reaction 1.10 is given by:

$$K_{1.10} = \frac{P_{CO}\ a_{MnO}}{P_{CO_2}\ a_{Mn}} \quad . \quad . \quad . \quad 1.11$$

where a is the activity of manganous oxide or manganese and P is the partial pressure of the respective gases.

If it is assumed that manganous oxide and manganese are not mutually soluble then $a_{MnO} = a_{Mn} = 1$, and

$$K_{1.10} = \frac{P_{CO}}{P_{CO_2}} \quad . \quad . \quad . \quad . \quad 1.12$$

From $$\Delta G^{o}_{T} = -RT \ln K \quad . \quad . \quad . \quad 1.13$$

the equilibrium values of P_{CO}/P_{CO_2} for reaction 1.10 can be calculated at various temperatures from equations 1.12 and 1.13.

Temperature ^{o}C	P_{CO}/P_{CO_2} (reaction 1.10)
1000	$8,5 \times 10^4$
1200	$2,3 \times 10^4$
1400	$7,5 \times 10^3$
1600	$3,1 \times 10^3$
1800	$1,5 \times 10^3$

The significance of the P_{CO}/PCO_2 ratios for the reduction process becomes apparent when the Boudouard reaction is considered.

$$CO_2 + C = 2CO \quad . \quad . \quad . \quad . \quad 1.14$$

$$\Delta G^{o}_{1.14} Jmol^{-1} = 170707 - 174,5T$$

$$K_{1.14} = \frac{P^2_{CO}}{P_{CO_2} a_C}$$

Since the activity of solid carbon is 1

$$K_{1.14} = \frac{P^2_{CO}}{P_{CO_2}}$$

If the total pressure, $P_{CO} + P_{CO_2}$, is taken as 101,325 kPa then the following values of P_{CO}/P_{CO_2} can be calculated.

Temperature ^{o}C	P_{CO}/P_{CO_2} (reaction 1.14)
1000	$1,28 \times 10^2$
1200	$1,15 \times 10^3$
1400	$6,10 \times 10^3$
1600	$2,26 \times 10^4$
1800	$6,50 \times 10^4$

Plots of log P_{CO}/P_{CO_2} against temperature, for reactions 1.10 and 1.14 are shown in Figure 1.2. It can be seen that at temperatures of 1420^{o}C or higher manganous oxide can be reduced by carbon monoxide in the presence of solid carbon. For this to occur the ratio of P_{CO}/P_{CO_2} has to be 6610 or higher, which shows that even small amounts of carbon dioxide in the system will inhibit reaction.

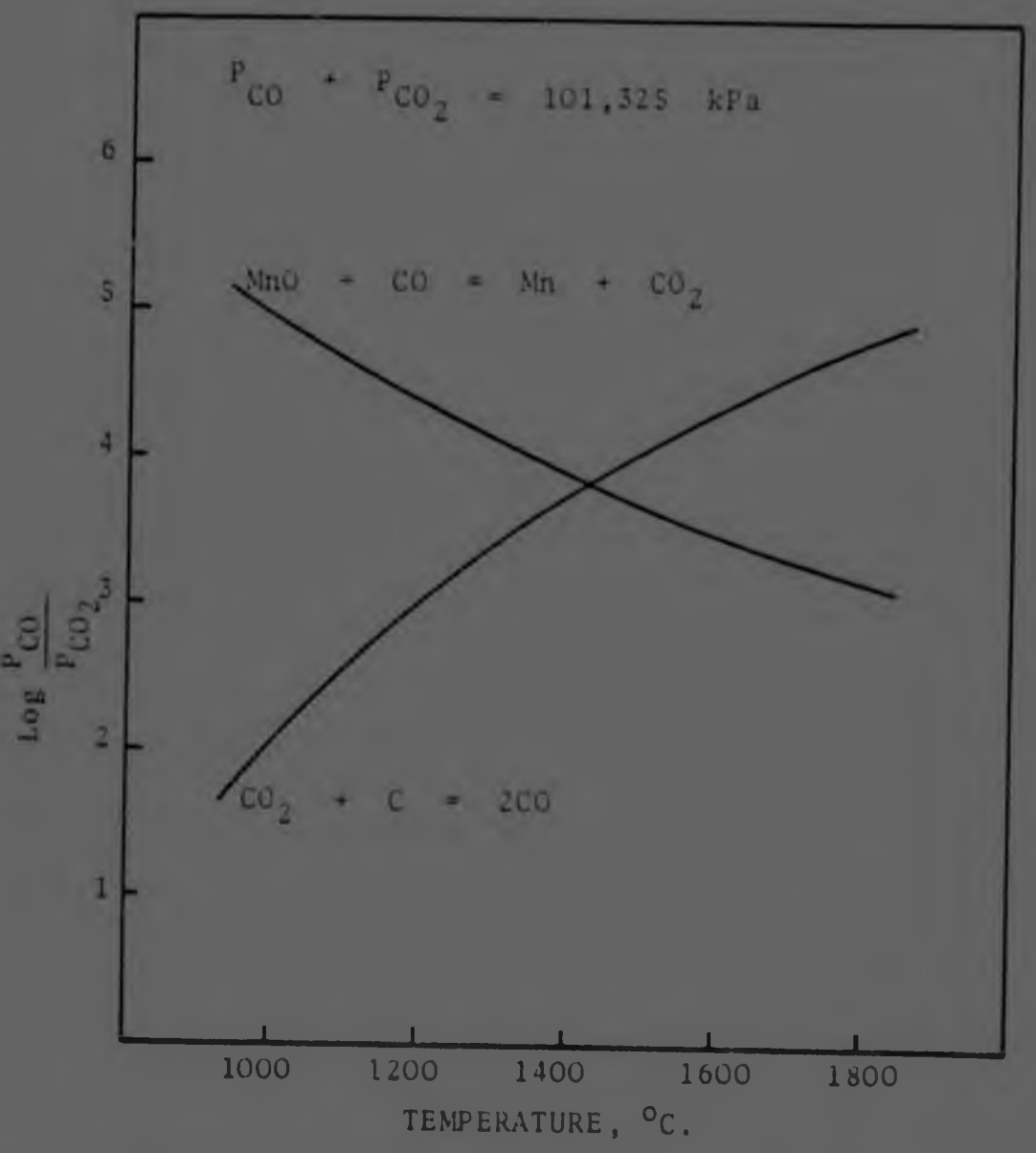


Figure 1.2 Plots of log P_{CO}/P_{CO_2} against temperature for two reactions.

It is very doubtful whether such high ratios of P_{CO}/P_{CO_2} exist in the upper regions of ferromanganese furnaces. It is probable however, that they exist in the vicinity of the electrode tips where the temperature is high and any carbon dioxide present will be reduced to carbon monoxide rapidly by reaction with carbon.

The reduction of manganous oxide by solid carbon has been dealt with by several investigators [3, 25, 34]. The reactions considered by Grimsley [3] and the corresponding changes of free energy with increasing temperature are shown in Figure 1.3. It can be seen that reduction of manganous oxide with solid carbon or iron carbide will take place preferentially according to the reactions

$$MnO + 10/7C = 1/7Mn_7C_3 + CO \quad . \quad . \quad . \quad 1.15$$
$$\Delta G^{o}\ Jmol^{-1} = 284220 - 180T \ (990\text{-}1360K)$$

and

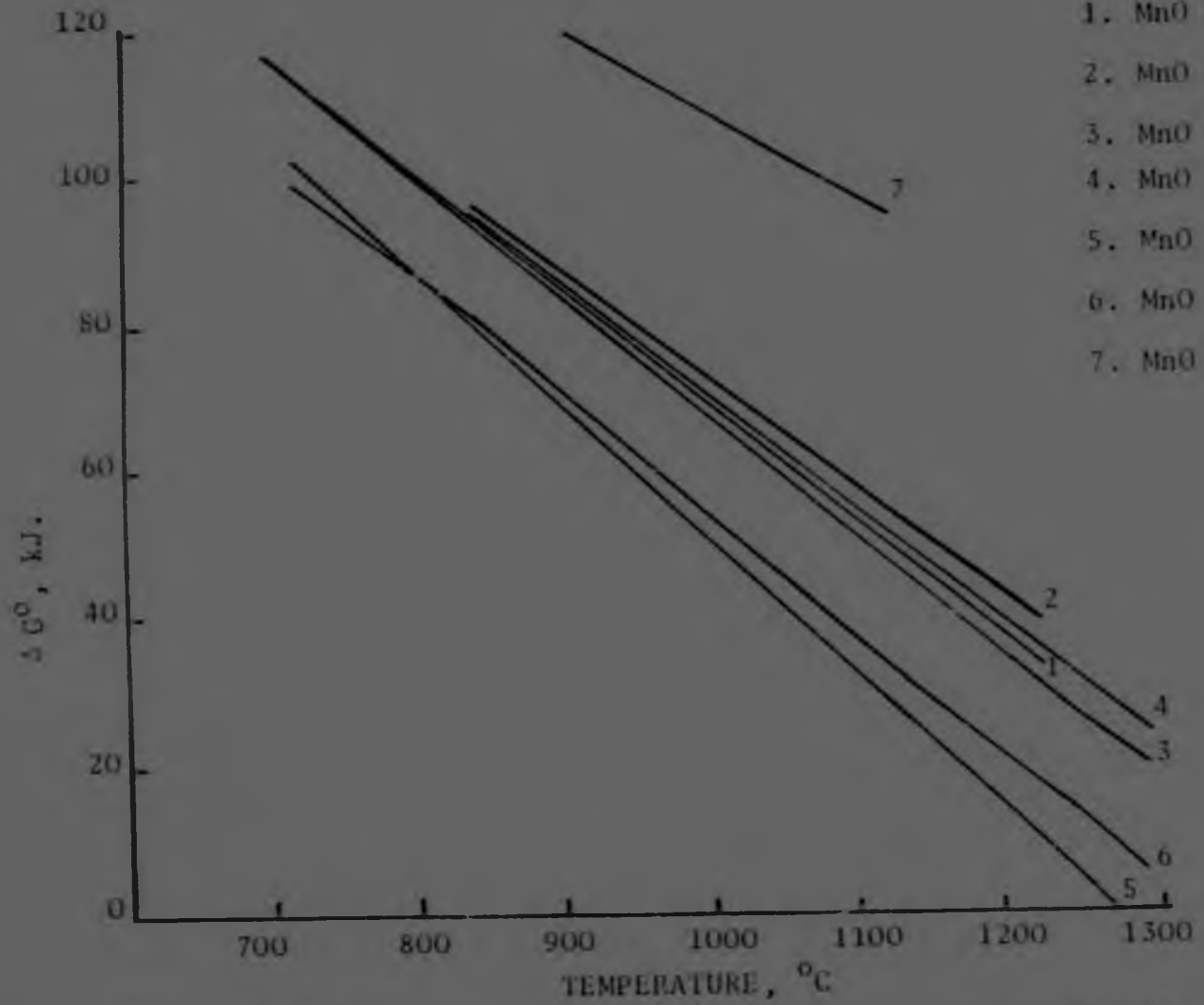
$$MnO + 10/7Fe_3C = 1/7Mn_7C_3 + 30/7Fe + CO \quad 1.16$$
$$\Delta G^{o}\ Jmol^{-1} = 246090 - 150T \ (990\text{-}1113K)$$
$$= 269420 - 170T \ (1113\text{-}1360K).$$

1.2.3. Reduction of Manganous Oxide from Slags

The reduction of manganous oxide from slags has not been investigated in any detail. The literature on this subject relates mostly to the reduction of manganous oxide from blast furnace slags in which the concentration of this oxide is relatively low.

Opinions vary with regard to the mechanisms of the reduction of manganous oxide from slags.

Tarby and Philbrook [35] found, that the reduction of manganous oxide and iron oxide from blast-furnace slags, by carbon saturated iron, occurred in two stages; a rapid initial stage due to stirring of the melt by the evolving carbon monoxide and a slower second stage after boiling had subsided and conditions were defined by natural convection. The two stages of reduction were also observed by other investigators [30, 37]. The rate of reduction of the two oxides was influenced by the



1. $MnO + {}^{4}/_{3}C = {}^{1}/_{3}Mn_3C + CO$
2. $MnO + 4/_{3}Fe_3C = {}^{1}/_{3}Mn_3C + 4Fe + CO$
3. $MnO + C = Mn + CO$
4. $MnO + Fe_3C = Mn + 3Fe + CO$
5. $MnO + {}^{10}/_{7}C = {}^{1}/_{7}Mn_7C_3 + CO$
6. $MnO + {}^{10}/_{7}Fe_3C = {}^{1}/_{7}Mn_7C_3 + {}^{30}/_{7}Fe + CO$
7. $MnO + {}^{1}/_{3}Mn_7C_3 = {}^{10}/_{3}Mn + CO.$

Figure 1.3 Free energy changes against temperature for the reduction of MnO (ref. 3).

temperature and the oxide concentration and was diffusion controlled. A diffusion controlled mechanism was also proposed by Yagi and Ono [38].

Contrary to the findings of Tarby and Philbrook [35] and Yagi and Ono [38], Daines and Pehlke [36] found that while temperature and melt geometry had a significant effect on the rate of reduction the rate of stirring had no effect, indicating that the reaction rate was controlled by chemical reaction at the slag/metal interface. Models derived by Daines and Pehlke and based on a diffusion controlled reaction step and on two chemical reaction steps, were tested using data obtained with varying stirring rate, temperature, melt geometry and reactant concentration. The results indicated that the anodic reaction,

$$O^{2-} = \underline{O} + 2e- \quad . \quad . \quad . \quad 1.17$$

was the rate limiting step. The cathode half cell reaction is,

$$Mn^{2+} + 2e- = \underline{Mn} \quad . \quad . \quad . \quad 1.18$$

From results obtained by varying the slag composition, the ambient pressure and the carbon activity Pomfret and Grievson [37] proposed that the fast reaction stage took place by the exchange mechanism,

$$(MnO) + [Fe] = [Mn] + (FeO) \quad . \quad . \quad 1.19$$

The authors concluded that the rate of reaction during the initial stage is controlled by mass transport in the slag phase and is influenced by the rate of evolution of carbon monoxide.

Kukhtin et al [39] investigated the kinetics of reduction of manganous oxide from slags, similar to those encountered in the production of high carbon ferromanganese. Gravimetric and electrochemical methods were used. They assumed that reduction would take plac. by the reaction

$$(MnO)_{slag} + C(gr) = Mn(l) + CO(g) \quad . \quad 1.20$$

and found that rotation of the graphite disc in the melt had no effect on the rate of reduction, which was

practically a linear function of the manganous oxide content of the slag.

The half cell reactions

$$C(s) + O^{2-} - 2e = CO \text{ and } \quad . \quad . \quad 1.21$$

$$Mn^{2+} + 2e = Mn^{o} \quad . \quad . \quad . \quad 1.22$$

were studied separately by means of polarizing measurements. It was established that reduction of MnO from the slags took place, on the whole, by electrochemical means, the limiting factors being the delayed anode oxidation of carbon which in turn was inhibited by desorption of carbon monoxide. Diffusion of manganous oxide in the slag was rapid at 1500 and 1650°C but the process was kinetically controlled.

1.3 The Mechanism of Reduction of Metal Oxides

The mechanism of reduction of metal oxides is an involved subject and in the general case, reduction occurs by more than one mechanism, depending on the nature of the oxide, the temperature and the furnace atmosphere. It is frequently the case that a number of potential reducing agents coexist in the system and this makes it impossible to isolate the effect of any one of them. Although the process that is most likely to occur under a given set of conditions can be determined from thermodynamic considerations, the kinetics of the process may be unfavourable and a different process may occur.

Kolchin [20] discussed four general mechanisms for the reduction of metal oxides by carbon.

Mechanism 1.

$$MeO + CO = Me + CO_2 \quad . \quad . \quad . \quad 1.23$$

$$CO_2 + C = 2CO \quad . \quad . \quad . \quad . \quad 1.24$$

According to this mechanism the oxide is reduced by carbon monoxide which is regenerated by reaction between solid carbon and carbon dioxide.

Mechanism 2.

$$2\,MeO = 2Me + O_2 \quad . \quad . \quad . \quad . \quad 1.25$$

$$C + nO_2 = CO_2 + pCO \quad . \quad . \quad . \quad . \quad 1.26$$

This mechanism is based on the dissociation of the oxide into the metal or its suboxide and oxygen with the subsequent oxidation of carbon.

Mechanism 3.

$$MeO + C = Me + CO \text{ or } CO_2 \quad . \quad . \quad 1.27$$

Reduction takes place by contact between solid carbon and oxide.

Mechanism 4.

$$MeO(g) + C(s) = Me + CO \text{ or } CO_2 \quad . \quad 1.28$$

This mechanism is based on the evaporation of the oxide and its reaction with solid carbon.

Kolchin [40] cites numerous examples to support one or the other of the four mechanisms proposed and concludes that the reduction process cannot be explained by a 'universal' mechanism and that reduction by carbon may take place by various mechanisms depending on the system and the specific conditions.

The mechanisms of reduction of iron oxides have been dealt with by many investigators [41-51]. Generally, the literature deals with systems in which an oxide of high purity is reacted with a solid or gaseous reducing agent. These systems are simplifications of actual processes since the possibility of slag formation and its effect on the process of reduction does not arise.

There is general agreement that the reduction of iron oxides by solid carbon occurs mainly through the intermediate gaseous reaction product CO. Thus

$$3Fe_2O_3 + CO = 2Fe_3O_4 + CO_2 \quad . \quad . \quad . \quad 1.29$$

$$Fe_3O_4 + CO = 3FeO + CO_2 \quad . \quad . \quad . \quad . \quad 1.30$$

$$FeO + CO = Fe + CO_2 \quad . \quad . \quad . \quad . \quad 1.31$$

$$CO_2 + C = 2CO \quad . \quad . \quad . \quad . \quad . \quad 1.32$$

The rate of reduction is determined by the rate of carbon solution. Therefore the reactivity of the reducing agent towards carbon dioxide has a significant influence on the rate of reduction.

Baldwin [45] considers that, in the blast furnace, glazing of the ore near its melting point would diminish the ease of gas penetration and contact between fayalite and coke would result in direct interaction. The apparent mechanisms and the rate of reduction of iron oxides change with changes in the lime to silica ratio [52].

The mechanisms for the reduction of the higher oxides of manganese are well established. It has already been indicated that reduction of MnO_2, Mn_2O_3 and Mn_3O_4 to MnO can take place by thermal dissociation, by gaseous reduction or by reaction with solid carbon. In the submerged-arc furnace reduction to MnO probably occurs mainly by carbon monoxide for two reasons. Firstly, the area of contact between solid carbon and ore is extremely limited and secondly rapid reduction by CO will take place even in atmospheres containing as little as 10 per cent of carbon monoxide [23]. Thus it can be assumed that all the manganese oxides in an ore such as Mamatwan ore will be reduced to MnO in the upper regions of the furnace bowl.

The mechanism for the reduction of preheated Mamatwan ore between 1000 and 1300°C has been investigated by Grimsley [3], who proposed a two stage reduction process as indicated in Figure 1.4. The first stage involves the reduction of Mn_3O_4

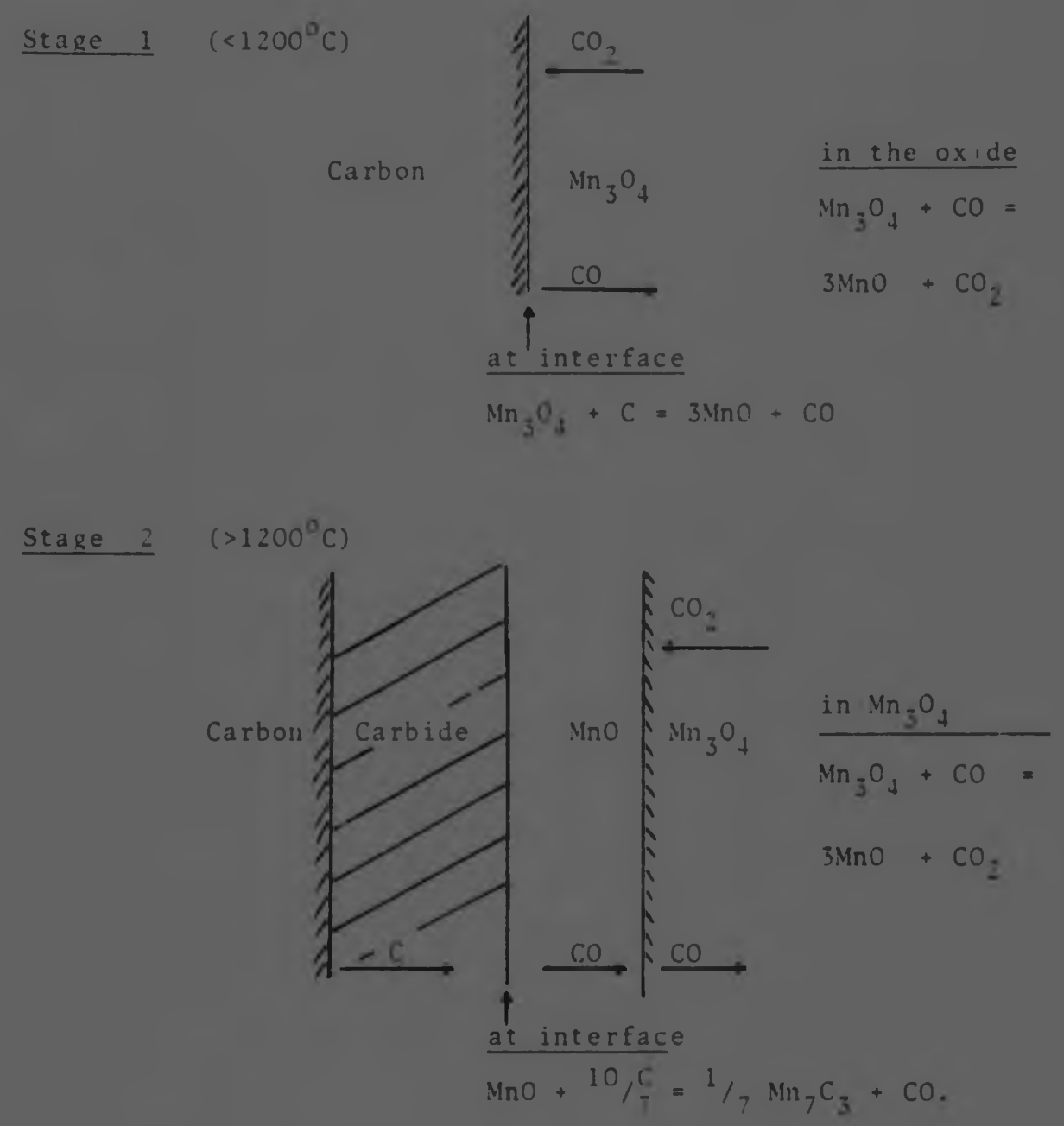


Figure 1.4 Scheme for the reduction of preheated Mamatwan manganese ore (ref. 3).

by carbon and carbon monoxide while the second stage involves the reduction of MnO by a carbide and of the remaining Mn_3O_4 by CO. Concerning the second stage of the proposed mechanism it should be pointed out that the possible influence of slag formation on the mechanism of reduction was not considered. The ore used by Grimsley [3] contained a total of 20,6 per cent of 'unreducible' oxides and 48.6 per cent MnO. It is easily seen that progressive reduction of MnO would increase the proportion of slag in the system. It is difficult therefore to visualise the maintenance of the interfaces proposed by Grimsley.

In comparative experiments it was established [3] that the reduction of preheated Mamatwan ore was faster than that of pure Mn_3O_4 during the second stage of the reaction. This was attributed to the presence of iron in the ore which may act as an intermediate carbide through which carbon is transported to the reaction interface. It is obvious however that the comparison is not entirely valid since the ore contained gangue oxides, the influence of which is not well known.

The influence of the formation of slag on the mechanisms and rates of reduction of oxides has not been investigated in great detail.

Urquhart [53] established that the addition of fluxing materials SiO_2) to a charge of Transvaal chromite and char increased the rate of reduction of chromium while the rate of reduction of iron from the ore was unaffected.

Barcza [54] also noted an increase in the rate of reduction of chromium from chromite ore upon adding silica to the mixture. The increased rate was attributed to the simultaneous reduction of chromium and silicon.

However, at temperatures of 1500°C or less Kucukkaragoz [55] found that the addition of silica to pure chromite spinel had a deleterious effect on the carbothermic reduction kinetics.

1.4 Previous Research Relating to the Metallurgical Applications of Mamatwan Manganese Ore

The amount of research that has been carried out on the metallurgical applications of Mamatwan ore is very limited. The thermal behaviour of Mamatwan ore has been investigated by De Villiers [56] who heated samples of the ore between 600 and 1000°C for 1 to 4 hours. The reducibility of Mamatwan ore has been studied by Pentz [2] who heated 5 kg sample to 1000°C in hydrogen and carbon monoxide. The thermal behaviour of the ore was also investigated. Grimsley [3] studied the characteristics, mechanism and rate of reduction of ore fines by solid carbon.

The findings of De Villiers [56] and Pentz [2] relating to the mineralogical changes which take place during heat treatment of the ore in air are summarised below.

i) Dolomite was present in samples heated to 600°C but disappeared at 700°C [56]. A significant loss of mass occurred between 600 and 900°C due to the dissociation of carbonates [2].

ii) Calcite started disappearing at 800°C but appeared sporadically at 900°C [56].

iii) $CaMnO_3$ started to appear at about 800°C [2, 56]

iv) $CaMn_2O_4$ formed at 900°C [56]

v) The spinel $MnFe_2O_4$ (jacobsite) started to form after heating at 900°C for 2 hours.

vi) Braunite decomposed above 900°C and this seemed to correspond to the formation of hausmannite (Mn_3O_4) and silica [56]. Pentz [2] found that braunite started decomposing at 880°C and two phases rich in manganese formed. One of the phases contained lime and the other silica.

De Villiers [56] found that the reactions started on the edges of oolites and carbonate grains to form reaction rims which

progressively increased in size with increased heat treatment. Evidence of fusion could not be found on heating at 1000°C for up to 4 hours.

Pentz [2] eated Mamatwan ore in hydrogen and observed three stages of reduction as follows:

i) A small loss of mass (3,2 per cent) between 400 and 600°C due to reduction of manganese and iron oxides.

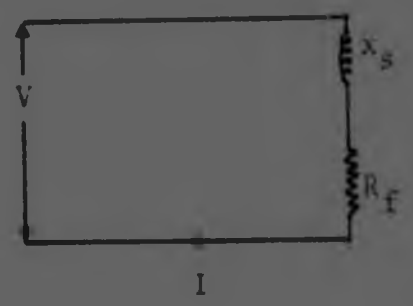
ii) An increased loss of mass between 600 and 800°C due to the dissociation of carbonates.

iii) Further reduction of the ore between 800 and 1000°C.

The findings of Grimsley [3] will not be discussed here as frequent reference has been made to this work.

1.5 Electrical and Thermal Aspects of Submerged-arc Furnace Operation

The electrical network of a submerged-arc furnace in balance can be represented by a simplified one-phase circuit as shown below if the small resistance of the conductors is disregarded [57].



V = voltage
I = current
X_s = system reactance
R_f = furnace resistance.

Figure 1.5 Single-phase circuit representing the electrical network of a submerged-arc furnace.

For this circuit the voltage is given by:

$$V = I \left[R_f^2 + X_s^2\right]^{\frac{1}{2}} \quad . \quad . \quad . \quad 1.33$$

the power factor by:

$$\cos\theta = \frac{R_f}{\left[R_f^2 + X_s^2\right]^{\frac{1}{2}}} \quad . \quad . \quad . \quad 1.34$$

and the effective or smelting power by:

$$P_E = I^2 R_f \quad . \quad . \quad . \quad . \quad 1.35$$

Thus the smelting power is determined by the voltage and the furnace resistance and an increase in R_f leads to an increase in power factor.

The resistance of a furnace is inversely proportional to electrode diameter as given by the Andreae equation [58]

$$R_f = \frac{k}{\pi D} \quad . \quad . \quad . \quad . \quad 1.36$$

where

k is a constant dependent on the charge and
D is the electrode diameter.

The dependence of furnace diameter, D_F, on electrode diameter has been dealt with by Kelly [58] who proposed the relationship

$$D_F = 5,6D \quad . \quad . \quad . \quad . \quad 1.37$$

Thus it is seen that larger furnaces will have a lower resistance and power factor.

The resistance, R_f can be adjusted by lowering or raising the electrodes. However, for a particular process the position of the electrodes is fixed within narrow limits for optimum metallurgical results. Outside these limits the resistance of the furnace has to be adjusted by altering the particle size and/or composition of the charge.

In furnaces used for the production of ferromanganese the electrodes should be kept deep in the charge in order to minimize manganese losses in the form of vapour and to maintain the temperature of the slag and alloy layers at an acceptable level. Losses due to vaporisation of manganese may account for up to 20 per cent [5] of the total manganese charged if good operating conditions are not achieved.

The resistance, R_f, can be expressed as the sum of two resistances in parallel [59]. These are the resistance of the charge, R_c, and the resistance of the reaction zone, R_r. The resistance, R_f, is then given by

$$\frac{1}{R_f} = \frac{1}{R_c} + \frac{1}{R_r} \quad . \quad . \quad . \quad 1.38$$

The contributions made to R_f by R_c and R_r are not known with accuracy for the different processes. It is known [59, 60], however, that the resistance of the reaction zone, R_r dominates R_f. The heat generated in the reaction zone and in the charge will be proportional to their respective resistance. Westly [59] considers that the heat generated in the charge will contribute to the melting of the raw materials which drip into the reaction zone where reduction is completed. If the resistance of the charge becomes comparable with the resistance of the reaction zone then an excessive amount of power will be dissipated in melting the charge and insufficient energy will be left over for reduction.

For optimum metallurgical results there must be a balance between the heat consumed in melting the raw materials and that left for reduction ie there must be a balance between R_c and R_r. Westly [59] defined a heat distribution factor, C, as

$$C = \frac{R_f}{R_c} \quad . \quad . \quad . \quad 1.39$$

The value of C will range from 0 to 1 and will be determined by R_f for a particular charge. Thus an increase in R_f must be followed by a proportional increase in R_c in order to

maintain C constant at its optimum value. In the production of ferromanganese it has been established [59] that short term variations in R_f without varying R_c lead to higher manganese losses in the slag.

From the foregoing it is clear that the resistance of the furnace, R_f, must be as high as possible for high power input and power factor. However, the choice of R_f is governed by the resistance of the charge R_c. Urquhart [53] found that 50 per cent of the power is dissipated from the electrode tip and 25 per cent from the last 300 mm of electrode length. This indicates that the resistance of the charge is much higher than that of the reaction zone and that it decreases significantly as the electrode tip is approached. Andersen's [61] pattern of the interior of furnaces used in the production of pig iron indicates a similar effect.

1.6 The Electrical Properties of Carbonaceous Reducing Agents

The reducing agents used in electrothermic reduction processes have a profound influence on the resistance of the furnace and a great deal of work has been carried out on their electrical properties to establish the factors which determine these properties.

The results of investigations show that each material possesses unique characteristics which are determined by its physical and chemical properties and the heat treatment received. Some useful trends and key values have been established which relate the variations in resistivity with temperature to the chemical properties of the material.

The main factors which influence the resistivity of carbonaceous reducing agents in the granular form are:

a) The temperature of carbonization
b) The volatile matter and ash contents
c) The particle size and
d) The pressure.

The profound influence of carbonization temperature on the resistivity of coal is shown in Figure 1.6 [62]. Measurements of resistivity with increasing temperature for different coals have shown that temperature has a much stronger effect on the resistivity of the 'coke' than the rank or composition of the original coal [62 - 64].

The resistivity of coke increases with increasing residual volatile matter and ash contents [64, 65] and the addition of inorganic substances such as sand has been suggested [66] to increase the resistivity of coke.

It is generally accepted that the resistivity of a bed of reducing agent is mainly determined by the number of contact points, between the particles and consequently the smaller the particle size the greater the resistivity will be. [53, 65, 67 - 72]

The resistivity of a packed bed decreases with increasing pressure due to a decrease in the 'contact resistance' between particles.

The mechanism of electrical conduction by carbonaceous reducing agents has been explained [62, 67, 72] on the basis of the physical and chemical changes which occur during heat treatment.

As the temperature rises a progressive loss of hydrogen atoms from the edges of the polycyclic aromatic structures causes the graphitic crystallites to move closer together and to increase their degree of ordering. As the graphitic crystallites move closer to one another the potential barriers are lowered and electrons can move more freely from one crystallite to the other. This explains why cokes or graphite show little variation in resistivity with temperature while coals show a drastic decrease in resistivity as the temperature increases until at about 900°C the resistivity of coals and cokes becomes virtually the same.

It has been established empirically, [62,68,73] that the

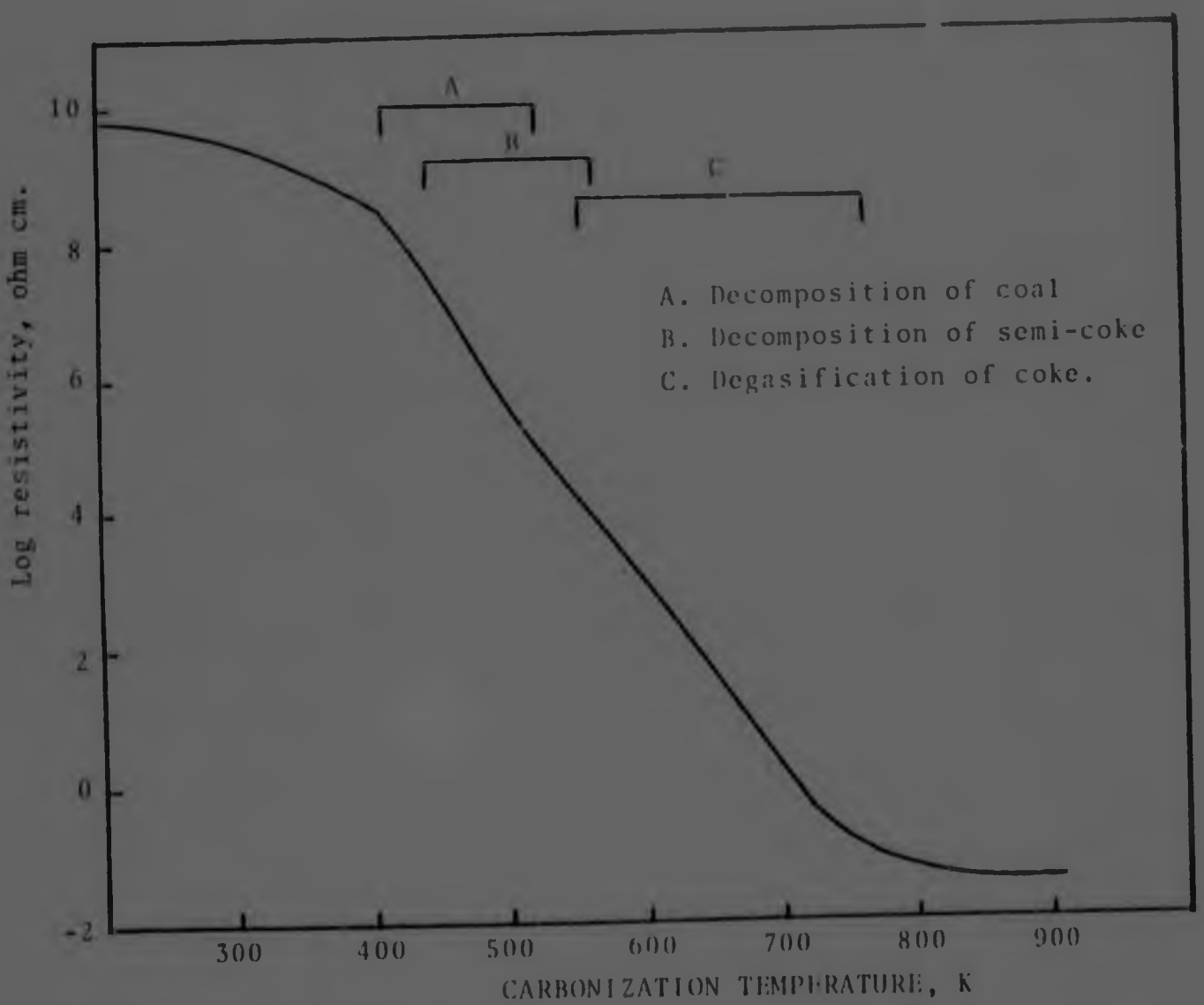


Figure 1.6 The influence of carbonization temperature on the resistivity of coal. (ref. 62).

resistivity (ρ) of a burden component or mixtures of burden components is related to temperature by the Arrhenius-type relationship:

$$\rho = Ae^{B/I} \quad . \quad . \quad . \quad . \quad 1.40$$

where A and B are constants and
I is the absolute temperature.

The values of A and B can vary in different temperature ranges. The activation energy for conduction (B) is a measure of the energy barrier through which electrons must be thermally excited before they become conducting ons. The value of the activation energy decreases with increasing temperature because the energy barrier becomes smaller. For a coal the width of the energy barrier drops from about 13,5Å at 80 per cent carbon content to 0Å at 100 per cent carbon content [74].

1.7 The Electrical Properties of Ores

The electrical properties of ores have not been studied to the same extent as those of reducing agents probably because in the past the resistivity of a furnace burden was considered to be predominantly dependent on the resistivity of the reducing agent and the molten slag. However, the electrical properties of the ore cannot be overlooked since the physical and chemical changes in the ore, particularly at high temperatures, can have a dramatic effect on its resistivity.

The main factors which influence the resistivity of a packed bed of ore at a given temperature are:

a) The particle size of the ore
b) The semiconduction characteristics of the ore
c) The oxygen content of the oxides in the ore
d) The distribution of the oxides in the ore
e) The amount, composition and distribution of the gangue minerals.
f) The pressure on the packed bed.

The influence of particle size on the resistivity of an ore has not been investigated in great detail. It has been established [70, 71] however, that the resistivity decreases as the particle size is increased.

The semiconduction characteristics of different ores have been shown to exert a dramatic influence on their resistivity. The resistivity of chromites [53, 75] decreases by several orders of magnitude by heating up to temperatures of 500°C. Rennie [71] noted an exponential decrease, between 500 and 600°C, in the resistance of a titaniferrous iron ore and attributed this to improved semi-conduction. Some investigators [76, 77], found that small amounts of impurities in an oxide can have a significant effect on its resistivity.

The effect of oxygen content and of doping on the resistivity of iron ores is shown in Figure 1.7 [67]. It is clear that the higher the proportion of oxygen in the ore the higher is its resistivity. The results of Rennie [71] and Silveira [68] on the resistivity of iron ores in different oxidation states are in general agreement with those shown in Figure 1.7.

The distribution of the metal oxides and the amount, composition and distribution of the gangue are interrelated [67]. If the proportion of gangue and its mode of occurrence are such that it forms a continuous network within the ore, the resistivity will be governed by that of the gangue. Fusion of the gangue at relatively low temperatures could have a profound influence on the resistivity of the ore.

The application of pressure on a packed bed of iron ore has been shown [71] to reduce the resistance although its effect is not as pronounced as that of the oxidation state of the ore.

Published work on the electrical properties of manganese ores is scarce. Silveira [75] found that during heating, the resistance of a manganese ore decreased up to 600°C, increased between 600 and 800°C and decreased again at

KEY TO FIGURE 1.7

a) Mill scale
b) Kiruna 'E' ore (53,2% Fe_2O_3, 24,9% FeO).
c) Itabira ore (96,2% Fe_2O_3)
d) Limonite-Ljubija 'B' (75,8% Fe_2O_3)
e) Frictal ore (54,7% Fe_2O_3)
f) Magnetite
g) Hematite
g') Hematite doped with 0,30 atom percent Ca^{2+}.

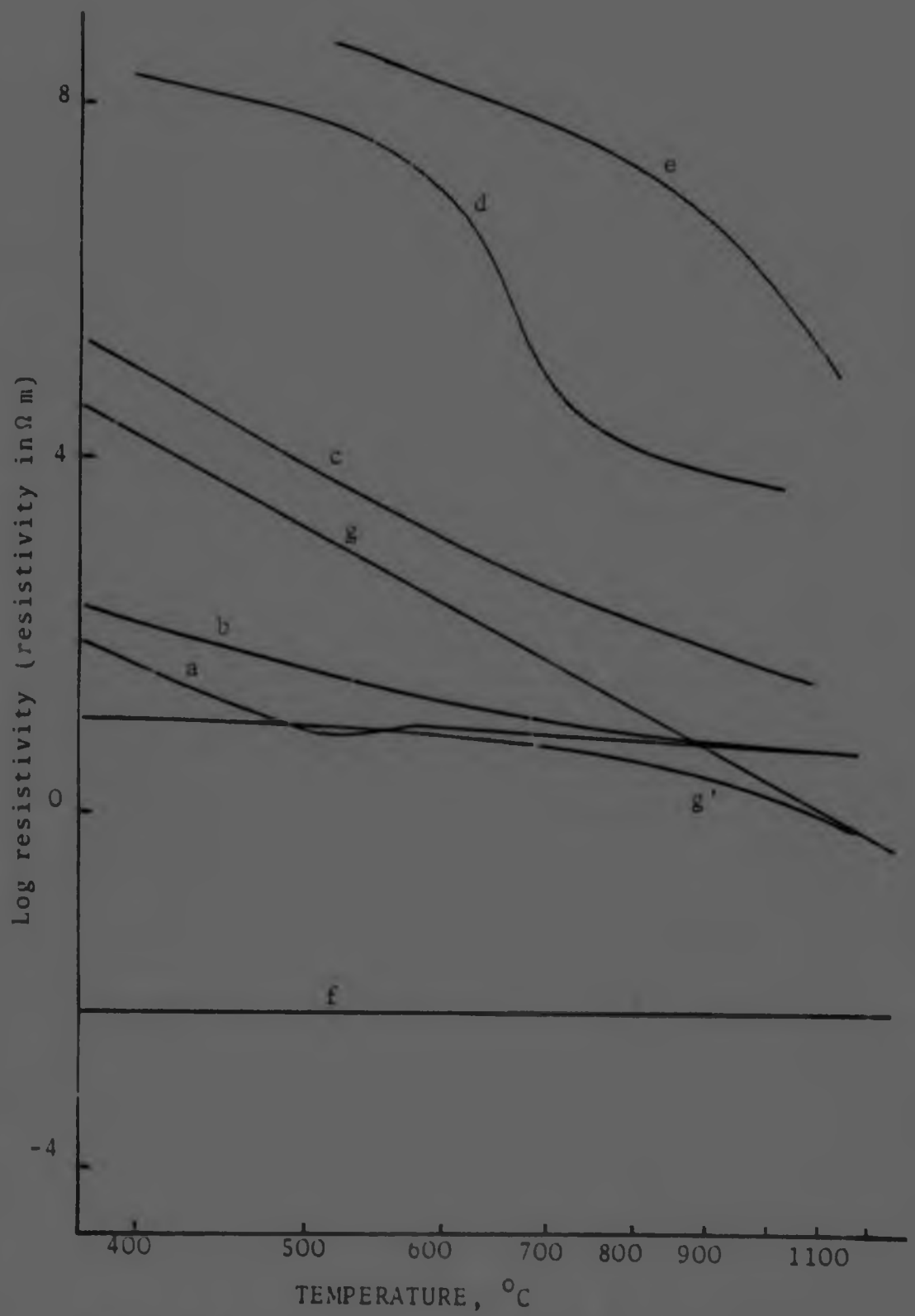


Figure 1.7 Resistivity as a function of temperature for iron ores or materials containing iron oxides (ref.67).

higher temperatures.

The dependence of the resistivity of ores on temperature can be described approximately by the Arrhenius type relationship of equation 1.38.

1.8 The Electrical Properties of Furnace Burdens

For convenience, the interior of a submerged-arc furnace may be divided into an upper region with a hign resistance and a lower region with a much lower resistance. The upper region may be assumed to consist of the burden from stock-line level down to the smelting zone, while the lower region occupies the rest of the furnace volume.

In the upper region the burden consists of a mixture of ore and reducing agent and it will be assumed here that the resistivity of the reducing agent is much lower than that of the ore. In this region, reduction, sintering and slag formation occur to a limited extent and the resistivity of the burden is mainly determined by the following factors:-

a) The particle size of the components.
b) The proportion by volume of ore and reducing agent.
c) The type of reducing agent.

Several authors [70, 71, 78] have found that a reduction in the particle size of either the ore or the reducing agent results in increased burden resistivity. However, recent work by Dijs [64] has shown that the resistivity of the burden is a function of the relative sizes of the ore and the reducing agent. Dijs found that the resistivity of the burden will decrease to a minimum with increasing particle size of the reducing agent and increase again with a further increase in the size of the reducing agent. The variations in the resistivity of the mixture with varying particle size of the reducing agent become less pronounced as the particle size of the ore is increased (Figure 1.8).

The resistivity of mixtures of two components, one of which is a conductor (reducing agent) and the other an

d_i = mean size of quartz, cm

volume fraction quartz = 0,5.

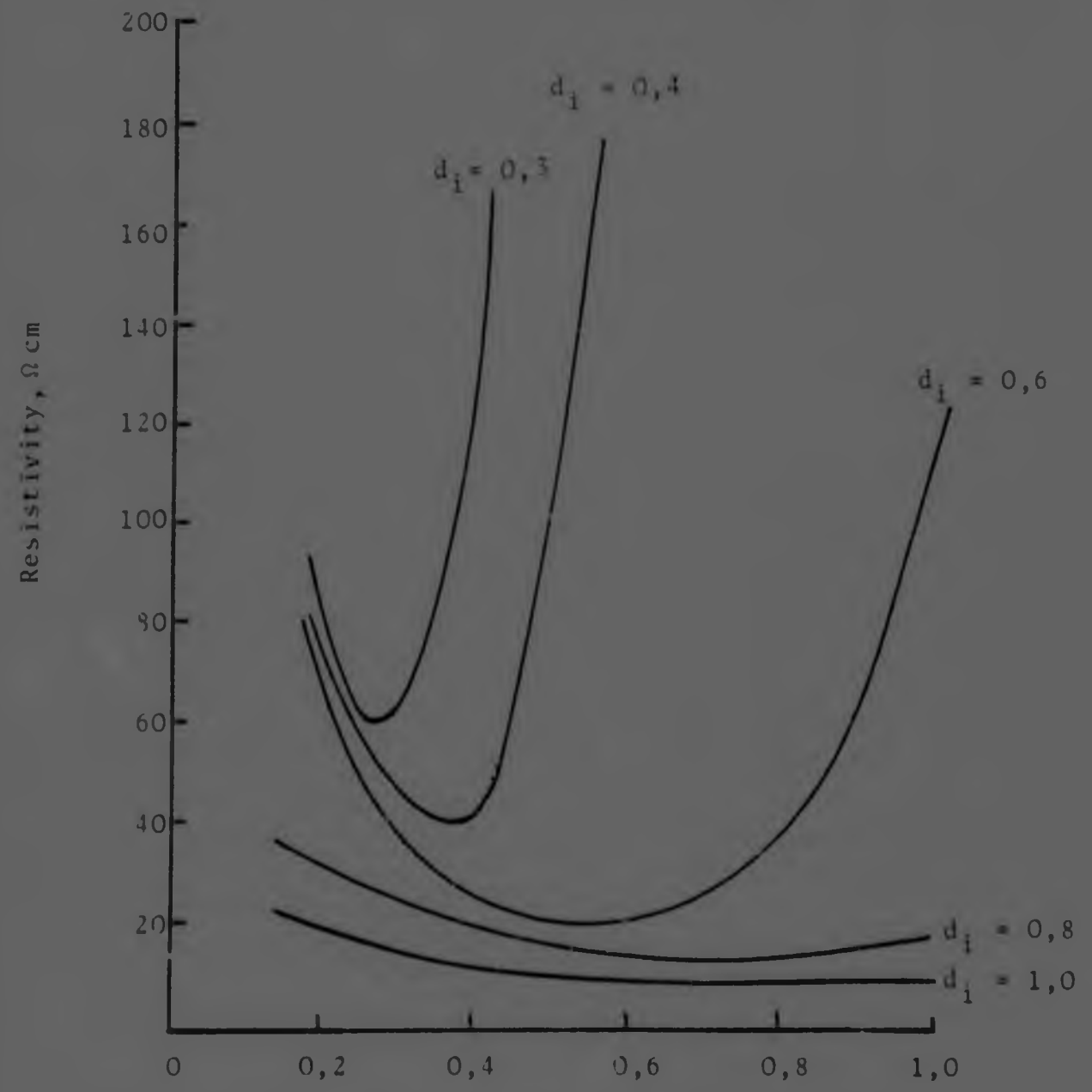


Figure 1.8 The influence of char particle size on the resistivity of mixtures of char and quartz, for various particle sizes of quartz. (ref. 64).

insulator (ore), drops abruptly [70, 75, 80] at a specific proportion by volume of conductor to insulator. This is due to the formation of continuous current paths by the conducting particles in the mixtures.

Buecke [80] considered a mixture of identical spheres and showed that the critical concentration of conducting spheres varie considerably with the type of lattice formed and the extent to which the lattice is filled. The situation becomes even more complex when actual systems are considered. Willand [70] found that the resistance of a mixture of chromite and charcoal increased steeply when the volume fraction of chromite exceeded 35 per cent (Figure 1.9). It is obvious however, that these proportions can change drastically with changes in the relative sizes of the two components. For instance, if the particle size of the ore is much greater than that of the reducing agent then the volume fraction of reducing agent necessary for the formation of continuous current paths will be reduced.

The influence of the type of reducing agent on burden resistivity has been studied by several investigators [64,70,71,75,81] who found that, at low temperatures, the resistivity of mixtures of ore and coal is higher than that of mixtures of ore and coke. At high temperatures (1200-1400°C) the resistance of burdens containing the same ore but different reducing agents is the same [64,70, 71]. This is partly due to the fact that the resistivities of coal and coke are the same at high temperatures and partly due to reduction reactions and slag formation. The latter effect reduces the influence of the particle size of the ore on the resistivity since Downing and Urban [69] found that molten slag and coke have comparable resistivities.

The conditions that prevail in the lower region of submerged-arc furnaces are not well known. It is known however [53,82] that most of the power supplied to the furnace is dissipated from the electrode tip to the molten bath underneath it. In the general case this bath can be assumed to be a mixture of molten slag and solid reducing agent, in

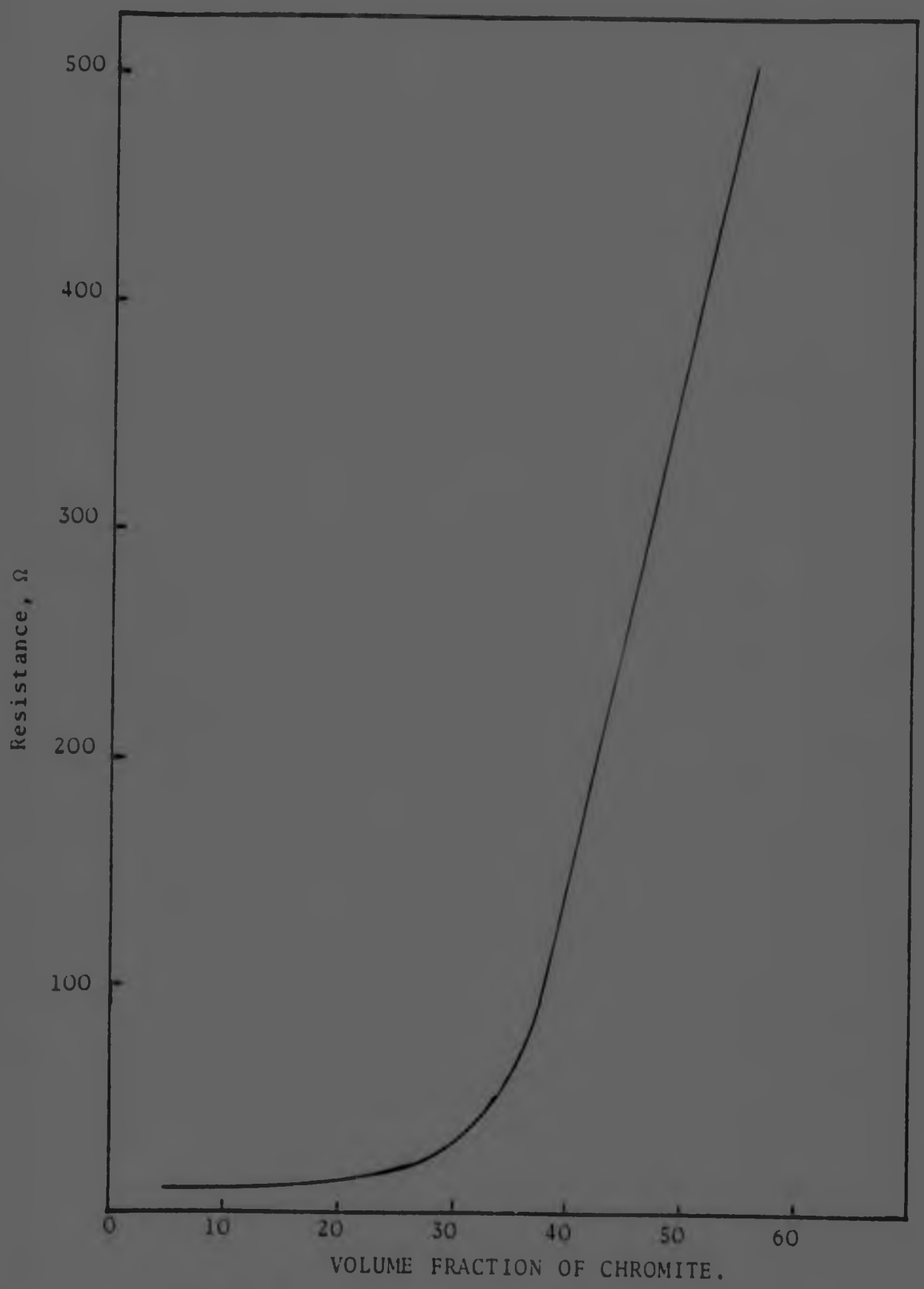


Figure 1.9 The influence of volume fraction of chromite ore on the resistance of a mixture of ore and char (ref.70).

a state of intense agitation due to reduction and evolution of gaseous products.

Investigators who studied the electrical properites of furnace burdens have generally concentrated on the properties of the solid burden or of burdens in which some slag formation occurred. Very few attempts have been made to simulate the conditions underneath the electrode tip [64, 82, 83]. Dijs [64] simulated this furnace region by using mixtures of brine and reducing agents. From basic considerations and by regarding the two phases in the mixture as resistances in parallel Dijs [64] derived the relationship

$$\frac{1}{\rho_m} = \frac{1}{\rho_r} + \frac{1-f}{\rho_s} \quad . \quad . \quad . \quad . \quad 1.41$$

where ρ_m is the resistivity of the mixture
ρ_r is the resistivity of the reducing agent
ρ_s is the resistivity of the solution and
f is the volume fraction occupied by the reductant.

Dijs [64] obtained reasonable agreement between experimental and calculated results, although it is difficult to assess the extent to which the results apply to industrial furnaces.

1.9 The Distribution of Zones in Submerged-arc Furnaces

Modern furnaces used for the production of ferroalloys consist of a cylindrical steel shell lined with refractory brick and carbon paste or blocks on the inside. Three electrodes of the Soderberg type are positioned in the furnace crucible at the vertices of an equilateral triangle and supply the energy required for the process. Carbonaceous reducing agents are used mainly to carry out the reduction of the ore.

The production of alloys of ferromanganese, ferrochromium and pig-iron is accompanied by the formation of substantial volumes of slag. In these processes the position and extent of the different phases and zones are determined by the

position and extent of the reaction zone near the electrode tip. The internal structure of different furnaces shows many similarities.

The work that has been carried out to investigate the internal structures of furnaces is very limited particularly in the case of furnaces for the production of ferromanganese. A good understanding of the processes occurring in submerged-arc furnaces and of the influence of the various zones on furnace operation is necessary for process control and optimization. Research dealing with the physical and chemical changes of the burden during its descent in the furnace is scarce, and the various zones that form have not been investigated or defined adequately for most processes. Usually five zones may be distinguished:

a) The burden zone.
This zone is situated at the top of the furnace where the higher oxides in the ore are reduced by CO to a lower oxidation state.

b) The smelting zone
This zone forms near the electrode tips and consists of a mixture of solid and fused material.

c) The coke bed
This zone consists of lumps of coke or of a mixture of coke and slag and can exist directly underneath the electrodes in the shape of a cone [81, 82], or as a layer between the burden zone and the smelting zone [84, 85] or between the molten bath and the smelting zone [86-89].

d) The molten bath
This zone includes the layers of molten alloy and slag in the furnace hearth.

e) The dead zone
This zone consists of accretions or stagnant burden which adheres to the furnace wall.

The zones beneath the electrode tip of a 150kVA, single-phase pilot furnace for the production of pig-iron have been investigated by Muller [82]. The furnace electrode was hollow to allow additional coke to be fed to the reaction zone to ensure that the electrode was riding on top of the coke bed at all times. Muller found that the coke bed had a conical shape and was symmetrical about the vertical axis of the electrode. The interstices between coke particles in the lower part of the coke bed were filled with molten slag. The shape and size of the coke bed and the temperature of the process varied with electrode position which determined the resistance of the furnace. A deep electrode position decreased the furnace resistance and resulted in a shallow but broad coke bed and a high process temperature.

Andersen [61] presented a pattern for the interior of an industrial pig-iron furnace (Figure 1.10) based on observations made during 'dig outs' of furnaces taken out of operation and on temperature measurements made during operation. The subject is treated qualitatively and full advantage of the 'dig outs' does not appear to have been taken.

Other investigators studied the internal structure of ferrochromium [89] and silicomanganese [84, 85] furnaces by freezing and sectioning experimental furnaces. The patterns presented by the different authors show many similarities although the patterns found in experimental furnaces [85, 89] are much more complex than those presented for industrial furnaces [61, 88]. The internal structure of an experimental furnace for high-carbon ferrochromium [89] is shown in Figure 1.11. It can be seen that the coke bed consists of a thin layer of coke particles between the molten slag and the unreacted burden.

The pattern of lining erosion and the internal structure of a 19 MVA furnace for high-carbon ferromanganese were investigated by Ozeki et al [88]. The contents of the furnace were removed after blasting and detailed observations of the furnace interior were not made. The authors however,

Figure 1.10

A. Coke bed.
B. Slag bath penetrating the lower part of the coke bed.
C. Metal bath.
D. Highest temperature zone (2000-3000^{o}C)
E. Pre-reduction and smelting zone
F. Preheating zone
G. Solidified slag
H. Sponge iron.

Figure 1.11

1. Charge layer
2. Electrodes
3. Coke Bed
4. Cavity
5. Slag layer
6. Layer of unmolten ore
7. Layer of molten ore
8. Metal pool
9. Residual metal
10. Tap hole
11. Alumina balls.

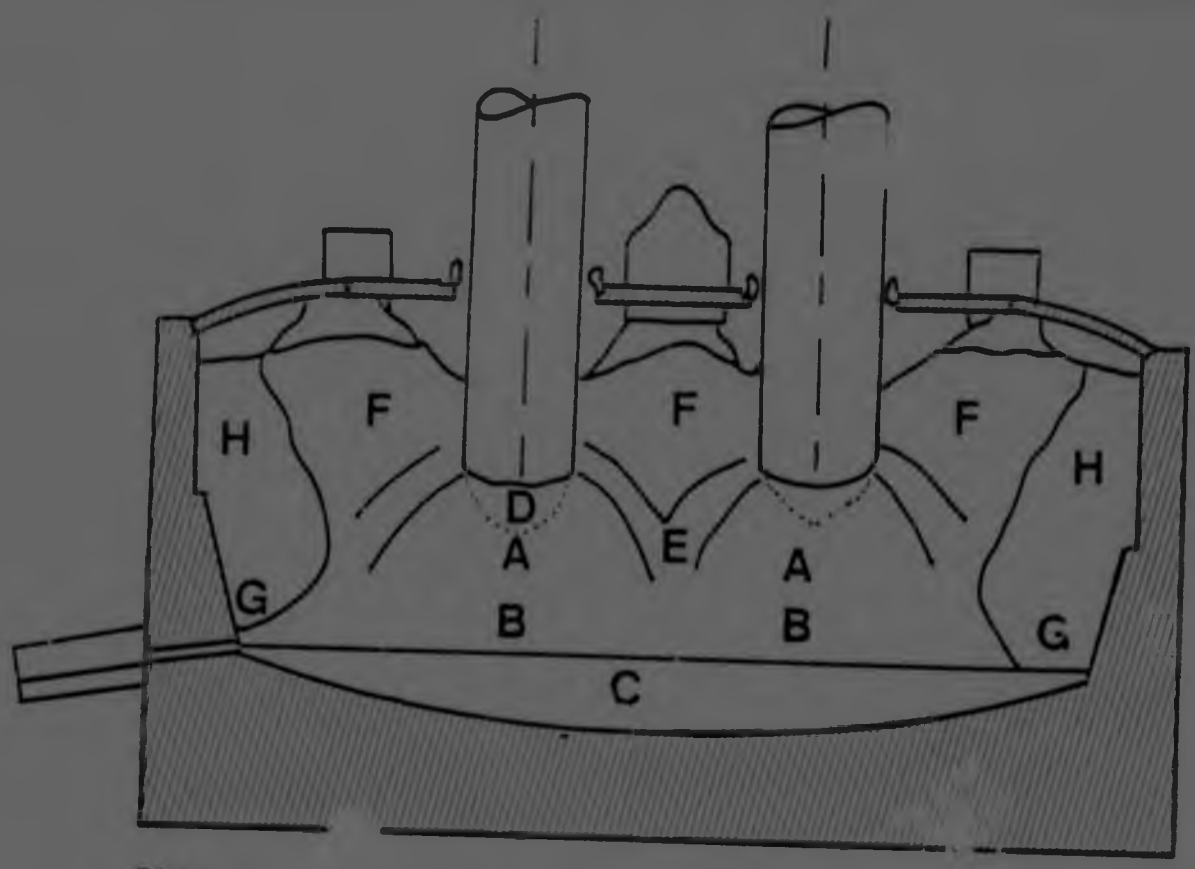


Figure 1.10 Principal pattern of the metallurgical structure of the interior of an electric pig-iron furnace (ref.61)

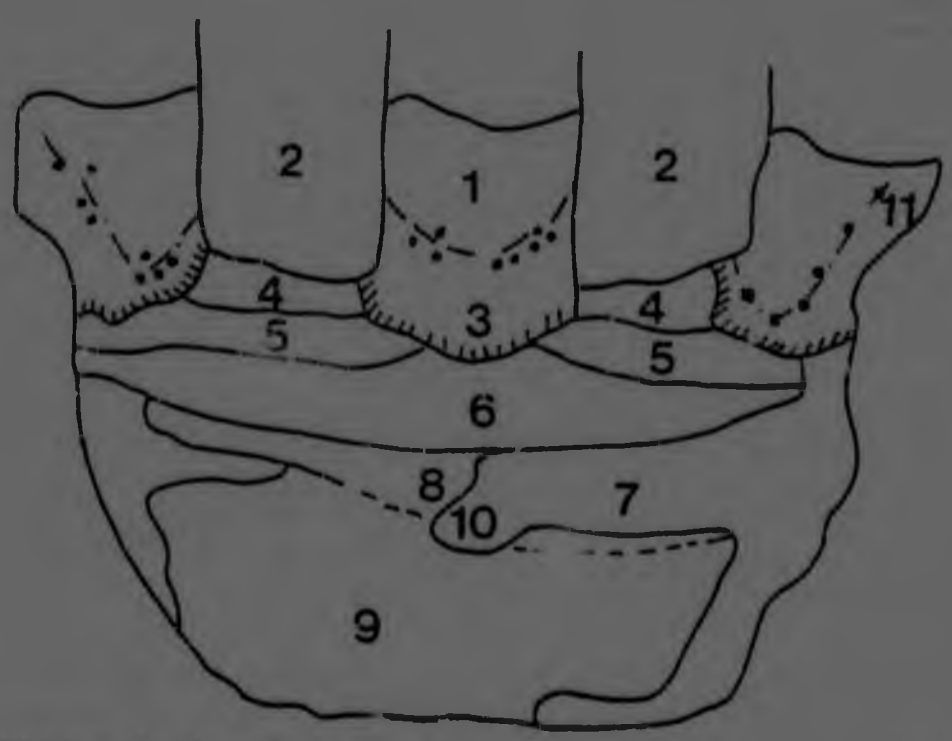


Figure 1.11 Cross section of an experimental two-phase ferrochromium furnace (ref.89).

constructed a simplified pattern of the furnace interior from information gained from a number of furnace sections which were studied in connection with lining erosion. This basic pattern, which is similar to that proposed by Dancoisne [86] is shown in Figure 1.12. The authors observed unexpectedly high erosion of the hearth and crust formation on the furnace walls, particularly between electrodes and in positions remote from the metal and slag tap holes. Segregation of coke towards the furnace walls resulted in a coke bed 1 m thick at the wall and 0,3 to 0,5 m thick in the centre.

Some of the zones in submerged-arc furnaces, especially the coke bed, may not be a permanent feature of the process, as their presence and extent is determined by the properties of the burden and the operating conditions. For instance, a decrease in the reactivity of the reducing agent or an increase in its size will result in an increase of the size of the coke bed. Volkert [87] has demonstrated that the resistivity of the burden has a strong influence on the size and geometry of the different zones. Thus a burden of lower resistivity results in a larger reaction zone because the electrodes have to be raised in order to obtain a high furnace resistance and power input. This is precisely the position with ferromanganese furnaces which can be operated with a partial 'dead zone' in the centre due to the low process temperature and the high electrical and thermal conductivities of the charge [90]. These properties of the charge would result in a proportionately larger reaction zone in comparison with a ferrochromium furnace in which the energy is concentrated in a relatively small volume below the electrode tips.

1.10 Conclusions

The large reserves of manganese ores and coal in the Republic of South Africa place the country in a highly competitive position in the field of ferromanganese production. The recent developments in submerged-arc electric smelting of manganese ores indicate that this practice will continue in the foreseeable future.

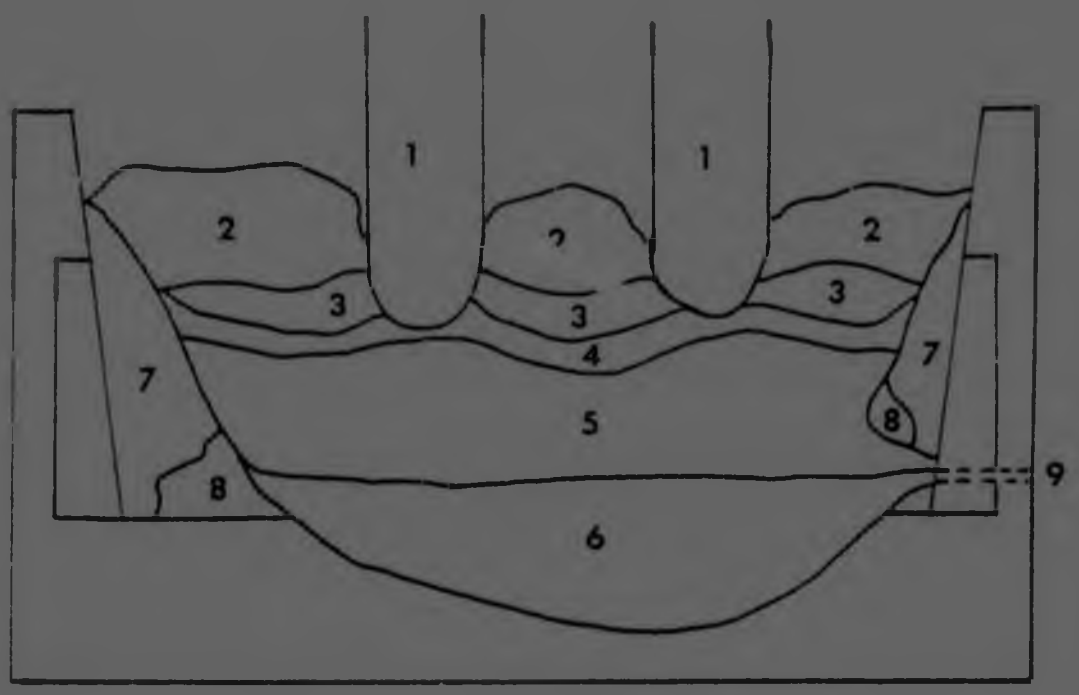


Figure 1.12 The basic structure of a submerged-arc furnace for the production of high-carbon ferromanganese (ref.88)

KEY

1. Electrode
2. Burden zone
3. Smelting zone
4. Coke bed
5. Molten slag
6. Alloy layer penetrating the furnace lining
7. Dead zone
8. Fused material.
9. Metal tap-hole.

The low-shaft blast furnace may be a feasible alternative to the submerged-arc furnace for the smelting of Mamatwan manganese ore. However, it will probably take several years and a considerable amount of research before this unit is able to compete with the submerged-arc furnace in terms of production.

The vast increase in the size of modern submerged-arc furnaces has resulted in lower furnace resistance and higher furnace sensitivity to changes in burden quality. Therefore, the attainment of stable operating conditions has become more difficult. The optimization of operating conditions can only be achieved through a deep understanding of the processes that take place in the furnace. These processes include the following:

1. The variations in the resistivity of the burden as it descends the furnace bowl.

2. The physicochemical changes that occur in the burden components at different positions inside the furnace.

3. The mechanisms of reduction of the oxides.

4. The segregation of components in a furnace.

5. The distribution of the different zones in a furnace.

Some of the above processes have already been examined to a greater or lesser extent. However, the experimental conditions used were such that it is difficult to determine the extent to which the results represent actual furnace conditions.

CHAPTER 2

2.0 EXPERIMENTAL

2.1 Choice of Experimental Technique

The conditions that prevail in a submerged-arc furnace are very complex and can be treated quantitatively only by the making of simplifications and assumptions that create doubts about the validity of the results. Hence, the design of laboratory tests that give results adequately related to the activity in industrial furnaces is very difficult.

Some investigators have frozen and sectioned experimental furnaces in order to study the processes that take place in furnaces used for the production of ferrochromium [89] and silicomanganese [84,85]. Although this technique supplied considerable information on the internal structure and the reactions occurring in these two types of furnace its use is limited by the scale and cost of the experiments.

The reduction of ores has generally been studied by use of reactants in a fine state of comminution. Studies of this nature have given valuable information with regard to the reduction characteristics of ores, mechanisms of reduction and reactivities of the reducing agents. However, the results of these investigations cannot be readily used to assess the processes that take place in industrial units.

Klemantaski[91], suggested the use of the "stationary charge in controlled environment" (SCICE) technique for the investigation of processes that occur in the stack of an iron blast furnace. This technique eliminates the arbitrary choice of experimental variables and has been used successfully[92] to investigate the processes that occur in the stack of a blast furnace.

The theory and uses of the SCICE technique have been given by Klemantaski[91] and other investigators[92,93]. Conditions in the stack of an iron blast furnace can be simulated without movement of the charge, the retention time and inlet gas composition being varied rather than the position of the charge. However, a knowledge of the rate of descent of the charge and the temperature variations experienced by it during its descent in the furnace stack are required. The SCICE technique is ideally suited to studies of the gaseous reduction of iron ores at relatively low temperatures (up to about 1100°C).

The SCICE technique as such cannot be used to investigate the reduction of manganese ore to metal owing to the high temperature[94] (>1280°C) required for the reduction of manganous oxide by carbon. At this temperature an appreciable amount of slag forms and the carbon monoxide permeability of the ore is reduced.

A variation of the SCICE technique was used by Urquhart[55] in a study of the production of high-carbon ferrochromium in a submerged-arc furnace. Since the rate of descent of the burden and the temperature profiles in submerged-arc furnaces are not well known, Urquhart heated the charge at a controlled rate of 400°C per hour to a predetermined temperature, maintained the temperature for a time, and then allowed the charge to cool.

Early work by Pentz[2] on the gaseous reduction of Mamatwan ore and later by Grimsley[3] and Dewar and See[95], who investigated the reduction characteristics of this ore at relatively low temperatures by a variety of carbonaceous reducing agents, indicated a lack of knowledge of the processes that occur in the hotter regions of ferromanganese furnaces when Mamatwan ore is treated with different reducing agents.

Since the rate of descent of the charge and the temperature profiles in ferromanganese furnaces are not well known, it was decided that the technique and heating rate in the work described here should be similar to those used by Urquhart[53]. The mass of the experimental charge, its composition and its particle size were such that an attempt could be made to simulate the conditions in the upper regions of a submerged-arc furnace.

2.1.1 Critical Appraisal of the Experimental Technique

The SCICE technique was used in an attempt to follow the processes occurring in an element of furnace burden as it descends the furnace bowl. Obviously, there are differences in the conditions experienced by the experimental charge and an element of furnace burden. In order to assess the extent to which the experimental technique simulates the conditions in an industrial furnace it is necessary to analyse the differences between the experimental conditions and the conditions that probably attain in a furnace.

The zones of greatest importance in a submerged-arc furnace are those around, and directly underneath the electrode as indicated in Figure 2.1(a). The zones further away from the electrode are partially or completely stagnant [61] and are practically impervious to gases due to sintering and decrepitation of the burden. The depth of penetration of the electrode below stockline level in a 48MVA furnace is on average about 3m.

Probable heating curves, for an element of furnace burden descending in the cone of fast moving material around the electrode of a 48MVA furnace, are shown in Figure 2.1(b). The experimental heating rate ($350^{o}C$ per hour) and holding temperatures are superimposed for comparison. It is obvious that a lower experimental heating rate would have been closer to furnace conditions but this would have

Since the rate of descent of the charge and the temperature profiles in ferromanganese furnaces are not well known, it was decided that the technique and heating rate in the work described here should be similar to those used by Urquhart[53]. The mass of the experimental charge, its composition and its particle size were such that an attempt could be made to simulate the conditions in the upper regions of a submerged-arc furnace.

2.1.1 Critical Appraisal of the Experimental Technique

The SCICE technique was used in an attempt to follow the processes occurring in an element of furnace burden as it descends the furnace bowl. Obviously, there are differences in the conditions experienced by the experimental charge and an element of furnace burden. In order to assess the extent to which the experimental technique simulates the conditions in an industrial furnace it is necessary to analyse the differences between the experimental conditions and the conditions that probably attain in a furnace.

The zones of greatest importance in a submerged-arc furnace are those around, and directly underneath the electrode as indicated in Figure 2.1(a). The zones further away from the electrode are partially or completely stagnant [61] and are practically impervious to gases due to sintering and decrepitation of the burden. The depth of penetration of the electrode below stockline level in a 48MVA furnace is on average about 3m.

Probable heating curves, for an element of furnace burden descending in the cone of fast moving material around the electrode of a 48MVA furnace, are shown in Figure 2.1(b). The experimental heating rate (350^{o}C per hour) and holding temperatures are superimposed for comparison. It is obvious that a lower experimental heating rate would have been closer to furnace conditions but this would have

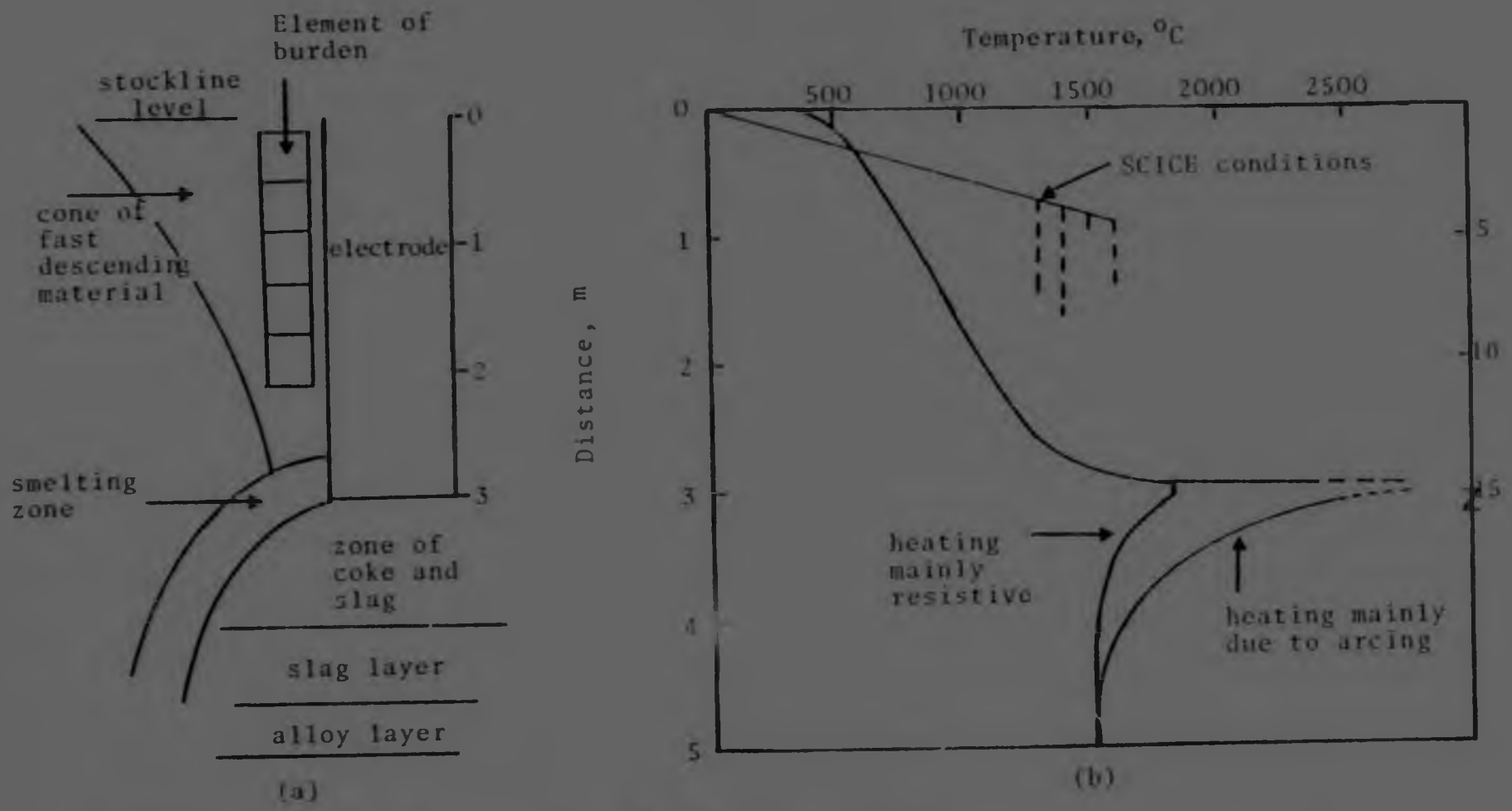


Figure 2.1 a) The zones near the electrode of a submerged-arc furnace and

b) probable heating curves for an element of furnace burden descending near the electrode. The heating conditions for the SCICE charges are superimposed for comparison.

resulted in unduly long experiments. On the other hand the influence of retention time on the degree of reduction of lumpy ore, at temperatures below about 1300°C is very limited. Therefore, the SCICE technique, as used in this work, should give results that would closely resemble the processes taking place near the electrode of the furnace, from stockline level to a few centimetres above the electrode tip.

The heating curves suggested in Figure 2.1(b) were constructed from observations made during furnace 'dig outs'[13,61], measurements of the mean residence time distributions of the charge in a 48MVA furnace[14], calculations of power dissipation from different parts of the electrode [53], studies of the modes of current transfer in furnaces[82,96,97] and from a knowledge of the tapping temperatures of high-carbon ferromanganese and 'discard' slag. Dyason[14] showed that in a 48MVA furnace, an element of charge, placed near the electrode takes about 15 hours to descend from slockline level to the tip of the electrode where fast reduction occurs.

The heating rate of an element of furnace burden is slow until it gets close to the tip of the electrode. Under conditions of mainly resistive heating, the temperature in the coke-enriched zone Figure 2.1(a) is probably of the order of 1800°C. With the formation of long arcs, the temperature in this zone probably increases to between 2500 and 3000°C. At these temperatures, both the slag and the manganous oxide would melt and rapid reduction would take place, accompanied by rapid evolution of gaseous reduction products and boiling of the molten material. The temperature decreases with increasing distance from the electrode tip and reaches about 1450°C in the alloy layer.

The above considerations show that the experimental conditions might be considered to resemble the conditions in a furnace between stockline level and the electrode tips and in regions at some distance from the electrode tips.

2.2 Materials and the Preparation of SCICE Charges

The materials used in this investigation were Mamatwan manganese ore, Iscor metallurgical coke and Delmas coal which were supplied by the Metalloys plant of Samancor at Meyerton in October 1975.

The materials were crushed and screened, and the size ranges retained for the SCICE experiments were 2,83 to 12,7 mm for the ore and 2,83 to 6,35 mm for the reducing agents. After crushing and screening, representative samples of each material were obtained by riffling.

Tables 2.1 and 2.2 give details of the proximate and ash analyses of the coarse fraction of Iscor coke and Delmas coal and of the analysis of Mamatwan ore. The fine fractions were also sampled and analysed to establish whether crushing and screening caused the segregation of any constituents. The fine and coarse fractions of the ore and the coke showed no significant differences in composition. The amount of volatile matter in the coarse fraction of the coal was lower than that in the fine fraction by 6,5 per cent, and the fixed carbon content higher by 4,7 per cent. It may be noted that 57 per cent of the coal was less than 2,83 mm in size.

The SCICE charges were made up of ore and reducing agent in stoichiometric proportions. (Stoichiometric carbon is defined as the amount of carbon required to reduce all the oxides of manganese and iron in the ore to the

TABLE 2.1

Proximate and ash analyses of the reducing agents*

CONSTITUENT		DELMAS COAL Mass %	ISCOR COKE Mass %
Fixed carbon		48,55	79,07
Volatiles		28,33	2,75
Ash		15,65	15,98
Moisture		6,11	1,28
Sulphur		1,20	0,20
Phosphorus		0,15	0,20
Ash Analysis	MgO	2,79	1,19
	Al_2O_3	26,38	30,05
	SiO_2	43,38	50,58
	CaO	7,87	4,37
	Mn_2O_3	0,95	0,40
	Fe_2O_3	7,74	7,37
	S	2,48	0,35

* All chemical analyses were carried out by The National Institute for Metallurgy

TABLE 2.

The chemical composition of Mamatwan ore

CONSTITUENT	MASS %
MgO	3,10
Al_2O_3	0,10
SiO_2	4,27
CaO	12,96
Mn_2O_3	55,93*
Fe_2O_3	5,99**
Cr_2O_3	0,36
P_2O_5	0,17
K_2O	0,21
CO_2	14,91
H_2O	0,54

* This is the total manganese content of the ore expressed as Mn_2O_3

** Total iron expressed as Fe_2O_3

respective metals,. A charge of ore and coal consisted of 960g of coal and 3040g of ore, while a charge of ore and coke consisted of 600g of coke and 3400g of ore. Fluxing materials were not added because it was desirable for the system to be as simple as possible and because Mamatwan ore is largely self-fluxing .

The ore and the reducing agent were mixed on a plastic sheet and transferred to a tray in which they formed a bed about 30 mm deep. From the tray the mixture was transferred in small batches to the crucible, which had been placed in the furnace. This method of charging was followed in order to minimize segregation. It was found that segregation could not be eliminated entirely due to differences in size and specific gravity between the ore and the reducing agents. During charging, a metal rod 3 mm in diameter was used to compress the charge and to avoid bridging and the formation of large voids.

2.3 Apparatus and Procedure

2.3.1 SCICE Experiments

The SCICE experiments that were carried out are listed in Table 2.3. The charge was contained in a graphite crucible of 150 mm internal diameter and 515 mm depth which acted as a susceptor when heated in a 40kW, 3kHz induction furnace. The crucible assembly is shown in Figure 2.2. The crucible was divided horizontally into a re-usable top and bottom.

The central graphite electrode was used for resistivity measurements which are reported at a later stage.

Two Pt-6%Rh/Pt-30%Rh thermocouples were used to measure the temperature, one positioned in the centre of the charge and the other 15 mm from the crucible wall. The central thermocouple was lowered down the electrode and the outer one into a graphite sheath of 10 mm inside diameter and

TABLE 2.3.

Details of the SCICE experiments

Heating rate		350°C/h
Particle size:	Ore	2,83-12,7 mm
	Reducing agent	2,83-6,35 mm

Temperature °C	Retention time at temperature h			
Iscor coke				
1300	0	1	2	-
1400	0	1	2	4
1500	0	-	-	-
1600	0	1	2	-
Delmas coal				
1400	0	-	2	4
1600	0	1	2	-

- No experiments conducted under these conditions.

KEY TO FIGURE 2.2

a graphite electrode
b electrode-centering device
c brass electrode
d asbestos cover
e water-cooled furnace top
f graphite lid
g aluminous-porcelain sheath
h graphite crucible
i alumina tube
j lagging of ceramic fibre
k silica tube
charge
m conducting part of electrode
n alumina bubbles
p water-cooled furnace base
q graphite sheath
r induction coil

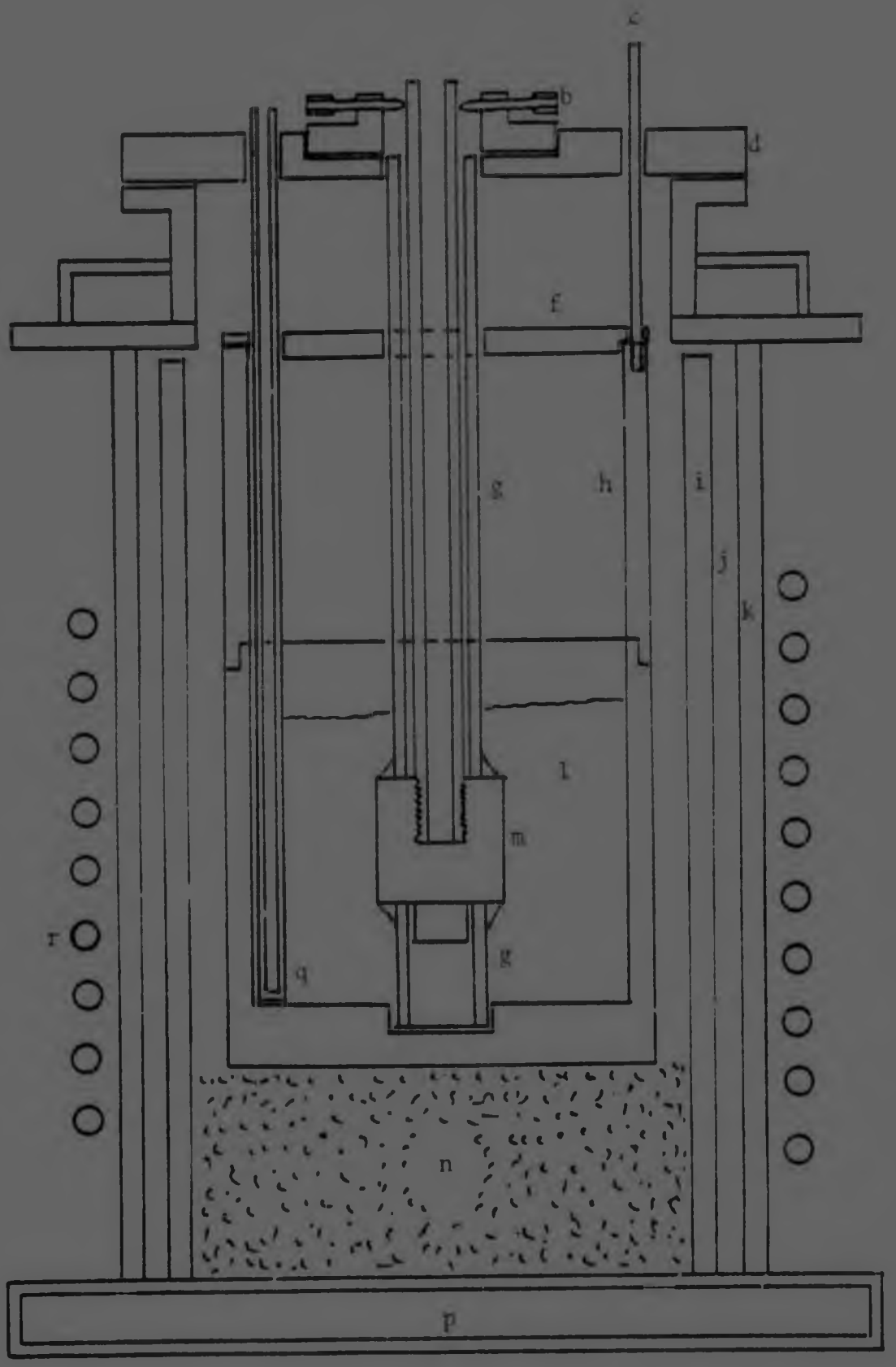


Figure 2.2 Schematic section of the SCICE apparatus

14 mm outside diameter. The outer thermocouple was used for temperature control, and all the temperatures quoted in this work refer to measurements made by use of this thermocouple, unless otherwise stated. All the temperature measurements were made with the thermocouple junctions 60 mm above the bottom of the crucible.

During the heating of a charge of ore and coke, there was a small temperature difference between the inner and the outer thermocouples at low temperatures, and this difference increased to about 140°C for temperatures between 400 and about 1000°C. The temperature difference decreased above 1000°C and was about 100° at 1200°C. Heating curves obtained during the heating of a charge of ore and coke are shown in Figure 2.3.

During the heating of a charge of ore and coal, there was a temperature difference of 140°C between the centre and the edge of the charge for temperatures up to 850°C. The difference increased between 850 and 900°C, and decreased above 1000°C. The temperature difference between the centre and the edge of the charge decreased to about 80°C for temperatures higher than 1200°C.

Similar cooling curves were obtained for comparably treated charges of ore and coke and of ore and coal. There was no significant temperature difference during cooling between the edge and the centre of the charge. Cooling curves for charges of ore and coal that were heated to 1400 and 1600°C are shown in Figure 2.4

The heating rate was controlled manually according to the temperature of the charge measured next to the crucible wall. The power imput was adjusted to maintain a heating rate of 350°C per hour. The temperature of the charge was controlled to within ± 5,5°C during retention at constant temperature.

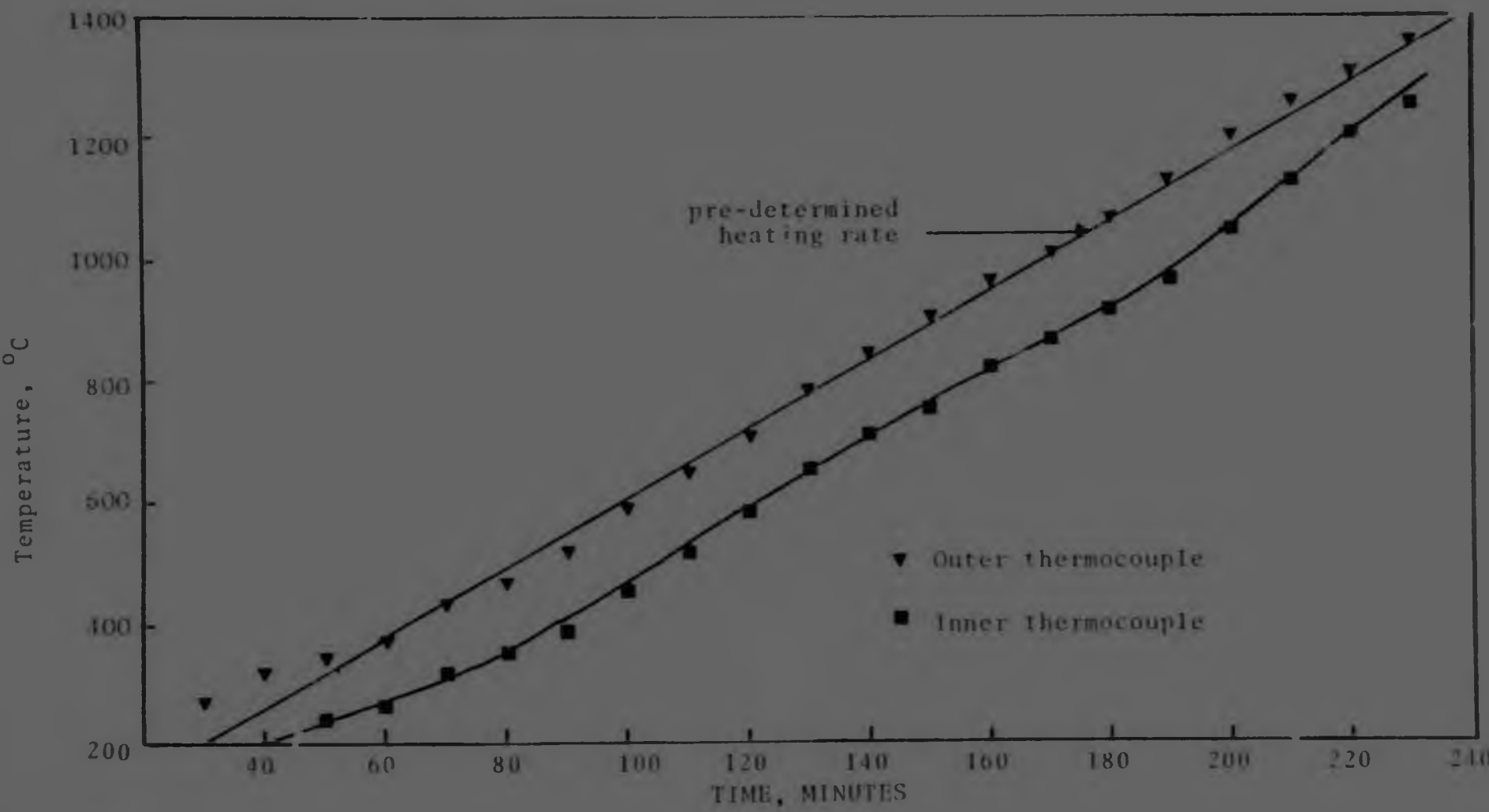


Figure 2.3 Temperatures recorded by the inner and outer thermocouples during the heating of a charge of ore and coke.

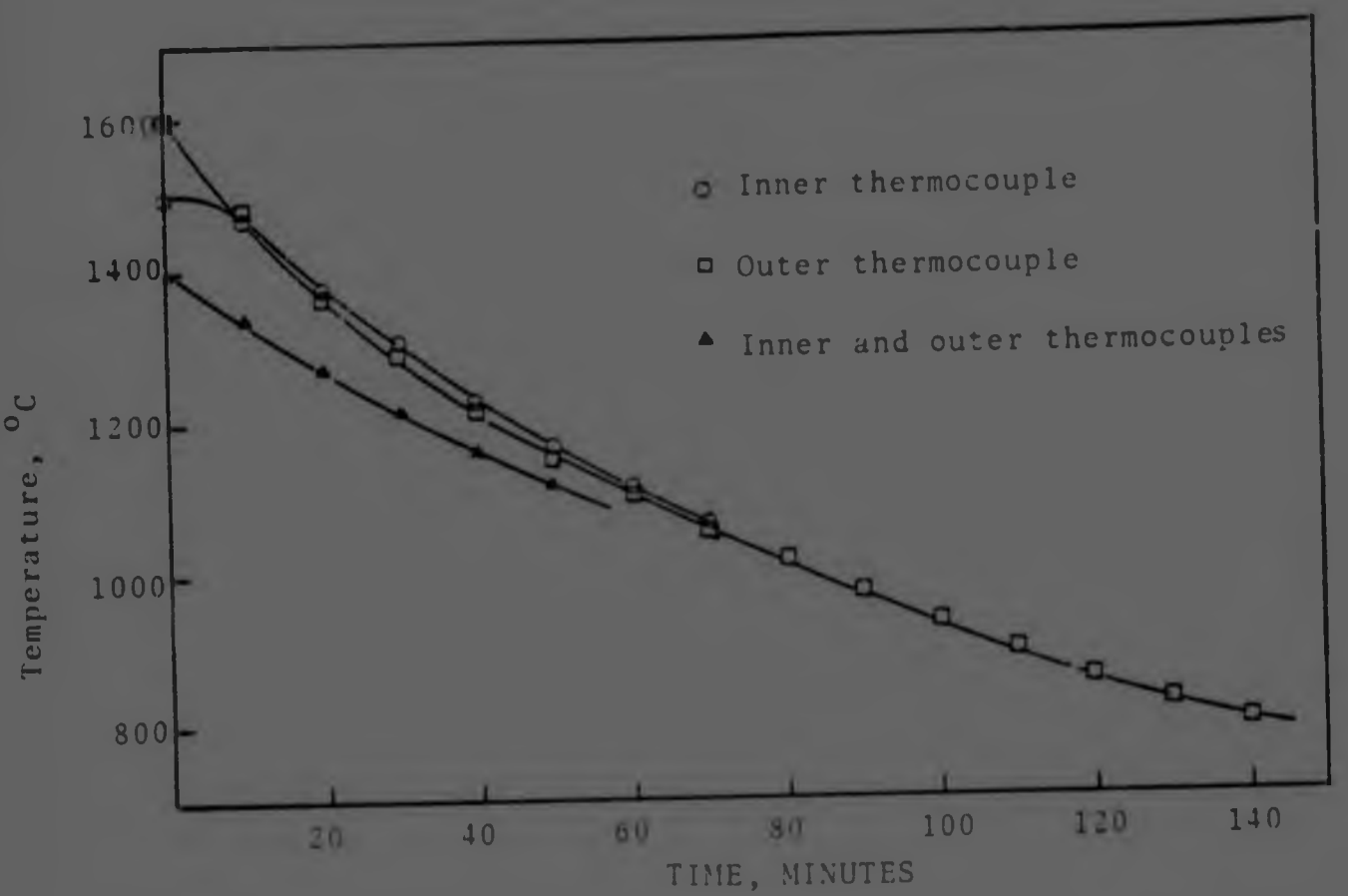


Figure 2.4 Cooling curves for charges of ore and coal after heating to 1600°C and after heating to 1400°C and maintaining that temperature for 2 hours.

The optimum position for the induction coil, relative to the position of the charge, was established by determining temperature profiles at constant temperature along the depth of a charge of alumina bubbles. An actual charge was not used because of the volume changes and reactions that occur at high temperatures. The temperature profiles obtained are shown in Figure 2.5. The temperature profiles in an actual charge may differ from those shown in Figure 2.5 owing to differences in thermal conductivity.

2.3.2 Additional Experiments

The purpose of these experiments was to provide additional information that would contribute to an understanding of the changes in structure and composition found in particles of ore reacted under SCICE conditions.

In one set of experiments, particles of ore between 4,7 and 6,35 mm were heated at 1300°C for 2, 4 and 15 hours in air.

In another set of experiments, particles of ore in the same size range were heated isothermally in a molybdenum-wound resistance furnace, in an atmosphere of pure carbon monoxide, for 1 hour at 1200°C and for 6 hours at 1450°C. A further experiment, in which a temperature of 1200°C was maintained for 1 hour, involved loading the ore into an alumina crucible placed inside a graphite crucible. The graphite crucible was used to ensure than any carbon dioxide generated by reduction of the higher oxides of manganese would be reduced to carbon monoxide.

In a large scale experiment, a 6,0 kg charge of ore, of particle size range between 2,83 and 12,7 mm, was heated in a graphite crucible at 350°C per hour to 1400°C and retained at 1400°C for 1 hour. The temperature was then raised to 1580°C within 15 minutes and the charge allowed to cool.

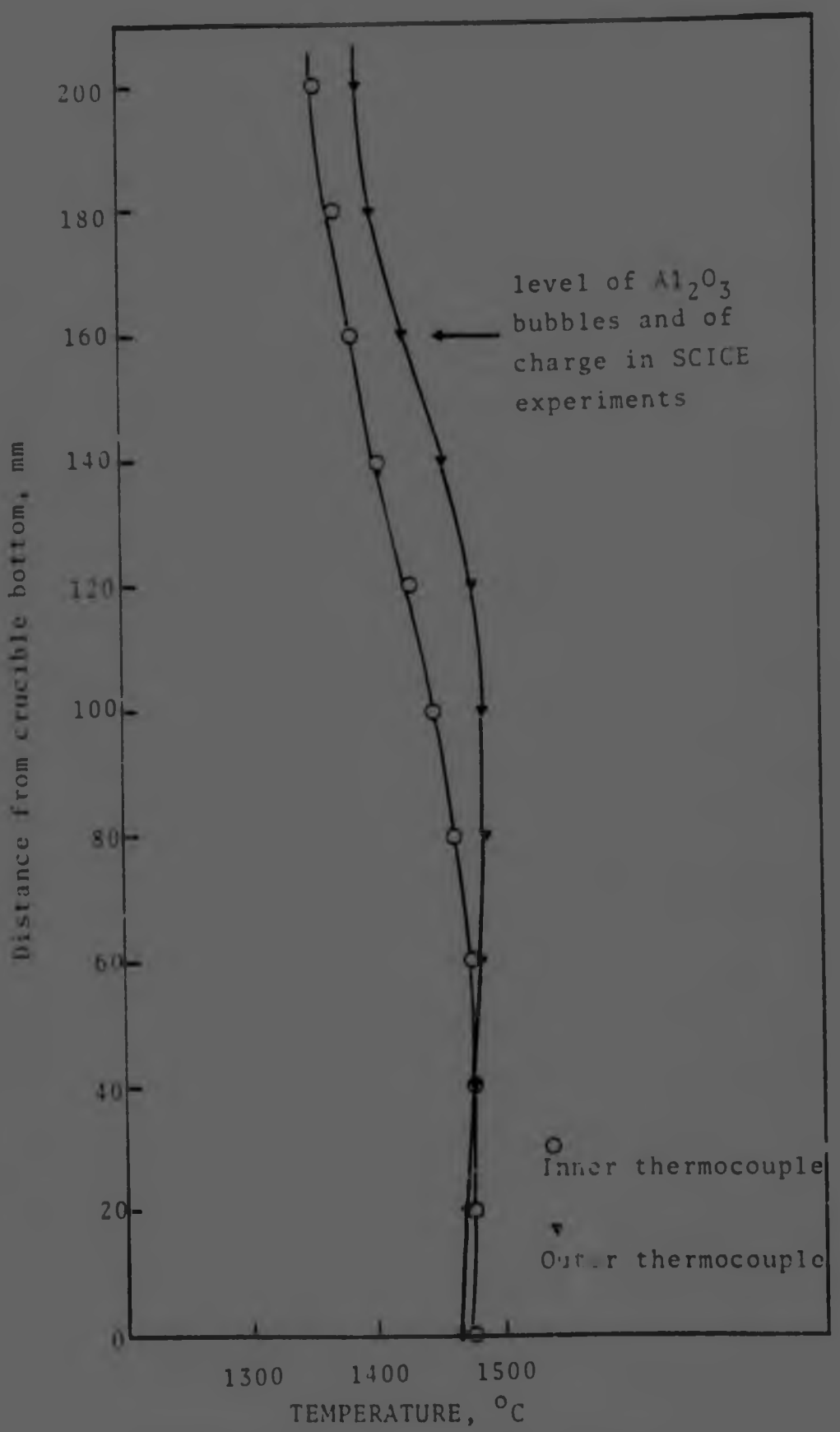


Figure 2.5 Temperature gradients in a charge of alumina bubbles.

2.3.3 Sampling and Examination of Reacted SCICE Charges

The reacted charges were initially examined visually. In those cases where, due to sintering or fusion, the charge could not be removed from the crucible, the charge was sectioned with a diamond impregnated circular saw. The charges were photographed, weighed and selected samples were taken. Samples for chemical analysis (to determine the percentage metallization), for X-ray diffraction analysis, and for microscopic examination were prepared by riffling the crushed charge. Attempts to determine the percentage metallization were unsuccessful. The techniques used and the results obtained are discussed in Appendix 1.

X-ray diffraction analysis was carried out by the diffractometric method. A Philips X-ray unit was used which consisted of a 1 kW X-ray generator (model PW 1010/80), a goniometer (PW1050/25), a proportional counter (PW1965/50), and a curved graphite crystal monochromator. Copper Kα radiation was used and the operating conditions were in general as follows: scanning speed $2^{o}(2\theta)$ per minute, divergent slit 1^{o}, receiving slit $0{,}25^{o}$, time constant 2s, chart speed 20 mm per minute, and a range of 400 counts per second, giving maximum sensitivity of the strongest diffraction peak. A stepscan control (model PW1374) and a digital printer (PM2468) were used when accurate determination of peak intensity and position were required.

2.3.4 Microanalysis by the Energy Dispersive System (EDS)

Microanalyses obtained with the EDS system give information on the composition of a very small volume (typically $1\mu m^3$) of material. These analyses are normally carried out by use of an energy dispersive detector on a scanning electron microscope. The system is usually used for qualitative analysis although semiquantitative and quantitative [98] determinations are also possible, provided that suitable standard specimens are available and that the experimental conditions are strictly reproduced.

The use of the energy dispersive detector on the scanning electron microscope and its principles of operation have been dealt with by several authors[99-101]. A limitation of the detector is that it will not detect elements lighter than sodium due to absorption by a beryllium window about 7 µm thick located between the sample and the detector[101]. The limit of detectability of the system is very low and Marshall[99] considers that the minimum mass fraction of an element that may be detected is about 0,01 per cent.

The equipment used for X-ray microanalysis in this work consisted of a Cambridge S4 scanning electron microscope equipped with an EDAX 'lithium-drifted detector', a 707B multichannel analyser and a NOVA 2 computer. The spectrum of the volume analysed was displayed on a video screen and a tabulated list of the elements and their proportion by mass was obtained by means of the computer and a teletypewriter. Standard specimens were not available so the analyses presented in this work are qualitative although they are presented as quantitative statements.

The equipment was used to obtain the analyses of selected spots or areas in the samples. X-ray distribution maps[100] were also obtained to show the major components in areas of interest. The samples were prepared by mounting in plastic resin, polishing and applying a carbon coating. Selected samples were analysed after etching.

"Spot" analyses[101] were carried out over a period of 100s. The accelerating voltage of the microscope was kept at 20kV to limit the depth of penetration of the electron beam and the lateral scatter of electrons in the specimen. These conditions gave excellent peak to background ratios for the major constituents in the alloy, the slag and the oxide phases.

The composition of an unknown specimen is determined quantitatively by comparing the number of characteristic X-ray counts arriving from the unknown specimen, (N_{spec}) with the number (N_{std}) arriving from a standard specimen in the same time and under the same experimental conditions. The concentration of the required element in the unknown specimen, C_{spec} should then be given by [101]

$$C_{spec} = \frac{N_{spec}}{N_{std}} \times C_{std} \quad . \quad . \quad . \quad 2.1$$

where C_{std} is the accurately known concentration of the element in the standard specimen and each value of N is a peak count minus a background count. Because, in the general case, the composition and the density of the unknown specimen are different to those of the standard specimen equation 2.1 may need correction for some or all of the three effects: atomic number (Z), absorption (A) and fluorescence (F). The origin of these effects has been discussed by Goodhew [101] and Marshall [99].

In the case of the samples under consideration, the computer was programmed to carry out corrections for Z, A and F. Without the use of standard specimens the computer makes the comparison shown in equation 2.1 by using values of N_{std} and C_{std} from a calibration curve that relates counting rate to the atomic number of the element for the K, L and M X-ray series. This procedure may introduce significant errors in the analyses because the computer programme is not precisely matched to the calibration curve. The accuracy is best for close atomic numbered elements.

Attempts to produce standard specimens were not made because of time limitations. Such specimens must conform to the most stringent specifications with regard to composition, porosity and homogeneity because of the extremely small volume analysed each time.

A number of tests were carried out to assess the accuracy and reproducibility of the analyses, which were normalised, without provision for oxygen, to 100 per cent and are presented in terms of cation concentration.

The reproducibility of the analyses was assessed by carrying out 'spot' analyses in the centre of a grain of impure manganous oxide. The electron beam was positioned successively at the vertices of a square with side 0,1µm. The results showed a high degree of reproducibility in the major constituent (Mn) while the reproducibility decreased for the constituents in lower concentration as indicated below. It may be noted that the diameter of the electron beam at the surface of a sample is about 1µm and increases with decreasing sample density and increasing accelerating voltage.

	Element, mass per cent			
	Mg	Si	Ca	Mn
Mean value	12,9	0,3	1,5	85,3
Standard deviation	0,59	0,15	0,02	0,73

The accuracy of the analyses was assessed by analysing an austenitic steel low in carbon and high in manganese, and the high-carbon ferromanganese produced by reacting the ore with coke at 1600°C for 1 hour. The composition of these two alloys was known from conventional chemical analyses.

The composition of the steel obtained by the two methods of analysis was as shown below.

	Fe	Mn	Cr	Si	C	P
Chemical analysis	NA*	12,87	NA*	0,56	1,23	0,045
EDS Analysis	86,3±1,3	11,4±1,2	1,4±0,2	1,0±0,3	ND+	ND+

NA* Not analysed
ND+ Not detected

The iron plus chromium content of the alloy obtained by the EDS method is within 3 per cent of that calculated from the conventional chemical analysis. It is well known [102,103] that this type of steel normally contains between 1 and 3 per cent chromium. Hence the major component of the steel (Fe) was determined to within less than 4,9 per cent of its actual value. The undetected carbon in the material does not alter the proportions of the other elements by a significant amount owing to its low concentration.

The error in the Mn content of the alloy is 11,4 per cent, and that in the Si content 84 per cent.

The composition of the high-carbon ferromanganese obtained by the two methods of analysis was as follows:

	Element, Mass per cent			
	Mn	Fe	Si	C
Chemical analyses	80,3	10,1	0,2	7,5
EDS analyses	92,4±0,6	7,1±0,8	0,4±0,1	ND*
Chemical analyses corrected for carbon	88,6	,1	0,21	

The major element (Mn) was determined to within 4,3 per cent of its actual value. The elements Fe and Si were determined to within 36,1 and 90 per cent respectively of their actual values.

The magnesium oxide content of the ore was 3,1 per cent. If during the early stages of reduction, 73 per cent by mass of the non-metallic component of the charge was oxide and 23 per cent slag and if all the magnesium oxide dissolved in the manganous oxide, then the magnesium oxide

---

ND Not detected

* Since carbon cannot be detected by the energy dispersive detector comparison between the values obtained by the two methods is carried out after recalculating the values obtained by conventional analysis disregarding the carbon content.

content of the oxide should rise to about 5,5 per cent by mass. The EDS analyses gave a much higher magnesium oxide level in the manganous oxide. This and the low accuracies obtained in the determination of the silicon content of the alloys discussed above, indicated that the error was higher for the lighter elements. The error was assessed by analysing analytical grade magnesium chloride. The results obtained are indicated below:

	Element, mass per cent	
	Mg	Cl_2
Calculated analyses	25	75
EDS analyses	42-6	58-6

Hence the magnesium content was determined to within 68 per cent and the chlorine to within 23 per cent of their actual values. These results do not necessarily hold in the case of a solid solution of manganous and magnesium oxides where the concentration of magnesium oxide is very low.

From the results presented above, the following conclusions may be drawn with regard to the EDS analyses.

a) The technique was consistent in detecting all the elements of atomic number greater than 10 and in its ability to indicate the major and minor elements in the volume analysed.

b) The reproducibility of the analyses was within 1,5 per cent of the mean value, for elements whose concentration in the oxide was greater than 85 per cent by mass. The reproducibility was within 12 per cent of the mean value for elements whose concentration in the sample was between 7 and 13 per cent. The reproducibility was generally much lower for elements in concentrations of less than about 2 per cent.

c) Iron and manganese in the alloys were determined to within less than 1,9 per cent of their actual values in samples containing these elements in proportions exceeding about 85 per cent. The accuracy for these elements decreased to about 36 per cent or less for samples containing iron and manganese in proportions between 11 and 13 per cent by mass.

d) The analyses were grossly inaccurate for the lighter elements which were present in low concentrations.

CHAPTER 3

3.0 RESULTS

3.1 The Mineralogy of the Ore

The mineralogy of the Mamatwan ore deposit has been investigated before[3,8, 50, 104, 105]. However, for the purpose of this investigation a certain amount of first hand experience was considered necessary.

The mineralogy of the batch of ore used was studied by the examination of polished sections, by X-ray-diffraction analysis and by X-ray microanalysis using the energy dispersive detector on the scanning electron microscope.

The microscopic examination of polished sections showed that the ore consisted in general of a fine aggregate of manganese and gangue minerals with local concentrations of gangue occurring in the form of veins and oolites. The composition of the ore varied significantly between particles and from point to point in the same particle (even in particles 3mm in size). Figure 3.1 shows a characteristic structure of the ore. In ore particles rich in braunite the latter formed the continuous phase and the gangue minerals appeared as isolated grains. Ore particles rich in gangue showed a matrix of gangue with dispersed grains of manganese and iron minerals.

The variations in the composition of individual ore particles become important in this investigation when the early stages of reduction and slag formation are considered. The morphology of grains of unreduced oxide, the amount of primary slag and the amount of manganous oxide dissolved in the slag will be influenced by the relative amounts of the different constituents in the ore particles.

The relative amounts of braunite, dolomite, calcite and hematite were determined by X-ray diffraction analysis in six random particles of ore, approximately 10 mm in size. For comparison the same determinations were carried out on a representative sample of ore.



Figure 3.1 Micrograph of Mamatwan ore showing a fine aggregate of metallic (bright) and gangue (grey)minerals. Gangue in the form of a vein and as an oolite is apparent. Porosity appears black. Polished, 480X.

The samples were ground dry in a Sieb mill to less than 149µm and then ground in alcohol for 3 minutes in a McCrone micronising mill using agate elements. Microscopic examination of the powders produced showed that the coarsest particles present had a diameter of about 8µm. The powders were compacted in aluminium holders and analysed, by scanning over the 100 per cent intensity peaks of braunite, dolomite and calcite and over the 50 per cent intensity peak of hematite at steps of $0,05^{o}(2\theta)$. A counting time of 20s was used at each step. The procedure was repeated 3 times on one of the samples to test the reproducibility of the technique.

The area under the different peaks was found by plotting counts per second at each step against angle, 2θ, and determining the width of the peak at background level. The integrated relative intensity, I, was then calculated from the relationship:

$$I = \frac{\theta_2 - \theta_1}{0,05}\left[(Y_1 + Y_2 + \ldots + Y_n) - (Y_m)\right] \quad . \quad . \quad 3.1$$

where

$\theta_2 - \theta_1$ is the width of the peak at background level

Y_1, Y_2 ... Y_n denote the number of counts per second at each step of $0,05^{o}(2\theta)$ and

Y_m is the mean number of counts per second for background radiation.

The relative intensity of the peaks, in relation to the strongest peak in each sample, is shown in Table 3.1 (a). Examination of Table 3.1(a) will show the enormous varations in the proportions of the different phases when individual ore particles are considered.

TABLE 3.1(a)

The integrated relative intensity of the more abundant phases in Mamatwan ore in relation to the strongest peak of each sample.

SAMPLE NO.	PHASE			
	CALCITE	DOLOMITE	BRAUNITE	HEMATITE
	Intensity, relative to the strongest peak of each sample			
Representative sample of ore	22,40	55,02	100	2,55
1	12,28	80,36	100	1,96
2	57,79	6,60	100	3,42
3 (a)	1,35	40,99	100	1,54
(b)	1,19	42,00	100	1,50
(c)	1,46	40,89	100	1,28
4	20,45	100	75,7	2,72
5	3,48	31,81	100	1,52
6	9,72	44,31	100	1,43

The relative intensity of the peaks in relation to the strongest peak of each phase is shown in Table 3.1(b). It can be seen that the amounts of the phases varied enormously between particles. The mean relative intensities for tests a, b and c of sample No. 3 and the maximum per cent variation about the mean are also shown in Table 3.1(b). It can be seen that the relative intensities of the dolomite and braunite peaks were reproduced within narrow limits. The reproducibility of the calcite and hematite peaks was rather poor due to the low peak to background counting rate ratios obtained for these phases.

The statistical error in the determinations of relative intensity was estimated by using data from Klug and Alexander[106], that relate the per cent error to the total number of counts for different ratios of peak to background counting rate. The approximate error varied from a minimum of 0,4 per cent for braunite to a maximum of 4,7 per cent for hematite.

The 50 per cent intensity peak of hematite was used because the 100 per cent peak overlaps the 100 per cent peak of braunite. If it is assumed that the 100 per cent hematite peak is of twice the intensity of the 50 per cent peak and that the intensities of hematite and braunite are additive then it can be seen from Table 3.1(a) that the hematite makes only a small contribution to the relative intensities determined for braunite.

X-ray diffraction analysis of the ore showed that its mineralogical composition is very complex. The phases identified are indicated in Table 3.2 together with the relative heights of the 100 per cent intensity peaks. Minor quantities of other minerals were present, but these were not positively identified owing to interference and overlapping of peaks.

TABLE 3.1(b)

The integrated relative intensity of the more abundant phases in Mamatwan ore in relation to the strongest peak of each phase.

SAMPLE NO.	PHASE			
	CALCITE	DOLOMITE	BRAUNITE	HEMATITE
	Intensity, relative to the strongest peak of each phase			
Representative sample of ore	75,26	38,67	61,72	66,85
1	55,60	76,10	83,15	68,29
2	100	2,39	31,78	45,53
3(a)	7,29	46,45	99,51	64,23
(b)	6,45	47,76	99,84	62,00
(c)	7,93	46,56	100	53,66
4	97,78	100	66,43	100
5	17,55	33,58	92,70	51,22
6	46,62	44,44	88,06	52,85
Mean intensity for tests a, b and c and maximum per cent variation about the mean	7,22	46,92	99,78	60,16
	10,7%	1,8%	0,3%	10,8%

TABLE 3.2

Qualitative X-ray diffraction analysis of Mamatwan ore

MINERAL	CHEMICAL FORMULA	RELATIVE HEIGHT OF THE 100 PER CENT INTENSITY PEAK
BRAUNITE	$MnO.3Mn_2O_3.SiO_2$ *	100
DOLOMITE	$CaMg(CO_3)_2$	36
CALCITE	$CaCO_3$	23
HAUSMANNITE	Mn_3O_4	11
HEMATITE	Fe_2O_3	11**
CRYPTOMELANE	KMn_8O_{16}	8

* This is the ideal composition of braunite

** This is the height of the 50 per cent intensity peak for hematite. The 100 per cent hematite peak overlapped the 100 per cent peak of braunite.

The mineralogy of the ore was investigated by X-ray micro-analysis. This technique gave a very clear indication of the mode of occurrence of the more abundant phases whose constituent elements were determined. Analyses, obtained by the EDS system, of the more abundant minerals in the ore are shown in Table 3.3.

The important findings of this part of the investigation may be summarised as follows:

a) Braunite and hematite occurred in general as fine grains of irregular shape.

b) Hausmannite occurred as very coarse grains sometimes associated with oolites.

c) Small amounts of quartz were found which occurred as coarse grains.

d) The calcite invariably occurred in the form of veins and oolites.

e) The dolomite occurred as fine grains dispersed in a matrix of braunite and as a matrix containing grains of metallic minerals. These forms of dolomite contained a high proportion of manganese.

f) All the minerals discussed above contained appreciable amounts of impurities except for quartz which was pure.

3.2 Observations during the Heating of SCICE Charges

When charges of ore and coke were heated a light haze (probably steam) was given off at temperatures between 100 and 350°C as measured by the outer thermocouple. At about 1100°C a considerable quantity of carbon monoxide was evolved which ignited at the top of the furnace.

TABLE 3.3

EDS Analysis of the more abundant minerals in Mamatwan ore

Element	Cation concentration** in mineral, mass per cent				
	BRAUNITE	HEMATITE	HAUSMANITE	DOLOMITE	CALCITE
Mn	84,6±2.8*	4.1	99,0±0,6	27,8±7,9	8,5±5,0
Fe	1,2±1,0	94,5	-	-	-
Si	12,4 9	0,5	0,4±0,1	Minor	Minor
Ca	0,9±0,3	0,5	0,5±0,4	38,3±3,1	88,1±8,1
Al	Minor	-	-	Minor	Minor
Mg	-	-	-	33,1±7,7	2,7±3,7
P	-	-	-	-	Minor
K	-	-	-	Minor	-

* The ± figures are standard deviations about the mean values given. High standard deviations indicate large variations in the composition of grains of the same mineral.

** Calculated on an oxygen-free basis.

When charges of ore and coal were heated, fumes appeared at 300°C, the quantity of fumes increasing until a temperature of 600°C was reached. Some tar condensed on the furnace cover. The amount of visible fumes decreased beyond 650°C, until no fumes were given off at about 750°C. At about 850°C, sufficient combustible gas was evolved to sustain a flame at the top of the furnace. At 1090°C the gases decreased in quantity and the flame was extinguished. More visible fumes were given off at 1430°C and the amount of fumes increased with temperature up to 1600°C.

3.3 Macro-examination of the Reacted SCICE Charges

Charges of ore with coal or coke reacted under the same conditions had a similar appearance.

The degree of metallization obtained, by heating up to 1400°C and holding the temperature for up to 4 hours, was very limited. Heating to 1500 and 1600°C resulted in significant reduction and a layer of alloy began to form at the bottom of the crucible. Holding of the charge at 1600°C for 1 or 2 hours resulted in the formation of a layer of alloy and a layer of slag. The slag layer formed at 1600°C for 1 hour contained an appreciable number of partially reduced ore particles which tended to settle at the interface between the alloy and the slag layers. The unreacted particles of reducing agent tended to float to the top of the slag layer although some were found embedded in the slag layer. Figure 3.2 shows the fractured surface of the slag layer formed by heating ore and coke to 1600°C and holding that temperature for 1 hour. The partially reduced particles of ore are clearly visible in the cementing slag.

The amount of partially reduced ore decreased significantly with an increase in the holding time, at 1600°C, from 1 to 2 hours.

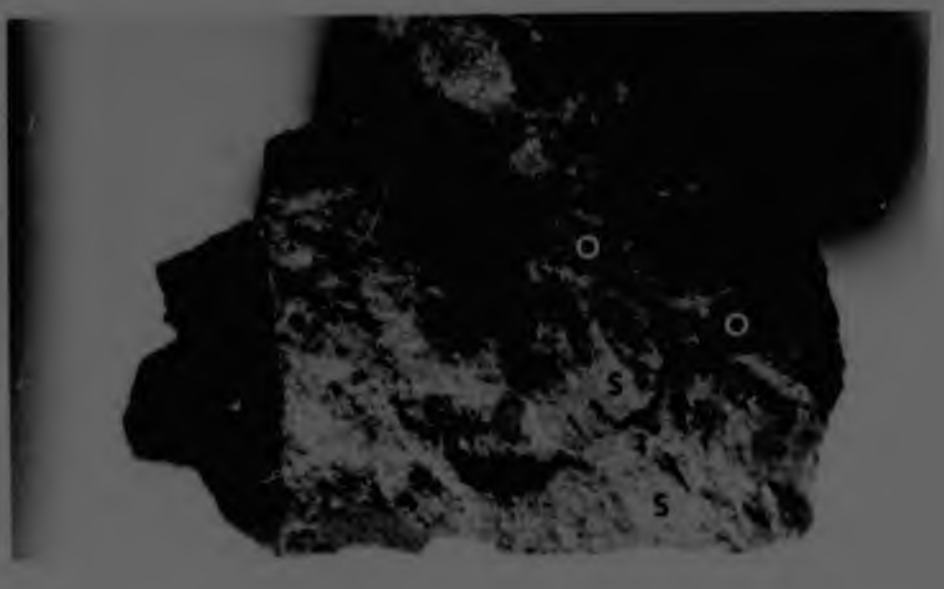


Figure 3.2 Partially reduced ore particles (O) in the slag (S) formed by heating ore and coke to 1600°C and holding that temperature for 1 hour. Magnification 3X.

The slag layer was porous and there were voids between it and the alloy layer. It appeared that significant amounts of carbon monoxide were given off during the cooling period. The carbon monoxide passed through the slag layer forming craters that became covered with minute crystals of graphite.

Four charges of ore and coal reacted under different SCICE conditions are shown in Figures 3.3 to 3.6.

A summary of the examination of charges of ore and coke reacted under different SCICE conditions is shown in Table 3.4

3.4 Microscopic Examination of the Reacted SCICE Charges

3.4.1 General Microscopic Examination of the Phases in Particles of Partially Reduced Ore

Samples from all the reacted SCICE charges were examined microscopically in an attempt to determine the processes that occur during the reduction of Mamatwan ore with Iscor coke and Delmas coal. Both reflected light and scanning electron microscopy were used.

The inhomogeneous nature of the ore resulted in variations in the structure of different particles of partially reduced ore taken from the same charge. A particular structure however was seen to repeat itself in the majority of cases (see figure 3.7).

Samples of ore taken from the two types of charge, reacted under the same conditions, showed no apparent differences in structure. The structural changes that occurred during the reacting of the ore with Iscor coke or Delmas coal are discussed here with reference to charges of ore and coke because a greater number of experiments were carried out using this mixture.

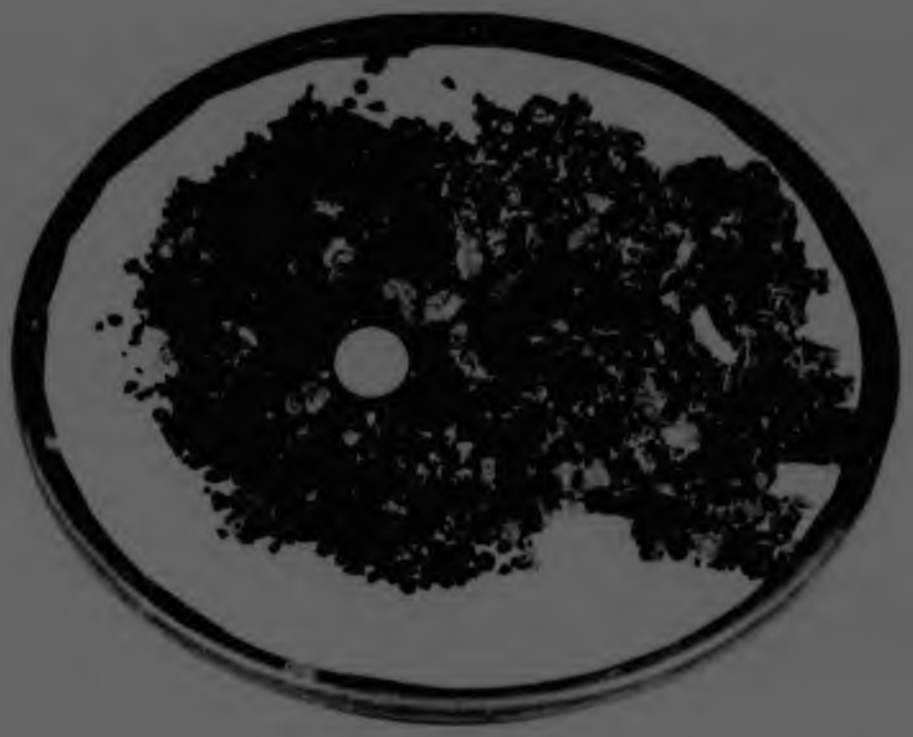


Figure 3.3 Sinter and loose particles in a charge of ore and coal that was heated to 1400°C and held at that temperature for 4 hours.
Coin 24 mm diameter.



Figure 3.4 Sinter and some loose particles in a charge of ore and coal that was heated to 1600°C and cooled.
Coin 24 mm diameter.

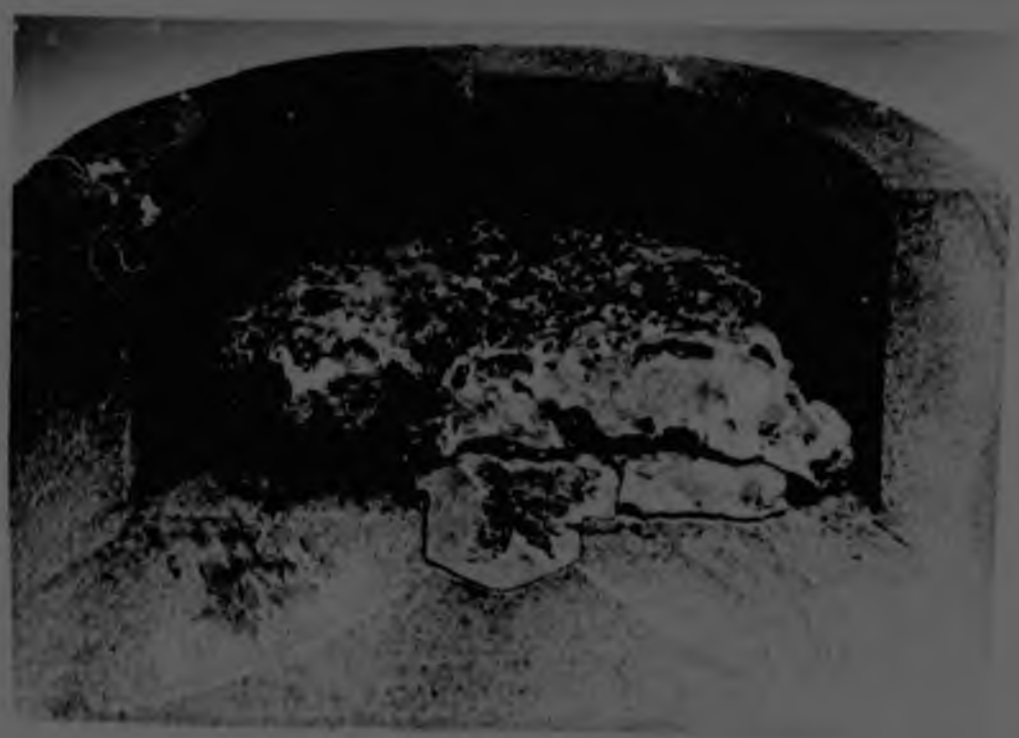


Figure 3.5 Slag and alloy formed by heating ore and coal to 1600°C and holding that temperature for 1 hour.



Figure 3.6 Slag and alloy formed by heating ore and coal to 1600°C and holding that temperature for 2 hours.

TABLE 3.4

Summary of the examination of charges of ore and coke reacted under different SCICL conditions

Temp °C	Holding time at temperature, hours			
	0	1	2	4
1300	Cracking of ore. Decomposition of carbonates with some free CaO and MgO appearing. Some sintering. Metallic prills appear on some ore particles. Generally ore particles appear light green.	Similar to charge heated to 1300°C and cooled	Similar to charge heated to 1300°C and cooled.	-
1400	Ore appears a darker green. Small increase in metallization and amount of sintering. Free CaO and MgO not observed	Similar to charge heated to 1400°C and cooled.	Small increase in sintering, slag formation and metallization.	The charge forms a single mass of weak sinter. Metallic prills about 1mm on ore particles
1500	Appreciable fusion. Ore appears a dark green. Lumps of alloy form which begin to drain to the bottom of the crucible.	-	-	-
1600	Extensive fusion and flowing of material. A discontinuous layer of alloy forms at the bottom of the crucible. The ore appears dark green.	A layer of alloy and a layer of slag separate out. Dark green particles of ore embedded in lighter green slag. Apparent decrease in size of ore particles which retain their basic form. Reducing agent tends to float on top of slag layer.	A layer of alloy and a layer of slag present. Decreased amount of partially reduced ore in the slag layer. Some reducing agent on top of the slag layer.	-

- No experiment conducted under these conditions.

When the charge was heated to 1300°C or higher the original structure of the ore broke down to form a network of slag surrounding grains of impure manganous oxide. Random metallic particles appeared throughout the ore particles. Generally the metallic particles adhered to the oxide grains and extended into the slag. In some cases metallic particles were observed in the interior of oxide grains. The amount of metal in the interior of ore particles from the same charge varied considerably from one particle to the other for charges reacted at temperatures between 1300 and 1600°C. The size and morphology of the oxide grains varied, due apparently to the amount of slag in the ore particle. This basic structure, which was retained until the final stages of the reduction, is illustrated in Figure 3.7. It can be seen that the size of the grains of oxide varied and that the metallic particles on the surface were much coarser. Coarser oxide grains can be seen in areas that were originally occupied by oolitic gangue material. The amount of metal associated with the oxide in the oolitic areas was small while the metallic beads at the interface between the oolitic areas and the matrix were coarser.

Small amounts of a mixed ferrite of calcium and manganese were found in ore particles reacted with coke at 1400°C for 1 hour. The mode of occurrence of the ferrite was similar to that shown in Figure 3.38

The size of the metallic particles on the surface of ore particles increased rapidly with increasing temperature and holding time. The number of metallic particles on the surface (Figure 3.8) appeared to be greater than the number of contact points between the ore and the reducing agent indicating that contact between solid reducing agent and metallic bead was not necessary for the bead to grow.

The proportion of slag in the interior of ore particles appeared to remain constant irrespective of experimental conditions. The thickness of a film of slag that formed on the



Figure 3.7 Metallic particles (bright), grains of oxide (light grey), slag (dark grey) and pores (black) in an ore particle that was heated with coke to 1300°C and cooled.
Polished, 60X, enlarged 33 per cent.

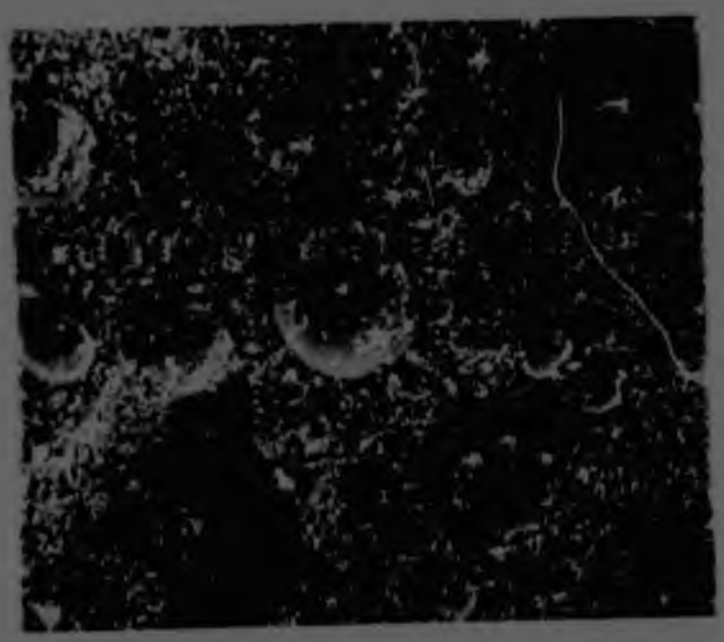


Figure 3.8 Beads of alloy on the surface of an ore particle that was heated with coke to 1400°C and cooled. The surface was covered with a film of dendritic slag.
SEM 100X.

surface of ore particles increased drastically with increasing temperature and holding time, for temperatures of 1500 and 1600°C. For lower temperatures, soaking periods of up to 4 hours had little effect on the proportion of slag formed.

Microscopic examination of lumps of sintered material composed of reducing agent, slag and partially reduced ore, showed that there was seldom direct contact between the alloy and the reducing agent.

Figure 3.9 shows a section through a lump of sinter from a charge of ore and coke that was heated at 1600°C and cooled. It can be seen that the basic structure of the partially reduced ore is very similar to that shown in Figure 3.7. Larger metallic particles occurred at the ore-slag interface. The slag had a duplex structure and contained many fine grains of oxide. Metallic particles at the slag-coke interface were not observed.

It has been seen that the particles of partially reduced ore became embedded in the slag layer when the charge was retained at 1600°C for 1 or 2 hours. Microscopic examination of the interface between the partially reduced ore particles and the cementing slag showed that the ore particles were in the process of breaking up. This resulted in isolated grains of oxide in the slag matrix.

Figure 3.10 shows the interface between a partially reduced ore particle and the slag matrix formed by reacting ore and coke at 1600°C for 1 hour. It can be seen that the slag matrix has a duplex structure and contains many fine oxide particles The appearance of the interior of the ore particle is similar to that shown in Figure 3.7 except for its coarser grain size.

The isolated grains of oxide in the slag appeared elongated in many cases as indicated in Figure 3.11. X-ray micro-analysis of these grains showed that they were enriched in

surface of ore particles increased drastically with increasing temperature and holding t[illegible] for temperatures of 1500 and 1600°C. [illegible] or lower temper[illegible]tures, soaking periods of up to 4 hours had little effect on the proportion of slag formed.

Microscopic examination of lumps of sintered material composed of reducing agent, slag and partially reduced ore, showed that there was seldom direct contact between the alloy and the reducing agent.

Figure 3.9 shows a section through a lump of sinter from a charge of ore and coke that was heated to 1600°C and cooled. It can be seen that the basic structure of the partially reduced ore is very similar to that shown in Figure 3.7. Larger metallic particles occurred at the ore-slag interface. The slag had a duplex structure and contained many fine grains of oxide. Metallic particles at the slag-coke interface were not observed.

It has been seen that the particles of partially reduced ore became embedded in the slag layer when the charge was retained at 1600°C for 1 or 2 hours. Microscopic examination of the interface between the partially reduced ore particles and the cementing slag showed that the ore particles were in the process of breaking up. This resulted in isolated grains of oxide in the slag matrix.

F[illegible] 3.10 shows the interface between a partially reduced ore particle and the slag matrix formed by reacting ore and coke at 1600°C for 1 hour. It can be seen that the slag matrix has a duplex structure and contains many fine oxide particles. The appearance of the interior of the ore particle is similar to that shown in Figure 3.7 except for its coarser grain size.

The isolated grains of oxide in the slag appeared elongated in many cases as indicated in Figure 3.11. X-ray microanalysis of these grains showed that they were enriched in



igure 3.9 Interfaces between partially reduced ore and slag (S) and coke (C) and slag. Note the fine oxide grains in the slag.
Polished, 60X, enlarged 33 per cent.

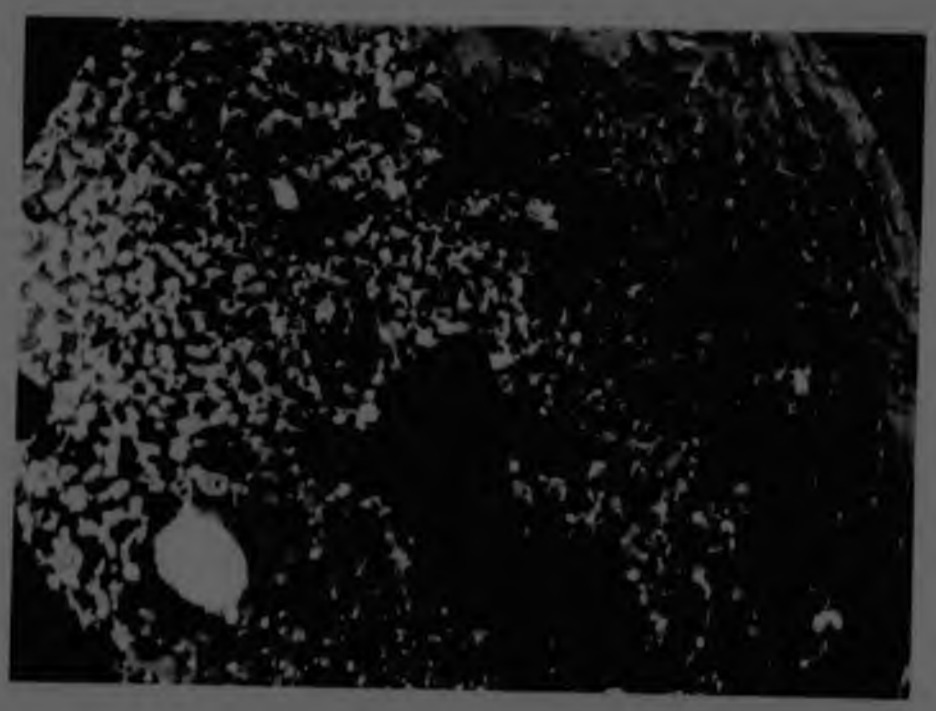


Figure 3.10 A particle of ore breaking up in the slag matrix formed by reacting ore and coke at 1600°C for 1 hour. Note the metallic particles in the interior of some oxide grains.
Polished 120X.

magnesium and depleted in manganese. The average composition of these grains on an oxygen free basis was; manganese 60,1 per cent, magnesium 34,4 per cent and calcium 3,7 per cent. Particles of graphite were also found in the slag as indicated in Figure 3.11. The precise origin of these graphite particles is not known. X-ray microanalysis showed that the graphite particles did not contain any of the ash constituents present in the coke.

The grains of oxide formed in particles of partially reduced ore exhibited a green halo when examined with the optical microscope. The frequency of this occurrence was low at 1300 and 1600°C and high at 1400 and 1500°C Etching and scanning electron microscopy indicated that the green haloes were caused by a reaction rim that formed round the oxide grains as shown in Figure 3.12. It can be seen that the etching characteristics of the reaction rim differed markedly from those of the interior of the oxide grains and the slag. Variations in the rate of dissolution of different areas within the grains themselves are apparent. It appeared that the thickness of the rim increased with increasing reduction as indicated in Figure 3.13. It can be seen that some of the oxide grains hardly etched at all.

3.4.2 Examination of the Metallic Component

From thermodynamic considerations, when a mixture of manganous and ferrous oxides is heated in a reducing environment, the ferrous oxide is preferentially reduced due to its lower stability.

The results of X-ray microanalysis showed that practically all the ferrous oxide was reduced before any significant reduction of manganous oxide occurred. This resulted in the formation of random metallic nuclei throughout the particles of ore. The size of the metallic particles on the surface of ore particles increased rapidly, partly due to the reduction of manganous oxide and partly due to the coalescence of smaller particles. It follows therefore that the

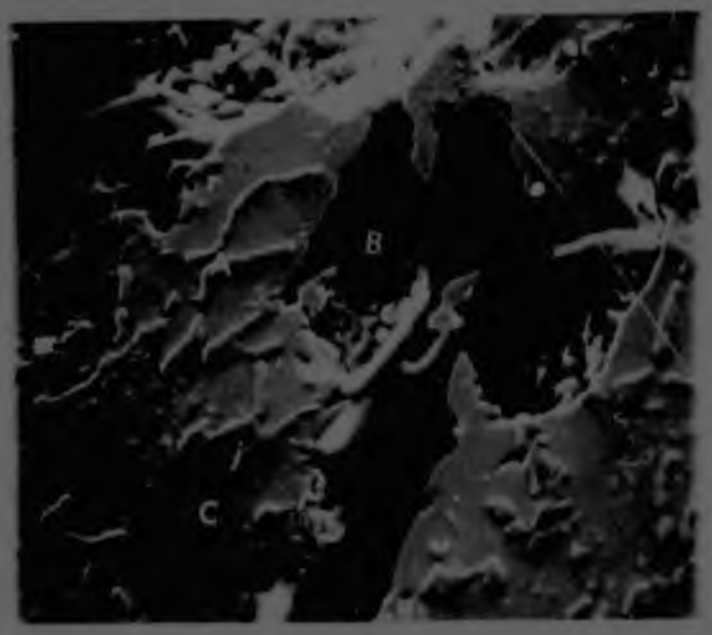


Figure 3.11 Elongated grains of impure manganous oxide (A) and particles of graphite (B) in a matrix of slag (C) formed by reacting ore and coke at 1600°C for 2 hours.
SEM, polished, 575X.



Figure 3.12 The reaction rim (A) that formed round grains of oxide (B) by heating ore and coke to 1400°C and cooling. Slag (C) and metallic particles (D) are indicated.
SEM, etched 2 per cent HCl, 10000X

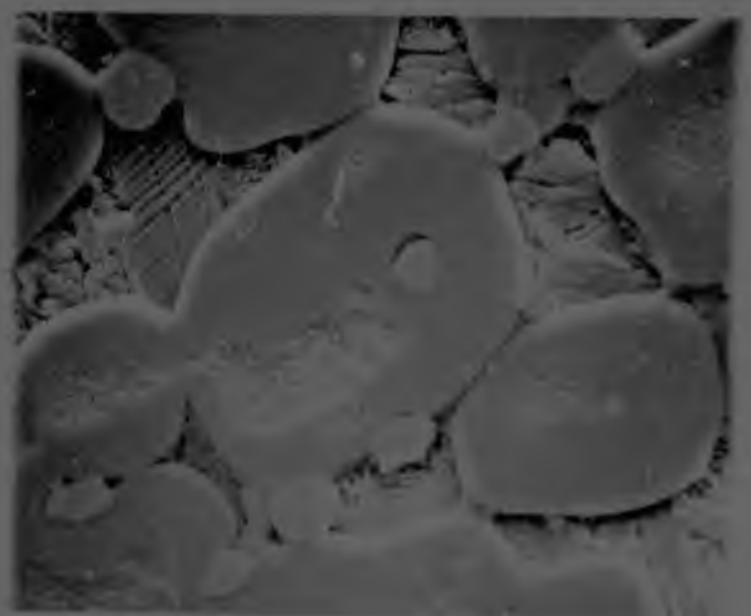


Figure 3.13 Spreading of the reaction rim towards the centre of oxide grains from a charge of ore and coke that was heated to 1000°C and cooled.
SEM, etched 2 per cent HCl, 10000X.

sequence of events occurring during the reduction of Mamatwan ore could be followed to some extent by the examination of the metallic component of reacted charges . It is clear however that the phase composition of metallic particles need not bear an absolute relationship to their size.

The diameter of the metallic nuclei in the interior of ore particles did not exceed 10um in the majority of cases, irrespective of experimental conditions. In some cases metallic particles with a diameter of up to 125µm were observed near the surface of ore particles and in positions where it appeared that metallic nuclei had coalesced to form bigger particles.

Etching tests showed that metallic nuclei with a diameter smaller than about 25um consisted of a single phase while nuclei with a diameter of between 50 and 125µm consisted of one or two phases. The metallic beads on the surface of ore particles consisted of at least two phases.

Examination of the structure of metallic beads from charges of ore and coke reacted at 1300°C for 0 to 2 hours gave a good indication of the reactions occurring during the early stages of metal formation, although the structure of individual beads varied due to variations in chemical composition. (Table 3.5).

The iron that formed by the reduction of ferrous oxide was carburised either by the carbon monoxide in the atmosphere or by solid coke. The structure was similar to that of hypereutectoid steel and consisted of a network of free carbide at the boundaries of grains of very fine pearlite. Structures similar to that of hypoeutectoid steel were not observed indicating that at 1300°C the carbon content of the metal was in excess of 0,8 per cent. From Table 3.5 it can be seen that both the carbide and the pearlite contained some manganese and that the manganese content of the free carbide was higher than that of the pearlite.

TABLE 3.5

The composition of different phases or components in metallic particles as obtained by X-ray microanalysis

Figure No.	Phase or componenet	Mode of analysis	Iron* Mass per cent	Manganese* mass per cent
	Free carbide in pearlitic particles	spot	96	4
	Pearlite	area	98	2
3.14	Carbide	spot	92	8
	Troostite	area	96	4
3.15	Carbide	spot	89	11
	Austenite	spot	92	8
. 16	Primary dendrites and dispersed constituent of eutectic	spot	85	15
	Carbide	spot	89	11

* Carbon free basis

The structure described above was slightly modified for small increases in the proportion of manganese in the alloy. The free carbide at the grain boundaries was retained while the pearlite changed to troostite (Figure 3.14), a form of extremely fine pearlite. The proportion of free carbide to troostite varied significantly in different particles due apparently to variations in the overall carbon content. Flakes of graphite were observed in some metallic beads and evidence was found that some of the beads containing free carbon had been in direct contact with solid reducing agent.

With a further increase in the manganese content of the alloy bead, the troostite decreased in quantity or disappeared completely and the structure consisted of equiaxed grains of a solid solution with free carbide at the grain boundaries and as Widmanstatten needles. Figure 3.15 shows an alloy bead with a reduced amount of troostite. X-ray diffraction analysis showed that the grains of solid solution were austenitic. The uneven distribution of the troostite indicated variations in composition across the diameter of the bead.

The absence of dendrites from the structures discussed thus far indicated that these alloy beads were in the solid state at 1300°C.

With an increase in the manganese content of the alloy, significant changes took place in the structure of the beads as indicated in Figure 3.16. The structure consists of primary dendrites of a solid solution in a eutectic of the solid solution and carbide. Comparison between the amount of carbide in Figure 3.16 and Figures 3.14 and 3.15 shows that an increase in the carbon content of the alloy was also involved. The appearance and the hardness (Table 3.6) of the solid solution in Figures 3.15 and 3.16 were similar, indicating that the solid solution in Figure 3.16 was austenite. The type of structure shown in Figure 3.16 varied

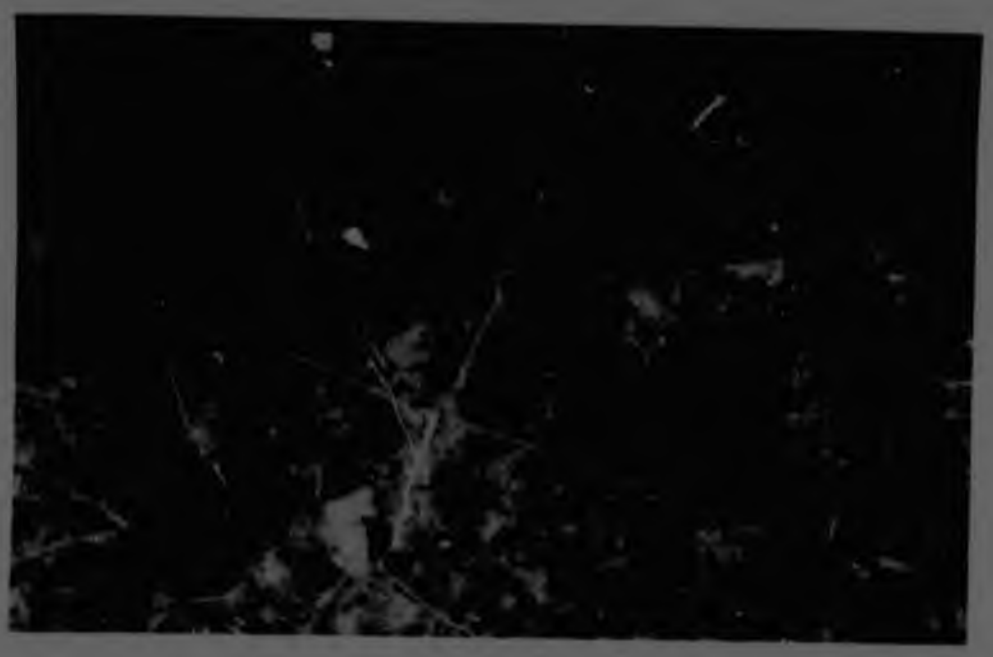


Figure 3.14 Grains of troostite delineated by a bright network of carbide precipitate in an alloy bead formed by heating ore and coke to $1300^{o}C$ and cooling.
Etched 2 per cent HNO_3 in alcohol, 60X, enlarged 33 per cent.



Figure 3.15 Grains of solid solution (light grey) and nodules of troostite (dark grey) surrounded by a thick network of carbide in an alloy bead formed by heating ore and coke to $1300^{o}C$ and cooling.
Etched 2 per cent HNO_3 in alcohol, 60X, enlarged 33 per cent.

TABLE 3.6

The hardness of the metallic component formed under SCICE conditions

Test No.	Description of test	Load g	Hardness VPN
1	Single-phase nuclei between 25 and 50 µm in diameter	15	190 ± 21 *
2	Two-phase nuclei between 50 and 125 µm in diameter	25	485 ± 20
3	Troostite in Figure 3.14	50	346 ± 26
	Carbide in Figure 3.14	50	1485 ± 56
4	Equiaxed grains of solid solution in Figure 3.15	50	262 ± 14
5	Primary dendrites in Figure 3.16	50	277 ± 21
	Carbide in Figure 3.16	50	1144 ± 37
6	Carbide in Figure 3.19	100	1699 ± 69
	Two-phase constituent in Figure 3.19	15	506 ± 125
7	Primary carbide in Figure 3.20	15	1602 ± 128
	Two-phase constituent in Figure 3 20	15	616 ± 74
8	Carbide in Figure 3.21	100	1619 ± 79

* The ± figures are the values of the standard deviation about the mean hardness value.

with apparent variations in the proportions of manganese and carbon in the alloy. In alloy beads of high carbon but low manganese contents the primary dendrites and the eutectic austenite transformed to troostopearlite upon cooling. In alloy beads of intermediate carbon and manganese contents the interior of the dendrites was austenitic while troostopearlite occurred as nodules or rims around the primary dendrites. The primary dendrites indicated that the alloy was in the liquid state at 1300°C.

The hardness of the phases or constituents in the metallic component of reacted charges was measured with a microhardness tester. Loads of 50 and 100g were used for the carbide, wherever possible, to obtain indentations with diagonals of about 10µm and so minimise errors in their measurement. Higher loads caused cracking of the carbide due to excessive deformation.

A completely eutectic structure of carbide and austenite (Figure 3.17) formed in alloy beads with an apparently higher carbon content.

Eutectic structures were also observed in alloy beads formed by heating ore and coke to 1400°C and maintaining that temperature for periods of up to 4 hours (Figure 3.18). Larger alloy beads from the same charge showed grains of carbide that were surrounded by a two-phase constituent as indicated in Figure 3.19. The proportion of carbide increased significantly with an increase in the size of the alloy beads.

The structure of alloy beads formed by heating ore and coke to 1500°C and then cooling was similar to that of beads formed at 1400°C although evidence was found of the precipitation of primary carbide (Figure 3.20).

The massive alloy formed by heating to 1600°C and maintaining that temperature for 0 to 2 hours consisted of carbide and traces of a second constituent. Specimens for microscopic examination were difficult to prepare from these alloys due



Figure 3.16 Dendrites of primary austenite (dark) in a eutectic of austenite and carbide in an alloy bead formed by heating ore and coke to 1300°C and cooling.
Etched 2 per cent HNO_3 in alcohol,
60X, enlarged 33 per cent.



Figure 3.17 Eutectic structure of austenite (dark) and carbide (bright) in an alloy bead formed by heating ore and coke to 1300°C and cooling.
Etched 2 per cent HNO_3 in alcohol, 60X,
enlarged 33 per cent.



Figure 3.18 Alloy beads with eutectic structure formed by reacting ore and coke at 1400°C for 4 hours. Carbide appears bright, austenite dark grey and pores appear black.
Etched 2 per cent HNO_3 in alcohol, 120X enlarged 45 per cent.



Figure 3.19 Grains of primary carbide surrounded by a two-phase constituent in an alloy bead formed by reacting ore and coke at 1400°C for 4 hours. Etched 2 per cent HNO_3 in alcohol, 270X, enlarged 33 per cent.

to their extreme hardness and their tendency to chip and crack. Figure 3.21 shows a polished section from the alloy formed by reacting the charge at 1600°C for 1 hour. The section shows obvious cracks and pores as well as many fine lines. Scanning electron microscopy showed that these lines were either cracks or deep ridges in the alloy.

The section in Figure 3.21 is shown in Figure 3.22 after prolonged etching. The differences in colour between Figures 3.21 and 3.22 appeared to be due to staining which could be removed rapidly by washing in 2 per cent hydrochloric acid in alcohol. The hardness of differently stained areas was similar indicating that these belonged to the same phase. The differential staining in Figure 3.22 is probably due to differences in the orientation of grains. Comparison between Figures 3.21 and 3.22 showed that the darker areas in Figure 3.22 were delineated by lines in Figure 3.21. It appears therefore that these lines might have been grain boundaries at which a constituent had segregated to form a film, which was removed during preparation. The existence of such grain boundaries would also explain the curved path followed by some of the lines. In a brittle material, cracks would be expected to follow a straight or jagged path as indeed was the case with the obvious cracks in the sample.

3.5 The Distribution of Elements in the Phases of Partially Reduced Ore

The microscopic examination showed that the three components present in reacted SCICE charges were metal, slag and unreduced oxide. It will be seen in section 3.5.2 that the unambiguous identification by X-ray diffraction analysis, of the phases in the reacted charges was difficult due to their complex composition.

The proportion of manganese to oxygen in manganous oxide varies with the partial pressure of oxygen in the system[27,107]. The green colour of the partially reduced ore in reacted charges suggested that the composition of the oxide was



Figure 3.20 Laths of primary carbide (bright) and an interstitial two-phase constituent in alloy beads formed by heating ore and coke to 1500°C and cooling.
Etched 2 per cent HNO_3 in alcohol,
120X, enlarged 45 per cent.

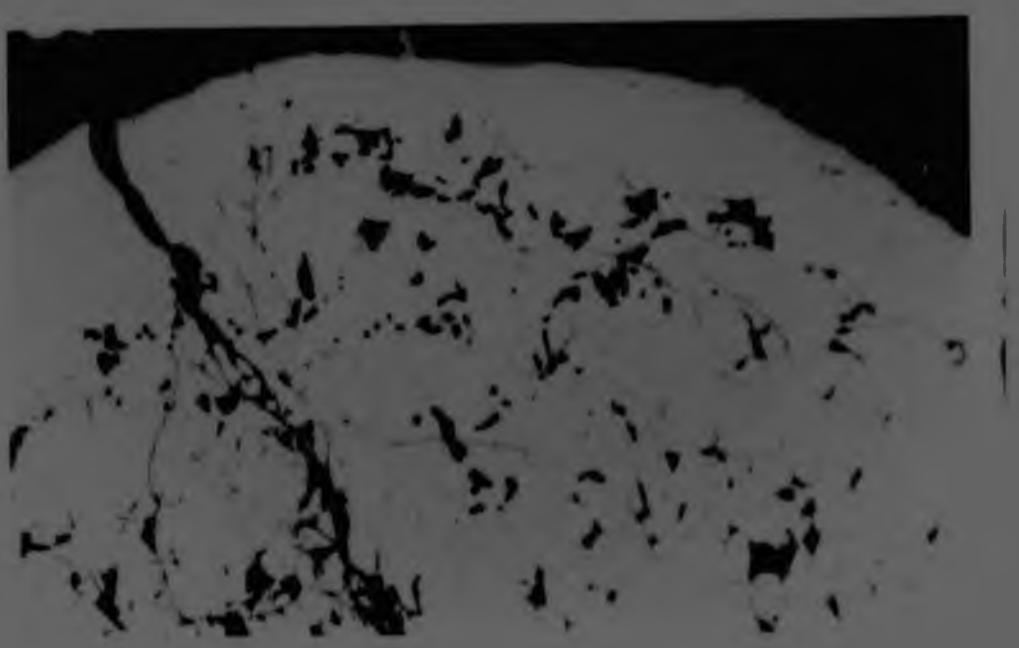


Figure 3.21 A section from the alloy formed by reacting ore and coke at 1600°C for 1 hour, showing porosity, cracks and fine lines of uncertain nature.
Polished 120X, enlarged 45 per cent.

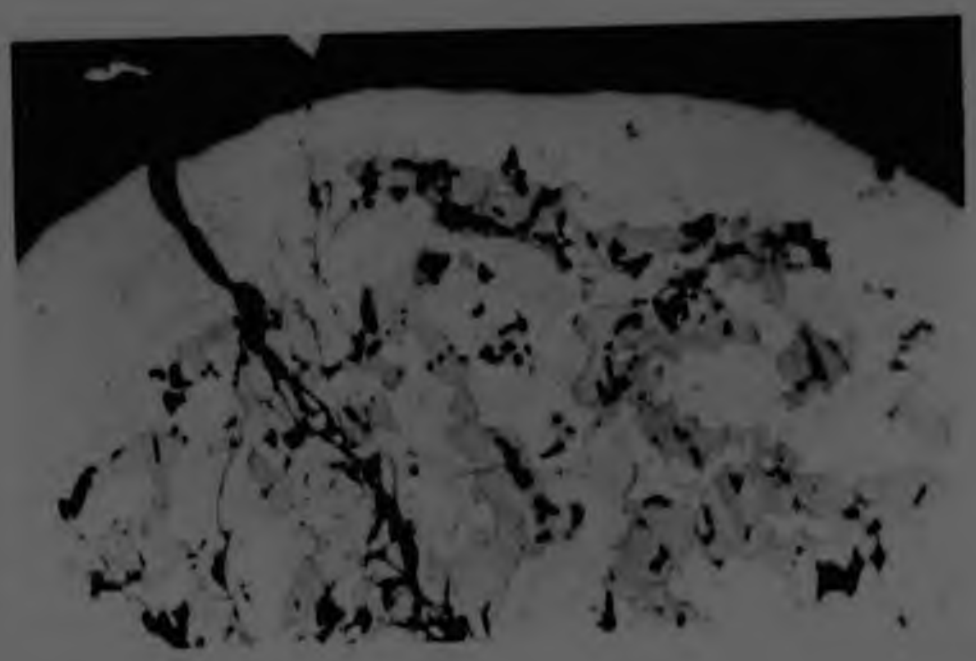


Figure 3.22 Differential staining in the alloy of Figure 3.21.
Etched 2 per cent HNO_3 in alcohol,
120X, enlarged 45 per cent.

stoichiometric or nearly so. The d-spacings of this phase however deviated significantly from those given for pure MnO. It was suspected that the differences in d-spacings were not caused by small deviations from stoichiometry which may have existed in the composition of the oxide since Klingsberg and Roy [17] found no systematic shift of X-ray diffraction lines in MnO that was prepared with different stoichiometries. The deviation of d-spacings could have been due to the formation of a solid solution.

The complex composition of the ore (Table 2.2) made it very difficult to predict which reactions would occur and what products would form at elevated temperatures. Further complications arise due to differences in the physical and chemical properties of the two reducing agents which could also influence the processes that occur and the composition of the phases that form at high temperatures.

In a previous study [3] of the reduction of Mamatwan ore with solid carbon it was claimed that the non-metallic phases in the partially reduced ore were manganous oxide and calcium manganate. These phases however do not account for the magnesium oxide (3,1 per cent) and the silica in the ore (4,3 per cent). The affinity of lime for silica is well known [108] and it would be reasonable to suppose that a reaction should take place preferentially between these two oxides.

Thus it became apparent that X-ray microanalysis was necessary in order to determine the constituents of each phase and the reactions that take place at elevated temperatures to form the various phases.

3.5.1 X-ray Microanalysis of Reacted SCICE Charges

The distribution of elements, in the three components, slag, alloy and oxide, formed under conditions of different temperature, retention time and reducing agent, is shown in Table 3.7. The values given are the means of four determinations. Although these results are not quantitative they give a clear indication of the distribution of elements in the three components.

TABLE 3.7

The distribution of elements in the alloy, the oxide and the slag that formed by reacting Mamatwan ore with Delmas coal or Iscor coke under various experimental conditions.

Reaction Temp. °C	Time at Temp. h	Reducing agent	Phase analysed	"Cation concentration, mass per cent"							
				Mn	Mg	Ca	Si	Fe	Al	S	
1400	0	D.C.	Oxide	97,3	1,9	0,5	0,3				
1400	2	D.C.	Oxide	76,8	18,0	2,6	0,6				
1400	4	D.C.	Oxide	83,4	13,5	2,3	0,9				
1400	0	I.C.	Oxide	86,0	13,4	0,6					
1400	2	I.C.	Oxide	86,1	13,0	0,4	0,5				
1400	4	I.C.	Oxide	73,7	13,4	12,2	0,1				
1600	0	D.C.	Oxide	84,3	13,7	1,6	0,4				
1600	0	I.C.	Oxide	75,0	22,3	1,8	0,3	0,3	0,1	0,1	
1400	0	D.C.	Slag	25,1	3,8	25,7	37,0		0,3	0,4	
1400	2	D.C.	Slag	1,9	0,3	63,1	33,7		0,8	0,2	
1400	4	D.C.	Slag	3,1	0,6	65,3	30,4		0,4	0,2	
1400	0	I.C.	Slag	28,3	1,5	20,1	47,9				2,3
1400	2	I.C.	Slag	20,2	6,1	26,4	31,5		14,8	0,2	0,8
1400	4	I.C.	Slag	16,9	2,2	40,5	1,2		39,2		
1600	0	D.C.	Slag	14,4	5,7	47,5	31,5		0,9	0,1	
1600	0	I.C.	Slag	4,3	4,3	59,0	31,6	0,1	0,7	0,1	
1400	0	D.C.	Alloy	33,0			0,3	66,7			
1400	2	D.C.	Alloy	36,0		0,7	0,3	63,0			
1400	4	D.C.	Alloy	60,8		0,3	0,7	38,2			
1400	0	I.C.	Alloy	0,7			0,4	98,8			
1400	2	I.C.	Alloy	41,5			0,3	58,1			
1400	4	I.C.	Alloy	35,8			0,6	63,6			
1600	0	D.C.	Alloy	26,7		1,7	0,6	71,0			
1600	0	I.C.	Alloy	35,9		0,8	0,3	62,5			

D.C. Delmas coal I.C. Iscor coke

Examination of Table 3.7 shows that the composition of the three components does not exhibit a clear trend with changing experimental conditions. This was probably due to inhomogeneities in the ore and the nature of the reduction process. The ore was not fluxed completely by heating to 1600°C and cooling and it is possible that the processes occurring at different points in the charge varied due to variations in the composition of the partially reduced ore particles. A comparison between the results obtained for charges of ore and coke and for charges of ore and coal showed that the distribution of elements in the three components was similar It also showed that the type of reducing agent did not affect the composition of the components for comparable experimental conditions. As pointed out earlier, the analyses of ore particles varied considerably and therefore variations in alloy analysis may be due to this factor as well as changing experimental conditions.

The main constituents of the alloy were iron, manganese and silicon. Minor quantities of other elements were detected at times. These probably occurred as inclusions in the alloy.

The main constituents of the oxide were manganese, magnesium and calcium with minor amounts of silicon. The relative proportions of magnesium and calcium varied owing to variations in the composition of the ore particles.

The main constituents of the slag were calcium, silicon and manganese. Smaller quantities of magnesium, aluminium and sulphur were also present. It may be noted that the proportion of magnesium in the slag was lower than that of the oxide. The variations in the analyses are due to the fact that the slag consisted of at least two phases.

The general distribution of the more abundant elements in a partially reduced ore particle is illustrated by the X-ray distribution maps of Figure 3.23.

Figure 3.23 The distribution of elements in an ore particle that was partially reduced by heating with coke to 1500°C and cooling.

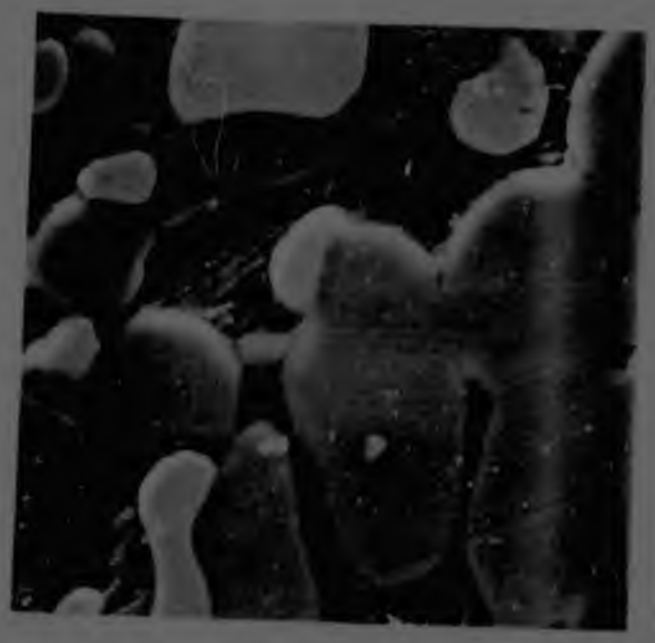
a) Grains of oxide and metallic particles surrounded by a network of slag in the partially reduced ore particle. SEM, 2700X

b) Calcium Kα X-ray-distribution map

c) Iron Kα X-ray-distribution map

d) Manganese Kα X-ray-distribution map

e) Silicon Kα X-ray-distribution map



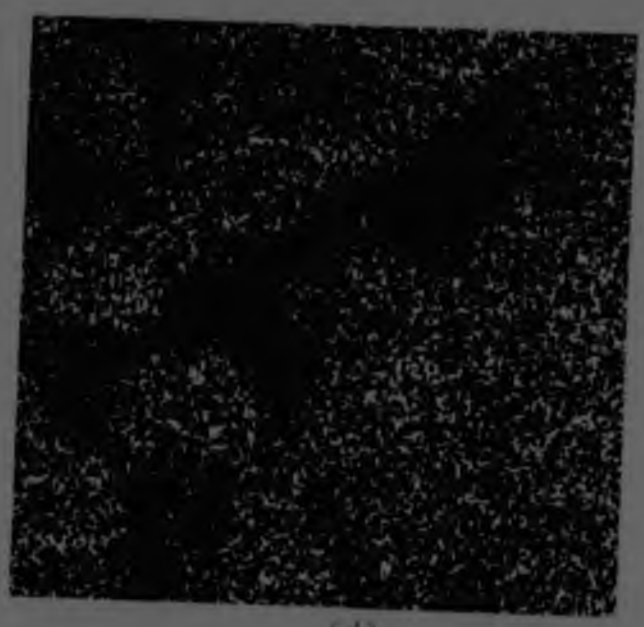
(a)



(b)



(c)



(d)



(e)

3.5.2 X-ray Diffraction Analysis

Representative samples from the charges that were reacted as indicated in Table 2.3 were analysed by X-ray diffraction. The alloys that formed with the two reducing agents at 1400 and 1600°C (temperature maintained for 0 to 4 hours and for 0 to 2 hours respectively) were analysed to enable better comparison between diffractograms. The slag that formed at 1600°C (temperature maintained for 1 and 2 hours) was also analysed.

The diffractograms obtained from charges of ore plus coke and ore plus coal were similar for comparable experimental conditions.

Parts of the diffractograms of charges of ore plus coke and ore plus coal that were reacted at 1600°C for 1 hour are compared in Figure 3.24. The similarities between the phases that formed and their approximate proportions are obvious.

The major component in charges of ore plus coke that were reacted at 1300°C for 0 to 2 hours was impure manganous oxide. Appreciable amounts of α-iron were also detected. Retention time at 1300°C did not have a significant effect on the phases present or their approximate proportions.

The same phases, and in approximately the same proportions, appeared in charges reacted at 1400°C for periods of 0 to 4 hours. Retention time at 1400°C did not have a significant effect on the proportions of the phases, although small peaks appeared due to the presence of small quantities of carbide.

The charge of ore and coke that was heated to 1500°C and cooled showed a small increase in the proportions of carbide and slag. Quantities of α-iron could still be detected.

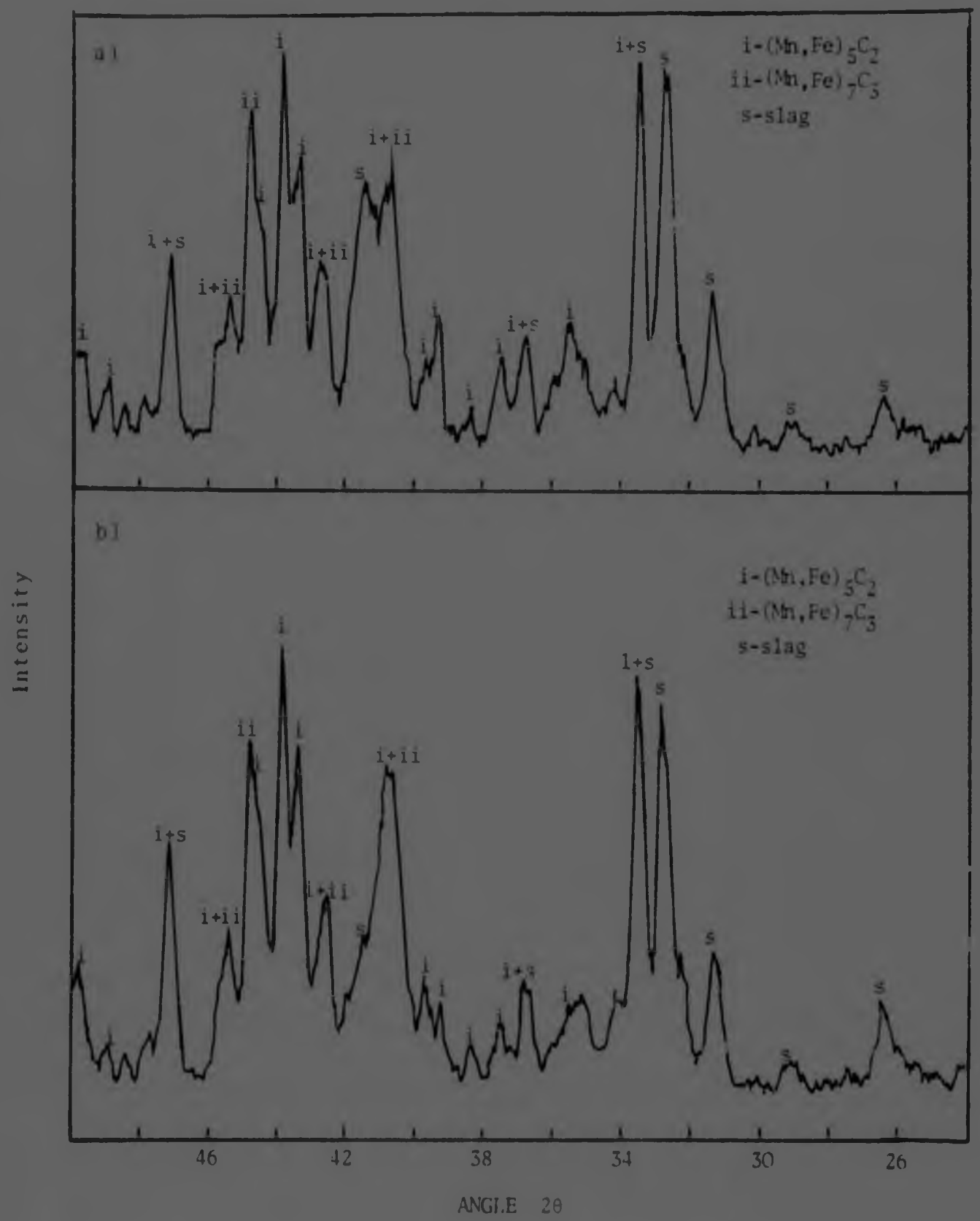


Figure 3.24 Comparison between the diffractogr m: obtained from charges of
a) ore and coke and
b) ore an: coal after reaction at 1600°C for 1 hour.

Charges reacted at 1600°C for periods of 0 to 2 hours showed a significant increase in the proportions of carbide and slag and a corresponding reduction in the amount of impure manganous oxide. Manganous oxide could not be detected in the tracings of the charges that had been reacted for 1 and 2 hours owing to the complexity of the tracings. The presence of this phase however was established by microscopy and X-ray microanalysis. The α-iron was present as small particles in the interior of partially reduced ore particles, but, the major peak of this phase was obscured by reflections from the carbide.

The alloy formed by heating to 1400°C and maintaining that temperature for 2 to 4 hours, by heating to 1500°C and cooling and by heating to 1600°C and maintaining for 0 to 2 hours gave almost identical diffractograms. The alloy formed at 1400 and 1500°C was picked from the surface of ore particles and was of a different composition to the metal occurring in the interior of the ore particles.

The alloy consisted mainly of the two carbides $(Fe, Mn)_5C_2$ and $(Fe, Mn)_7C_3$ as indicated in Figure 3.25(b). Identification of these phases was effected by comparing Figures 3.25 and 6.25.

The diffractograms of the alloy formed with coke at 1400°C for 4 hours and with coal at 1600°C for 2 hours are compared in Figure 3.25.

The phases in the slag were not identified precisely. The major peaks from the slag appeared in approximately the same positions irrespective of experimental conditions. It appeared that the phases in the slag formed by heating up to temperatures of 1600°C and cooling were calcium orthosilicate (α'-Ca_2SiO_4) and calcium manganese silicate $(Ca,Mn)_2SiO_4$ The slag that formed at 1600°C appeared to be similar to calcium magnesium silicate $(2CaO.SiO_2)_{5,6}$ $(3CaO.MgO.2SiO_2)_{4,4}$. The major peaks of this phase occur at approximately the same angular positions as those of calcium orthosilicate.

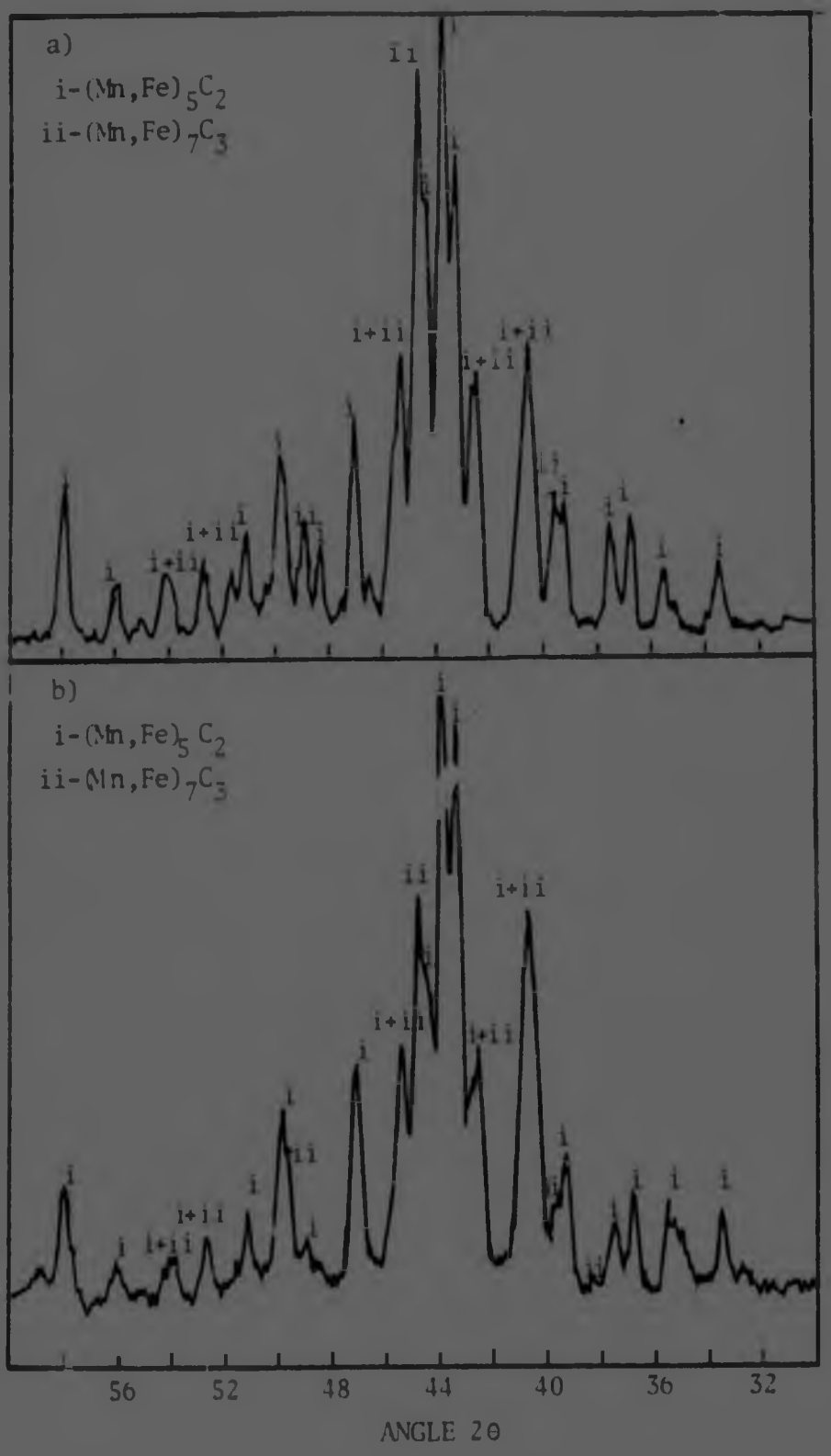


Figure 3.25 Comparison between the diffractograms of the alloy formed with coal after 2 hours at 1600°C (a), and with coke after 4 hours at 1400°C (b).

3.3.3 Mass Losses and Alloy and Slag Compositions

The mass losses that occurred under different experimental conditions are shown in Table 3.8. The values given for charges reacted at 1600°C for 1 or 2 hours are approximate since these charges were sectioned before weighing.

The mass losses are plotted against retention time at temperature in Figure 3.26. The two types of charge exhibited similar trends for comparable experimental conditions. The influence of retention time at the lower temperatures on the final mass of the charge was relatively small. Retention time at 1600°C had a more pronounced effect on the final mass of the charge. The mass losses that occurred by heating charges of ore and coke to temperatures between 1300 and 1600°C and cooling are plotted in Figure 3.27. It can be seen that the rate of loss of mass increased drastically between 1400 and 1500°C and decreased above 1500°C.

The compositions of the alloys and slags that formed under different experimental conditions are shown in Table 3.9. It should be pointed out that the amount of alloy that formed at temperatures below 1500°C was very small and that beads of alloy were picked from the surface of ore particles. These alloys therefore were not representative of the metallic component present in the charge. The alloy that formed in charges of ore and coke at 1300°C was analysed by EDS area-analyses on globules of alloy that had been mounted and polished. This procedure was used because the amount of alloy that could be separated from these charges was not adequate for conventional chemical analyses.

The variations in the manganese and iron content of the alloys formed by the heating of charges of ore and coke, and of ore and coal, between 1300 and 1600°C are plotted in Figure 3.28 The alloy formed in the early stages consisted mainly of iron Its manganese content increased with temperature changing at a slower rate at temperatures greater than about 1450°C,

TABLE 3.8

Effect of experimental conditions on the mass of various charges

Reaction temperature °C	Reaction time h	Reducing agent	Mass loss per cent
1300	0	I.C.*	23,2
	1	I.C.	24,6
	2	I.C.	25,4
1400	0	I.C.	24,0
	1	I.C.	26,6
	2	I.C.	27,2
	4	I.C.	28,8
1500	0	I.C.	31,6
1600	0	I.C.	34,0
	1	I.C.	38,4
	2	I.C.	40,9
1400	0	D.C.**	30,8
	2	D.C.	34,2
	4	D.C.	34,9
1600	0	D.C.	35,2
	1	D.C.	42,2
	2	D.C.	43,2

* Iscor coke

** Delmas coal

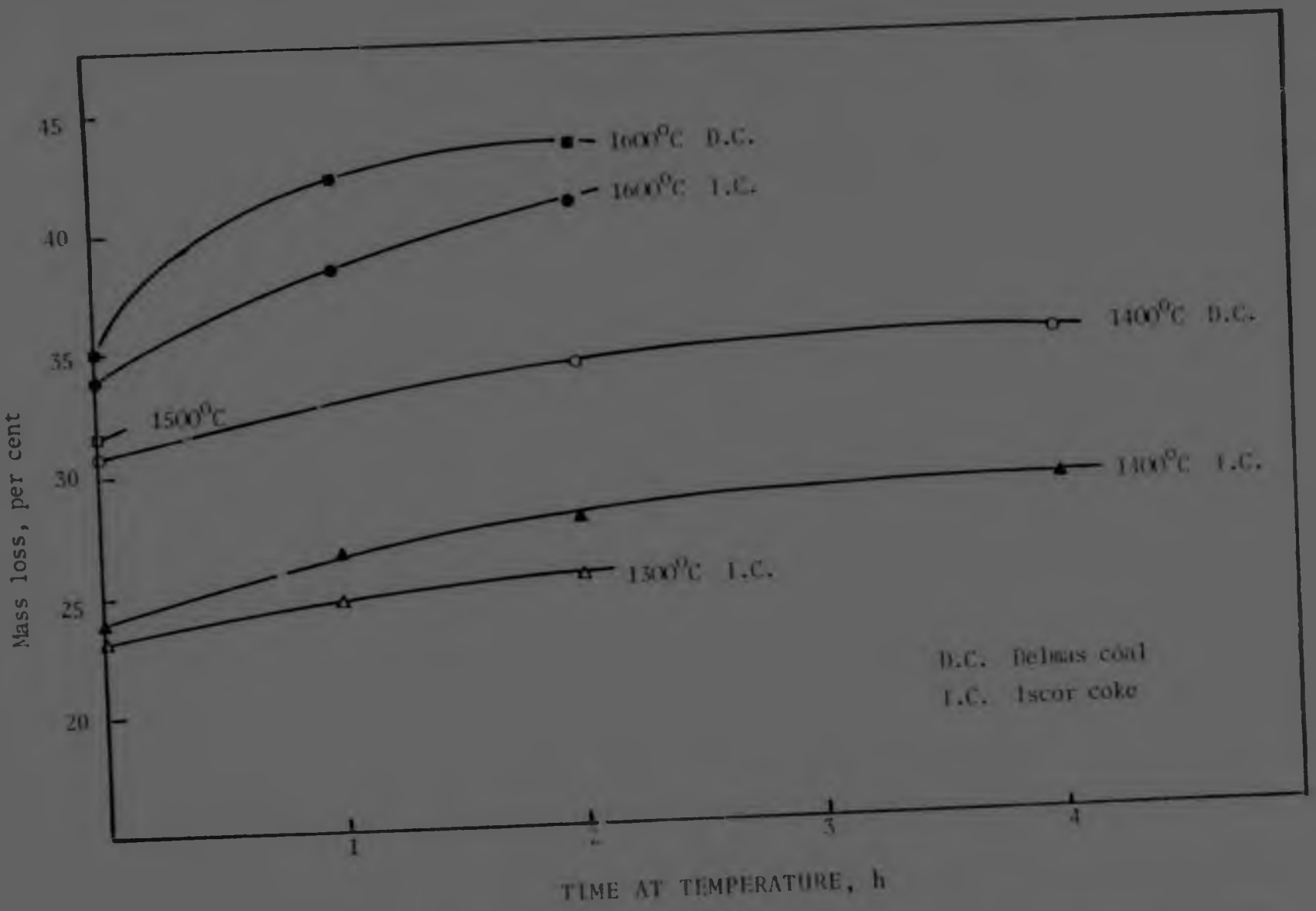


Figure 3.26 Plots of mass loss against holding time at temperature for mixtures of ore with coal or coke.

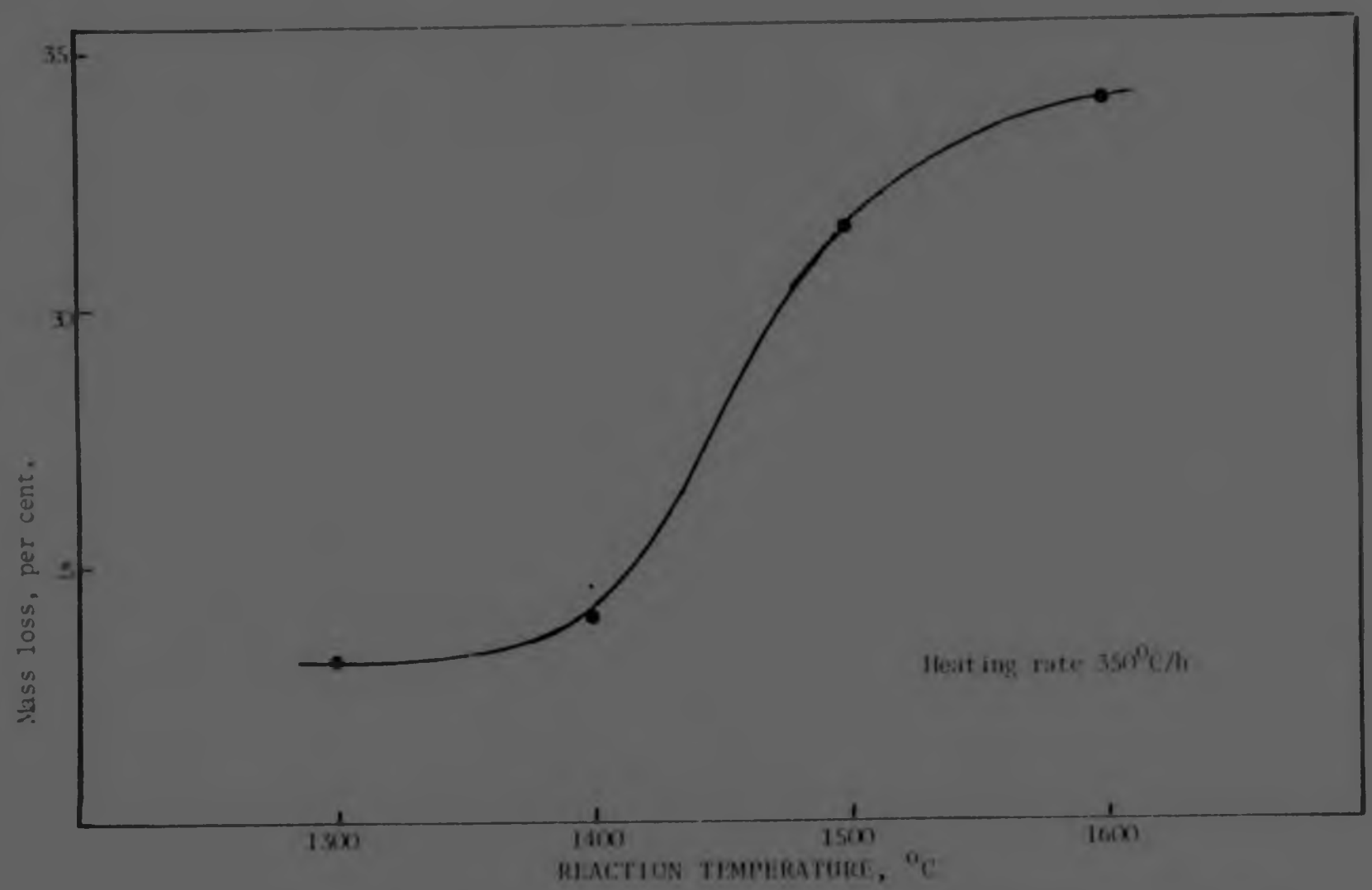


Figure 3.27 Plot of mass loss against reaction temperature for mixtures of ore and coke.

TABLE 3.9

The composition of alloys and slags formed under different experimental conditions

	Temperature of reaction °C	Retention time h	Reducing agent*	ELEMENT					
				Mn	C	Fe	Si	P	S
Alloys	1300+	0	I.C.	10,6 ± 2,66	-	89,4 ± 2,66	-	-	-
	1300+	1	I.C.	13,1 ± 8,73	-	86,6 ± 8,73	-	-	-
	1300+	2	I.C.	10,8 ± 5,22	-	89,2 ± 5,22	-	-	-
	1400	0	I.C.	51,4	6,1	41,1	0,13	-	-
	1400	1	I.C.	57,8	6,0	31,5	0,36	0,09	0,04
	1400	2	I.C.	59,6	5,5	31,9	0,30	0,09	0,05
	1400	4	I.C.	67,5	6,1	23,8	0,34	0,07	0,04
	1400	0	D.C.	48,9	5,6	41,0	0,59	0,17	0,06
	1400	2	D.C.	53,0	6,0	39,6	0,12	0,08	0,02
	1400	4	D.C.	67,1	6,1	23,0	0,45	0,09	0,13
	1500	0	I.C.	73,6	6,9	18,2	0,15	0,09	0,02
	1600	0	I.C.	79,1	7,0	11,2	0,23	0,06	0,01
	1600	1	I.C.	80,3	7,5	10,1	0,19	0,06	0,02
	1600	2	I.C.	81,3	7,4	10,5	0,05	0,06	0,01
	1600	0	D.C.	78,7	7,1	12,0	0,22	0,07	0,03
	1600	1	D.C.	80,5	7,7	10,5	0,13	0,06	0,02
	1600	2	D.C.	81,5	7,2	11,0	0,03	0,05	0,01
				MgO	Al_2O_3	SiO_2	CaO	MnO	Fe_2O_3
Slags	1600	1	I.C.	8,98	6,59	16,70	34,92	30,02	3,64
	1600	2	I.C.	11,19	8,63	22,51	45,32	10,43	2,27
	1600	1	D.C.	8,33	5,25	16,23	33,70	35,55	5,21
	1600	2	D.C.	10,64	9,30	23,54	43,95	10,41	1,41

* I.C. = Iscor coke, D.C. = Delmas coal

+ These compositions were determined by EDS area analyses and are approximate (See 2.5.1). The figures given are the means of three determinations and their standard deviation.

owing to the increased volume of alloy present. The composition of the alloys was not affected significantly by the type of reducing agent used.

The influence of retention time on the manganese content of the alloys is shown in Figure 3.29. The alloys formed at 1600°C with Iscor coke and Delmas coal had very similar compositions. The alloys formed at 1400°C with Iscor coke appeared to be richer in manganese than the corresponding alloys formed with Delmas coal for retention periods of less than 4 hours. The discrepancy could be due to errors in sampling since representative samples of the metallic component in these charges were difficult to obtain.

The composition of the slags formed at 1600°C for retention periods of 1 or 2 hours is shown in Table 3.9. A sharp reduction in the manganous oxide and ferric oxide contents occurred when the retention time at 1600°C increased from 1 to 2 hours. The slags contained lumps of partially reduced ore and dispersed grains of impure manganous oxide. The iron was present mainly as metallic globules in the slag and partially reduced lumps of ore.

3.6 Results of Additional Experiments

3.6.1. Ore heated in air

Microscopic examination of the ore samples that were heated in air showed that the ore consisted of oxide grains that were surrounded by a matrix of slag. The oxide grains had a cuboidal shape as indicated in Figure 3.30 and their size increased significantly with retention time at 1300°C.

X-ray diffraction analysis showed that the oxide was hausmannite (Mn_3O_4). The phase(s) in the slag were not identified precisely.

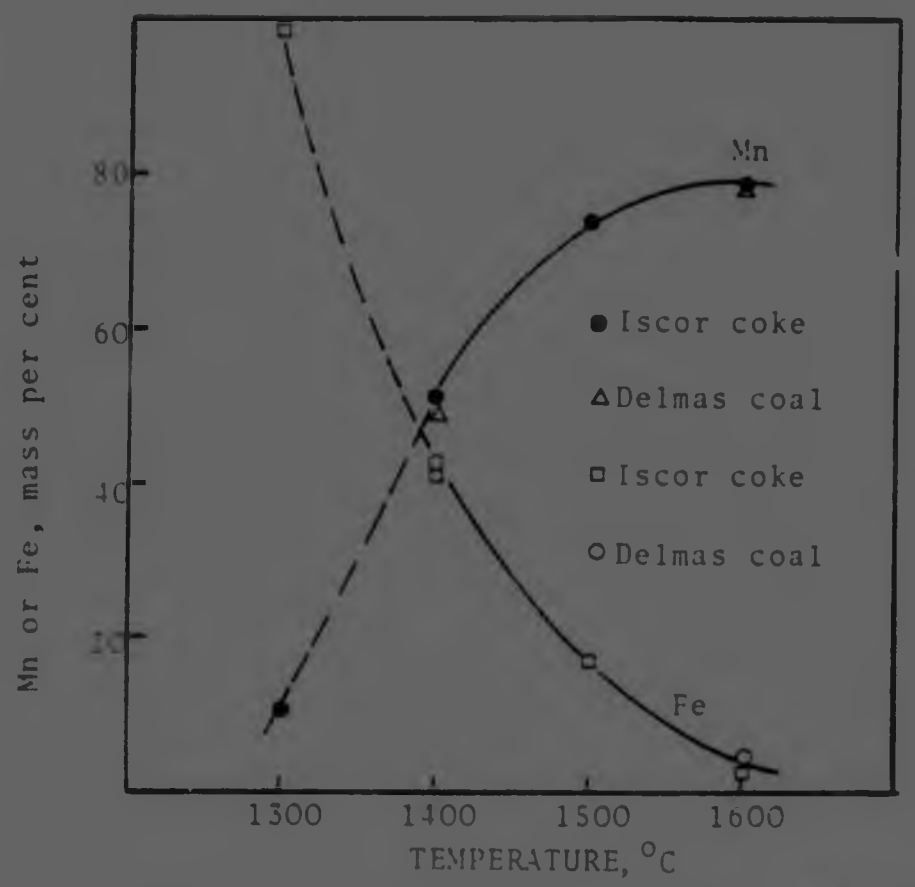


Figure 3.28 Variation of manganese and iron in the alloy on heating charges to different reaction temperatures and cooling.

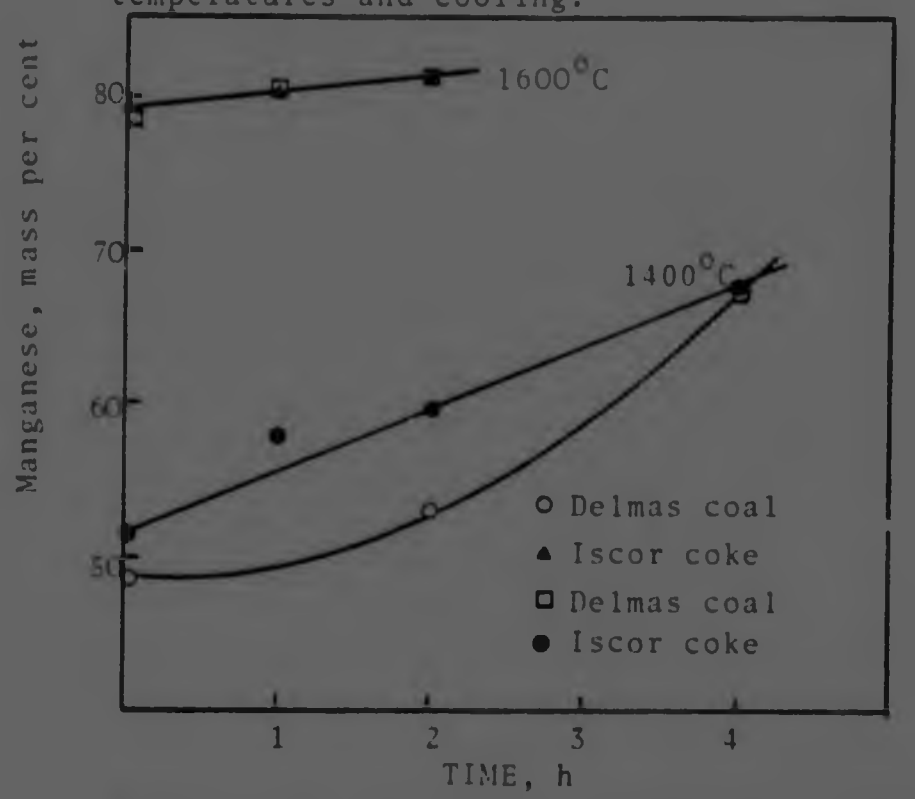


Figure 3.29 Variation in manganese content of the alloy with time at temperature.



Figure 3.30 Cuboidal grains of impure hausmannite in a matrix of slag formed by heating Mamatwan ore at 1300°C for 4 hours in air.
SEM, polished, 500X.

X-ray microanalysis showed that the hausmannite contained all the iron that was in the ore. The concentration of magnesium was approximately the same in the oxide and in the slag. The oxide also contained minor amounts of aluminium, calcium and silicon.

The slag contained mainly calcium and silicon with appreciable amounts of manganese and magnesium.

The composition of the oxide and the slag, as obtained by EDS analyses, is shown in Figures 3.31 and 3.32 respectively.

3.6.2 Ore Heated in Carbon Monoxide

The structures of the ore samples reduced at 1200°C in carbon monoxide with and without solid carbon in the furnace worktube were similar.

The phases observed were impure manganous oxide, slag and metal. Very limited fusion occurred and the amount of metal varied between ore particles and from point ot point in the same particle, owing to differences in the chemical composition of the ore particles. The colour of the ore changed in places to a light green.

The structure of an ore particle heated in carbon monoxide at 1200°C for 1 hour in the presence of graphite is shown in Figure 3.33. The composition of the metallic phase was investigated by EDS analyses and was shown to average (in mass per cent) 2,0 calcium, 2,0 manganese, and 96,0 iron. Small amounts of calcium may have been present in the metallic phase in the form of inclusions. It is evident from thermodynamic considerations that calcium oxide could not have been reduced under the conditions used.

Sectioning of the crucible containing ore particles between 4,7 and 6,35 mm that had been heated in carbon monoxide, without graphite in the worktube of the furnace, and had been maintained at 1450°C for 6 hours showed the following :

1. The ore formed a coherent mass and individual particles of ore became indistinguishable due to fusion and formation of slag. The charge attained a brilliant green colour and appreciable

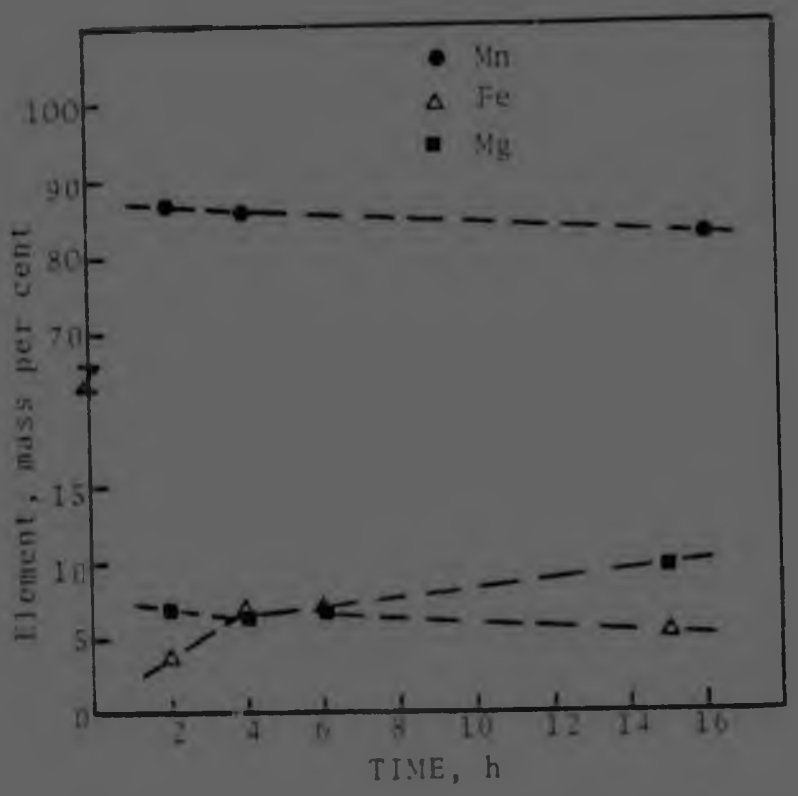


Figure 3.31 EDS analyses of the oxide formed by the heating of ore at 1300°C in air.

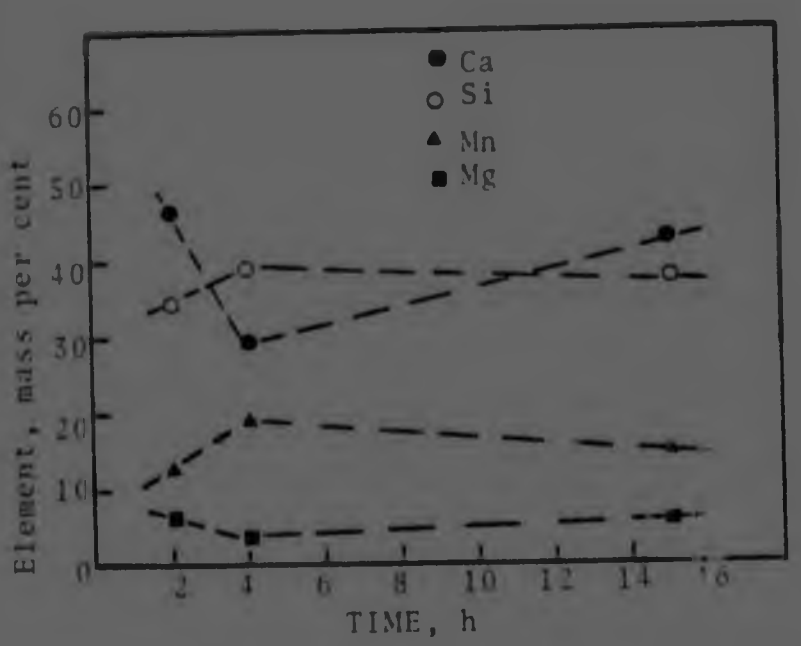


Figure 3.32 EDS analyses of the slag formed by the heating of ore at 1300°C in air.

reaction occurred between it and the alumina crucible.

2. Considerable metallization took place and the metallic particles showed a distinct tendency to migrate towards the crucible wall where they coalesced to form bigger particles. Etching in 3 per cent nitric acid in alcohol and hardness testing showed that the metallic component etched unevenly and extremely slowly and had a structure (Figure 3.34) and hardness (87VPN) similar to those of α-iron.

3. The grains of impure manganous oxide were rounded and extremely coarse as indicated in Figure 3.34. It can be seen that after etching some grains appeared almost black while others were light grey. Reaction rims round the grains are apparent. Oxide in the form of dendrites was found near the crucible wall indicating that precipitation of oxide from the molten slag occurred during cooling (Figure 3.35).

It can be seen from Figure 3.35 that the etching characteristics of the dendrites were different to those of the rounded grains and similar to those of the reaction rims. Scanning electron microscopy revealed that the slag surrounding the dendrites and the rounded grains was in relief showing that the etchant attacked both the dendrites and the grains but in different ways. Polishing effects can be excluded since the oxide polishes in relief due to its higher hardness.

The structure of the interior of an oxide grain is shown in Figure 3.36. It can be seen that the grain was attacked differentially to reveal clusters of slowly dissolving material in the matrix which appeared to consist of a regular network of thin planes and cementing material. The rate of

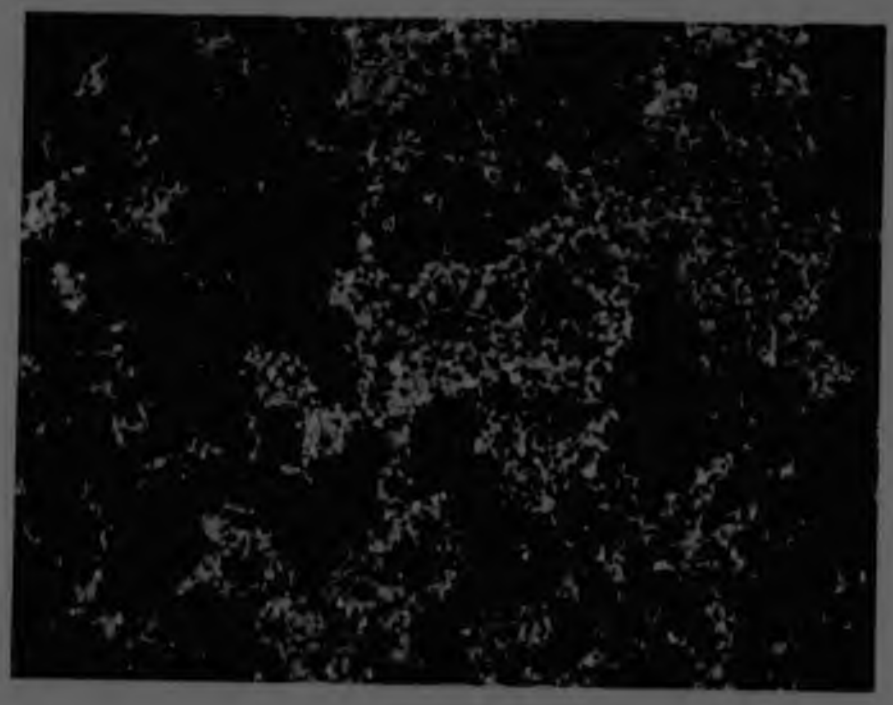


Figure 3.33 The structure of an ore particle that was partially reduced at 1200°C in carbon monoxide. Rounded grains of impure manganous oxide (light grey) and metallic particles (bright) are surrounded by a thin film of slag. Porosity appears black.
Polished, 120X.



Figure 3.34 Rounded grains of oxide and metallic particles in a slag matrix formed by heating ore at 1450°C for 6 hours in carbon monoxide.
Etched 3 per cent HNO_3 in alcohol 400X.



Figure 3.35 Dendrites and rounded grains of impure manganous oxide in the slag matrix near the wall of the alumina crucible. Metallic particles appear bright and grains of a complex mixture of manganese, aluminium and magnesium oxides appear dark grey.
Etched 2 per cent HCl in alcohol, 270X, enlarged 45 per cent.

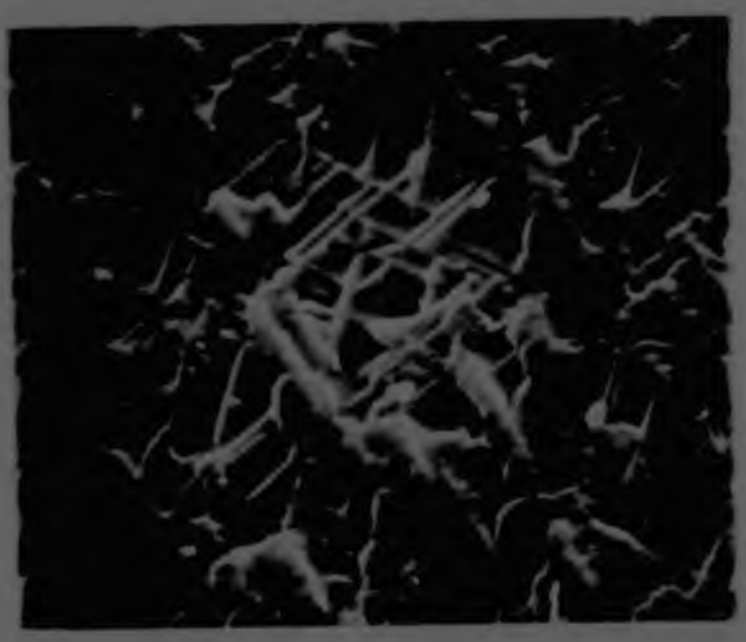


Figure 3.36 The structure of a grain of oxide after reaction at 1450°C for 6 hours in carbon monoxide.
SEM, etched 2 per cent HCl in alcohol, 10000X.

dissolution of the cementing material was the highest while the regular planes dissolved at an intermediate rate between that of the cementing material and the clusters. The clusters showed a definite orientation in the matrix and it appears that the differences in the reflectivity of oxide grains (Figure 3.34) were due to orientation effects. It is of interest to note that metallic particles were not observed in the centre of oxide grains.

The metallic phase, the slag, and the impure manganous oxide were analysed bythe EDS method. The results obtained showed a high degree of consistency, indicating long-range diffusion of species. The slag contained a high proportion of alumina owing to reaction with the crucible. The composion of the metallic phase (in mass per cent) was 97,8 iron and 1,3 manganese. Minor amounts of aluminium, silicon and calcium were also detected. The composition of the impure manganous oxide was 85,6 per cent by mass manganese, 12,6 magnesium, 1,5 calcium and 0,3 silicon. The composition of the dendrites of oxide was not significantly different from that of the rounded grains. The slag contained 46,0 per cent by mass aluminium, 26,4 calcium, 9,8 silicon and 17,9 manganese.

3.6.3 Ore Heated in Graphite Crucible.

Sectioning of the crucible and its contents showed that the final volume was about 44 per cent of the original, and that the ore had formed a coherent, porous mass because of extensive fusion. It is important to note here, that charges of ore and reducing agent held at 1400°C for 4 hours showed only a limited amount of fusion (Figure 3.3). Also charges heated to 1600°C and cooled did not form a coherent mass (Figure 3.4). A slab of 'sintered ore' extending to a depth of about 30mm from the side of the graphite crucible, was taken from a vertical section through the centre of the charge.

The section (Figure 3.37) was green to a depth of about 10 mm, and metallic particles were found to a maximum depth of about 15mm. The hardness of the metal on the surface of the section was about 1100VPN, and that of metal 2 mm away from the surface was about 100VPN.

The grains of impure manganous oxide in the green zone were finer than those away from the edge of the section. Green haloes were observed with the optical microscope round grains of oxide only in the metallized region. In some areas of the non-metallized region the grains of oxide showed rims and needles or areas of a different phase as shown in Figure 3.38. These rims were of a distinctly different nature to those described earlier in that they had precipitated from the oxide during cooling and a definite interface existed between the oxide grains and the rims. X-ray microanalysis showed that the rims consisted of a mixed ferrite of calcium and manganese. Microanalyses carried out on grains of oxide at distances of about 3 and 25 mm from the edge of the section showed that the oxide in both regions contained appreciable amounts of magnesium and smaller amounts of calcium. These anlyses did not indicate a definite difference in the composition of the oxide from the two regions.

The slag in the metallized region was green while that away from the edge of the region was black. An interface existed between the two types of slag, evidenced by differences in reflectivity. The slag contained mainly calcium, silicon and manganese with smaller amounts of magnesium, aluminium and potassium. In the non-metallized region iron was detected in the oxide grains only.

Evidence for the dissolution of manganous oxide in the slag and its precipitation during cooling was found in both regions. Figure 3.39 shows a section through the metallized region. Many minute grains of oxide can be seen in the slag. Some of these grains are elongated and appear to have precipitated at the boundaries of the slag grains.

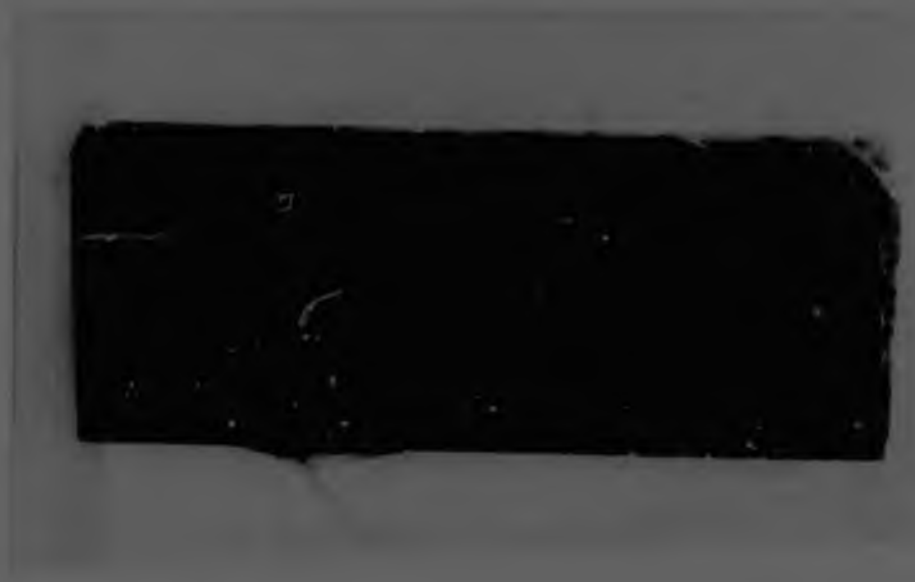


Figure 3.37 Section of sinter formed by heating a 6 kg charge of ore in a graphite crucible.
Polished, 1,6X.

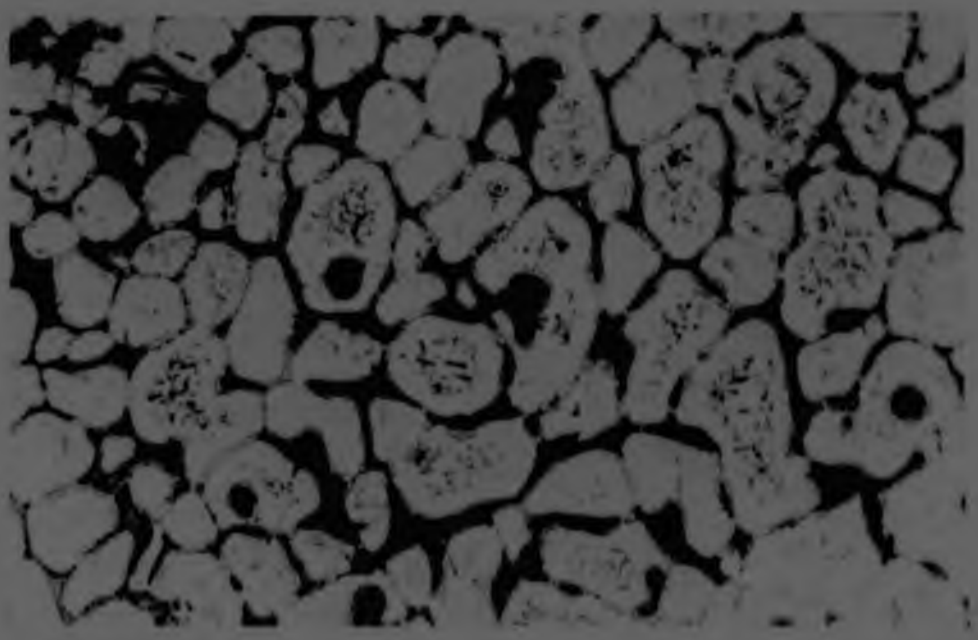


Figure 3.38 Precipitation of a calcium-manganese ferrite on the periphery and in the interior of grains of oxide in a matrix of slag.
Etched 2 per cent HCl in alcohol, 120X, enlarged 45 per cent.



Figure 3.39 Precipitation of fine grains of oxide (light grey) in a slag matrix (dark grey). Polished 60X, enlarged 33 per cent.

The nature of the slag and of the impure oxide, from the two regions, was further investigated by X-ray diffraction analyses, samples being taken from the top 5 mm of the section and from between 5 to 20 mm below the surface.

The X-ray tracings of the two samples showed significant differences in the positions of the peaks of the oxide and the slag.

The exact position of the oxide peaks was determined by scanning at steps of 0,05° (2θ) and counting over a period of 10s. The position that gave the highest count was taken as being the apex of the peak. This method established the position of the peaks within 0,025° (2θ) assuming that errors from other sources [106] were negligible. The maximum error in d-spacings introduced by an error of 0,025° 2θ in the position of a peak is about 0,08 per cent. This error decreases rapidly with increasing angle. The d-spacings of the oxide peaks are shown in Table 3.10 and are compared with the d-spacings of 'pure MnO'.

The lattice parameter of the oxide from the two regions was determined from the last three d-spacings shown in Table 3.10 by using the formula [106]

$$a_o = d\sqrt{h^2 + k^2 + l^2} \quad . \quad . \quad . \quad 3.1$$

where a_o is the lattice parameter and
d is the spacing between planes with indices h k l.

The lattice parameter was determined for the three different d-spacings in each case and plotted against $\cos^2\theta$. A straight line was fitted to the points by the method of least squares and extrapolated to $\cos^2\theta = 0$, the intercept giving a_o. This method [106] minimises the errors in a_o.

TABLE 3.10

Comparison of X-ray diffraction data for manganous oxide from different sources

d-spacings for pure MnO*	I/I_1 for MnO	d-spacings for MnO in metallized region	Relative height of peak for MnO	d-spacings for MnO in non-metallized region	Relative height of peaks for MnO
2,568	60	2,565	52	2,576	30
2,223	100	2,220	100	2,233	100
1,571	60	1,569	40	1,579	25
1,340	20	1,338	20	1,343	15
1,283	14	1,281	15	1,287	10
1,112	12	1,109	5	1,116	10

* Data from ASTM card No. 7-230

The relationship between a_o and $\cos^2\theta$ for the sample from the metallized region was :

$$a_o = 4,430 + 0,0111 \cos^2\theta. \ \text{Å} \quad . \quad . \quad 3.3$$

For the sample from the non-metallized region the relationship was :

$$a_o = 4,498 - 0,058 \cos^2\theta. \ \text{Å} \quad . \quad . \quad 3.4$$

The method described above for the determination of d-spacings and lattice parameters is not normally used [106] because its accuracy is relatively low. The accuracy of the method was assessed by determining the lattice parameter of pure MnO obtained by the oxidation of volatilized manganese and of chemically pure MgO.

The relationship obtained for MnO was :

$$a_o = 4,452 - 0,009 \cos^2\theta. \ \text{Å} \quad . \quad . \quad 3.5$$

The relationship for MgO was :

$$a_o = 4,216 + 0,022 \cos^2\theta. \ \text{Å} \quad . \quad . \quad 3.6$$

The lattice parameters are shown in Table 3.11 together with ASTM data for CaO, MgO and FeO. It can be seen that the values of a_o may contain an error of about 0,7 per cent. It is clear however that the lattice parameter of the oxide from the two regions is different.

TABLE 3.11

The lattice parameter and crystal structure of some oxides

Oxide	Source of Oxide	Lattice Parameter Å	Crystal Structure
MnO	From metallised region	4,430	cubic
MnO	From non-metallised region	4,498	cubic
MnO	From volatilised Mn	4,452	cubic
MgO	Chemically pure	4,216	cubic
MnO	ASTM card 7-230	4,445	cubic
MgO	ASTM card 4-829	4,213	cubic
FeO	ASTM card 6-617	4,307	cubic
CaO	ASTM card 4-777	4,811	cubic

The positions of the major peaks of the slag were determined by scanning at steps of $0{,}05^{o}$ 2θ and counting for 10s at each step. Plots of counts against angle 2θ are shown in Figure 3.40. The slag from the non-metallized region was very similar to calcium orthosilicate (α' - Ca_2SiO_4). The slag from the metallized region showed a greater deviation from calcium orthosilicate although the tracings of Figure 3.40 show some similarity.

The major constituent of the metallic phase was α-iron. Minor amounts of carbides were present also.

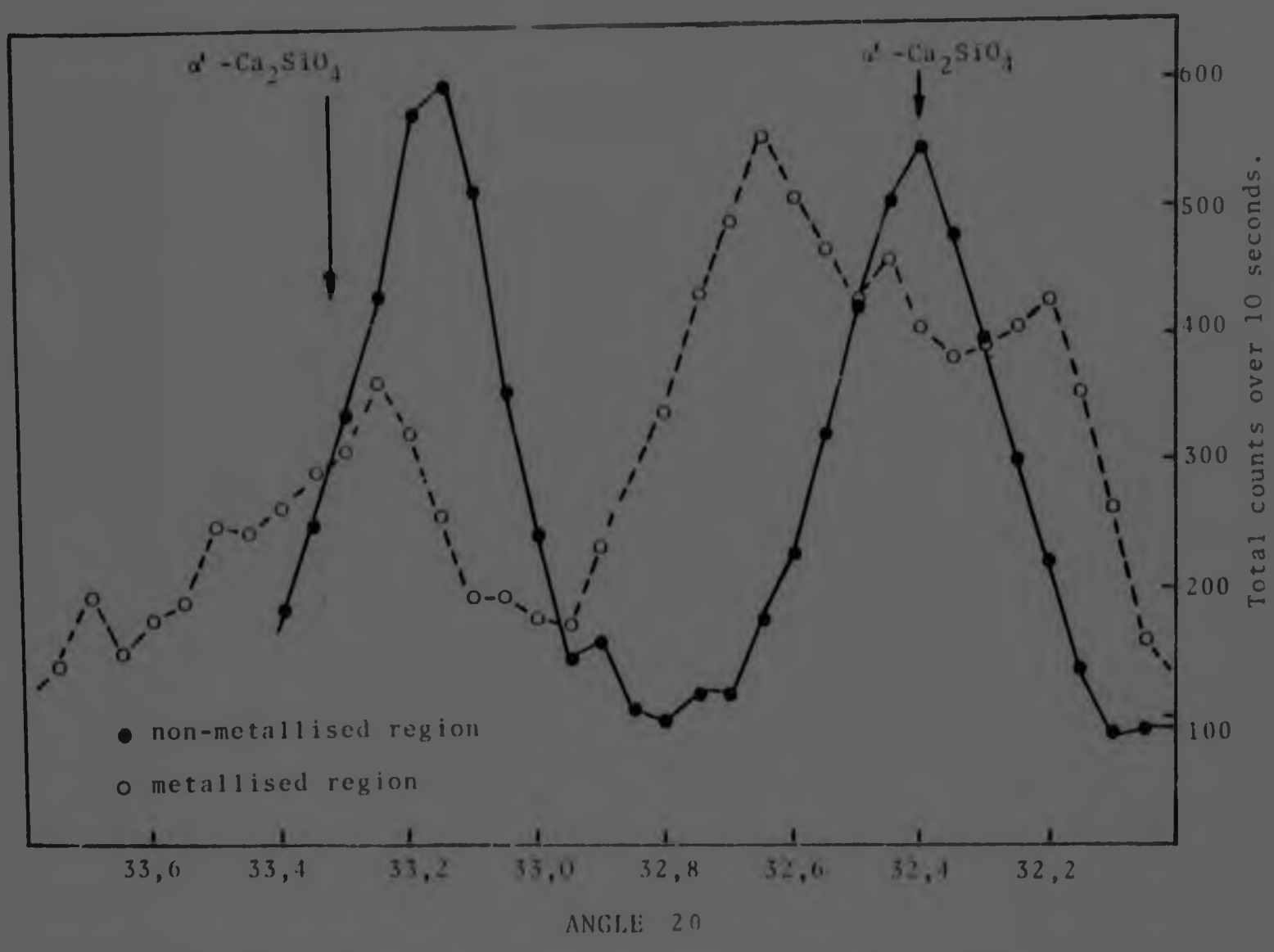


Figure 3.40 Comparison of the diffraction patterns of the slag from the metallised and non-metallised regions. The positions of the major peaks of calcium orthosilicate are indicated.

CHAPTER 4

4.0 DISCUSSION

4.1 Some Practical Considerations on the Use of Mamatwan Ore in Submerged-arc Furnaces

The mineralogy of Mamatwan ore,[2, 8, 56] the mineralogical changes which occur in oxidizing[2, 8] and reducing atmospheres[2] and the rate and mechanisms[3] of its reduction by solid carbon have been considered by various investigators while the physicochemical processes that occur in the ore at temperatures greater than 1000°C have received little consideration.

It has been seen that sintering and consolidation of the charge are much more pronounced when the ore is heated in the absence of a reducing agent (compare Figures 3.4 and 3.37). The reasons for these differences may be as follows:

a) In a mixture of ore and reducing agent, the ore particles are physically separated from each other by the reducing agent and therefore a more open structure results upon heating to high temperatures. Evidence is presented in Chapter 5 (Figure 5.5) which shows that the particles of reducing agent hinder the subsidence of the charge probably by forming a type of super-structure throughout the charge.

b) In the absence of a reducing agent, reduction of the ferrous oxide in the ore does not take place. The incorporation of this oxide in the slag would result in a slag of lower melting point and viscosity which would aid the relative movement of ore particles.

In the submerged-arc furnace, segregation of the ore and the reducing agent are bound to occur due to differences in the specific gravity of the components and due to the presence of the cone of fast descending burden around the electrode. Segregation of the reducing agent towards the wall of a ferro-manganese furnace was observed by Ozeki et al [88]. Muller [82] found that an uneven distribution of the charge around the electrode of an experimental furnace resulted in the segregation of reducing agent in the cone of fast descending material which manifested itself in the form of a distorted coke bed underneath the electrode.

The slow rate of movement of the burden in the furnace [14] can be taken as being equivalent to the retention of elements of burden at a series of temperatures for prolonged periods of time. In a segregated charge this would result in extensive consolidation and reduced gas permeability. The gaseous products of reduction generated underneath the electrode tip escape mostly through the cone of fast descending material which may have a diameter only slightly greater than that of the electrode at the level of the electrode tip (see Chapter 6). Any consolidation of the charge at this level would hinder the passage of gaseous products and cause an increase of pressure underneath the electrode. This could eventually result in a furnace eruption which is known to occur [1, 109].

From the above considerations it is clear that steps should be taken to minimise the segregation of charge components particularly such segregation as may occur due to the common practice of charging the furnace by use of a number [14] of chutes located round the electrodes. It is probable that the use of charging shafts concentric with each electrode might reduce segregation.

Van der Walt and Gericke [1] have pointed out that current paths in 48MVA furnaces may be controlled to some extent by charging burden of a higher or lower conductivity in selected furnace locations.

The results of this investigation show that the control of current paths should not be attempted by altering the stoichiometry of the charge, that is, by adding more or less of the reducing agent in different parts of the furnace. A charge of variable stoichiometry will result in a primary slag of variable composition and viscocity, and the flow of the burden will be altered in an unpredictable way.

Reservations concerning the suitability of Mamatwan ore for use in the submerged-arc furnace have been based on the high gangue content of the ore [7]. In his investigation of the mineralogy of natural and heat treated samples of Mamatwan ore, De Villiers [56] also considered possible methods of enriching the ore by removing gangue minerals. From the mode of occurrence of the metallic and gangue minerals in, and the extremely fine texture of the natural ore, De Villiers concluded that such enrichment would not be economical.

In the present study it has been shown that the structure of the ore can be altered considerably by treatment at temperatures of 1200°C or higher, in reducing or oxidising atmospheres. However, the texture of the "altered ore" still remains very fine and elimination of the gangue, which now occurs as a slag, would still not be feasible on a large scale. Since the slag occurs as the continuous phase, its removal would result in a powder product consisting of grains of oxide which would require agglomeration before use in a submerged-arc furnace. It appears therefore that the only practical means whereby Mamatwan ore can be upgraded is by the removal of ore lumps rich in gangue minerals. Otherwise the required furnace characteristics can be obtained by blending Mamatwan ore with an ore of higher grade as has been the practice in industry.

Sintering of Mamatwan ore fines, (<25mm) has been tried by Featherstone [7] in an attempt to improve the permeability of the burden to gases and to increase alloy production. He reported that the strength of the sinter was very low and that excessive quantities of fines were generated during handling of the sinter on the plant. Featherstone does not

report the conditions used for sintering. In this study it is shown that an extremely strong sintered product can be obtained (Figure 3.37) provided a high enough temperature is attained. From Figure 5.5 (Curve I) it is estimated that a temperature of about 1400°C would have to be used for appreciable sintering to occur in a reasonably short period of time. The statement that Mamatwan ore "begins to melt" at 1450°C and that it is "completely molten" at 1550°C is ambiguous. The indications are (Figure 5.5) that liquid begins to form at temperatures of the order of 1000 to 1200°C. It has been shown however (Figure 3.2) that the ore particles retain their basic character even after being held at 1600°C for 1 hour.

The conditions necessary for the agglomeration of ore fines by sintering must be such that the gangue minerals in the ore are completely reacted to form a slag which will hold ore particles together. At low temperatures some disintegration of the ore will occur during sintering due to the amount and mode of occurrence of gangue minerals. Thus, the dissociation of veins of calcite and of dolomite particles will result in the splitting of ore particles and the generation of fines. Agglomeration of ore particles will take place only when sufficient time at temperature is allowed for the silica that is liberated from the braunite to react with the lime to form a liquid slag. Reactions leading to the formation of slag are considered in more detail in Section 4.3.

4.2 Reduction of Higher Oxides to Manganous Oxide

It has been shown (Section 1.2.1) that the reduction of the higher oxides of manganese by carbon monoxide is very favourable thermodynamically and will occur at temperatures much lower than those required for the thermal dissociation of the oxides. Reduction of these oxides can be achieved with very low concentrations (10 per cent) of carbon monoxide in the atmosphere [23].

The concentration of carbon monoxide in equilibrium with carbon dioxide and solid carbon at a total pressure of 1 atmosphere, rises steeply from about 10 per cent at 500°C to about 90 per cent at 800°C as predicted by the equilibrium constant of the Boudouard reaction [110]. Equilibrium conditions were probably never attained during the SCICE experiments. However, a high concentration of carbon monoxide in the atmosphere must have been attained since metallic iron was formed by heating the charge to 1300°C and cooling.

The kinetics of solid-solid reactions are unfavourable and such reactions would be extremely slow in a system such as the one used in this work, due to the coarse size of the reactants. Therefore reduction of the higher oxides in the ore took place by carbon monoxide. Evidence for this was supplied by the randomly distributed metallic nuclei throughout the particles of ore. The gaseous reduction of the higher oxides in the ore is greatly facilitated by the porosity generated upon decomposition of the finely dispersed carbonate particles (Figure 3.1). The reduction of the higher oxides may be described by the following reactions :

$$3Mn_2O_3 + CO = 2Mn_3O_4 + CO_2 \quad \cdot \quad \cdot \quad \cdot \quad 4.1$$

$$Mn_3O_4 + CO = 3MnO + CO_2 \quad \cdot \quad \cdot \quad \cdot \quad 4.2$$

During the smelting of Mamatwan ore the reduction of the higher oxides to manganous oxide would occur in the higher regions of the furnace bowl. The rate of movement of the burden [14] is very low, even in the cone of fast descending material next to the electrode. Under normal operating conditions the probability of encountering any of the higher oxides near the electrode tip is very low. Pentz [2] considers that reduction of the higher oxides takes place over a very limited height of the furnace bowl and in positions where the temperature is greater than 1000°C.

This outlook is very conservative in view of the fact that an element of charge in the cone of fast descending material can take more than 15h to reach the electrode tip [14] and that the gaseous reduction of the higher oxides to MnO in braunitic ores is complete at 800°C [23]. The above considerations show that, from the viewpoint of power consumption in an industrial furnace, no benefit will be accrued by pre-calcining the ore. A similar conclusion was reached by Tulstogusov [29] from a consideration of the exothermic nature of the reactions leading to the reduction of the higher manganese oxides.

The manganous oxide occurred as more or less rounded grains in a matrix of slag indicating that a nucleation and growth mechanism was operative. The mode of occurrence of a solid oxide in liquid slag is related to the surface energies of the liquid, the solid and the solid-liquid interface [111]. The amount and type of gangue oxides varied in different ore particles (Table 3.1) and it appears that the differences in size and morphology of the oxide grains were due to the varied composition and quantity of slag in different ore particles.

X-ray microanalysis (Table 3.7) showed that more magnesium oxide was in solution in the manganous oxide than in the slag. It is known [20] that magnesium oxide, calcium oxide and iron oxide are soluble in manganous oxide in all proportions. The preferential dissolution of magnesium oxide by manganous oxide was probably due to the more favourable size factor for this reaction (Table 3.11). Another possible reason may be the fact that magnesium oxide forms less stable compounds with silica than does calcium oxide [108].

The magnesium oxide can be expected to decrease the reducibility of manganous oxide by decreasing its activity in the impure oxide.

The microscopic examination of samples showed that the grains of oxide dissolved in the slag and that re-precipitation of at least some of the dissolved oxide took place during cooling (Figures 3.9, 3.11, 3.39).

The increased magnesium oxide content detected in grains of the impure oxide during the final stages of reduction could be due to the gradual dissolution of manganous oxide by the slag or the simultaneous re-precipitation of manganous and magnesium oxides from the slag. A progressive increase in the amount of magnesium oxide in manganous oxide would lead to a rapid increase in its melting point as predicted by the MnO-MgO phase diagram [20]. This would impair the kinetics of reduction of manganous oxide by solid reducing agent or carbon dissolved in the alloy in a submerged-arc furnace since physical contact between the two reactants would be necessary.

The melting point of manganous oxide can vary by several hundred degrees depending on the partial pressure of oxygen in the atmosphere, as indicated by the Mn-O phase diagram presented by Hed et al [107]. It is not entirely certain that the melting point of stoichiometric manganous oxide has been accurately determined yet. However, a value of about 1800°C can be deduced from various sources [20, 107, 112]. The incorporation of 10 per cent magnesium oxide would push up the melting point to over 2000°C [20]. Thus, the melting of impure manganous oxide in a furnace would be possible only in the immediate vicinity of the electrode tips.

It is well known that manganous oxide is a non-stoichiometric compound, possessing an excess of oxygen ions in the lattice. Electrical neutrality is achieved due to the presence of Mn^{3+} ions in the lattice. Klingsberg et al [17] have suggested that manganous oxide may also occur as an oxygen depleted compound. However there appears to be doubt as to whether these investigators achieved their aim of preparing samples ranging in stoichiometry between $MnO_{0,80}$ to $MnO_{1,15}$.

Changes in the stoichiometry of manganous oxide are associated with a change in the colour of the oxide from black to green as the stoichiometric composition is approached or actually achieved. The exact composition of the oxide at the point of the colour change is not known precisely.

Davies and Richardson [27] observed the colour change in manganous oxide and measured the extent to which this oxide departs from the stoichiometric composition as the partial pressure of oxygen is raised from 10^{-8} or 10^{-9} kPa to 10^{-2} kPa at temperatures between 1500 and 1600°C.

In the SCICE experiments, the colour of the ore changed to green at temperatures between 1300 and 1600°C while nuclei of iron appeared throughout the ore particles. The equilibrium partial pressure of oxygen for the reduction of ferrous oxide to iron at temperatures of 1300 and 1600°C may be calculated from the reaction :

$$FeO_{(s)} = Fe_{(s)} + \tfrac{1}{2}O_{2(g)} \quad . \quad . \quad . \quad 4.3$$

$$\Delta G^{o} = 259617 - 62,6\ T\ Jmol^{-1} (298\text{-}1642K)$$

On the assumption that iron and ferrous oxide occur as pure substances in the system the equilibrium constant, K, for reaction 4.3 will be given by

$$K_{4.3} = P^{\frac{1}{2}}_{O_2}$$

From the relationship,

$$\Delta G^{o} = -RT \ln K \quad . \quad . \quad . \quad 4.4$$

the partial pressure of oxygen in the system at 1300°C may be calculated as $1,98 \times 10^{-9}$ kPa and at 1600°C as $5,73 \times 10^{-7}$ kPa. Thus, the value of oxygen partial pressure in the system must have been lower than $1,98 \times 10^{-9}$ and $5,73 \times 10^{-7}$ kPa at temperatures of 1300 and 1600°C respectively for metallic iron to form in the ore. These values for the partial pressure of oxygen are consistent with the formation of stoichiometric manganous oxide [27].

The behaviour of the grains of oxide towards the etchant is of interest.

From Figures 3.12 and 3.13 it can be seen that the slag matrix was rapidly attacked while different parts of the oxide grains were attacked at different rates. The rapid attack of the slag made it impossible to determine whether the reaction rim surrounding the oxide grains was attacked at all or whether it dissolved evenly over the entire surface. The obvious conclusion to be drawn from the appearance of the etched grains is that the differential rate of attack was due to differences in the chemical composition of different parts of the grains. X-ray microanalyses did not show a definite difference between the composition of grains that etched and grains that appeared not to be attacked. Previous investigators [17, 18, 27] point out that precipitation of some Mn_3O_4 may take place in the oxide during cooling. Klingsberg and Roy [17] found this to occur when the O:Mn ratio exceeded 1,10. It is not certain whether precipitation of Mn_3O_4 occurred in the samples under consideration, due to re-oxidation during cooling, or whether the differences observed were due to other factors such as the presence of impurities in the oxide.

The appearance of grains of oxide formed by reduction in carbon monoxide (Figure 3.33) was similar to that of grains formed under SCICE conditions. The slag that formed by reacting the ore in an alumina crucible at 1450°C appeared not to be attacked by the etchant. Scanning electron microscopy showed that both the reaction rim and the dendrites of manganous oxide were attacked by the etchant leaving the slag in relief. This indicated similarities between the dendrites which originated from manganous oxide that had dissolved in the slag and the reaction rim which appeared to be an integral part of the oxide grains.

The d-spacings of the oxide formed under SCICE conditions between 1300 and 1600°C and those of the green oxide formed by heating the ore in a graphite crucible (Table 3.10) were lower than the d-spacings found by Klingsberg and Roy [17] and those given in ASTM card 7-230. The discrepancy was probably

due to the presence of magnesium oxide in the manganous oxide. From Table 3.11 it can be seen that the lattice parameter of magnesium and ferrous oxides is lower than that of green manganous oxide. From Vegard's rule it follows that the incorporation of either of these oxides in the MnO lattice will reduce the lattice parameter of the resultant impure oxide.

The difference in lattice parameter between black and green manganous oxide (Table 3.11) were probably due to variations in the concentration of solute in the oxide. Klingsberg and Roy [17] found no systematic variation in the lattice parameter of manganous oxide for nominal compositions ranging between $MnO_{0.80}$ and $MnO_{1.15}$. A similar observation was made by Davies and Richardson [27] for manganous oxide ranging in composition between MnO and $MnO_{1.045}$. Those authors attributed the phenomenon to the precipitation of Mn_3O_4 in the MnO lattice but did not indicate whether the presence of Mn_3O_4 was actually established.

The X-ray tracings of green and black manganous oxide did not show Mn_3O_4 as a constituent phase. It appears therefore that the lower lattice parameter of the green manganous oxide was due to a higher concentration of magnesium oxide in the lattice. This may have been the result of the dissolution of a higher proportion of Mn^{2+} ions from the oxide grains by the slag. The differences in X-ray patterns of the slags from the metallized and non-metallized regions suggest that the concentrations of Mn^{2+} ions in the two slags were different.

It is obvious that the nature of the processes that take place in the grains of manganous oxide during reduction should be subjected to a much more detailed investigation. However the nature of this study and the numerous variables involved did not warrant a more thorough examination of these processes.

4.3 Reactions to Form the Slag

The softening of the SCICE charges at about 1100°C and the rapid reduction in volume at temperatures between 1000 and 1200°C (Figure 5.5) indicate that liquid started to form at about 1000°C.

From a consideration of the composition of the ore and the relevant phase diagrams [113] it can be established that eutectics with a melting point well below 1000°C can form in the systems K_2O-SiO_2, K_2O-FeO-SiO_2 and K_2O-CaO-SiO_2. The formation of the compound $K_2O.SiO_2$ is very favourable thermodynamically [108] and this was probably the first liquid phase that formed. The amount of potassium oxide in the ore is very small and the rapid reduction in the volume of the charge was probably not related to the formation of liquid $K_2O.SiO_2$. The rapid reduction in volume probably occurred when sufficient liquid had formed to wet the grains of the impure manganous oxide. An increase in the amount of slag could take place readily by the incorporation of calcium oxide or iron oxide into the potassium silicate.

In the systems FeO-CaO and FeO-CaO-SiO_2, eutectics form that have a melting point of 1100°C. Eutectics with a melting point between 1175 and 1200°C form in the systems, FeO-SiO_2, FeO-MnO-SiO_2 and MnO-CaO-SiO_2 [113].

At temperatures greater than 1000°C ferrous oxide will be reduced by carbon monoxide to metallic iron according to the reaction

$$FeO + CO = Fe + CO_2 \quad . \quad . \quad . \quad . \quad 4.5$$

The equilibrium constant for reaction 4.5 at 1000 and 1300°C may be calculated as 0,466 and 0,510 respectively. These values, which may be used as simple guidelines, indicate that there will be an appreciable tendency for the iron oxide to be reduced to metallic iron as the furnace gas is nearly pure CO.

The absence of iron from the slag and from the unreduced manganous oxide, upon reacting at 1400°C or higher (Table 3.7) indicates that practically all the iron oxide was reduced under these conditions. It follows therefore that the slag formed by heating to 1400°C or higher should consist mainly of MnO, CaO and SiO_2. Table 3.7 shows that this was in fact the case. The variations in the proportions of the different components can be attributed to the analytical method used and the fact that the slag consisted of a mixture of phases. The variations in the composition of different ore particles would also have a significant effect on the phases formed, since the ore particles did not disintegrate in the slag. Thus, particles with a high initial CaO to SiO_2 ratio would result in an increased solubility of MnO in the slag.

The phases in the slag were not identified precisely due to their complex nature. Thermodynamic data [108] shows that mono-, di- or tricalcium silicate should form in preference to silicates of MnO and MgO. However, the kinetics of formation of these compounds are unfavourable due to their relatively high melting point. The lowest melting eutectic in the CaO-SiO_2 system contains only about 37 per cent CaO and has a melting point of 1436°C [113]. Therefore the slag present at temperatures below 1436°C must have been a manganese silicate which probably contained some lime. The formation of a magnesium silicate is more favourable thermodynamically [108], but kinetically it is unfavourable due to the high melting point of these silicates [113].

The appearance of loose particles of lime in charges reacted at 1300°C indicates that this component was in excess and dissolved gradually in the slag as the temperature increased. The strong affinity of lime for silica probably caused the displacement of manganous oxide from the slag that formed originally.

The 1:1, 2:1 and 3:1 ratio of CaO to SiO_2 necessary for the formation of mono-, di- and tricalcium silicate would not be satisfied in all ore particles due to the enormous variations in the calcite to braunite ratio in different ore particles (Table 3.1a). Therefore the phases in different ore particles could well be expected to differ or vary in composition. The excess lime in ore particles would go into solution in the unreduced manganous oxide while a deficiency of lime would cause the dissolution of manganous oxide into the slag.

4.4 Reactions to Form the Alloy

The reduction of Mamatwan ore was a continuous process although the dominant reaction mechanism changed at different stages due to the physical and chemical changes that took place in the charge. For convenience, the reactions leading to the formation of the alloy will be discussed under three headings.

4.4.1 Nucleation of Metal

The mode of occurrence of the metallic nuclei in particles of ore and the similar microstructures observed in ore particles reduced under SCICE conditions and in carbon monoxide indicated that reduction of the iron oxide took place by reaction with carbon monoxide. The iron oxide was in solution in the Mn_3O_4 (Figure 3.31) and later in the MnO (Figure 3.38). Reduction of wustite by carbon monoxide proceeds at an appreciable rate at temperatures of about 1000°C or higher. Since the iron oxide was in solution its reduction probably took place at an appreciable at temperatures greater than 1000°C. It has been seen that quantities of a mixed ferrite were detected in ore reacted at 1400°C.

The reduction of iron oxide was accompanied by the formation of slag and a rapid decrease in the volume of the ore (Figure 5.5). Slag formation and the increased density of the ore reduced its permeability to carbon monoxide and carburization of the metallic nuclei in the interior of ore particles did not occur. This was evident from the single phase observed in these nuclei and from their hardness (Table 3.6).

The manganese content and the hardness of the metallic nuclei formed in the SCICE charges were higher than those formed in the absence of a solid reducing agent. This indicated that the reduction of MnO in the interior of ore particles proceeded further when solid reducing agent was present. The manganese content of metallic nuclei formed under SCICE conditions (Table 3.7) showed significant variations due to differences in the size of the nuclei analysed. It is shown at a later stage (Figure 6.30) that an increase in the size of the nuclei was accompanied by a significant increase in their manganese content. It is important to note that iron was present in all the nuclei that were anlysed, indicating that fresh nucleation of metal did not occur after the iron oxide had been reduced.

Reduction of manganous oxide in the interior of ore particles could take place by a number of reactions.

Pomfret and Grievson [37] consider that manganous oxide could be reduced to a limited extent by the exchange reaction :

$$(MnO) + [Fe] = (FeO) + [Mn] \quad . \quad . \quad . \quad 4.6$$

If a pure iron nucleus of 5 um in diameter is considered it can be shown that the addition of $4,1 \times 10^{-9}$ g of manganese would result in an alloy of 50 per cent iron and 50 per cent manganese. Manganese oxide could also be reduced by solid carbon deposited in the pores of ore particles by the reaction.

$$2CO = CO_2 + C \quad . \quad . \quad . \quad 4.7$$

Deposited carbon was not observed in the ore although evidence for carbon deposition has been found by other investigators[23,26,28], particularly in manganese ores that contained iron.
The fact that the metallic nuclei in the interior of ore particles did not, in the general case, exceed 10um in diameter, irrespective of the experimental conditions, indicated that the reduction of MnO ceased at an early stage or that the rate of reduction decreased to a very low level in the interior of ore particles.

4.4.2 Growth of Metallic Nuclei

The metallic nuclei on the surface of ore particles grew by coalescence and by reduction of manganous oxide. The presence of iron in all the alloy beads from the surface of ore particles indicated that growth of the beads occurred by the incorporation of all other metallic species into the nuclei of iron that formed originally. The phases observed in these alloy beads can be accounted for by reference to the Fe-Fe_3C and the Fe-Mn-C phase diagrams [114].

The iron formed initially was carburized by carbon monoxide or solid carbon to form a solid solution of carbon in iron. Since actual contact between solid carbon and iron would be required for carburization to occur, the dominant carburizing reaction must have been that between iron and carbon monoxide. The carburizing reaction has been represented [31] by the formula :

$$3Fe + 2CO = Fe_3C + CO_2 \quad . \quad 4.8$$

However, it is evident from the Fe-Fe_3C phase diagram that Fe_3C would not be present as such in the alloy due to the high temperatures used. Therefore the carburization reaction resulted in the formation of a solid solution of carbon in iron (austenite). The austenite begins to melt at 1300°C when its carbon content is about 1,3 per cent.

The structure in Figure 3.14 shows clearly that the alloy consisted of austenite with a carbon content somewhat in excess of 0,8 per cent. During cooling the austenite transformed to proeutectoid carbide and troostite. For very low manganese contents pearlite rather than troostite would form.

With an increase in manganese content, which increases the solubility of carbon in the alloy [115 - 117], the austenite remained stable down to room temperature as shown in Figure 3.15. This structure again indicates the presence of austenite, at 1300°C, from which some carbon is rejected during cooling due to a decrease in its solubility with decreasing temperature.

With a further increase in the manganese and carbon contents the liquidus temperature of the alloy is reduced and liquid formed as is clear from Figure 3.16. During cooling primary austenite was precipitated followed by the simultaneous precipitation of eutectic carbide and austenite. Here again the point of interest is that carbide did not exist as such at 1300°C.

From the structure of Figure 3.16, it follows that the alloy bead was of a hypoeutectic composition and that the appropriate increase in the carbon to manganese ratio would form an alloy of eutectic composition. This in fact was the case as indicated in Figure 3.17.

The phases observed in alloy beads formed at 1300°C and containing an appreciable amount of manganese are in good agreement with those depicted in the 600°C isotherm of the Fe-Mn-C system (Figure 4.1). Thus, for manganese contents of between 2 and 34 per cent and carbon contents of between 0,2 and 6,7 per cent the phases in the alloy should conform to one of the following possible combinations :

1. M_3C + α-Fe (cf Figure 3.14)

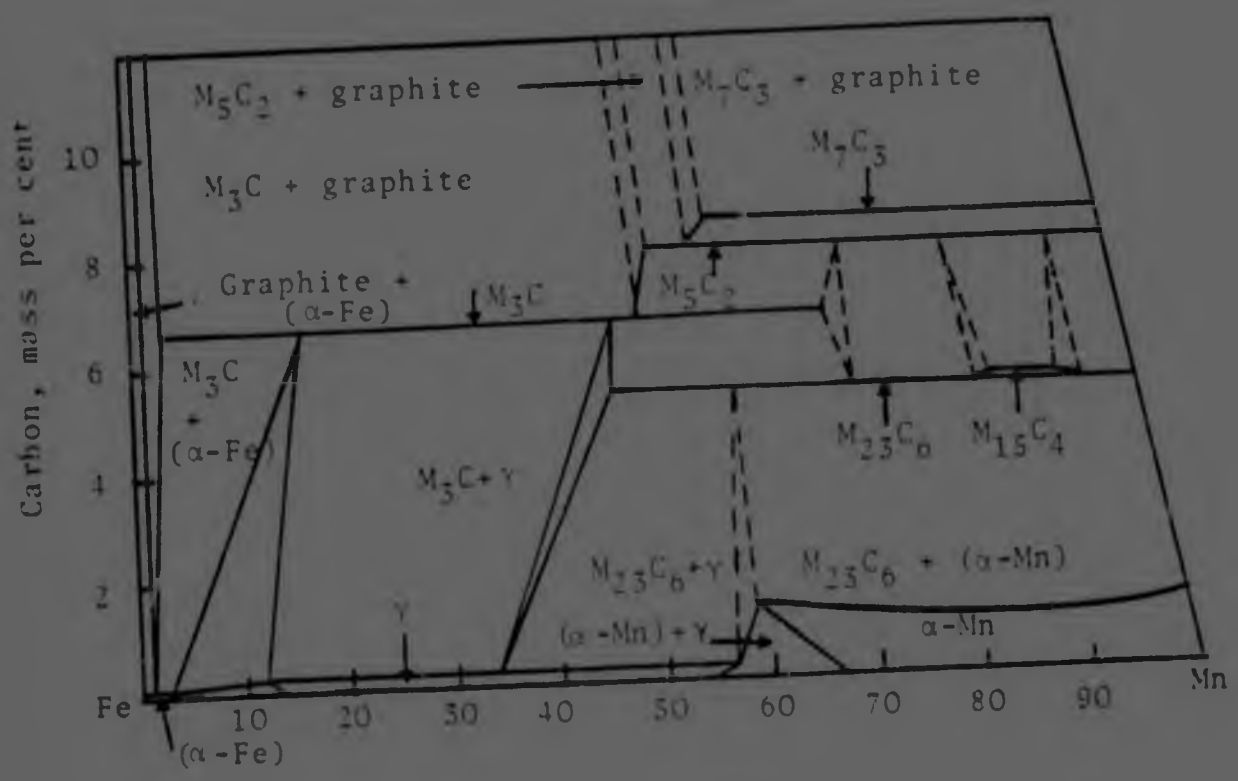
2. M_3C + α-Fe + γ (cf Figure 3.15)

3. M_3C + γ (cf Figures 3.16 and 3.17).

M_3C refers to a mixed carbide in which some of the iron has been replaced by manganese. From Figure 4.1 it can be seen that the ratio of manganese to iron in M_3C can vary considerably.

Since the alloy beads adhered to the surface of the ore particles, reduction of MnO by carbon dissolved in the alloy would be more favourable, kinetically, than reduction by solid carbon. Therefore the reduction of MnO during this stage of the process may be represented by the reaction

$$MnO + [C]_{alloy} = [Mn]_{alloy} + CO. \quad \cdot \quad \cdot \quad 4.9$$



MANGANESE, MASS PER CENT

Figure 4.1 The 600°C isotherm of the Fe-Mn-C system (Ref.114).

The manganous oxide could be in the form of solid grains or in solution in the slag. Reduction of solid or dissolved oxide would be equally favourable, thermodynamically, since the activity of the oxide in the solid and in the slag would be close or equal to unity. This disregards the low concentration of magnesium oxide in the solid and assumes that the slag was saturated in the oxide. The reduction process would continue only if the alloy were carburized continuously and if it remained in contact with the oxide or the slag. During the early stages of reduction these conditions could be satisfied due to the low proportion of slag in the charge.

As can be seen from Figure 3.8 the alloy beads were not completely covered by the slag film and carburization could easily take place by the reaction :

$$2CO = [C]_{alloy} + CO_2 \quad . \quad . \quad . \quad . \quad 4.10$$

The reduction of manganous oxide is often [3, 118] considered to take place by Fe_3C and the metallic product of the reaction is given as a manganese carbide. This is not accurate since neither Fe_3C nor the manganese carbide are stable at the temperatures considered.

4.4.3 Formation of the Alloy Layer

Since the heating rate of the SCICE charges was constant, the initial reactions to form the metal must have been similar irrespective of the temperature reached ultimately. Comparison of Figures 3.17 and 3.18 shows obvious similarities between the structures of small alloy beads formed at 1300 and 1400°C. With increasing manganese and carbon contents, the alloy attained a hypereutectic composition from which crystals of primary carbide formed during cooling (Figures 3.19 and 3.20). The remaining liquid became depleted in carbon and solidified interstitially between the carbide crystals. The alloy layer formed at 1600°C consisted almost entirely of carbide at room temperature and was liquid at 1600°C.

The transformations undergone by manganese-rich alloys during cooling from the liquid are difficult to interpret owing to the lack of published data on the phases in Fe-Mn-C alloys at temperatures greater than 1100°C.

The chemical composition of the alloys formed at 1400 and 1600°C showed that the phases in these alloys should be different. However, the diffractograms of the alloys showed distinct similarities (Figure 3.25). The alloys formed at 1400°C with coal or coke belong to the $M_3C + M_{23}C_6$ phase field of the Fe-Mn-C system, while the alloys formed at 1600°C belong to the $M_5C_2 + M_{15}C_4$ field. The apparent discrepancy can probably be explained by the fact that the diffractograms of the binary carbides Fe_3C and Mn_5C_2 show many similarities and it is probable that the ternary carbides, which form by substitution of manganese for iron, could also show structural similarities. Thus the carbide M_3C, for example, might be expected to show a diffraction pattern similar to that of M_5C_2.

With increasing reduction the alloy beads increased in size and the proportion of slag also increased. Thus, the larger alloy beads drained to the bottom of the crucible while a layer of slag of increasing thickness formed around the partially reduced ore particles. The formation of a substantial proportion of slag enhances consolidation of the charge and contact between slag and solid reducing agent is improved. Under these conditions the carburization of metallic beads at the interface between partially reduced ore particles and the slag layer may be expected to be inefficient owing to the extremely low solubility of carbon in the slag. Diffusion of carbon monoxide through the slag is not expected to be of significant importance. During this final stage of the process, reduction can take place by a number of mechanisms.

i) The reduction of MnO by carbon monoxide, bubbling through the melt, according to the reaction

$$MnO + CO = Mn + CO_2 \quad . \quad . \quad . \quad 4.11$$

is possible. However, thermodynamic considerations (1.2.2) show that this reaction is unlikely in the presence of carbon.

ii) Solid MnO or MnO dissolved in the slag may be reduced at the interface between the alloy and slag layers by carbon dissolved in the alloy. The more important reaction was probably that between dissolved MnO and carbon in the alloy since contact between crystalline MnO and the alloy must have been limited.

iii) The partially reduced ore particles may be reduced further by dissolution of MnO in the slag and diffusion to the slag-solid carbon interface where reduction is possible. Evidence for the dissolution of MnO in the slag has been presented on numerous occasions.

It is difficult to state with certainty whether reduction by carbon dissolved in the alloy or by the solid reducing agent was the dominant reaction. If the rate of reduction of MnO at both the alloy-slag and the slag-solid carbon interfaces is controlled by the rate of the chemical reaction, as proposed by Daines and Pehlke [38] and by Kukhtin et al [39] respectively, then reduction by solid carbon would be the dominant process owing to the greater surface area of the slag-solid carbon interface. Reduction at the interface between the alloy and slag layer would become increasingly important as the amount of solid carbon decreases. There is evidence [119, 120] that the rate of reduction of solid MnO by carbon dissolved in Fe-Mn-C melts is controlled by the rate of the chemical reaction and it is probable that chemical reaction is the rate-controlling process during reduction of MnO dissolved in the slag by the carbon of the alloy.

If significant reduction occurred at the alloy-slag interface the alloy would dissolve carbon from the graphite crucible to maintain a carbon content close to its saturation point. The crucibles were attacked by the alloy to a limited extent but it was not possible to relate the extent of attack to the significance of reactions at the slag-alloy interface. The fact that graphite linings in furnaces last for several years indicates that reduction of MnO by the molten alloy occurs to a very limited extent.

The absence of alloy in direct contact with solid reducing agent was probably due to differences in the surface free energies of the two components. This leads to the question of what becomes of the metal that forms by the reduction of MnO by solid carbon. There appear to be two possibilities.

i) The metal is transported through the slag back to the slag-oxide interface where it is absorbed by existing nuclei (Figure 3.9).

ii) It diffuses through the slag and is absorbed in the alloy layer at the bottom of the crucible.

Both of these processes suggest that, at any time, there is a certain concentration of metal atoms or metallic molecules in the slag.

4.5 The Influence of Reducing Agent on the Reduction Process

The speed of a reduction process may be influenced by the reactivity of the reducing agent towards carbon dioxide.

It is generally [44, 45, 47, 48] accepted that the reduction of iron oxides by carbon occurs via the intermediate gaseous reaction product CO, thus

$$3Fe_3O_4 + CO = 2FE_3O_4 + CO_2 \quad . \quad . \quad . \quad 4.12$$

$$Fe_3O_4 + CO = 3FeO + CO_2 \quad . \quad . \quad . \quad 4.13$$

$$FeO + CO = Fe + CO_2 \quad . \quad . \quad . \quad . \quad 4.14$$

$$CO_2 + C = 2CO \quad . \quad . \quad . \quad . \quad . \quad 4.15$$

For this reaction sequence the rate of regeneration of carbon monoxide will influence the rate of reduction and this is well substantiated experimentally [47].

The rate of reduction of Mn_3O_4 has been found [24] to be dependent on the reactivity of the reducing agent towards carbon dioxide, indicating that reduction of this oxide by carbon proceeds through carbon monoxide.

Grimsley [3] showed that the rate of reduction of Mamatwan manganese ore fines, by carbons of widely varying reactivity varied during the initial stages of reduction only. This indicates that the reduction of the higher manganese oxides and of the iron oxide in the ore occurred by carbon monoxide. The rate of reaction beyond about 35 per cent reduction was found not to be influenced significantly by the type of reducing agent, indicating that carbon monoxide was not an effective reductant for manganous oxide. Similar results were obtained by Lisniak and Evseev [121] during the reduction of iron-containing chromite ores by reducing agents of different reactivities.

The results obtained from the SCICE experiements indicate that the use of coal or coke as the reducing agent does not affect the rate of reduction significantly. Since the temperatures used were 1300°C or higher the influence of the reducing agent on the early stages of reduction could not be investigated. It can be seen from Figure 3.26 that the rate of mass loss of ore-coke and ore-coal mixtures heated at 1400°C for up to 4 hours was virtually identical indicating that the rate of reduction was similar in the two cases. Comparison of the mass losses effected at 1600°C is difficult since as stated earlier these charges were sectioned and losses occurred during this process. It is also evident from Figures 3.28 and 3.29 that the rate of reduction was almost identical since the compositions of the alloys produced, with the two reducing agents under otherwise similar experimental conditions was practically the same. These results supply further evidence that reduction of MnO during the later stages of the process occurred by solid reducing agent or by carbon dissolved in the alloy.

The similarities in X-ray diffraction patterns (Figure 3.24) obtained from charges of ore plus coal and ore plus coke reacted under similar conditions is further evidence that the type of reducing agent did not affect the reduction process significantly.

4.6 Conclusions

1. During its reduction by carbonaceous reducing agents, Mamatwan manganese ore consists of the two phases slag and impure oxide. The slag contains mainly lime and silica while the oxide contains mainly manganous oxide.

2. The reduction of Mamatwan ore by coal or coke was shown to involve the following three steps:

   a) The dissociation of gangue minerals and the gaseous reduction of hematite to metal and of the higher manganese oxides to manganous oxide. Slag formed by reaction between lime and silica. The manganous oxide content of the slag varied with the lime to silica ratio in individual ore particles.

   b) The growth of metallic particles on the surface of ore particles due to reduction of manganous oxide by carbon dissolved in the alloy and the formation of a slag layer on the surface of ore particles.

   c) The reduction of manganous oxide dissolved in the slag by solid reducing agent or by carbon dissolved in the alloy.

3. Reduction of manganous oxide occurred mainly from the slag

4. The rates of reduction of Mamatwan ore by coal or coke were similar for comparable experimental conditions.

CHAPTER 5

5.0 THE RESISTIVITY OF MIXTURES OF MAMATWAN ORE AND COKE OR COAL

5.1 Materials, Apparatus and Procedure

The resistance of mixtures of Mamatwan ore of constant particle size and Delmas coal or Iscor coke was determined for three different particle size ranges of the reducing agents. The ore was used in the size range 2,83 to 12,7 mm and the size ranges of the reducing agents were 2,83 to 6,35 mm, 6,35 to 9,5 mm and 9,5 to 12,7 mm. A description of the technique for the preparation of the charge has already been given. Segregation of the charge components became more pronounced with increasing particle size of the reducing agent.

The resistance measurements were made on the apparatus shown in Figure 2.2. The central graphite electrode was made of two parts. The upper part was 25 mm in diameter and 620 mm long, screwed into a lower part 40 mm in diameter and 50 mm in length. Aluminous-porcelain sheaths and alumina cement were used where necessary to ensure that conduction took place over a constant surface area of electrode irrespective of the level of the solid or partially fused charge in the crucible.

The lower edge of the conducting part of the electrode stood 40 mm above the bottom of the crucible in the bottom of which a recess 10 mm deep had been drilled. The bottom section of the electrode was located in this recess, and, by use of a bridge during charging and a centering device thereafter, the correct positions of the electrode and the control thermocouple were ensured.

5.1.1 Determination of Resistance

Initially, a Siemens meter developed by the National Institute for Metallurgy was used in conjunction with a furnace temperature programmer to measure the conductance of the charge.

CHAPTER 5

5.0 THE RESISTIVITY OF MIXTURES OF MAMATWAN ORE AND COKE OR COAL

5.1 Materials, Apparatus and Procedure

The resistance of mixtures of Mamatwan ore of constant particle size and Delmas coal or Iscor coke was determined for three different particle size ranges of the reducing agents. The ore was used in the size range 2,83 to 12,7 mm and the size ranges of the reducing agents were 2,83 to 6,35 mm, 6,35 to 9,5 mm and 9,5 to 12,7 mm. A description of the technique for the preparation of the charge has already been given. Segregation of the charge components became more pronounced with increasing particle size of the reducing agent.

The resistance measurements were made on the apparatus shown in Figure 2.2. The central graphite electrode was made of two parts. The upper part was 25 mm in diameter and 620 mm long, screwed into a lower part 40 mm in diameter and 50 mm in length. Aluminous-porcelain sheaths and alumina cement were used where necessary to ensure that conduction took place over a constant surface area of electrode irrespective of the level of the solid or partially fused charge in the crucible.

The lower edge of the conducting part of the electrode stood 40 mm above the bottom of the crucible in the bottom of which a recess 10 mm deep had been drilled. The bottom section of the electrode was located in this recess, and, by use of a bridge during charging and a centering device thereafter, the correct positions of the electrode and the control thermocouple were ensured.

5.1.1 Determination of Resistance

Initially, a Siemens meter developed by the National Institute for Metallurgy was used in conjunction with a furnace temperature programmer to measure the conductance of the charge.

The conductance decreased when the furnace power was switched off, and the temperature readings were often erratic. The frequency of the furnace current increased rapidly at times and gave a very rapid increase in temperature, which resulted in failure of the thermocouples. Stray signals from other equipment altered the frequency of the furnace current and affected the heating rate of the charge. It was decided therefore that the temperature should be controlled manually. In addition, the limited range (0,05 to 5S) of the Siemens meter and the uncertainties in the measurements led to the use of a voltmeter and an ammeter to measure the resistance of the charge. This arrangement which is shown in Figure 5.1, increased the range of measurable resistance, and made possible the measurement of the resistance of ore and coke mixtures, ore and coal mixtures or any of these materials individually. Urquhart [55] who used a similar circuit for ferrochromium charges, established that this circuit did not exhibit any inductance effects.

Long coaxial leads twisted round each other were used to connect the measuring instruments positioned about 2 m away from the furnace and so minimize the effect of induced fields. The current through the charge was measured with an ammeter and the voltage across the charge was determined with a digital multimeter with an impedance of 10MΩ. The voltmeter was connected across the charge itself so that errors would be at a minimum.

The error introduced by the relatively low impedance of the multimeter is high at low temperatures for coal and for mixtures of ore and coal, but decreases rapidly with increasing temperature. The error in the resistance of these charges at room temperature is 17,6 per cent, decreasing to 0,2 per cent at about 600°C. The error in the resistance of charges of ore alone and of mixtures of ore and coke at room temperature is negligible. By use of this apparatus, the effect of temperature on the resistance of the following charges was determined.

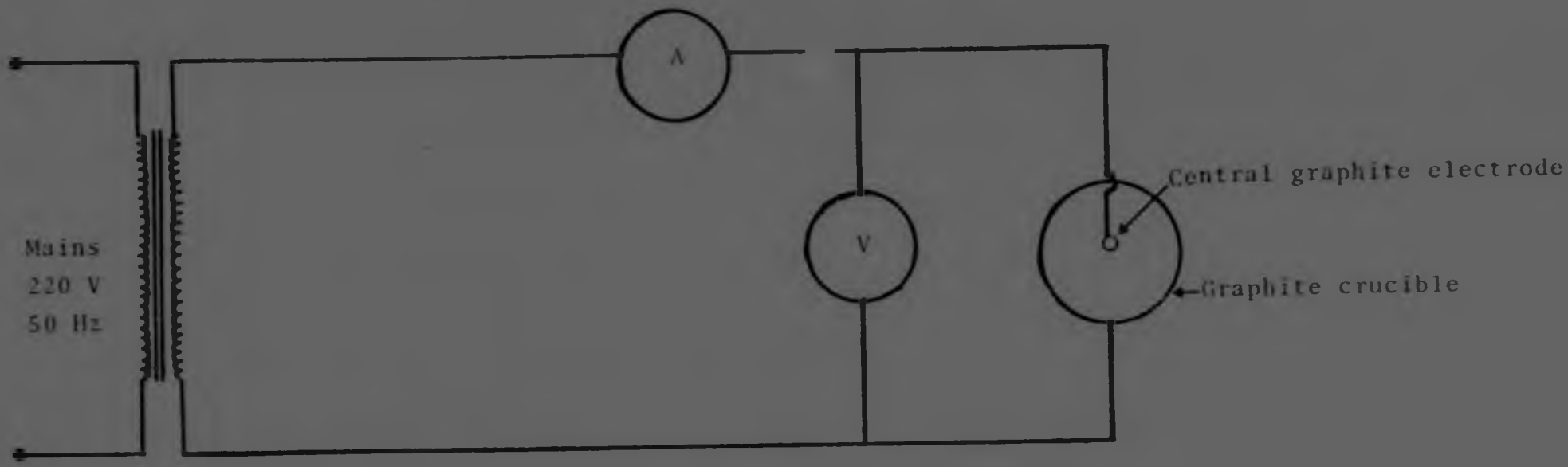


Figure 5.1 Circuit for the measurement of charge resistance.

CHARGE	SIZE RANGE OF REDUCING AGENT mm
Ore	
Iscor coke	2,83 - 6,35
Delmas coal	2,83 - 6,35
Ore and coke	2.83 - 6,35
Ore and coke	6,35 - 9,5
Ore and coke	9,5 - 12,7
Ore and coal	2,83 - 6,35
Ore and coal	6,35 - 9,5
Ore and coal	9,5 -12,7

The size of the ore particles ranged between 2,83 and 12,7 mm The resistance of the different charges was converted to resistivity by determination of the cell constant (shape factor) of the apparatus. The method used to determine the cell constant is indicated in Appendix 2.

5.1.2 Variation in Volume Fractions of Components

One variable that has a significant influence on the resistivity of a charge is the proportion by volume of the ore and the reducing agent [10]. The volume fractions of the components in the SCICE charges were estimated by independent measurements of the volume of reducing agents and ore, followed by measurement of their combined volumes when the mixture is not compacted. Compaction of the mixture during charging reduced the volume by about 1 per cent. It is clear that volume fractions measured in this way are meaningful only when the particle size and shape of the ore and the reducing agent are approximately the same.

The coke constituted 15 per cent by mass of coke-ore mixtures and the coal 24 per cent by mass of coal-ore mixtures, while the proportion by volume was found to be 38 per cent coke in coke-ore mixtures and 45 per cent coal in coal-ore mixtures. These measurements were made with ore particles ranging in size between 2,83 and 12,7 mm and particles of reducing agent ranging in size between 2,83 and 6,35 mm. The volume of the charges was found to remain approximately constant irrespective of the size range of the reducing agent used. The volume fractions were therefore assumed to remain approximately constant at room temperature.

It has been suggested [70] that variations in resistance between 400 and 1200°C in a chromite-char mixture could be due to expansion and contraction of the charge components. This theory was tested on the charges under consideration by measurement of the effect of increases of temperature on the volume changes of the different charges.

The measurement of changes in volume with increases of temperature could also provide information on the rate of increase in the volume fraction of the reducing agent in the mixture because the ore and the reducing agent diminish in volume at different rates. This could significantly affect the variation of the resistivity of the charge with increases of temperature.

The change in volume of ore, ore and coke, and ore and coal was measured by noting the variation of the level of the charge in the crucible as the temperature increased. A graphite slab 20 mm thick was placed on top of the charge and a mass of 2,5 kg was placed on top of the slab. The level of the charge was determined by the lowering of an alumina sheath through the cover of the furnace until it touched the top of the mass.

5.2 Results and Discussion

5.2.1 Effect of Temperature on Resistivity of Individual Charge Components

The values of resistivity with increasing temperature for the individual charge components and for mixtures of ore with coal or coke are shown in Appendix 2. In the ensuing sections plots of resistivity against temperature or time are presented.

Plots of resistivity against temperature for the individual materials are shown in Figure 5.2. Most refractory materials exhibit a resistance-temperature relationship that approaches the Arrhenius type relationship proposed by Rasch and Hinrichsen [73].

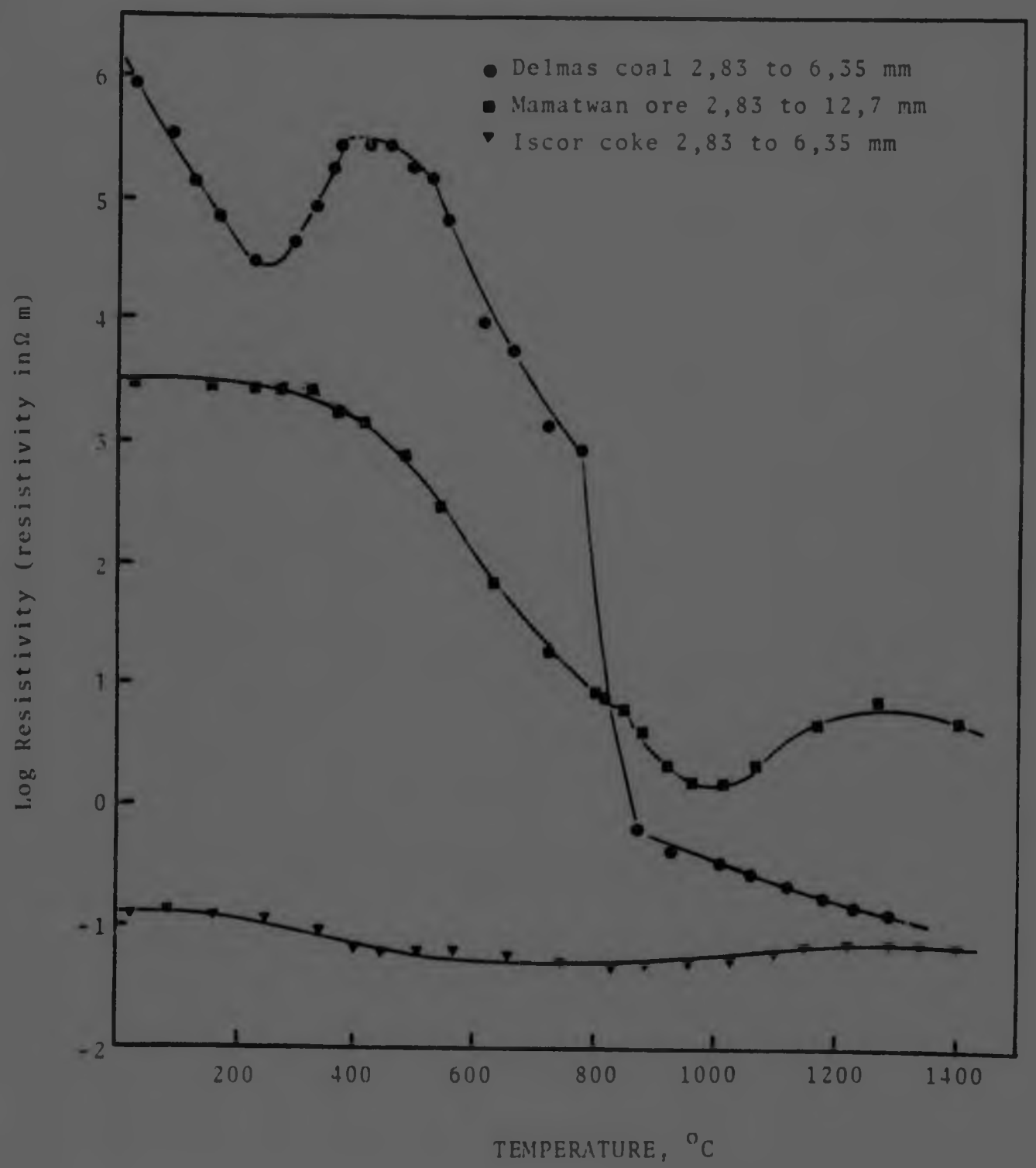


Figure 5.2 The effect of temperature on the resistivity of Mamatwan ore, Iscor coke and Delmas coal.

The relationship may be expressed as follows :

$$\rho = Ae^{B/T} \quad . \quad . \quad . \quad . \quad . \quad 5.1$$

where ρ is the specific resistance
T is the absolute temperature and
A and B are constants.

The value of A and B vary within the temperature range considered.

Plots of $\ln\rho$ against reciprocal temperature for the individual materials are shown in Figure 5.3. It can be seen that the variation of resistivity with temperature follows the Arrhenius type equation to a good approximation. The resistivity of the ore deviates from this relationship for temperatures higher than 1000°C due to the formation of liquid slag and a change from semiconduction to ionic conduction.

The changes in resistivity and in activation energy for conduction with increasing temperature are related to the structural and chemical changes that take place in the materials. It can be seen from Figure 5.2 that the resistivities of Delmas coal and Mamatwan ore change markedly with increasing temperature, whereas the resistivity of coke changes only slightly with temperature. While precise interpretation of the curves for the ore and the coal is difficult owing to the vast complexity of the processes that take place in these materials during heating the following features are noted .

The decrease in the resistivity of coal between 25 and 250°C appears to be due to loss of moisture, whereas the increase between 250 and 450° appears to be due to loss of some volatile matter. The increase in resistivity suggests that the loss of volatile matter during this stage results in a more random or porous structure. Urquhart [53] attributed similar variations in resistivity during the heating of coal char to the initiation of the loss of volatile matter. Further loss of volatile matter between 450 and about 800°C resulted in a very marked decrease in resistivity. The very steep decrease in resistivity between

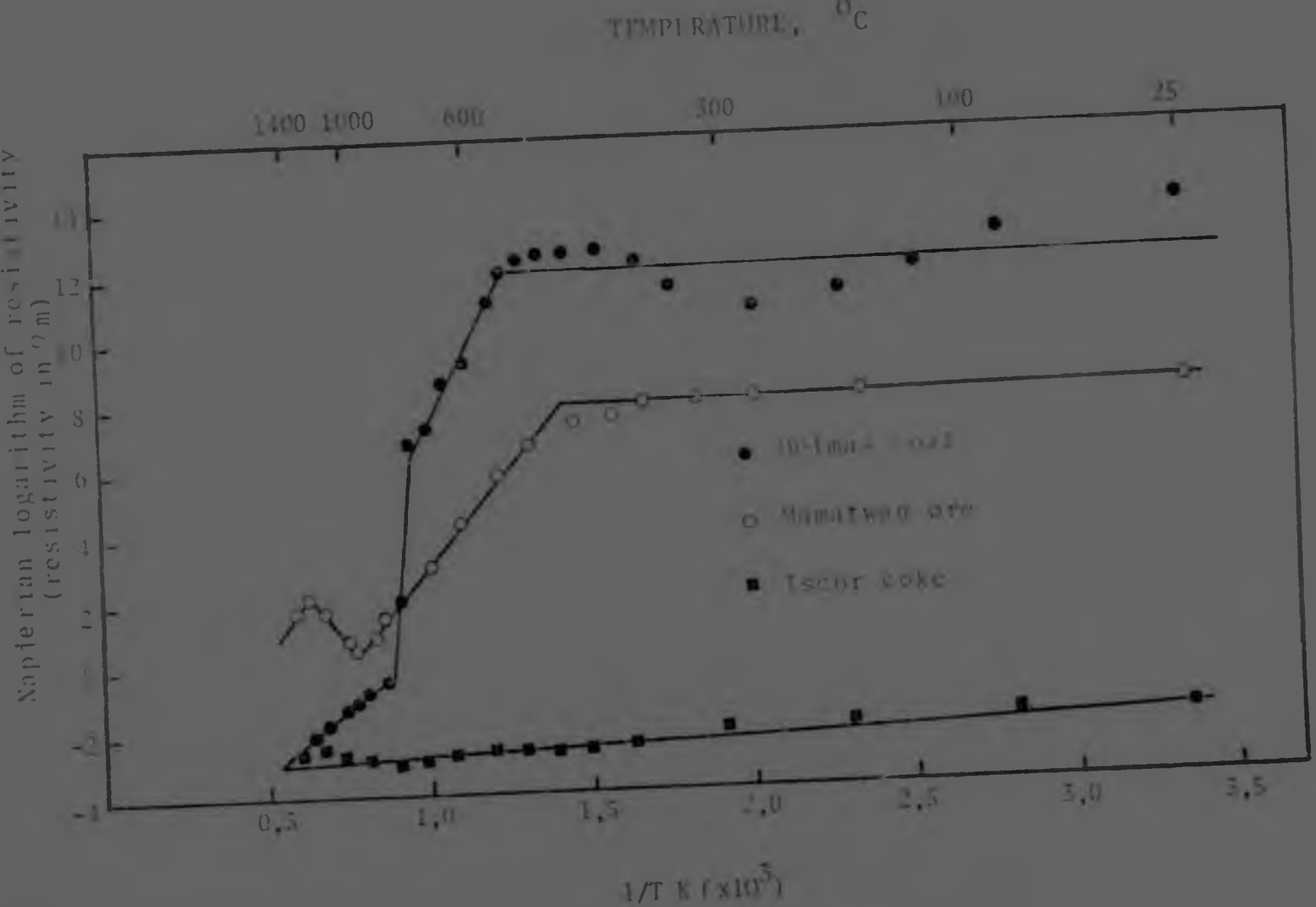


Figure 5.3 Arrhenius plots of the resistivity of Mamatwan ore, Iscor coke and Delmas coal.

about 800 and 900°C coincided with an increase in the thermal conductivity of the coal evidenced by a significant decrease in the temperature difference between the edge and the centre of the charge during heating (Figure 5.4). Figure 5.5 shows that the rate of change of volume of the coal-ore mixture changed between 800 and 900°C. Comparison of curve II with curves I and III shows that this rate change was due to a relatively rapid contraction of the coal up to 800°C and a reduced contraction rate above 900°C. The slow decrease in resistivity above 900°C was due to a gradual loss of volatile matter and an increase in the size and degree of ordering of the graphite crystallites in the coal structure. At 1200°C or higher, the resistivity of the coal becomes practically the same as that of the coke. Rennie [71] obtained similar results during a study of the electrical characteristics of coke, anthracite, charred coal, and charred anthracite. These results conform to the findings of other investigators [62, 122] according to which the resistivity of a carbonaceous reducing agent is primarily a function of heat treatment and not of the rank and composition of the original coal.

The resistivity of the ore decreased only slightly between 25 and 350°C as there is little change in its structure over this temperature interval. The decrease in resistivity between 400 and 1000°C is due to the decomposition of carbonates, and the formation of lower oxides of manganese and iron. That the resistivity of oxides decreases as the ratio of metal to oxygen in the oxide increases has been established by a number of investigators [67, 68, 71]. This is due to a decrease in the concentration of higher valency cations (eg M^{3+}) and an increase in the number of electrons associated with the cation sublattice [123].

The structural changes that occur in the ore at temperatures between 400 and 1000°C are not well known. Pilter [23] showed that carbon monoxide concentrations of as little as 10 per cent in the atmosphere will reduce the higher oxides of manganese to manganous oxide between 25 and 800°C. Because the ore in the present study was heated in a graphite crucible, an appreciable

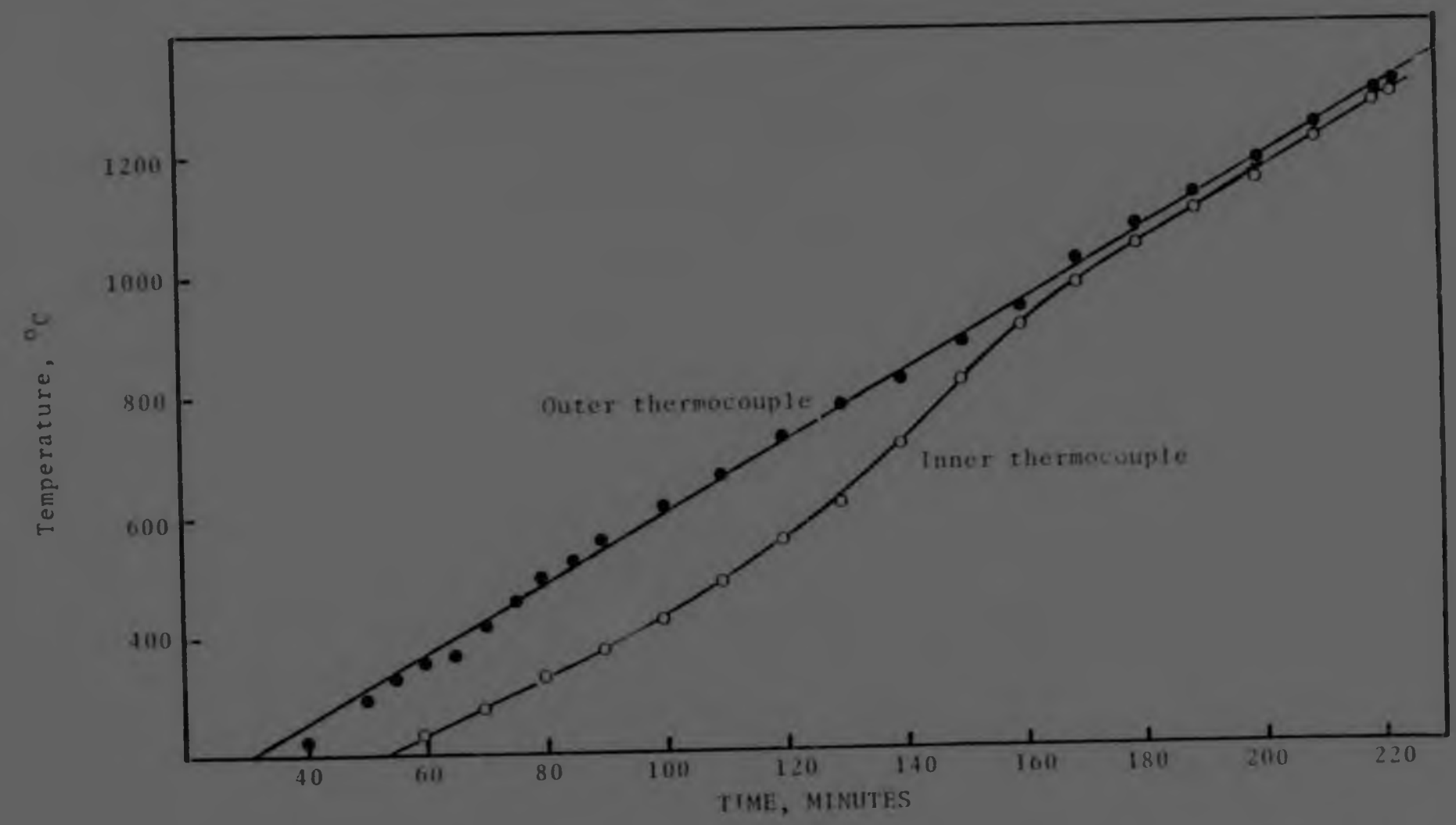


Figure 5.4 Temperature differences between the inner and outer thermocouples during the heating of Deimas coal.

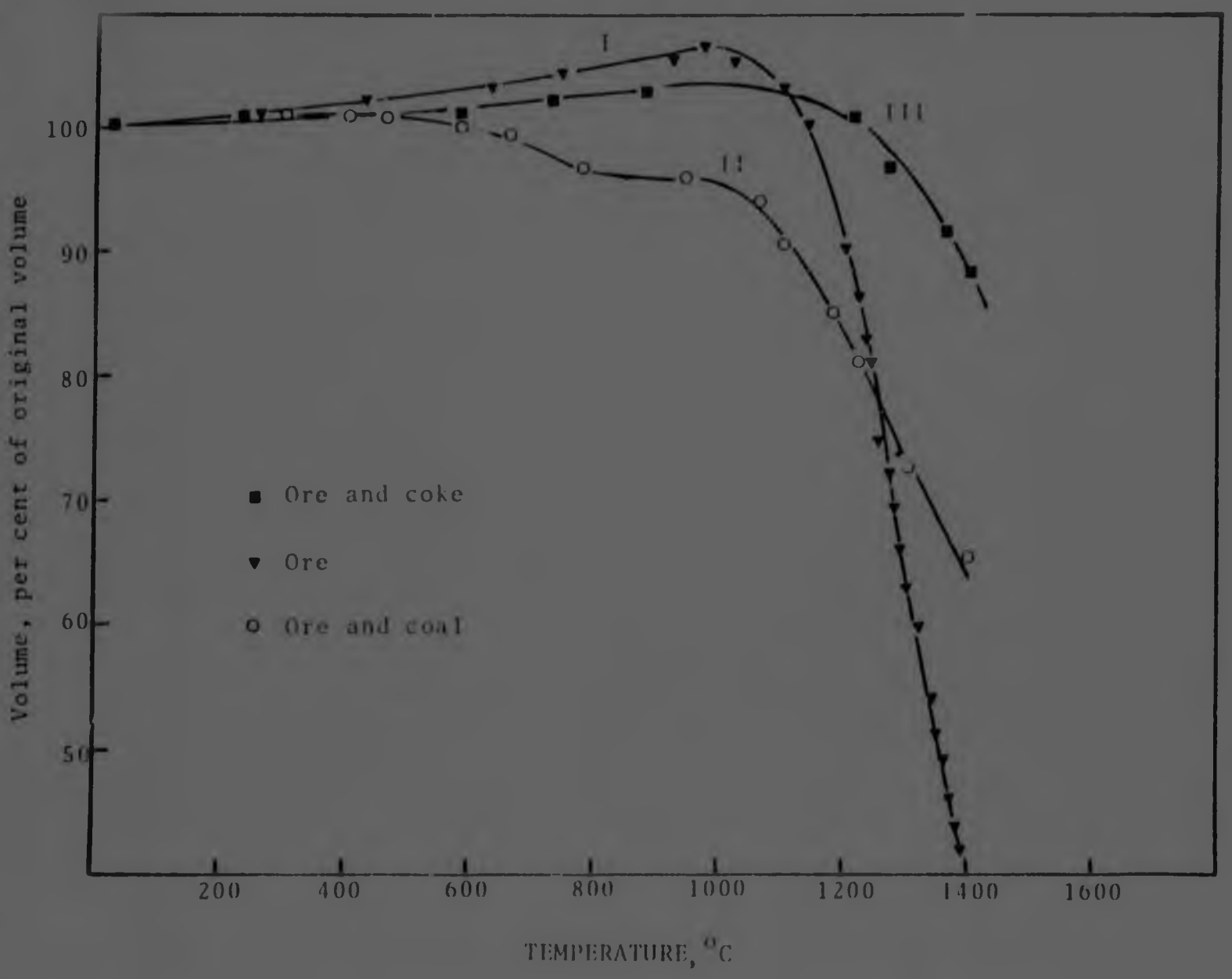


Figure 5.5 Volume changes with increasing temperature for various charges.

amount of carbon monoxide must have been present, and the equilibrium concentration of carbon monoxide in the presence of carbon dioxide and solid carbon rises [110] steeply from about 2 per cent at 400°C to about 99 per cent at 1000°C.

The resistivity minimum at 1000°C corresponds with the maximum volume of the charge of ore in Figure 5.5. The volume of the charge decreases rapidly at about 1000°C, whereas the resistivity increases between 1000 and 1300°C. The rapid decrease in the volume of the charge above 1000°C shows that drastic changes took place in the structure of the ore.

The results of De Villiers [56], and the examination of furnace samples (Figure 6.19) indicate that the initial stages of the reduction of the ore involve the formation of a spongy substance which contains most of the metallic oxides while the products of the decomposition of carbonates occur as loose particles in the interstices. Free silica, liberated from the braunite is probably also present. With an increase in temperature above 1000°C the spongy substance collapses to form grains of impure manganous oxide while the gangue oxides react to form the slag, both processes resulting in a rapid reduction in the volume of the ore. The mode of conduction then changes from electronic conduction through the spongy oxide to ionic conduction through the slag which now forms a more or less continuous path through the charge. This is accompanied by an increase in the resistivity which could be due to the low mobility of conducting ions within the slag phase at this temperature. The decrease in the resistivity above 1300°C could then be due to an increase in the mobility and concentration of these ions.

The resistivity of the coke varied only slightly between 25 and 1400°C owing to the high thermal stability of this material. Some variation in the resistivity of the coke can be expected due to reaction and fusion of the ash constituents at high temperatures. The resistivity of the coke measured at room temperature in this investigation is approximately the same as that of coal char [53] at 1400°C.

amount of carbon monoxide must have been present, and the equilibrium concentration of carbon monoxide in the presence of carbon dioxide and solid carbon rises [110] steeply from about 2 per cent at 900°C to about 99 per cent at 1000°C.

The resistivity minimum at 1000°C corresponds with the maximum volume of the charge of ore in Figure 5.5. The volume of the charge decreases rapidly at about 1000°C, whereas the resistivity increases between 1000 and 1300°C. The rapid decrease in the volume of the charge above 1000°C shows that drastic changes took place in the structure of the ore.

The results of De Villiers [56], and the examination of furnace samples (Figure 6.19) indicate that the initial stages of the reduction of the ore involve the formation of a spongy substance which contains most of the metallic oxides while the products of the decomposition of carbonates occur as loose particles in the interstices. Free silica, liberated from the braunite is probably also present. With an increase in temperature above 1000°C the spongy substance collapses to form grains of impure manganous oxide while the gangue oxides react to form the slag, both processes resulting in a rapid reduction in the volume of the ore. The mode of conduction then changes from electronic conduction through the spongy oxide to ionic conduction through the slag which now forms a more or less continuous path through the charge. This is accompanied by an increase in the resistivity which could be due to the low mobility of conducting ions within the slag phase at this temperature. The decrease in the resistivity above 1300°C could then be due to an increase in the mobility and concentration of these ions.

The resistivity of the coke varied only slightly between 25 and 1400°C owing to the high thermal stability of this material. Some variation in the resistivity of the coke can be expected due to reaction and fusion of the ash constituents at high temperatures. The resistivity of the coke measured at room temperature in this investigation is approximately the same as that of coal char [53] at 1400°C.

5.2.2 Volume Changes during Heating of Charges

The ore and reducing agent diminish in volume at different rates during heating and the resistance of the charge is influenced by the volume of ore and reducing agent at any given time.

The volume changes during the heating of three charges are shown in Figure 5.5. The ore loses about 18 per cent of its mass when calcined [2, 3] at 1000°C owing to the decomposition of carbonates and the thermal dissociation of higher to lower oxides. The loss of mass in the case under consideration must have been even higher than 18 per cent because the ore was heated in a graphite crucible and the higher oxides of manganese and iron were reduced to their lowest oxidation states. Yet the volume of the ore at 1000°C was higher than its initial volume. This volume increase was due to a more open structure which probably resulted from the cracking of the ore and the decomposition of carbonates. The volume began to decrease beyond 1000°C owing to the formation of slag. When different charges were probed with an alumina rod, it was found that the charge softened at about 1100°C

The mixture of ore and coke showed reduced expansion compared to the charge of ore. This could be due to a small amount of contraction of the coke or a decrease in the amount of expansion of the ore caused by the reduction to lower oxides. The volume of the mixture decreases between 1200 and 1400°C at a rate much slower than that for the charge of ore, indicating that the ore diminishes in volume at a higher rate than the coke.

The initial volumes of ore and coke in the mixture were 1800 and 1100 ml respectively, whereas the combined volume was 2800 ml. From the curve of volume against temperature for the ore (curve I), the calculated volume of ore in the coke-ore mixture at 1300°C is 1470 ml if it is assumed that the presence of coke does not affect the volume of the ore. The volume of the mixture at 1300°C is 2720 ml, which gives a theoretical volume of coke in the mixture of 1259 ml at 1300°C if it is assumed that the coke does not take part in any chemical reactions.

Hence the volume fraction of the coke in the mixture increases with heating. The coke inhibits subsidence of the charge, probably by forming a more or less continuous network throughout the charge, which increases the conductivity.

The charge of ore and coal showed very little expansion between room temperature and 500°C indicating that the coal begins to contract as soon as heating starts. The charge contracted significantly between 500 and 800°C due to the evolution of volatile matter. Contraction was very slow between 800 and 1000°C and very rapid above 1000°C. It has been seen that the thermal and electrical conductivities of the coal increase considerably above 800°C when most of the volatile matter has been eliminated.

The charges of ore plus coal and ore plus coke showed similar rates of contraction during the stage of rapid contraction.

5.2.3 Resistivities of Charges of Ore and Reducing Agents

The variation in the resistivity of mixtures of ore and coke with temperature is shown in Figure 5.6. The curves of resistivity against temperature for the individual charge components, ore and coke, are superimposed for comparison. It was observed that the current through the charge was unstable at temperatures below 400°C and small vibrations of the furnace were sufficient to cause the current to fluctuate. This effect was attributed to arcing between particles. The current became increasingly more stable at temperatures higher than 400°C. Evidence for arcing was not observed when ore or coal were used on their own or when mixtures of ore and coal were heated. However, when coke was used on its own, arcing occurred at voltages above 3V. Urquhart [53] observed arcing in charges of char and in mixtures of chromium ore and char and determined a critical voltage for arcing with increasing temperature. He found that this critical voltage increased steeply with increasing temperature.

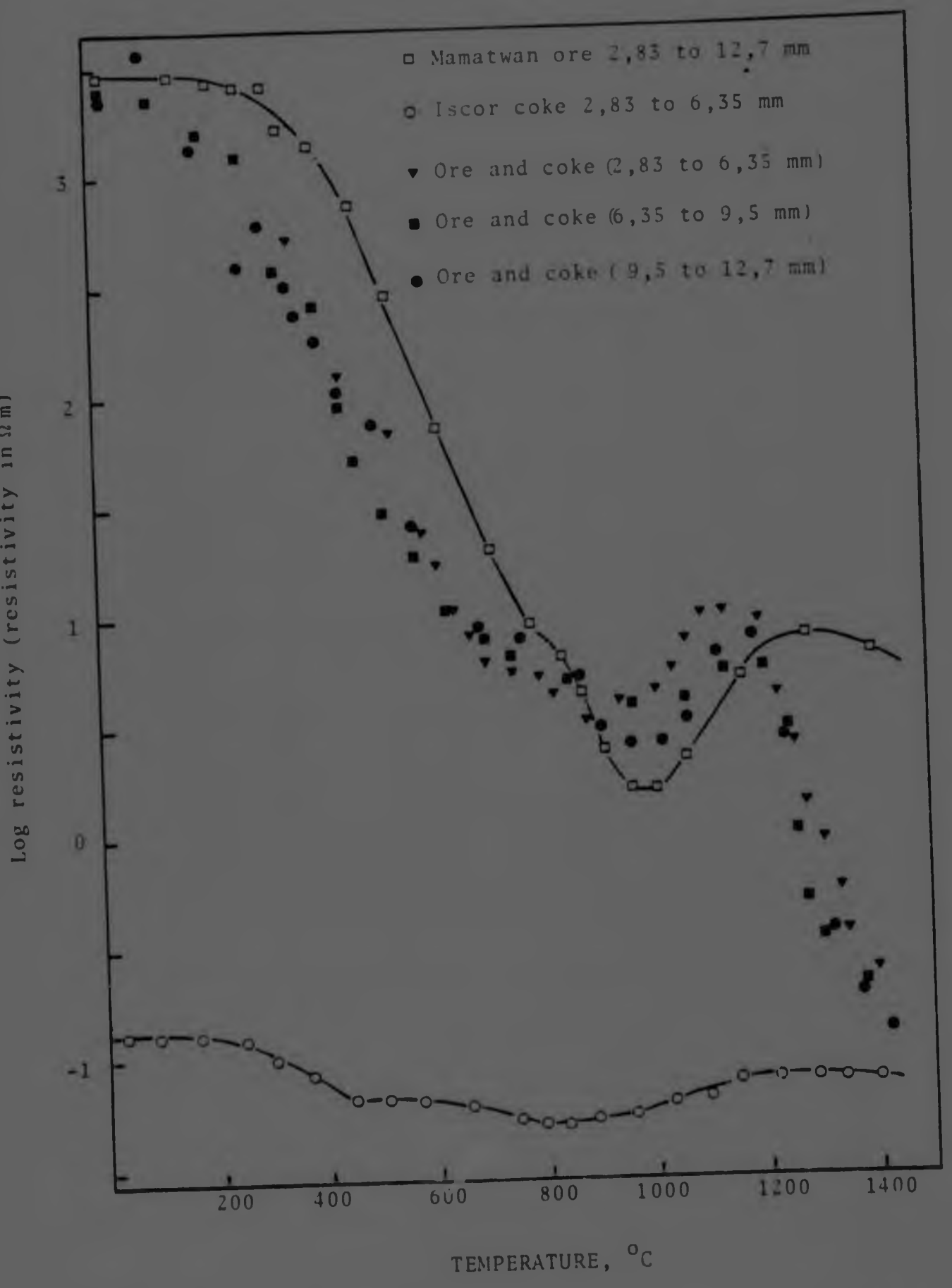


Figure 5.6 The influence of temperature on the resistivity of mixtures of ore and coke.

The mechanism for arcing proposed by Urquhart [53] involves the dissipation of power and an increase in temperature at points of contact between particles. A sufficiently high temperature at points of contact induces reaction between carbon and oxygen from the ore or the atmosphere to produce carbon monoxide. This generates a gap between the particles which if sufficiently small may satisfy the voltage gradient for arcing in CO (3kV/mm). The striking of an arc increases the temperature and further reaction takes place until the gap between the particles is too large for the prevailing voltage to sustain an arc and the arc is extinguished.

The behaviour of the coke-ore charges below 400°C was similar to that of the charges investigated by Urquhart [53] and a similar mechanism for arcing probably prevailed.

Arcing did not occur in charges of ore or coal or mixtures of these two materials owing to their much higher resistivities. The resitivity of coke at room temperature is about $10^{-1}\Omega m$ and that of coal is $10^{6}\Omega m$ (Figure 5.2). If it is assumed that these measurements were made under identical conditions then the following relationships may be written :

For the charge of coke

$$V = I_1 R_1 \quad . \quad . \quad . \quad 5.2$$

and for the charge of coal

$$V = I_2 R_2 \quad . \quad . \quad . \quad 5.3$$

Since $R_1 = \rho_1 K$ and $R_2 = \rho_2 K$

where ρ_1 is the resistivity of coke,
ρ_2 is the resistivity of coal and
K is a constant (the shape factor)

$$\frac{I_1}{I_2} = \frac{\rho_2}{\rho_1} = \frac{10^6}{10^{-1}} = 10^7$$

$$\therefore \quad I_1 = 10^7 I_2$$

It is thus seen that for a given voltage, the current flowing through the charge of coal is 7 orders of magnitude smaller than the current flowing through an identical charge of coke. Consequently the heat generated in the charge of coal is 7 orders of magnitude smaller since the heat generated is proportional to the product of current and voltage. Therefo e the probability of increasing the temperature at points of contact between particles in a charge of coal, to that required for reaction to occur between carbon and oxygen, is very limited. Arcing should occur in beds of materials of high resistivity only at extremely high voltages.

From Figure 5.6 it can be seen that the resistivity of mixtures of ore and coke is determined mainly by the resistivity of the ore, although coke does lower the resistivity of the charge between 25 and 900°C. This decrease in resistivity results from the low resistivity of coke and the reduction of oxides to a lower oxidation state. The more important factor is probably reduction to lower oxides with lower resistivities [67, 68, 71]. Figure 5.6 shows that the resistivities of the ore and of the mixture of ore and coke are similar at 25°C indicating that the coke has little influence on the resistivity of the mixtures at this temperature.

Systems composed of particles of a conductor and an insulator show an abrupt increase in resistivity when the volume fraction of insulator particles exceeds a certain critical value [70, 79, 80]. Willand [70] found that the resistance of mixtures of chromium ore and char increased dramatically when the volume fraction of ore was increased above 35 per cent. The resistance of the system showed only slight changes when the volume fraction of char was increased above 70 per cent. Since the volume fraction of ore up to 1200°C was about 60 per cent this could explain the similarity in resistivities between coke-ore mixtures and ore alone at these temperatures.

The resistivity of the mixtures begins to drop as soon as heating starts, whereas that of the ore remains constant up to 350°C. As shown in Figure 5.5 the changes in volume experienced by a charge of ore and by a mixture of ore and coke between 25 and 900°C are not very different, indicating that the volume fraction of coke in the mixture remains reasonably constant. These results

support the theory that the decrease in the resistivity of mixtures of ore and coke between 25 and 900°C is mainly due to the reduction of the higher oxides of manganese and iron to a lower oxidation state.

The resistivity of a mixture of ore and coke is higher than that of the ore between 900 and 1200°C. This increased resistivity could be related to the physical and chemical changes that take place in this temperature range. It has already been indicated (3.6.3) that sintering and consolidation of the ore were much more pronounced in the absence of a reducing agent. This could be due to either the fact that reduction of ferrous oxide to metallic iron does not occur, or due to the physical separation of ore particles by coke particles in the ore-coke mixtures. In the presence of coke, a slag of the fayalite type with a low melting point would not be formed due to reduction of the iron oxides to iron.

The resistivity of the mixture drops above 1200°C owing to the rapid contraction of the ore and slag formation. The contraction of the ore results in an increased volume fraction of coke in the mixture and improved contact between particles. Willand [70] showed that small increases in the proportion of conductor reduced the resistance of the system significantly in that range of compositions where the resistance of the mixture is primarily determined by the resistance of the insulator.

Downing and Urban [69] found that equal volumes of coke and molten slag have comparable resistances. However, in the mixtures considered in this investigation the proportion of slag formed by heating to 1400°C and then cooling was very small. It can therefore be said that the reduction in resistivity between 1200 and 1400°C was mainly due to the rapid contraction of ore particles, which resulted in an effective increase in the volume fraction of coke in the charge.

It can be seen from Figure 5.6 that no definite changes occurred in the resistivities of ore-coke mixtures for coke in the ranges 2,83 to 6,35 mm and 9,5 to 12,7 mm. Hence, for temperatures below 1200°C, the resistivity of the charge was determined mainly by the resistivity of the ore. The differences between the curves of the three mixtures were no greater than the differences obtained in duplicate experiments. Some variations between curves obtained from identical charges can be expected owing to segregation and some re-arrangement of the bed during heating.

For temperatures below 1200°C, the coke did not form continuous current paths through the charge. Thus, the use of coke of different size ranges cannot be expected to influence the resistivity ofthe charge significantly.

The influence of time at constant temperature, on the resistivity of mixtures of ore and coke containing coke in different size ranges, is shown in Figure 5.7. The resistivity showed an initial steep decrease and then remained essentially constant. The time period for the rapid decrease in resistivity was longer at 1200°C and the resistivity varied by less than one order of magnitude after 2 hours at temperatures between 1200 and 1400°C. The size range of the reducing agent did not have a definite influence on the resistivity for temperatures of 1300 and 1400°C.

That the resistivity remains essentially constant after the initial drop is explained by the fact that the rate of mass loss (Figure 3.26) is very low during retention of the charge at temperatures of up to 1400°C. This indicates that under these conditions, the proportion of slag and the volume fraction of reducing agent in the charge remain approximately constant.

The resistivity at 1400°C of the coke-ore mixtures is slightly lower than that of the coke at the same temperature.

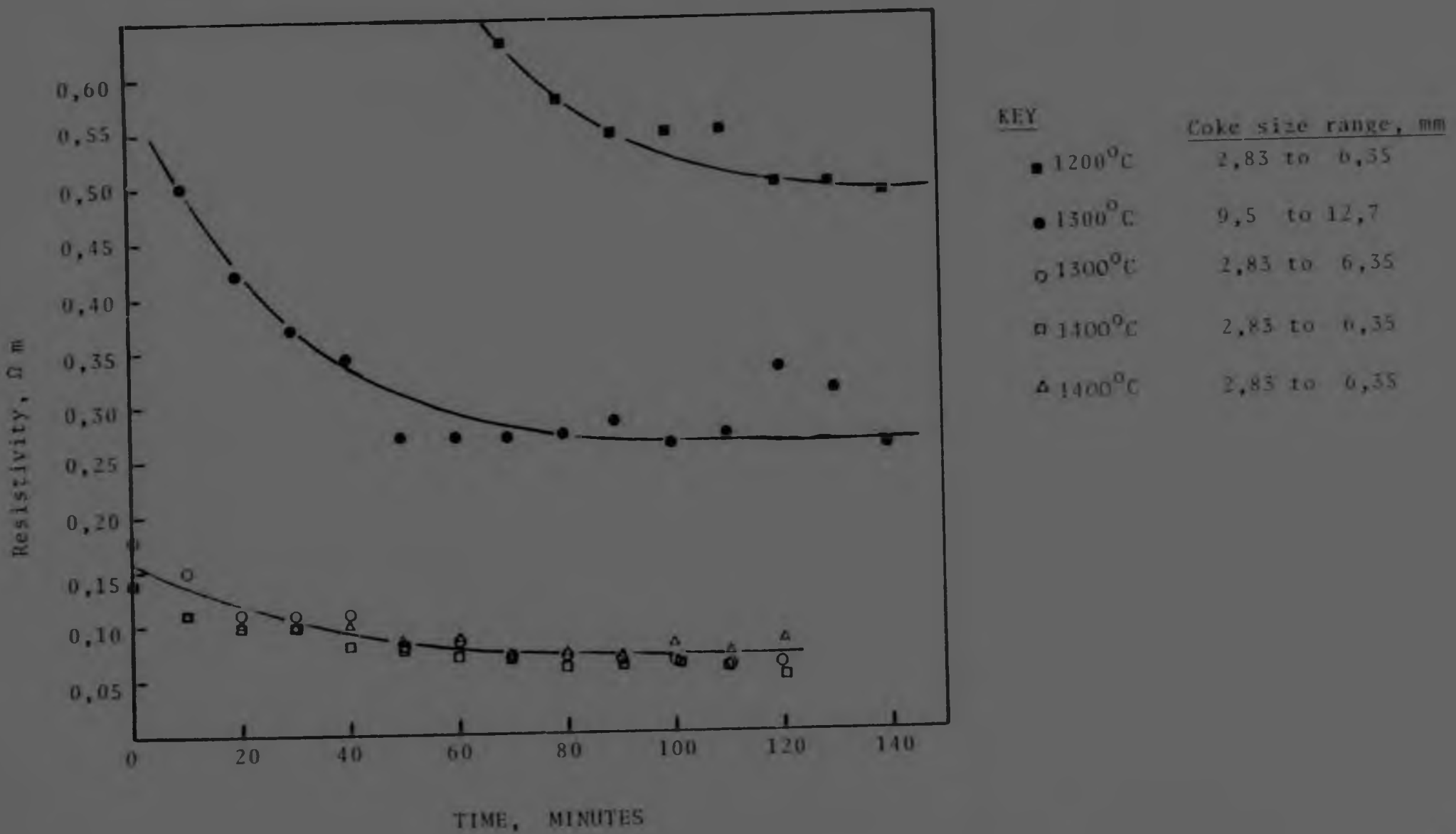


Figure 5.7 Variations in resistivity with time at temperature for mixtures of ore and coke.

The variation in the resistivity of mixtures of ore and coal with increasing temperature is shown in Figure 5.8. The curves of resistivity against temperature for the ore and the coal individually are superimposed for comparison. It can be seen that, at temperatures less than 600°C, the resistivity of the mixtures is influenced strongly by the resistivity of the coal. Between 600 and 750°C, the resistivity of the mixtures appears to be influenced by the resistivities of both the coal and the ore. As shown in Figure 5.5 the coal begins to contract at 600°C and reduces the volume fraction of coal in the mixture. The resistivity of the mixtures continues to drop beyond 600°C when the volume of the charge (Figure 5.5) has reduced to less than the original volume. Hence the changes in resistivity cannot be related to the expansion and contraction of the charge.

The resistivity of the ore-coal mixtures is higher than that of either the ore or the coal between 800 and 1200°C. The effect is similar to that observed with mixtures of ore and coke.

With mixtures of ore and coal, the decrease in resistivity starts at about 1050°C, as compared with 1200°C with mixtures of ore and coke. This appears to be related to the fact that mixtures of ore and coal begin to contract at 1050°C while for mixtures of ore and coke contraction starts at 1200°C. This is further evidence that the decrease in resistivity at high temperatures is mainly due to an increase in the volume fraction of the reducing agent.

At a constant temperature of 1300°C the resistivity of ore-coal mixtures decreased rapidly during the first 40 mintutes and remained reasonably constant during the next 80 minutes as shown in Figure 5.9. As for the lower temperatures, the size range of the coal did not have a definite influence on resistivity. The resistivty of the mixtures after 2 hours at 1300°C is slightly higher than that of the coal at the same temperature.

Plots of $\ln \rho$ against reciprocal temperature are shown in Figure 5.10 for mixtures of ore and coal and ore and coke containing reducing agents in the size range 6,35 to 9,5 mm. It can be seen that the activation energies for conduction at temperatures

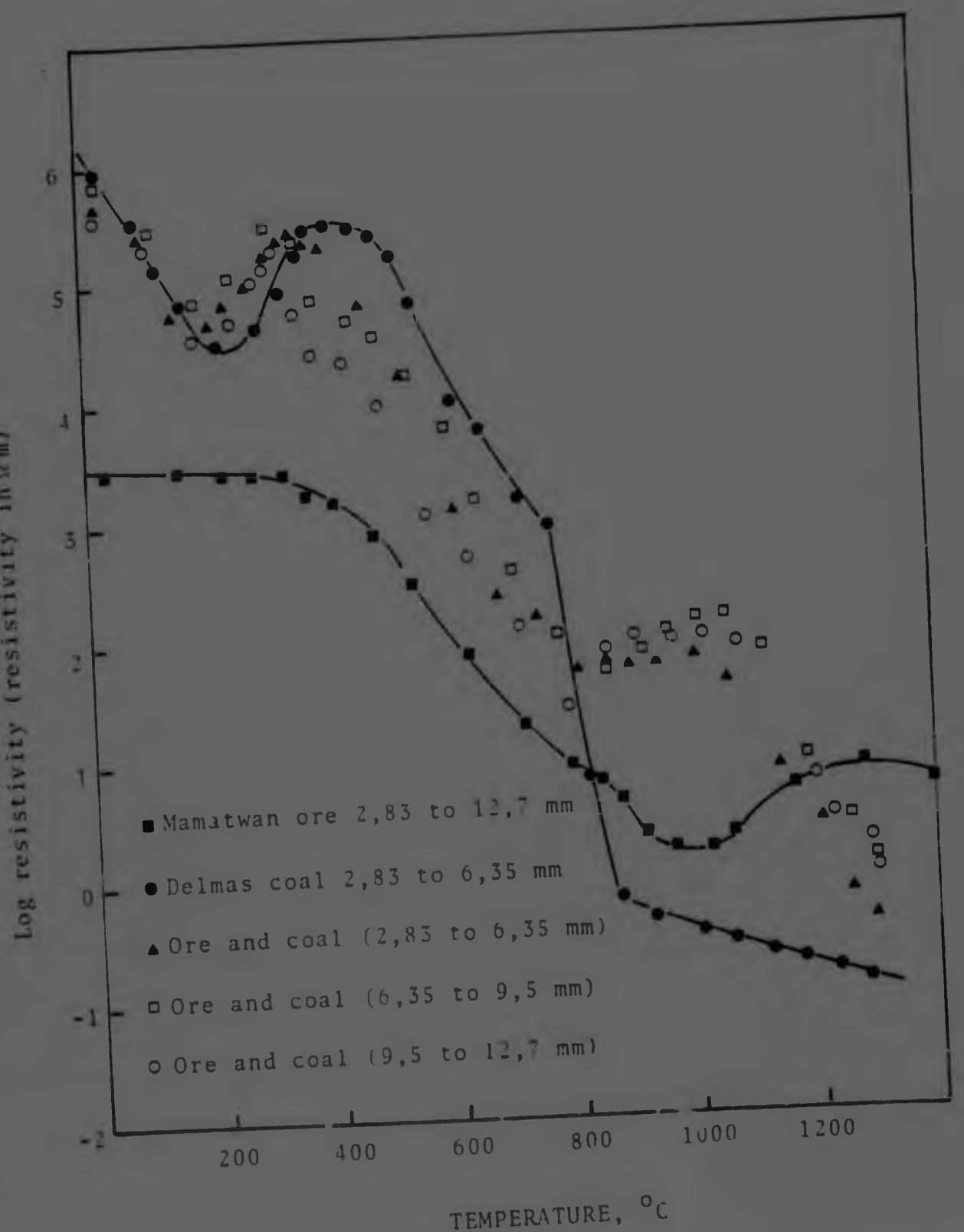


Figure 5.8 The influence of temperature on the resistivity of mixtures of ore and coal.

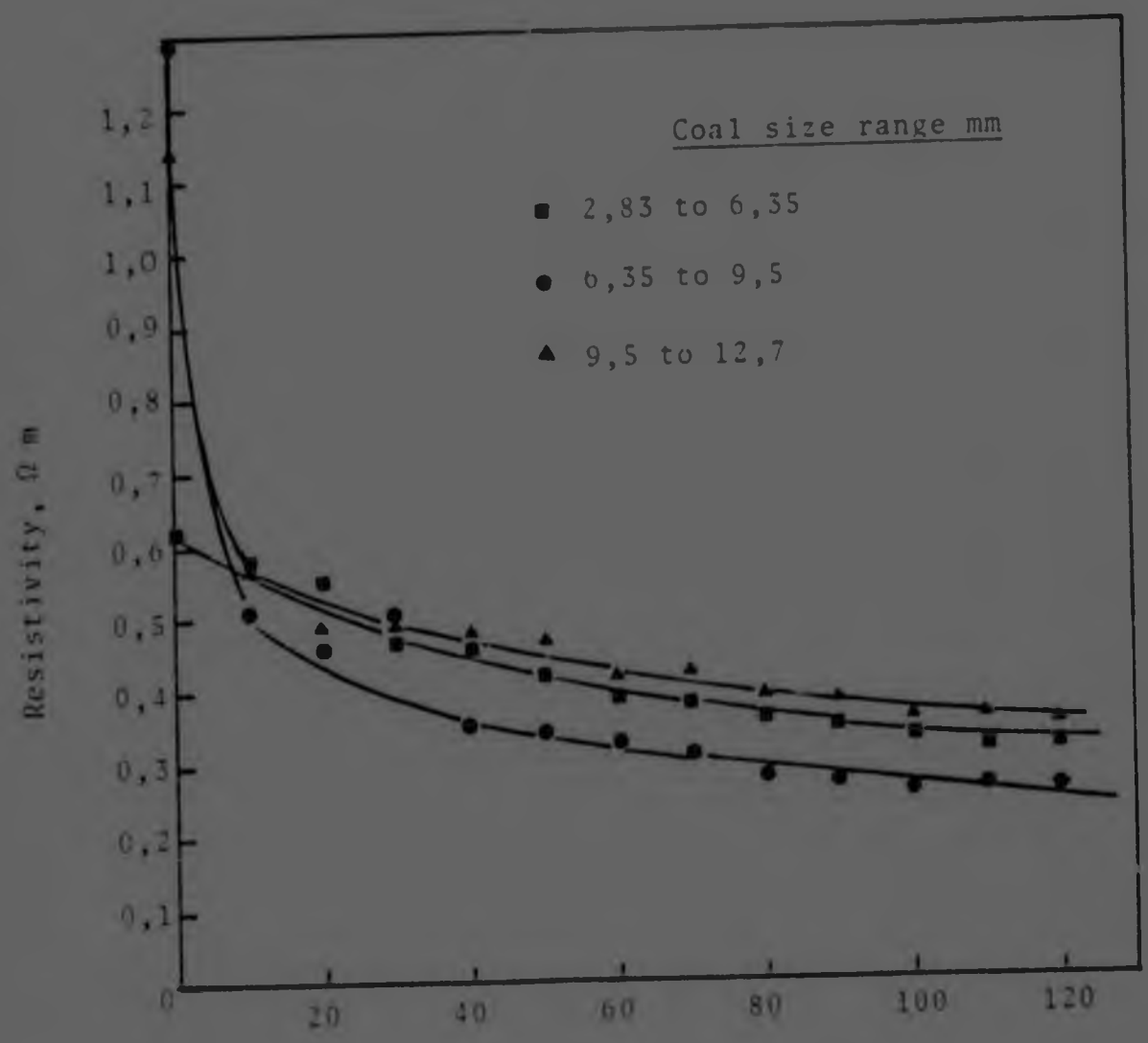


Figure 5.9 Variations in the resistivity of mixtures of ore and coal with time at 1300°C.

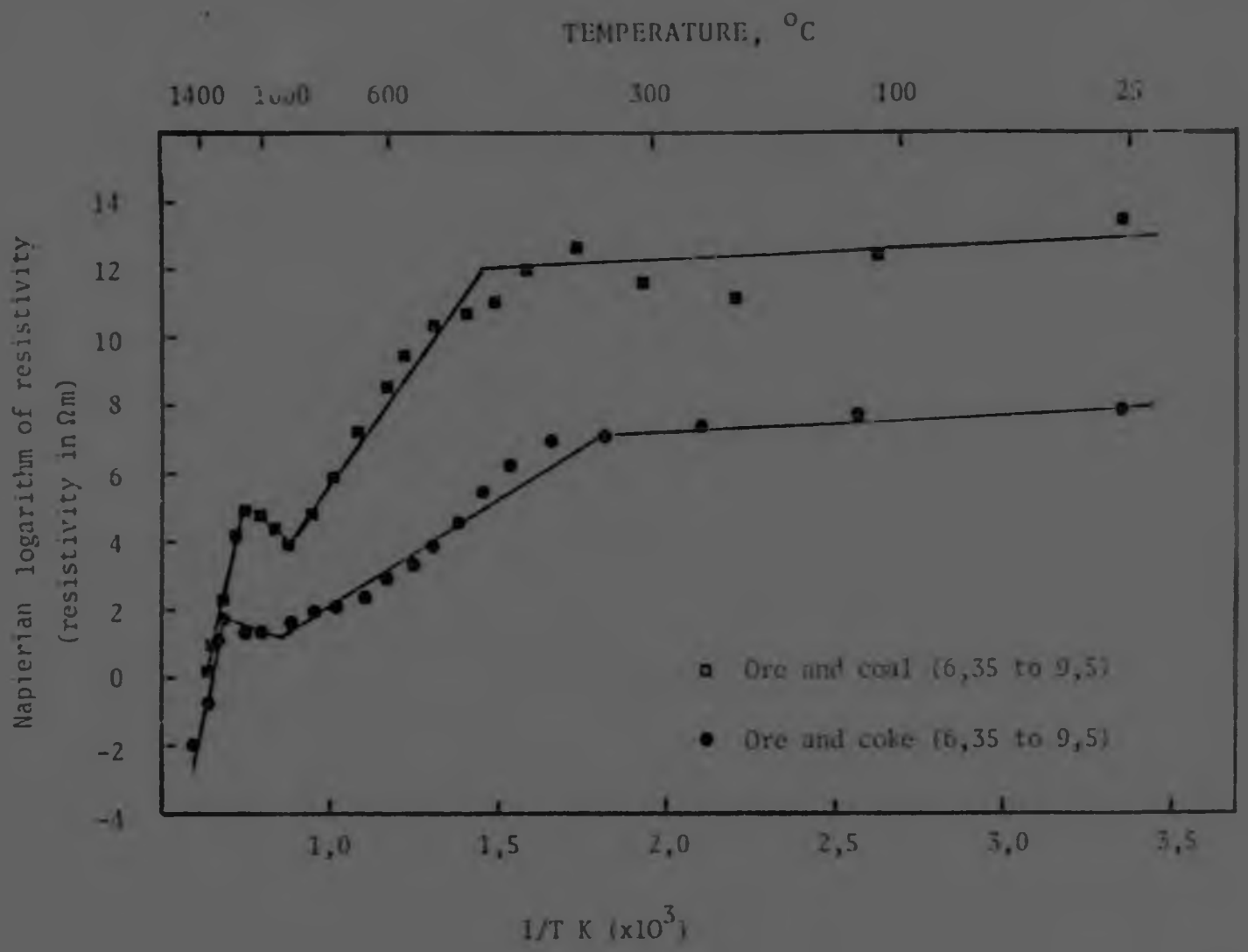


Figure 5.10 Arrhenius plots for mixtures of ore and coke and ore and coal.

greater than about 1080°C are very simil . for the two types of mixture indicating that the mechanism for conduction is the same in the two cases.

Up to now it has generally [53, 67, 68, 70-72, 78] been accepted that the resistivity of a bed of materials decreases with increasing particle size of its components. This has been attributed to the fewer 'contact resistances' which result from an increase in the particle size of the materials. Hensler and Henry [77] however, found the re[illegible] of magnesite compacts to increase with increasing gr[illegible]. Recent work by Dijs [64] shows that the resistivity of a bed of ore of fixed size and reducing agent decreases to a minimum as the size of the reducing agent is increased, and then increases again with a further increase in the size of the reducing agent. The variations in resistivity diminish rapidly as the mean size of both the reducing agent and the ore increases. When the mean size of the ore is 10 mm, no appreciable variations in resistivity will occur even though the mean size of the reducing agent is varied between 5 and 10 mm.

These results were obtained at room temperature for mixtures of silica and char in the proportions 1:1 by volume. They cannot therefore be applied direct to explain the results obtained in the present investigation. However, they show that the resistivity of mixtures of ore and carbonaceous reducing agent can remain reasonably constant even through considerable variations in the size of the reducing agent occur.

The variation of resistivity with temperature for mixtures of ore and coke and ore and coal are shown as resistivity bands in Figure 5.11. It will be seen that the resistivities of the two types of mixture are markedly different at low temperatures but are similar at about 1200°C. This result could be expected in view of the fact that, the resistivity of the two types of mixture is strongly influenced by the resistivity of the reducing agent for temperatures greater than 1000°C and that the resistivity of the two reducing agents is very similar at 1200°C.

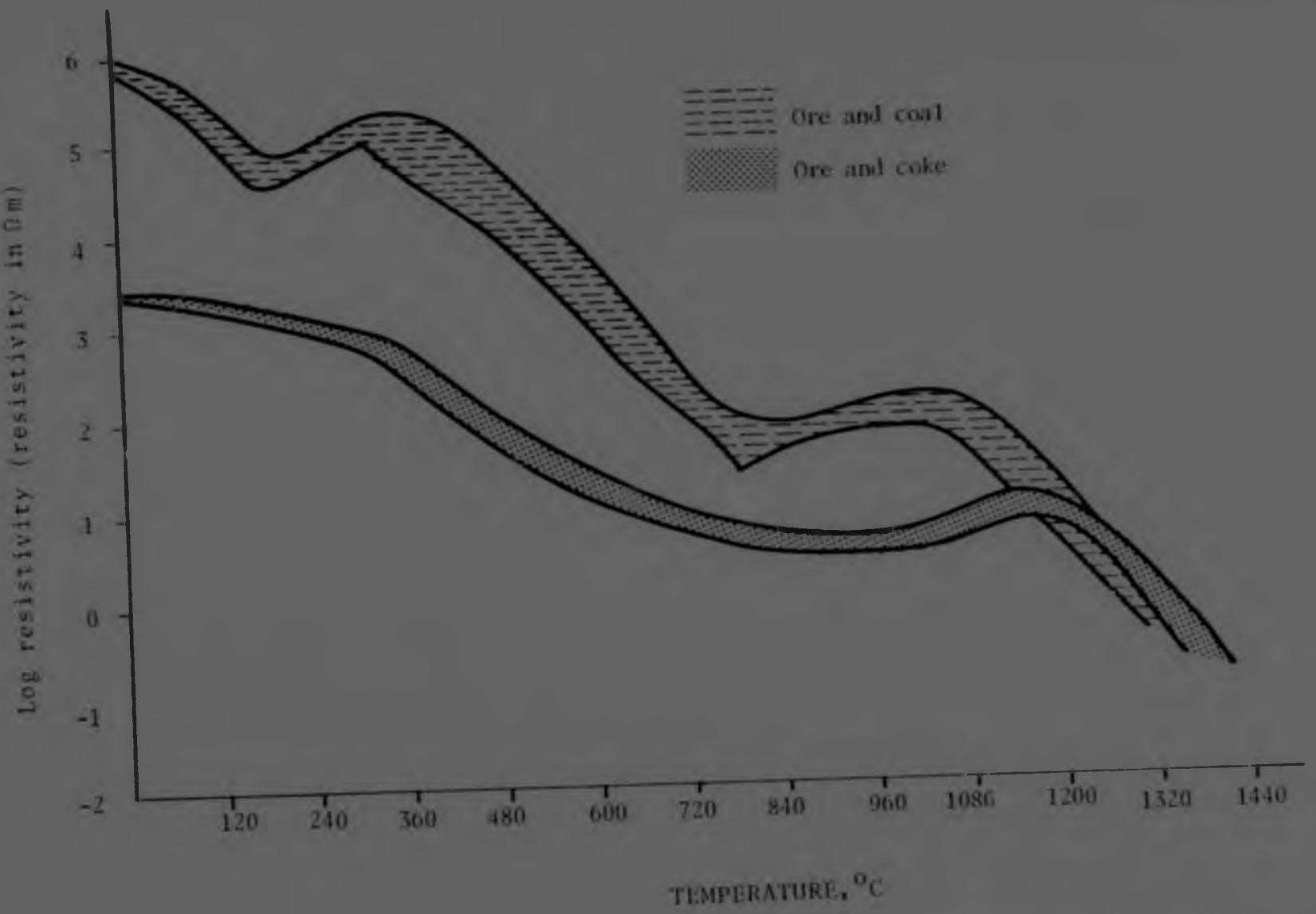


Figure 5.11 A comparison of the resistivities of mixtures of ore and coke and ore and coal for different particle sizes of the reducing agent.

5.3 Resistivity measurements and furnace resistance

The resistivity of electric furnace feed materials has been measured by numerous investigators in an attempt to establish the factors that govern furnace resistance. The direct application of experimental results to determine furnace resistance and power distribution in the furnace has been hampered by a number of factors. These include the unavoidable differences between experimental and furnace conditions [64, 67] and the possibility of current transfer by arcing in the furnace [63, 67, 71, 96].

In general, the results of experimental investigations have been used as very broad guidelines to increase furnace resistance and production rates. For instance, the higher resistivity of coal over coke, up to temperatures of about 1200°C, has led to the use of this material in varying proportions in the charge for ferromanganese production [1]. Silveira [75] reports increased production rates upon use of reductant of reduced size which led to increased furnace resistance.

These examples show that the deductions drawn from laboratory investigations can be used to advanta However, it is not entirely certain that the improveme in furnace operation were directly related to the alterations made on the basis of laboratory tests.

The furnace resistance R_f may be represented as the sum of two resistances in parallel [59] so that,

$$\frac{1}{R_f} = \frac{1}{R_r} + \frac{1}{R_c} \qquad . \quad . \quad . \qquad 5.4$$

where R_r is the resistance of the reaction zone and
R_c is the resistance of the charge.

This model is obviously very crude, since as indicated in Figure 5.11 the resistance of the burden changes in a gradual rather than in an abrupt manner. It may be used however to assess the apparent influence of different reducing agents on furnace resistance.

Figure 5.11 indicates that the resistance of the furnace will be determined predominantly by the resistance of the reaction zone which will be lower than that of the solid or partially fused charge by several orders of magnitude. Since the resistance of coal-ore and coke-ore mixtures is the same for temperatures greater than 1200°C the furnace resistance should remain constant irrespective of the type of reducing agent used. However, it is found in practice that coal increases furnace resistance. This may be due to factors such as the physical and chemical properties of the coal. During its descent in the furnace, coal undergoes carbonization which increases its porosity and reactivity [124]. Fragmentation of the coal will take place with increasing temperature and depth in the furnace due to thermal and mechanical stresses as well as the melting of ash constituents which usually occur as layers in the coal lumps. Coke remains unaltered in physical characteristics except for the gradual reduction in size due to reaction with the ore or slag. It follows therefore that no direct comparisons can be made between the resistance of a furnace operating on coal and that of the same furnace operating on coke of the same initial size. Volkert [87] considers that use of a reducing agent of coarser size and lower reactivity results in the formation of a coke bed of increased size. This suggests that the type of reducing agent will determine the geometry, the size, the temperature and the chemical composition of the zones near the electrode tip. It is evident therefore that a reduction in the size or type of reducing agent in the burden will have a number of side effects that may be of significant importance in determining furnace resistance.

The influence of reducing agent size on the resistivity of experimental charges has been found to vary. Lorenz and Marincek [67] report a slight change while Silveira [68] found significant changes in resistance upon changing the size of the reducing agent. In the present investigation the influence of reducing agent size on the resistance of the charge was not strong enough to detect by the techniques used. One of the reasons for this is believed to be the fact that pressure was not applied to the charge.

These findings show that the influence of reducing agent size on charge resistance is not well understood. The recent findings of Dijs [64] go a long way towards establishing the importance of reducing agent size relative to the size of the ore in the charge. Dijs [64] found that it is not the absolute size of the reducing agent that determines the resistance of the charge but its size relative to the size of the ore. Furthermore he found that the variations in resistance decrease enormously, when the size of the ore is increased, irrespective of the size of the reducing agent. It is clear therefore that what is needed now is an extension of the basic theory formulated by Dijs [64]. The determination of the electrical characteristics of particular charges in the laboratory appears to have little to offer in improving furnace resistance.

5.4 Conclusions

1. The resistivities of Mamatwan ore and Delmas coal decrease by several orders of magnitude during heating owing to the physical and chemical changes that occur with increasing temperature. The resistivity of coke is little affected by temperature changes.

2. The resistivities of ore-coal and ore-coke mixtures are vastly different at low temperatures, decrease by several orders of magnitude during heating and attain the same value at about 1200°C.

3. Use of coal and coke in three different particle size ranges in mixtures of the two reducing agents and ore of a constant particle size did not influence the resistivity of the charges significantly.

4. Conduction of current in the higher regions of a submerged-arc furnace is practically non-existent and therefore the resistance of the furnace is determined by the conditions underneath the electrode tips.

5. The higher resistance of furnaces operating on coal, compared to the resistance obtained with coke of the same initial size, appears to be the result of the physical disintegration of the coal and the attendant changes in the internal structure of the furnace rather than to the higher resistance of the coal at low temperatures.

6. In order to determine the factors which govern furnace resistance it is necessary to carry out experiments under conditions similar to those obtaining in the molten regions of a furnace.

CHAPTER 6

6.0 EXAMINATION OF FURNACE SAMPLES

6.1 General

The samples discussed in this chapter were taken from furnace M1O at the Kookfontein plant of Metalloys Limited. The excavation of this furnace, and the collection and examination of samples was undertaken for two main reasons. Firstly it was believed that the excavation of the furnace would supply valuable information on a macroscopic scale with regard to the zones in a 75MVA unit. The number of production and pilot furnaces that have been excavated and examined to date is very limited. The furnace M1O is the first ferromanganese furnace to be excavated and certainly the first furnace of this size to be studied in this way. Secondly the detailed examination of samples from furnace M1O could provide valuable information with regard to the reactions that occur in the different furnace zones. A comparison between the results obtained from the furnace samples and those obtained from the SCICE experiments could indicate the extent to which the SCICE technique simulates furnace conditions and indicate refinements or alterations in experimental method.

The furnace under consideration was commissioned [1] in 1973 and had since been used for the production of high carbon ferromanganese. The values of the more important parameters of the furnace are shown in Table A3.1 of Appendix 3.

During the ten days prior to close down, control of the furnace operation was erratic and the furnace load was at a reduced level. The total power input for the last two days prior to close down on the 20th of September 1977, was 494 and 422 MWH respectively. The total power consumption per day under good conditions is about 840MWH.

The types of raw materials and the quantities charged to the furnace during the last ten days of operation are shown in Table A3.2 of Appendix 3. The size analyses of the raw materials for that period are shown in Table A 3.3 of Appendix 3.

Under normal operating conditions feed to the furnace is through 13 chutes, 4 around each of the three electrodes and one in the centre of the furnace roof. During the period 10 to 20th September 1977, feed to the central chute consisted of Mamatwan and Hotazel ores and quartz. An extra 50kg of quartz per batch* of charge was added to the mix of the central chute. Reducing agents were not fed through the central chute during this period. The central chute normally drew three batches of charge per day, while during the period 10 to 20th September 1977 it drew 1 batch of charge per day.

On the last day of operation 45 tons of metal were tapped from the furnace. After tapping, the furnace was operated for a further 2 hours and then closed down. Normally a 'heel' of metal is left in the furnace after each tap. With the procedure used to close the furnace down and the routine normally used for tapping an appreciable quantity of metal could be expected to have remained in the furnace.

The furnace was quenched with water for about 1 hours after close down. The quenching was interrupted when it was realised that the water gas reaction was occurring in the hot charge. Thus the furnace burden cooled down extremely slowly.

6 2 Sampling Procedure and Sample Identification

The excavation of furnace M10 commenced on the 11th of October 1977 when the top layers of the charge were reasonably cool. Sampling of the contents of the furnace was carried out on a 24 hour basis by a team of scientists and technicians provided by the National Institute for Metallurgy.

---

* A batch of charge consists of 2800 kg of ore plus the appropriate amounts of reducing agents, 'return' slag and flux.

Samples were mainly taken from the three planes indicated in Figure 6.1. The plan for sampling in the three planes is shown in the vertical section of Figure 6.2

Access to the furnace interior was gained at the No. 1 electrode (Figure 6.1) by removing an arc of steel shell subtending an angle of about 75^{o} at the centre of the furnace. A front-end excavator and a back hoe, which could enter the furnace via a ramp, were used to remove excess material as the excavation progressed.

The excavation commenced by knocking down part of the brickwork and carbon lining from the top of the exposed arc to level C approximately (See Figure 6.2). Loose material from the top layers of the charge was then removed manually through the opening in the wall. The brickwork and carbon paste were removed in successive stages until the hearth of the furnace was reached. As the excavated plane approached the hearth, the working area was increased by removing material from the adjacent wall to minimise the possibility of contamination by collapsing burden.

During the excavation, samples were taken, observations made, sketches drawn and many photographs were taken to provide visual evidence of the internal structure of the furnace. The location of a sample was established by using measuring tapes, the roof, the shell and the electrodes of the furnace serving as reference points. The sample location was then photographed together with an identifying marker and the sample taken. A number of samples appearing on the plan for sampling (Figure 6.2) were not taken due to collapsing of the burden and contamination.

The samples were identified with reference to electrode number, level and position. Electrode number refers to the proximity of a sample to a particular electrode. Sample level refers to the vertical distance between the sample locality and the highest point of the furnace shell and sample position refers

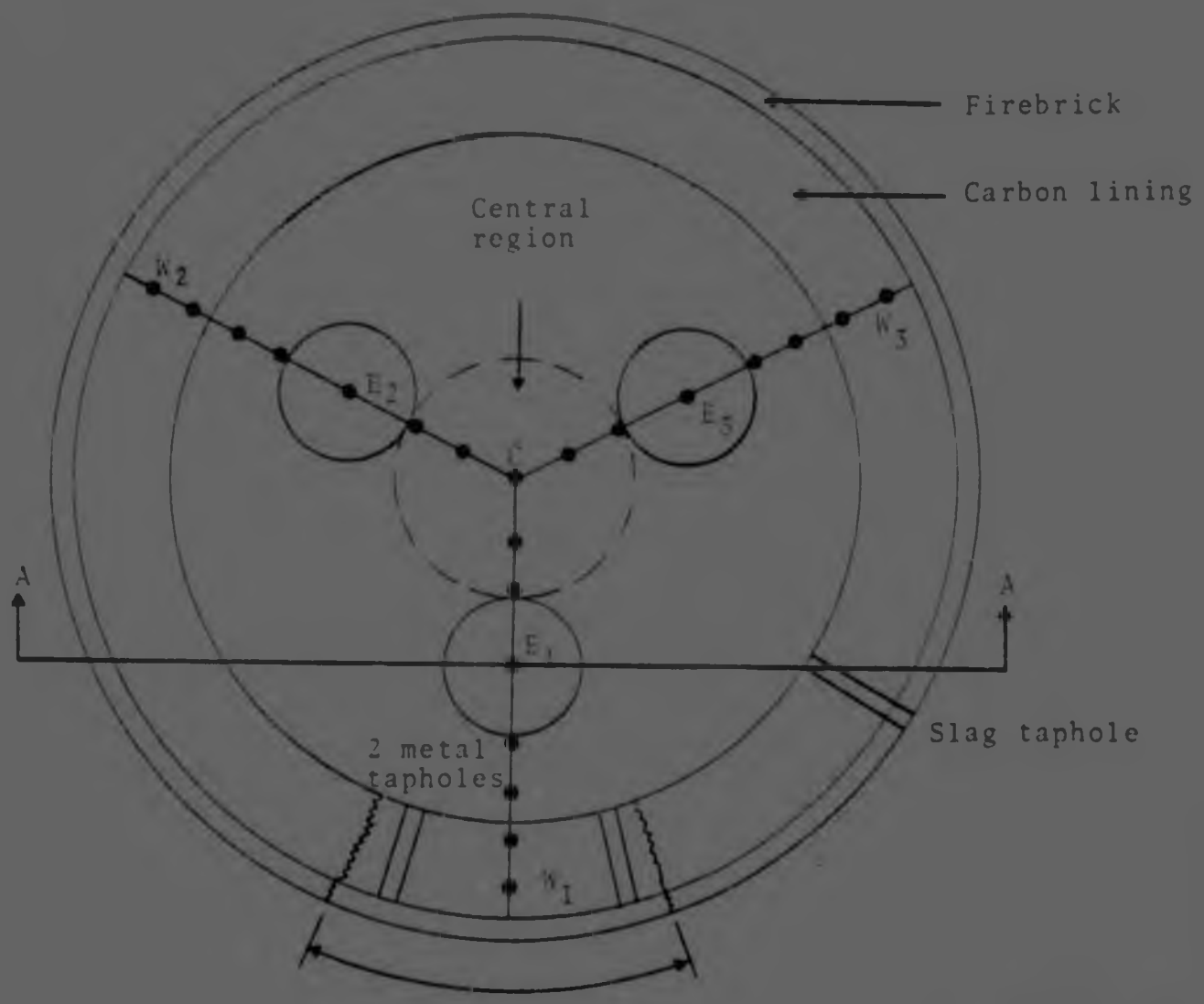
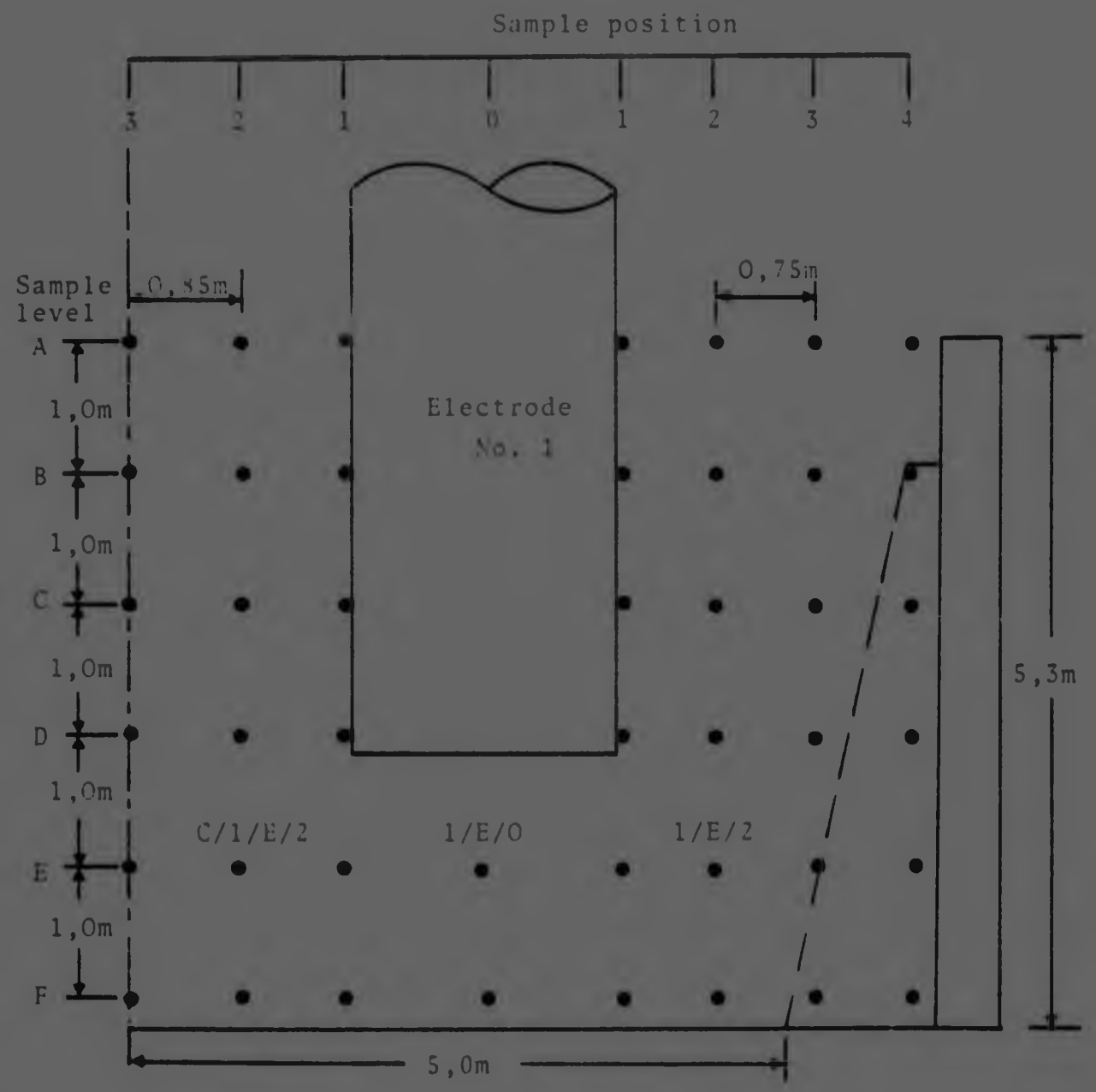


Figure 6.1 Section of furnace M10 in plan showing the position of the electrodes, the furnace diameter at roof and hearth levels and the planned sampling localities.



Scale 20mm = 1m

Figure 6.2 Vertical section through the furnace along radius CE_1W_1 (Figure 6.1) showing the planned positions for sampling.

to the horizontal distance between the electrode and the locality of a sample. Position O refers to samples taken at any level directly underneath the centre of an electrode. Thus the sample designated by 1/E/2 (Figure 6.2) was taken in the sampling plane CE_1W_1 (Figure 6.1) at level E and in position 2. Similarly, sample 1/E/O was taken in the same plane at level E and in position O which is directly underneath the electrode (Figure 6.2). The identifying code of samples that were taken from the central region (Figure 6.1) starts with C. For example, sample C/1/E/2 (Figure 6.2) was taken from the central region in plane CE_1W_1 at level E and position 2.

6.3 Appraisal of the Furnace Excavation

Ideally the excavation of a furnace such as that considered here should be carried out manually with possible use of small pneumatic or other mechanised equipment. The burden should be removed from the top downwards in layers of about 0,5 m and samples taken at intervals of 0,5 m both in the vertical and horizontal directions, in predetermined vertical planes. These planes should be chosen in such a way as to facilitate a detailed analysis of the processes occurring in the entire volume of the furnace.

A procedure such as the above would furnish samples from localities known with precision. A disadvantage of this method would be that synoptic visual evidence of the different zones in the furnace would not be obtained in any one vertical plane. However, since the sampling intervals would be small it would be relatively easy to construct the picture of a plane that was sampled. The gradual removal of the burden would allow ample time for a meticulous visual examination of the burden at the different levels. In addition it would allow the furnace to cool down far enough for manual excavation to be undertaken comfortably. It is obvious that such a procedure would furnish a great number of samples and their examination would probably be beyond the scope of an investigation such as the present. Also the cost of such a venture would be enormous.

The manual excavation of furnace M10 would have been an enormous task due to the enormous proportions (nett volume = 405 m^3) of this furnace. Also, a close-down period of unlimited duration would not be considered by any plant. Therefore, a compromise had to be made between manual and mechanised operations.

The gradual excavation of the burden around electrode No. 1 made it possible for many samples to be taken from plane E_1W_1 (Figure 6.2). The zones in the vicinity of electrode No. 1 were successfully exposed, sketched, measured and photographed. Some samples from plane E_1W_1 were not taken due to contamination from collapsing burden.

In order for the excavation to continue electrode No. 1 had to be removed. Removal of this electrode caused several tonnes of material from the central region to collapse into the excavated area. Thus most of the samples from the top layers of the burden in the central reg were not taken. Samples from the central region were mainly taken from levels E and F.

Sampling in planes E_2W_2 and E_3W_3 (Figure 6.1) was successful from level C downwards. The samples from level B were not taken due to contamination. Overall, only 62 per cent of the planned samples were successfully retrieved.

Approach to the Nos. 2 and 3 electrodes was from within the furnace and a detailed exposure of the zones around these electrodes was not obtained due to the collapsing of burden and its removal by excavator.

The use of excavators offered the advantage of removing large quantities of loose or sintered material very rapidly. However, it was not always possible to remove material to an accurately predetermined level.

The heat from the charge and the dust from the collapsing burden made it very difficult for the sampling team to remain in the furnace for very long periods at a time to carry out very accurate measurements and pin-point the sampling localities. The sampling localities given are estimated to be within 0,25 m of the planned localities.

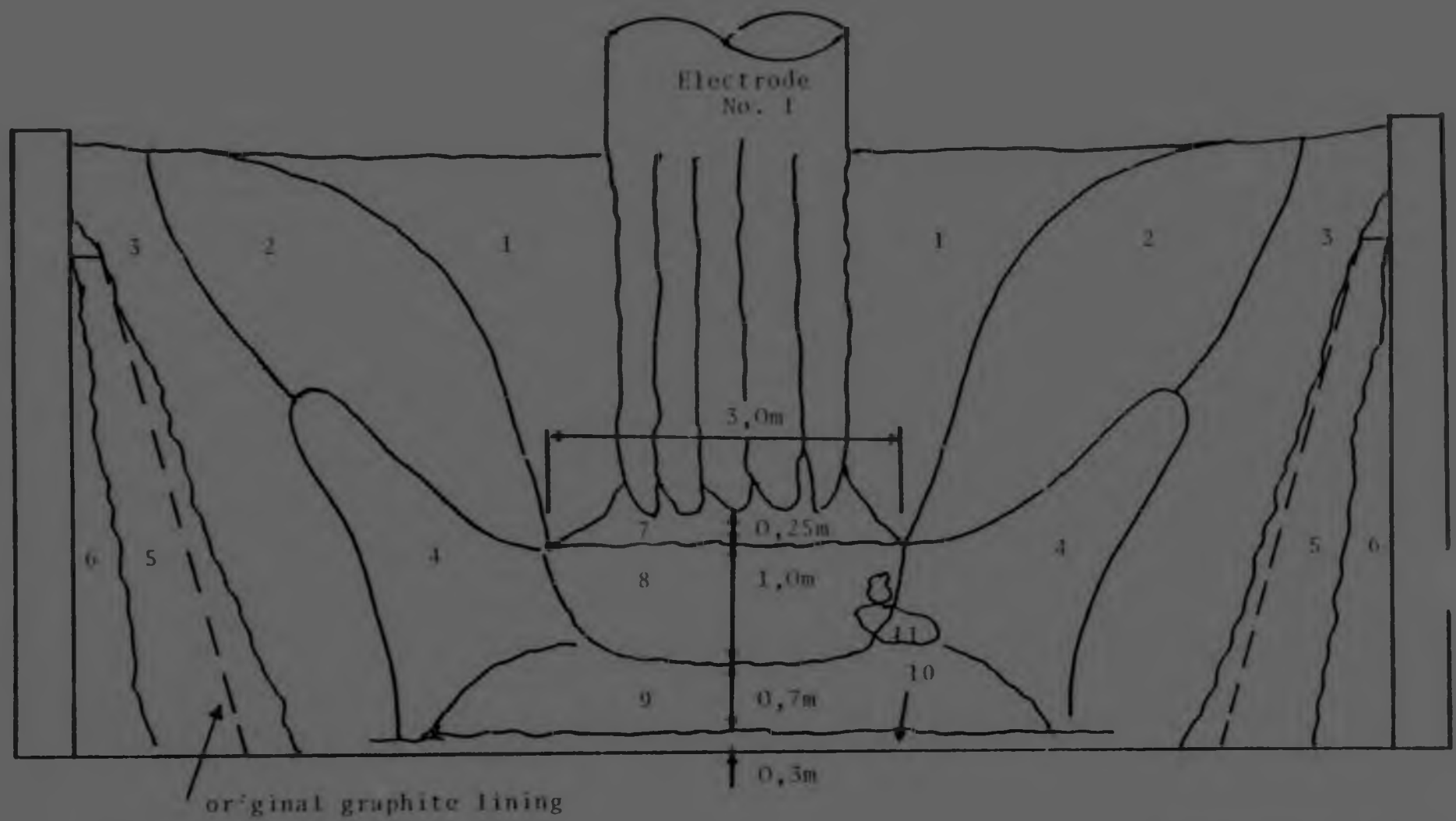
6.4 The Internal Structure of Furnace M10

The internal structure of furnace M10 is described with reference to the observations and measurements made around the No. 1 electrode since this electrode was exposed more successfully than electrodes 2 and 3.

Figure 6.3 shows section AA indicated in Figure 6.1. The different zones around the electrode are delineated by discrete boundaries a though the boundaries in the furnace were diffuse. The different zones were distinguished by differences in the size of the charge components, the colour of the charge, its composition and the apparent stage of reaction reached. The appearance of the different zones in the vicinity of electrode No. 1 is shown in Figure nd described briefly below.

Zone 1 : This is the cone of fast descending burden around the electrode. The aterial at the top was loose and had undergone little physical ange. Sintering of material was apparent at level C with considerable fusion and consolidation of the charge at level D. The charge in zone 1 retained its lumpy character.

Zone 2 : This zone consisted of loose charge at the top and loosely sintered material at the level of the electrode tip. An enrichment in reducing agents was apparent. Significant decrepitation of material had occurred and the colour of the charge was brown. The amount of decrepitation indicated that the charge had been retained at relatively high temperatures for prolonged periods. The boundary between zones 1 and 2 was enriched in reducing agents particularly at level B where substantial volumes of reducing agent were seen oxidising during the excavation. The oxidation of reducing agents produced ash which indicated clearly the areas enriched in reducing agents. The boundary between zones 1 and 2 is shown in Figure 6.5. The segregation of reducing agent evidenced by the light colour of the ash is clearly visible.



Scale 20mm = 1m

Figure 6.3 The distribution of zones in the vertical section AA of Figure 6.1



Figure 6.4 The appearance of the zones in the vicinity of electrode No.1.



Figure 6.5 The diffuse boundary between zones 1 and 2 (Figure 6.3) made apparent due to segregation of reducing agents. Note the penetration of the furnace shell.

Zone 3 : The material in this zone was loose at the top and loosely sintered at the bottom. Decrepitation of the charge and segregation of reducing agents were very extensive. The rate of movement of material in this zone was probably extremely low.

Zone 4 . This zone consisted of loosely sintered charge and extended upwards from the hearth as indicated in Figure 6.3. Sintering and slag formation were more extensive than in zones 2 and 3.

Zone 5 : This zone consisted mostly of accretions of carbonaceous material and occupied the position of the original carbon lining of the furnace.

Zone 6 : This zone consisted of the original carbon lining of the furnace which had not reacted with the charge. The thickness of the carbon lining varied from place to place in the furnace being completely absent in some areas.

Zone 7 : This zone consisted mainly of reducing agents and some slag and corresponded to what is commonly referred to as the 'coke bed'. The material was firmly packed around and under the electrode tip leaving no cavities, as was also the case with electrodes 2 and 3.

Zone 8 : This zone was a mixture of slag and reducing agents. The material could be broken easily owing to the crumbly nature of the slag. Zone 8 was similar to 7 except for its lower concentration in reducing agents Zones 7 and 8 are illustrated in Figure 6.6. Figure 6.7 is a close-up view of zone 8 and shows the decrepitating nature of the slag and the reducing agent embedded in it. The lumps of reducing agent exhibited a smooth surface indicating erosion due to reduction and mechanical action.

Zone 9 : This was a layer of slag with some reducing agents. The slag was powdery underneath the electrode and had a sandstone consistency further to the sides of zone 9. Towards the edge of the zone the slag was hard and crystalline. Part of

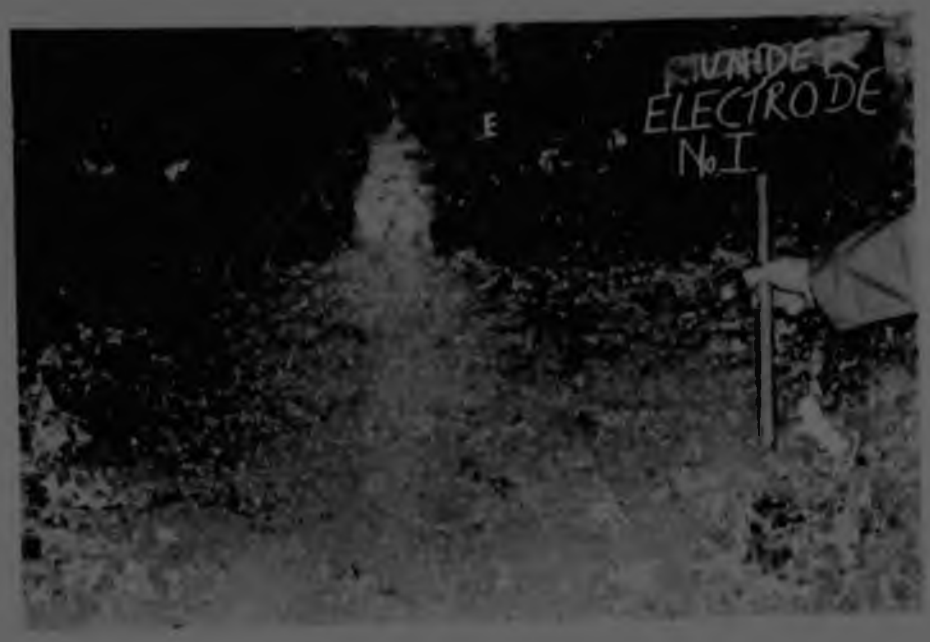


Figure 6.6 The 'coke bed' directly underneath the electrode (E) and the coke-enriched zone at some distance from the electrode tip.

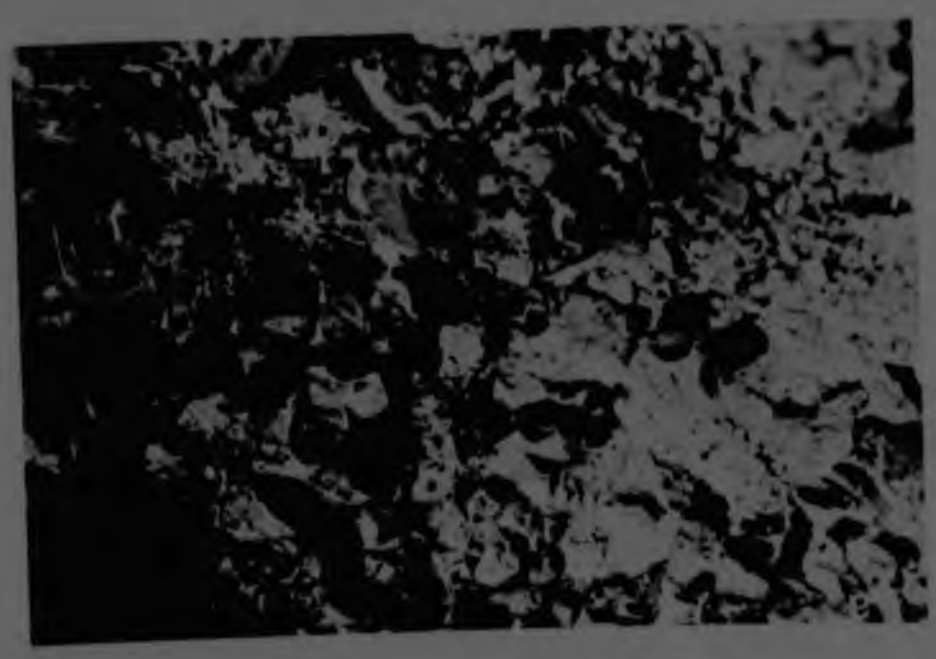


Figure 6.7 A close-up view of zone 8 (Figure 6.3) showing lumps of reducing agent embedded in the slag.

zone 9 is shown in Figure 6.8 together with some of the neighbouring zones. Lumps of slag with the sandstone consistency can be seen in the layer of powdery material.

Zone 10 : Zone 10 consisted of alloy and slag. The alloy in some regions contained graphite flakes and cleaved along these flakes under pressure. Alloy that contained graphite flakes was also found higher in the furnace.

Pieces of carbon paste that had broken off from the electrode are indicated in Figure 6.3 as zone 11. A layer of slag was present around the lumps of paste (Figure 6.8) indicating reduction of the ore by the electrode paste.

The casing of the electrode had been eroded by reaction with the environment and the electrode tip showed a 'finger-like' structure due to reaction and erosion. The mild steel 'ribs' used to re-enforce the electrode had been removed close to the electrode tip and it appeared that most of the gaseous products of reaction escaped through the channels so created. The shape of the tips of electrode Nos. 2 and 3 was similar to that of Electrode No. 1 except for a less pronounced 'finger-like' appearance. The diameter of the electrode was slightly reduced over a distance of about 800 mm from the tip. The appearance of the tip of the No. 1 electrode is shown in Figure 6.9.

The dimensions of some of the zones were obtained from measurements made during the excavation and are shown in Figure 6.3. The boundaries of the zones that were not measured were drawn to a first approximation from sketches made during the excavation and from photographs.

The zones around electrodes 2 and 3 were not observed in great detail due to the collapsing of the burden upon removal of the No. 1 electrode.



Figure 6.8 The variable consistency of zone 9.



Figure 6.9 The 'finger-like' appearance of the tip of electrode No. 1.

A large heap of sintered charge in the central region from Level E downwards indicated a partially 'dead zone' in the centre of the furnace. In this region the lumps of reducing agent were surrounded with slag and appreciable amounts of metal were observed at the interface between the slag and the reducing agent as indicated in Figure 6.10. This mode of occurrence of metal was not observed in other areas of the furnace.

6.5 Processing of Furnace Samples

It is to be expected that samples taken from an industrial furnace would be heterogeneous even on a scale of a few tens of millimetres. It was therefore necessary to take fairly large samples in order to ensure that maximum benefit was gained from them. The mass of the samples varied with locality being in general greater than 2kg. The samples taken from face CE_1W_1 ranged in mass between 2 and 10 kg the average mass being 4,6kg.

The samples were processed according to the general scheme shown in Figure 6.11. Through this procedure it was possible to investigate aspects of furnace operation such as the decrepitation of the burden, segregation of the reducing agent and the reduction of the ore. It is clear that the procedure shown in Figure 6.11 could not be used with all the samples since some of them consisted entirely of slag or metal.

The approximate temperature in a limited number of furnace localities was determined by establishing the phases in lumps of quartzite flux.

The phases present in lumps of partially reduced ore or in the metal were studied by the microscopic examination of mounted sepcimens, by X-ray diffraction analysis and by X-ray microanalysis. Chemical analyses were carried out mainly on the metallic component of the samples to determine the processes occuring in the formation of the alloy.



Figure 6.10 The appearance of the partially dead zone in the central region of the furnace. Lumps of reducing agent are embedded in the slag and alloy appears at the interface between the slag and the reducing agent.

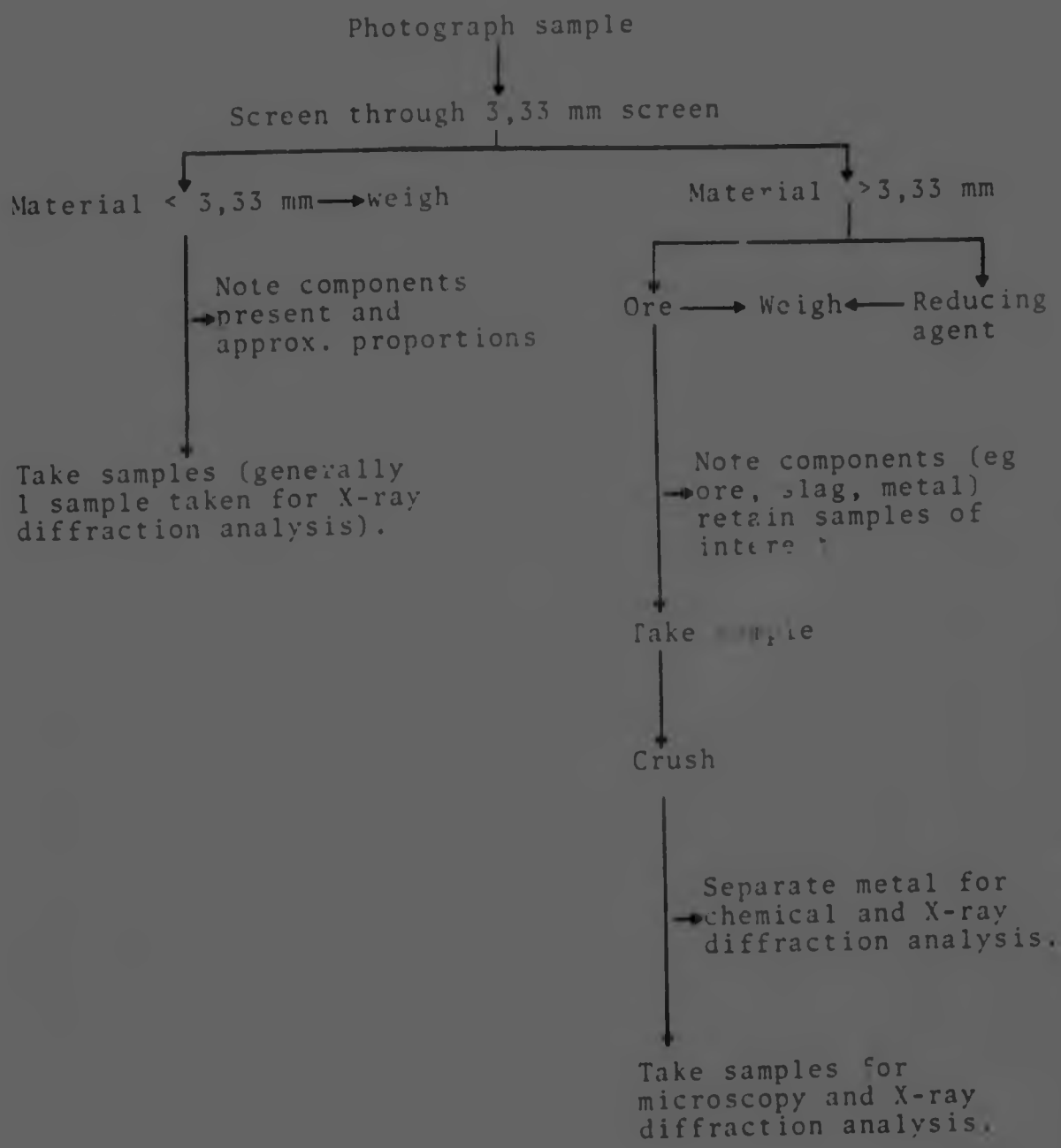


Figure 6.11 Scheme for the processing of furnace samples.

6.6 Examination of Samples from Face CE_1W_1

6.6.1 Visual Examination

The samples that were successfully taken from face CE_1W_1 are shown in Figure 6.12. A summary of the visual examination of the coarse fraction of these samples is shown in Table 6.1 The fine fraction consisted mainly of reducing agent and some ore or slag.

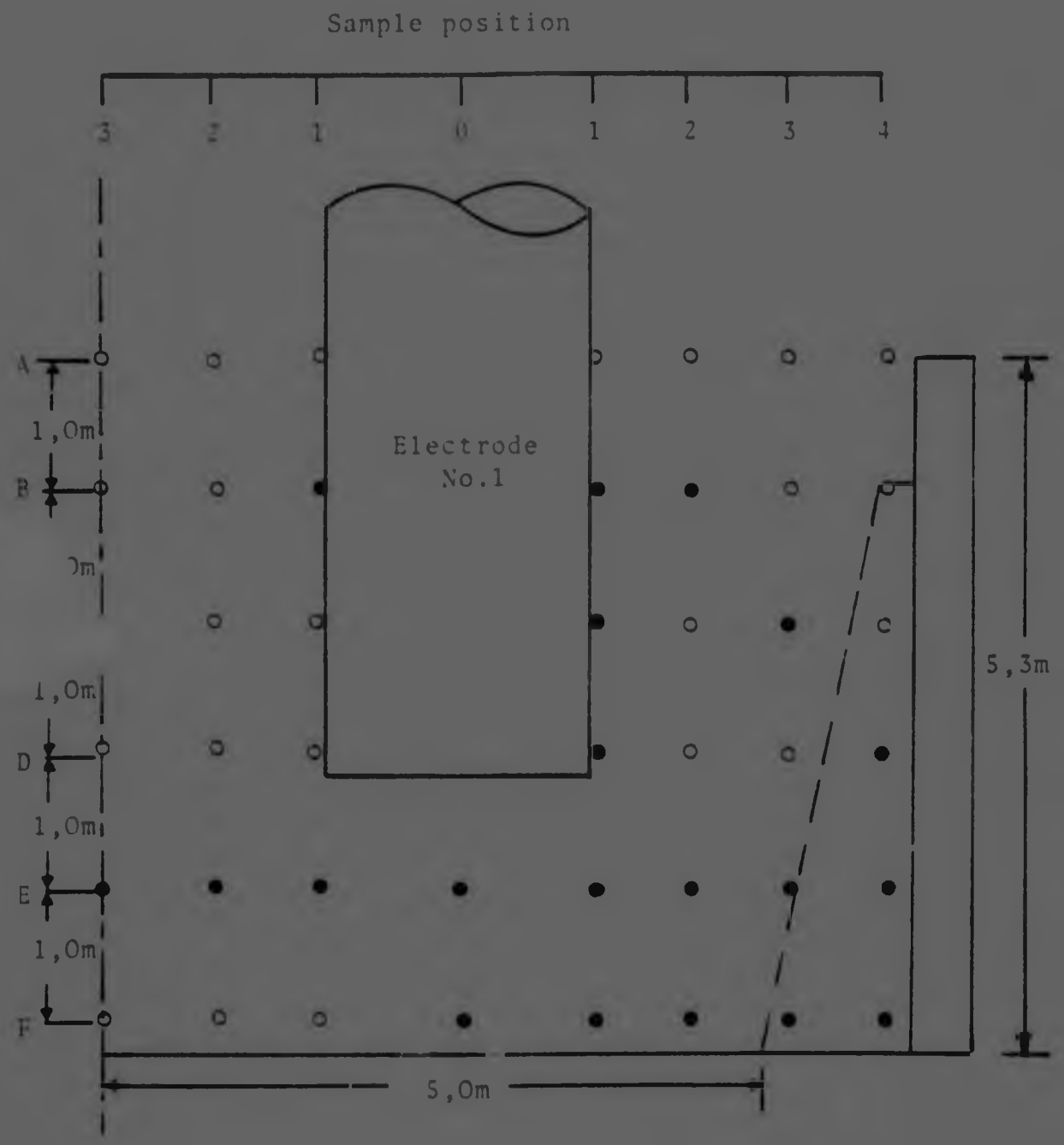
The term slag in Table 6.1 is used in a very broad sense to describe a product formed by the fusion and fluxing of burden components that was more or less homogeneous on a macroscopic scale. The appearance of the slag varied with furnace locality and the differences will become apparent in subsequent sections where the results of microscopic investigations and X-ray diffraction analysis are considered.

The samples from level E in the central region of face CE_1W_1 showed extensive sintering and metallization although the original ore lumps could still be distinguished.

The slag at level E underneath the electrode was powdery as shown in Figure 6.13 and indicated that the material in this locality had been in the liquid state. The slag at level F was coherent and consisted of the hard crystalline and sandstone varieties as indicated in Figure 6.14.

The alloy in this sample occurred as globules disseminated in the slag, as 'graphitized' lumps and as lumps that showed no apparent graphitization. This type of mixture was encountered in samples from levels E and F. In such cases chemical analyses were carried out on the different types of alloy.

The samples from position 1 between the electrode and the furnace wall formed a continuous series and supplied a lot of information with regard to the physical and chemical changes undergone by the ore during its descent towards the hearth.



Scale 10mm = 1m

Figure 6.12 Vertical section through plane CE_1W_1 (Figure 6.1)
Closed circles indicate samples that were taken
Open circles indicate samples that were not taken.

Table 6.1

Summary of the visual examination of the coarse fraction of samples from face CE_1W_1

Sample level	SAMPLE POSITION							
	3	2	1	0	1	2	3	4
B	X	X	B		B	B	X	X
C	X	X	X		B+S+A	X	B	X
D	X	X	X	X	S+A	X	X	S+R
E	SL+S+A+R	S+R	S+R	SL	SL+A	SL+A+R	A	SL+R
F	X	X	X	SL+A	SL+A	SL+A	SL+A	A

Key

B = burden-mixture of unreacted or partially reacted ore and reducing agent.
S = sinter-mixture of any number of constituents held together by slag.
A = alloy-any metallic phase
R = reducing agent - any carbonaceous material
SL = slag - a homogenous constituent (macroscopically) formed as a result of fusion and fluxing
X = samples not taken from these localities



Figure 6.13 Powdery slag in sample 1/E/O.

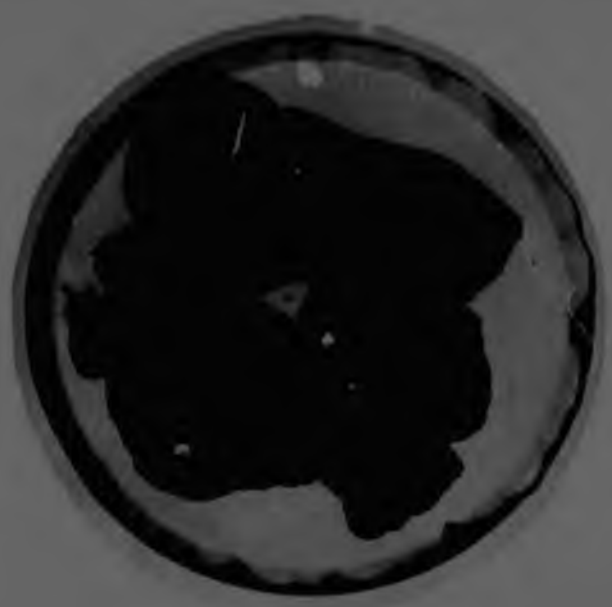


Figure 6.14 Lumps of slag with associated alloy in sample 1/F/O.

A faint green colour in the ore at level B indicated that reduction of manganese oxides to manganous oxide was taking place. It has been seen from the results of the SCICE experiments that this colour change takes place under conditions that would cause the reduction of iron oxide to metallic iron.

At level C considerable sintering occurred and appreciable amounts of alloy appeared as globules on the lumps of ore. A lump of sinter from sample 1/C/1 is shown in Figure 6.15. The ore is covered with a layer of slag of the order of 1 to 2 mm thick and a lump of coke is cemented in the centre. Metallic globules appear as fissures on the surface of the sintered ore. This structure shows clearly that direct contact between coke and ore or slag is not necessary for reduction to metal. It will be seen from Table 6.5 that the alloy contained 54 per cent by mass of manganese.

At level D the proportion of slag increased significantly as indicated in Figure 6.16 which shows a section through a lump of sinter. The positions from where lumps of reducing agent became dislodged are indicated. The general distribution of metallic globules in the section is indicated for clarity by circles or dots. It can be seen that there is little direct association between the solid reducing agent and the alloy and that the bigger metallic particles are situated at the interface between the partially reduced ore and the slag.

The structure shown in Figure 6.16 was not encountered in samples from levels E and F. The nature of the samples from these localities indicated that as the sintered material from level D descended to level E it entered a region of very high temperature and vigorous stirring. These conditions made the slag that held together lumps of ore and grains of oxide very fluid causing the complete dispersal of the oxide grains in the slag. The mixture formed a coherent mass upon cooling and solidification. The appearance of samples from levels E and F was similar to that shown in Figure 6.14.

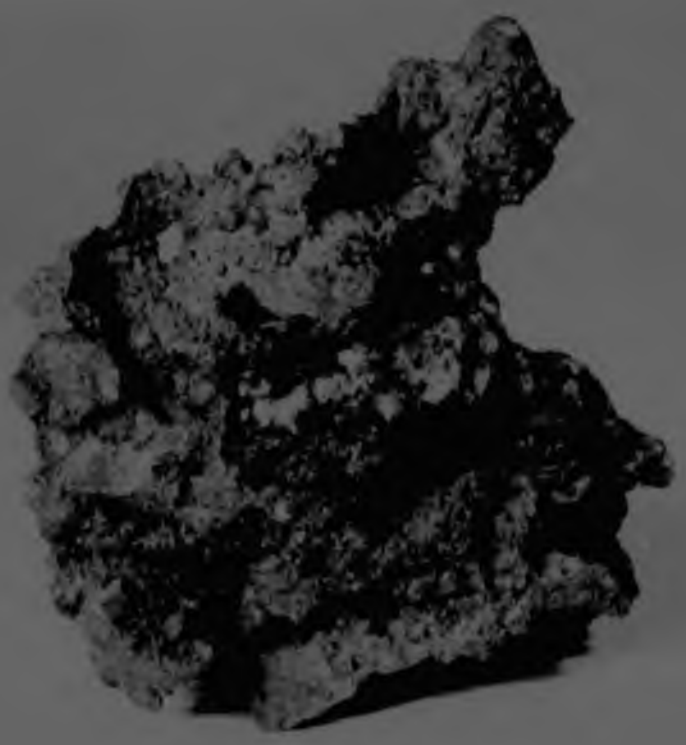


Figure 6.15 Sinter from sample 1/C/1 showing the distribution of metallic particles.
Actual size.

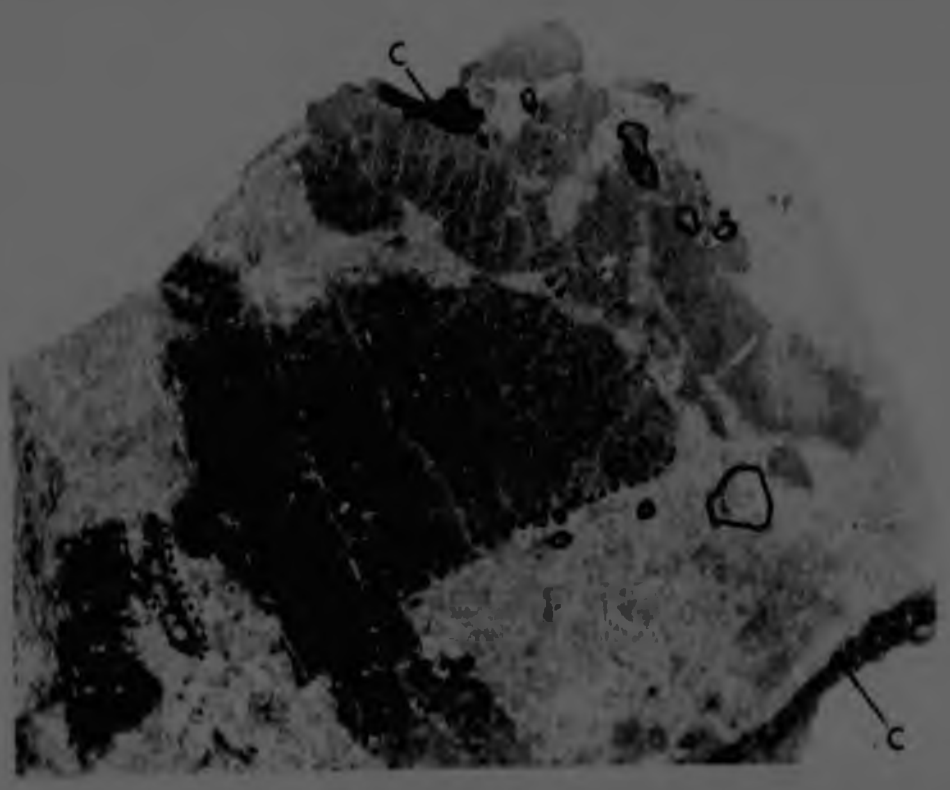


Figure 6.16 Sinter from sample 1/D/1 showing partially reduced ore (dark grey), slag (light grey), alloy, and the positions of particles of reducing agent (C).
Polished 4X.

Samples further away from the electrode showed less extensive reduction and a higher proportion of reducing agent and fine material at all furnace levels.

The fine material that resulted from the oxidation of reducing agents during the excavation and from the decrepitation of burden components is illustrated in Figure 6.17 which shows sample 1/B/2.

The segregation of reducing agent and excessive decrepitation of the burden are illustrated in Figure 6.18 which shows sample 1/C/3. Samples from position 4 showed a similar appearance to sample 1/C/3 with a greater or lesser proportion of ore or slag.

The proportions of fine material (less than 3,33 mm) and reducing agent in samples that contained these components are indicated below.

Sample	Fine fraction, mass per cent	Reducing agent in coarse fraction mass per cent
1/B/2	19,5	0
1/C/3	33	63
1/D/4	40	63
1/E/4	78	88

6.6.2 Microscopic examination

All the samples taken from face CE_1W_1 were examined microscopically. The changes that occurred in the ore were similar to those observed in samples taken from the SCICE experiments. The progressive changes in the structure of the ore, with increasing depth in the furnace, and the changes in the alloy will be discussed by reference to the samples taken from position 1 in plane CE_1W_1 (Figure 6.2).

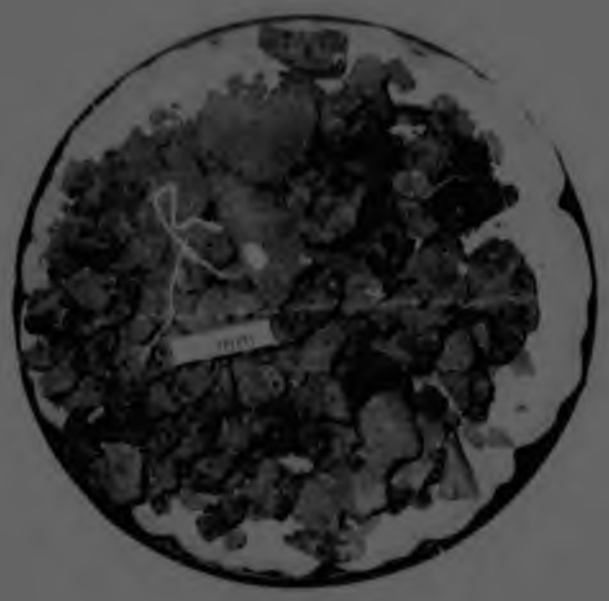


Figure 6.17 Fine material in sample 1/B/2 generated by the oxidation of reducing agents and decrepitation of ore lumps.

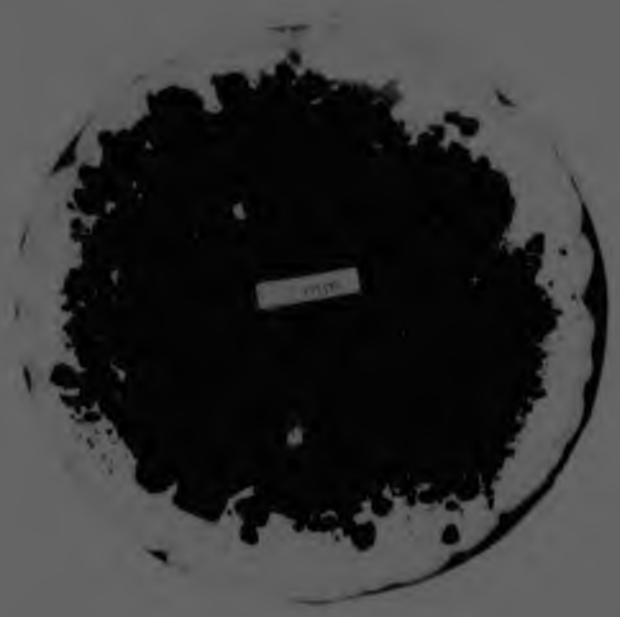


Figure 6.18 Segregation of reducing agents and excessive decrepitation of the burden in sample 1/C/3.

The dissociation of gangue minerals and the reduction of higher manganese oxides to manganous oxide occurred at level B in the furnace. These reactions led to the formation of a sponge-like mass of oxide as indicated in Figure 6.19. The pores in the structure were probably filled, in part, by oxides such as CaO, MgO and SiO_2 resulting from the decomposition of calcite, dolomite and braunite. Traces of metal were present in some ore particles.

At level C the gangue minerals reacted to form a slag while the spongy oxide began to break up into discrete particles as indicated in Figure 6.20. An appreciable amount of metal formed and the amount of porosity was reduced due to the surface tension of the viscous slag. The pores began to attain a more or less rounded configuration.

At level D the amount of porosity in the ore was reduced to a very low level, the oxide grains in the slag matrix attained a well rounded shape and increased in size, the number of metallic particles in the interior of the ore particles increased while their size was basically unaltered and the size of metallic globules on the surface of ore particles increased drastically. The metallic particles in the interior of ore particles showed a single phase while the alloy globules on the surface consisted of at least two phases (Figure 6.21). The structure of alloy globules on the surface of ore particles varied from hypoeutectic to hypereutectic. The large alloy globule shown in Figure 6.21 has a eutectic structure showing dispersed particles of austenite in a matrix of carbide.

The structures observed in samples 1/E/1 and 1/F/1 were drastically different to the ones already described. These two samples consisted of 'slag' of the sandstone and hard crystalline varieties. Microscopic examination showed that the hard crystalline material consisted almost entirely of MnO which occurred as extremely coarse grains (Figure 6.22). These grains were surrounded by a thin film of slag while metallic particles occurred interstitially between oxide grains. Some metallic particles were found in the interior of oxide grains. These were invariably smaller than interstitial metallic particles.

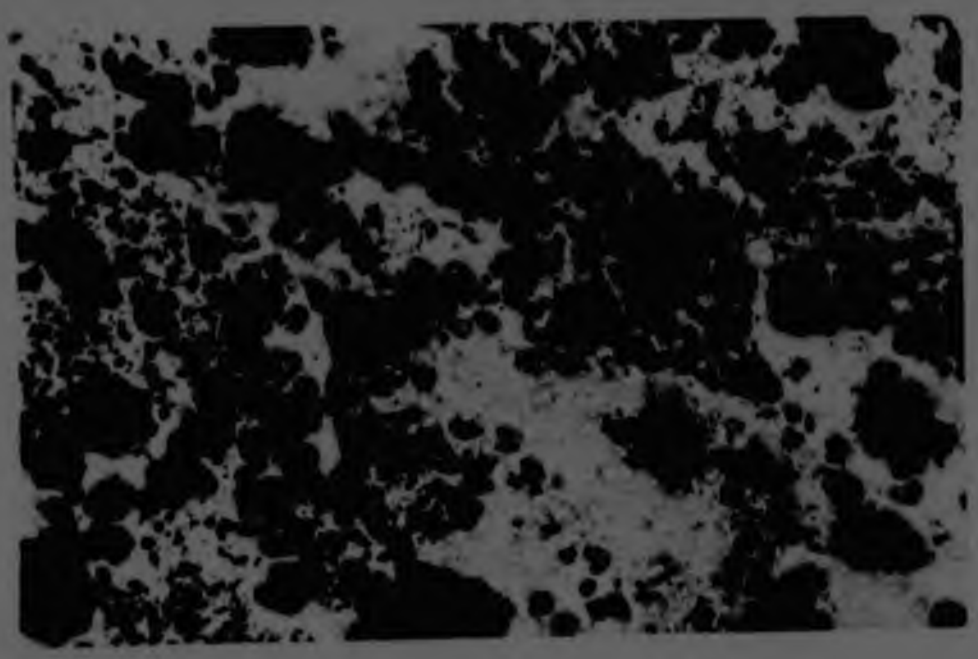


Figure 6.19 The porous structure of partially reduced ore from sample 1/B/1.
Polished 120X, enlarged 45 per cent.

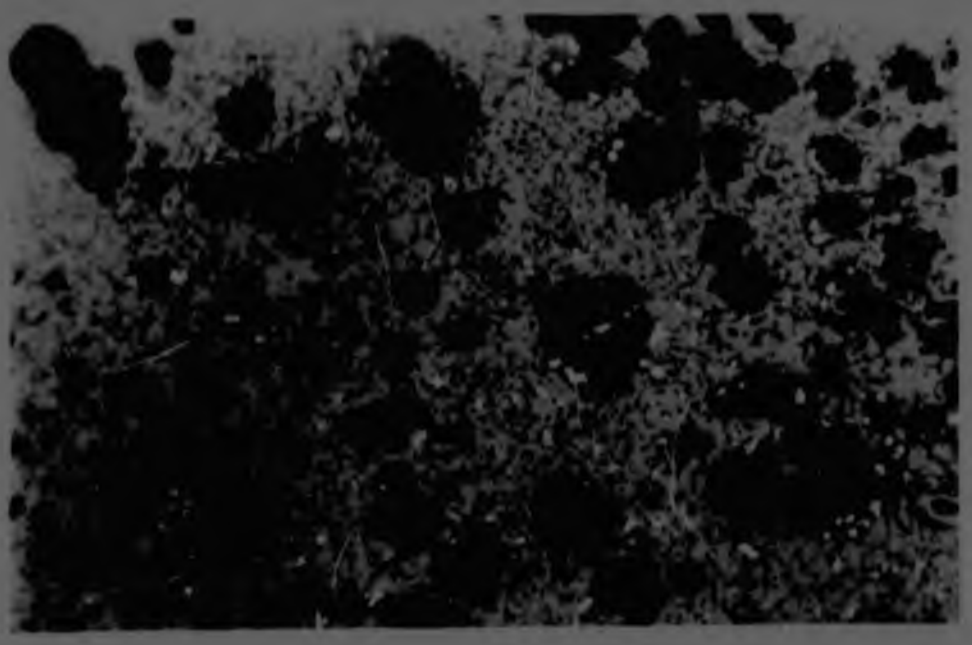


Figure 6.20 An ore particle from sample 1/C/1 showing MnO particles (light grey) and metallic particles (bright) in a matrix of slag. Pores appear black.
Polished 120X, enlarged 45 per cent.

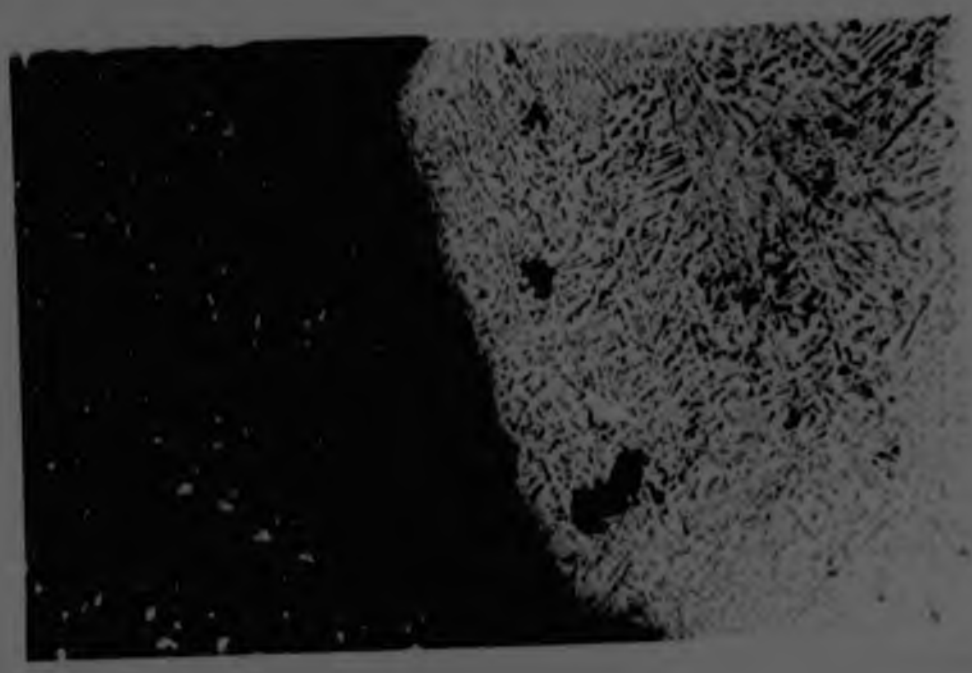


Figure 6.21 Metallic nuclei and grains of MnO in a matrix of slag. An alloy globule of eutectic composition adheres to the surface of the ore particle from sample 1/D/1.
Etched 2% HNO_3 in alcohol, 120X, enlarged 45 per cent.

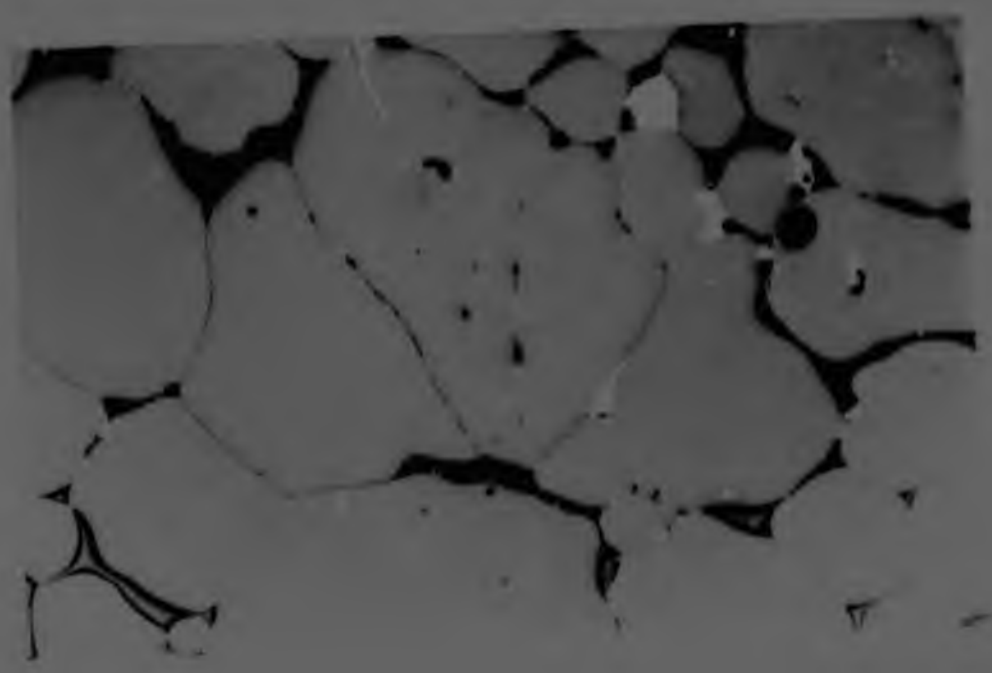


Figure 6.22 Coarse grains of MnO surrounded by a film of slag in sample 1/E/1.
Polished, 60X, enlarged 33 per cent.

The sandstone-like material was similar in structure to that described above although the proportion of slag was much higher and the oxide grains significantly smaller (Figure 6.23).

The 'massive' alloy in samples 1/E/1 and 1/F/1 was of two different varieties the one consisted of crystalline material while the other showed flakes of precipitated graphite. The graphite flakes reduced the strength of the alloy to the extent that it could be broken by hand. Figure 6.24 shows thick flakes of graphite in the alloy from sample 1/F/1. Very thin flakes of graphite were also found in the alloy. Lines in the alloy, similar to those shown in Figure 3.21 were probably due to extremely thin graphite flakes which could not be resolved.

6.6.3 X-ray Diffraction Analysis

6.6.3.1 Analysis of the Non-metallic Constituent

X-ray diffraction analyses were carried out on all the samples from face CE_1W_1. Table 6.2 shows the phases identified in samples which contained mostly non-metallic material. Lumps of alloy were not included in these samples in order to obtain better peak to background intensity ratios from the phases present. The phases are given in decreasing order of abundance. It may be noted that the phases identified in samples from position 1 between the electrode and the furnace wall confirm the results of the microscopic examination given in the preceding section.

Further X-ray diffraction analyses were carried out on selected constituents of some of the samples from face CE_1W_1. The constituents analysed and the phases identified are shown in Table 6.3 in decreasing order of abundance. It may be noted that the presence of carbon as the major constituent of the fine fraction of many samples confirms the results of the visual examination of these samples.

6.6.3.2 Analysis of the Alloy

The phases in the metallic component of the samples were investigated in more detail by X-ray analysis. Samples were prepared from lumps of alloy or from alloy globules separated from slag or sinter.



Figure 6.23 Grains of MnO and metallic particles in a matrix of slag from sample 1/F/1.
Polished, 60X, enlarged 33 per cent.



Figure 6.24 Thick flakes of graphite in the alloy from sample 1/F/1 .
Polished 120X, enlarged 45 per cent .

Table 6.2 The phases in the partially reacted ore samples from face CE_1W_1

Sample level	SAMPLE POSITION							
	3	2	1	0	1	2	3	4
B	X	X	BR $CaCO_3$ MnO Mn_3O_4	Electrode No 1	MnO CS, trace	Mn_3O_4 MnO BR	X	X
C	X	X	X		MnO Fe CMS	X	MnO Mn_3O_4 BR	X
D	X	X	X	X	MnO CMS Fe	X	X	CMS C x
E	MnO CMS Fe	MnO CMS Fe	MnO CMS Fe	CMS MnO-trace	MnO Mn	MnO Mn Fe CS, trace	A	MnO Fe x
F	X	X	X	MnO CMS Fe	MnO Mn Fe CMS, trace CS, trace	MnO Mn Fe	MnO Mn Fe, trace CS, trace	A

KEY:

BR - braunite

CS - calcium silicate (Ca_2SiO_4)

CMS - calcium manganese silicate ($(Ca,Mn)_2SiO_4$)

A - samples consisting of alloy only

X - samples not taken from these localities

x - a phase in appreciable proportion that was not identified.

Table 6.3 The phases in selected constituents of some samples from face CE_1W_1

Sample Code	Description of constituent analysed	Phases present
1/B/2	Material < 3,33 mm	Mn_3O_4, MnO, Braunite, C
	Material < 0,42 mm	C, Mn_3O_4, MnO, Braunite
1/C/3	Material < 3,33 mm	C, Fe, Mn_3O_4
1/D/4	Material < 3,33 mm	C, $(Ca, Mn)_2SiO_4$, MnO
1/E/4	Material < 3,33 mm	$(Ca,Mn)_2SiO_4$, MnO, Fe
C/1/E/2	Quartzite	Low alpha christobalite, tridymite, alpha quartz
C/1/E/1	Quartzite	Alpha christobalite, tridymite

The phases identified are shown in Table 6.4. It should be noted that constituents in low proportions in the alloy were also present but they were not positively identified from the diffractograms. For samples 1/F/O and 1/F/2 analyses were carried out on alloy of two different chemical compositions (Table 6.5). The 'graphitized' alloy from sample 1/F/O exhibited $(Fe, Mn)_7C_3$ as the major phase. The 'crystalline' alloy contained mainly $(Fe, Mn)_7C_3$ with a small proportion of $(Fe, Mn)_5C_2$.

The 'graphitized' alloy in sample 1/F/2 showed $(Fe, Mn)_7C_3$ and $(Fe, Mn)_5C_2$ while the alloy globules that were separated from the slag showed a pattern that agreed well with that of $Fe_{0,4}Mn_{3,6}C$ and Mn.

It can be seen from Table 6.4 that the lower carbides form in the higher regions of the furnace while the higher carbides form in the lower furnace regions. Discrepancies occur in samples which did not contain alloy in the massive form.

The diffractograms obtained were, in most cases, significantly different to those obtained from SCICE samples. Definite changes in the diffractograms were found with increasing carbon content of the alloy as shown in Figure 6.25. For a carbon content of 7,7 per cent (sample 1/F/O, Table 6.4) the diffractogram (Figure 6.25a) was similar to those of SCICE samples (Figure 3.25). As the overall carbon content increased the intensity of certain peaks was reduced until they finally disappeared (Figure 6.25 b and c). This sequence indicated that an increase in the overall carbon content was accompanied by an increase in the proportion of combined carbon in the alloy.

The phases $(Fe, Mn)_3C$ and $(Fe, Mn)_7C_3$ in Table 6.4 were not arrived at by direct comparison of experimental and known d-spacings but by comparison with the data for Fe_3C and Cr_7C_3. The carbide Fe_3C is isomorphous with Mn_3C [125] which is isomorphous with $(Fe, Mn)_3C$ [126].

Table 6.4 The phases in the metallic component of samples from face CE_1W_1

Sample level	SAMPLE POSITION							
	3	2	1	0	1	2	3	4
B	X	X		Electrode No. 1				
C	X	X	X		$(Fe,Mn)_3C$	X		X
D	X	X	X		$(Fe,Mn)_3C$	X	X	
	$(Fe,Mn)_7C_3$		α - Fe		α - Mn	$(Fe,Mn)_7C_3$	$(Fe,Mn)_7C_3$	
	$(Fe,Mn)_5C_2$	$(Fe,Mn)_3C$	$(Fe,Mn)_3C$		α - Fe	$(Fe,Mn)_5C_2$	C	
F	X	X	X	$(Fe,Mn)_7C_3$	$(Fe,Mn)_7C_3$	$(Fe,Mn)_7C_3$	α - Mn	$(Fe,Mn)_7C_3$
				$(Fe,Mn)_5C_2$	$(Fe,Mn)_5C_2$	$(Fe,Mn)_5C_2$	α - Fe	$(Fe,Mn)_5C_2$
						$(Fe_{0.4}MN_{3.6}C$		
						α - Mn		

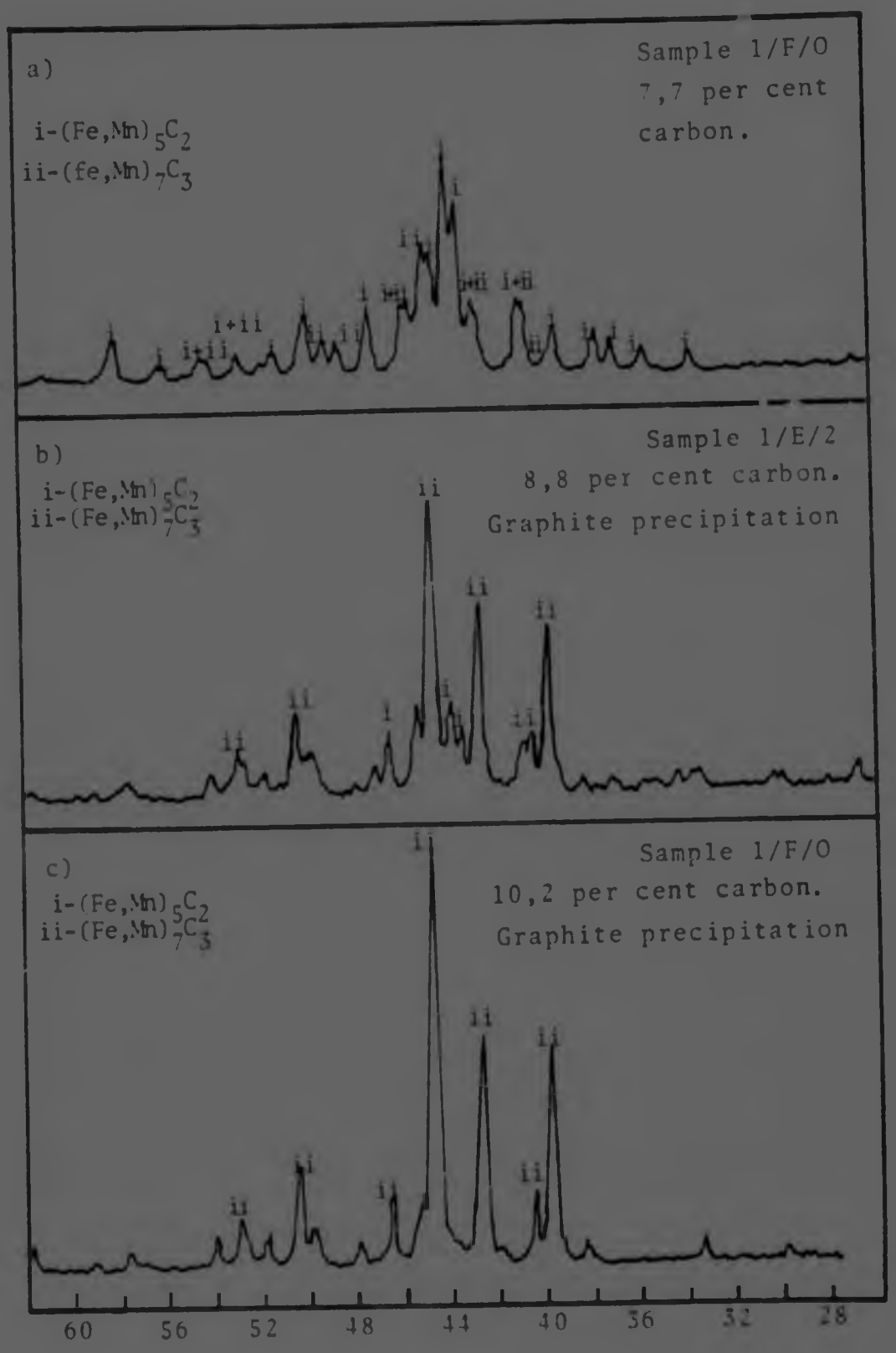


Figure 6.25 Variations in the X-ray patterns of the alloy with increasing carbon content.

Similarly, Cr_7C_3 is isomorphous with Mn_7C_3 [125] which is isomorphous with $(Fe, Mn)_7C_3$ [126].

It should be noted from Table 6.4 that in some samples ε-Mn and α-Fe occurred as separate phases and not as a solid solution or austenite as predicted by the Fe-Mn phase diagram [114]. This indicates that the manganese formed by the melting of previously volatilised material which condensed in the colder furnace regions.

6.7 The Chemical Composition of Alloys

Chemical analyses were carried out on the metallic component of samples from face CE_1W_1 in an attempt to establish possible trends in the composition of the alloy and deduce the processes that occur during furnace operation. The results are shown in Table 6.5 and Figure 6.26, 6.27 and 6.28.

Figure 6.26 shows the composition of alloys from position 1 between the electrode and the furnace wall. It can be seen that the alloy became richer in manganese as it descended from level C to E. The decrease in manganese content between levels E and F was due to a drastic increase in the carbon content of the alloy. The iron content of the alloy decreased with increasing depth in the furnace. It is clear that the hematite in the ore was mainly reduced between levels A and C in the furnace. The carbon content of the alloy increased between levels C and D and decreased between levels D and E. These changes in carbon content can probably be explained on the basis of the physical condition of the charge. Carburization of the metal between levels C and D by carbon monoxide, was possible due to the porous nature of the sinter (Figure 6.15). The carburisation of alloy globules at level E was probably not efficient due to the absence of porosity (Figure 6.22). Therefore any reduction of manganous oxide by carbon dissolved in the alloy would result in an alloy of reduced carbon content. The alloy at level F formed a pool and dissolved carbon from the reducing agent with which it was in contact.

Table 6.5 The chemical composition of the metallic constituent from samples in plane CE_1W_1 (Numbers designate mass per cent Mn, Fe and C in this order)

Sample level	SAMPLE POSITION							
	3	2	1	0	1	2	3	4
B	X	X		Electrode No.1			X	X
C	X	X	X		54,0 37,4 5,2	X		X
D	X	X	X	X	66,8 25,7 6,3	X	X	
E	71,5 22,8 8,2	G 33,7 50,4 10,8	9,4 82,6 4,8		A.S 75,1 21,5 1,2	G 73,9 11,4 8,8	G 50,6 9,1 31,6	
F	X	X	X	G 75,0 14,0 10,2	C 78,4 13,8 7,7	G 70,8 13,4 12,7	G C 73,7 73,4 13,5 18,8 12,5 5,0	A.S 64,1 33,2 1,0	G 74,0 13,8 10,2

G - massive alloy showing graphite flakes; C - massive alloy with no apparent graphite
A.S. - alloy globules extracted from slag.

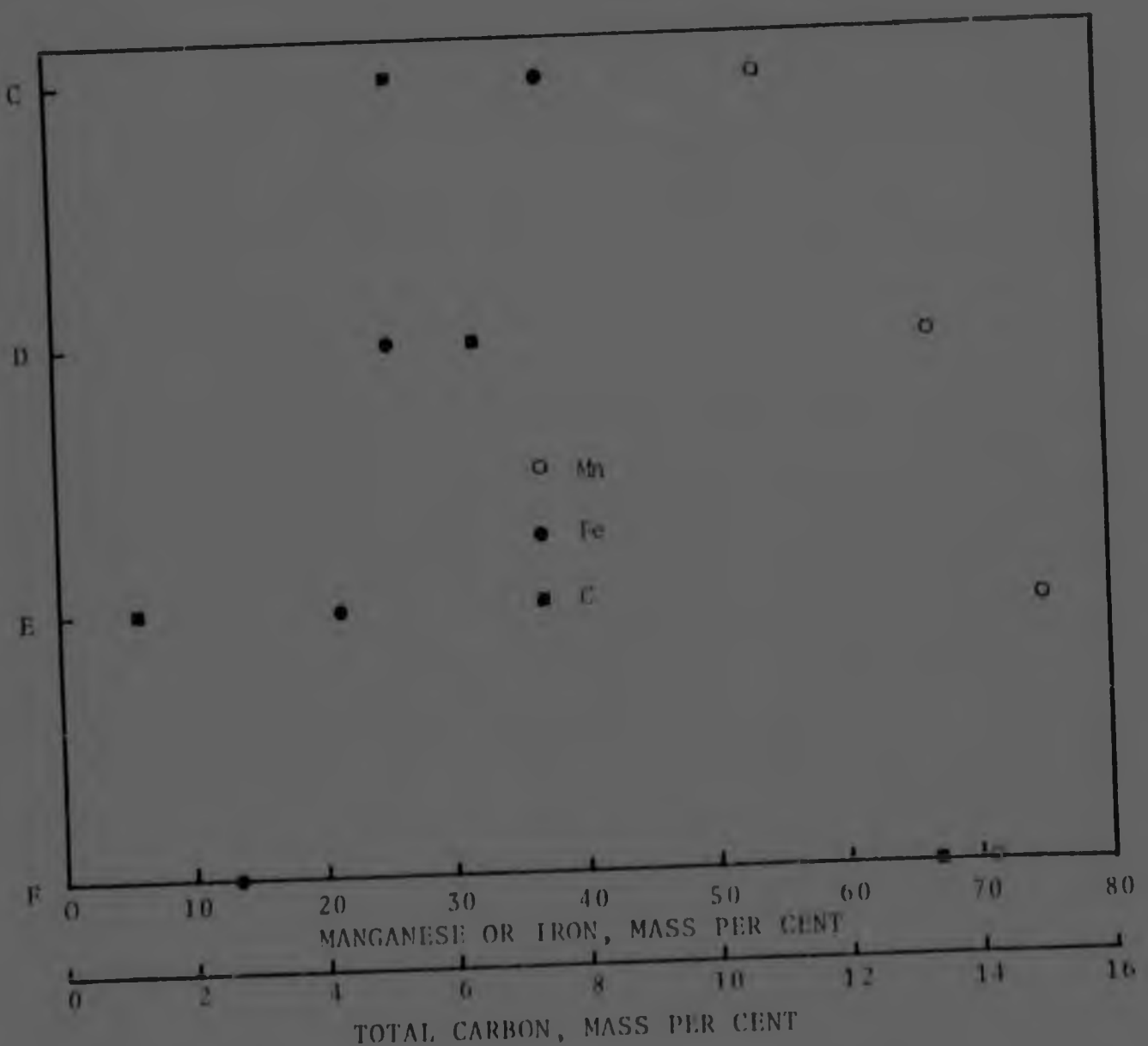


Figure 6.26 The composition of the alloy in samples from position 1 between the electrode and the furnace wall.

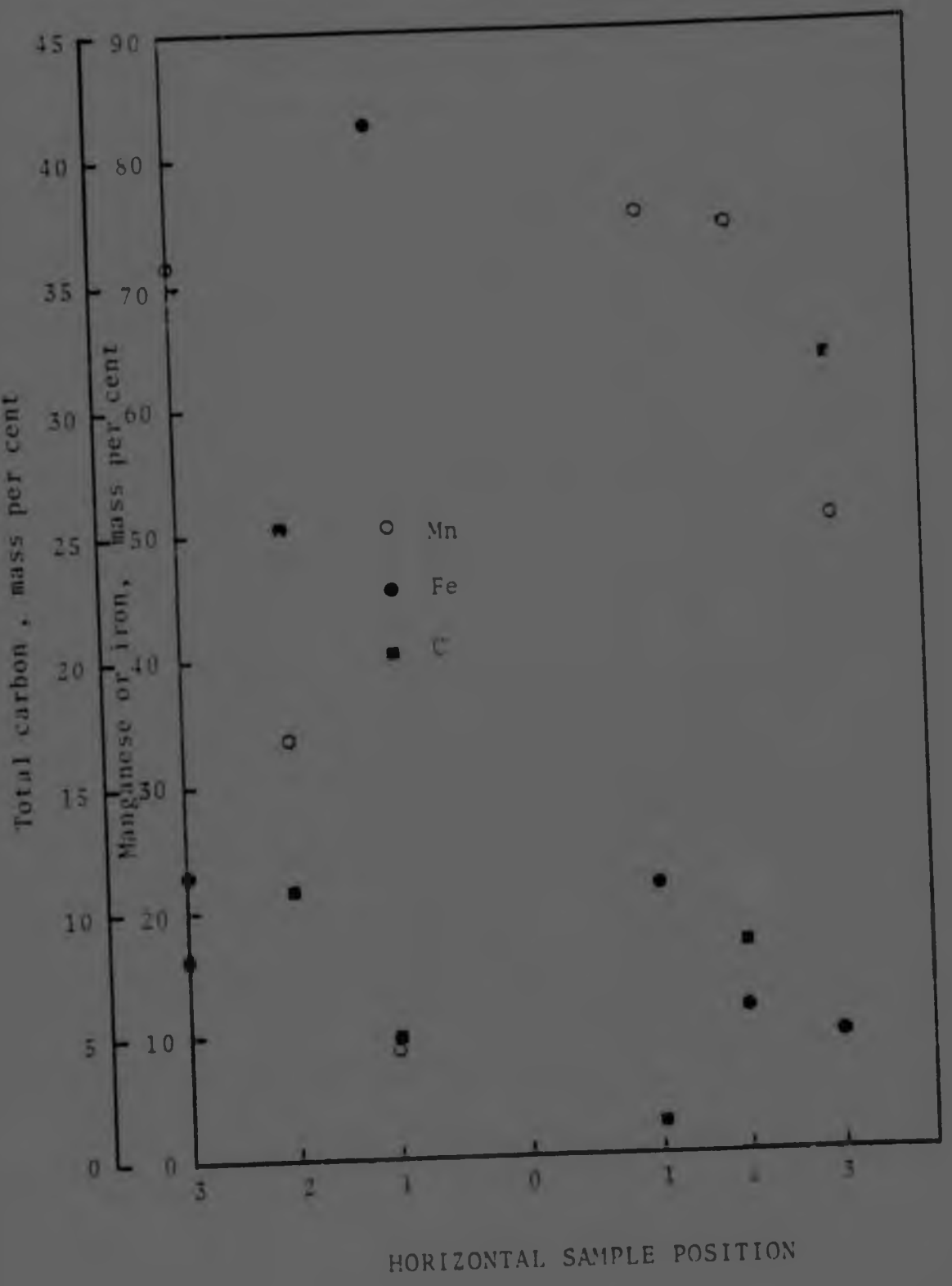


Figure 6.27 The composition of alloys at level E and at various distances from the centre of the furnace hearth.

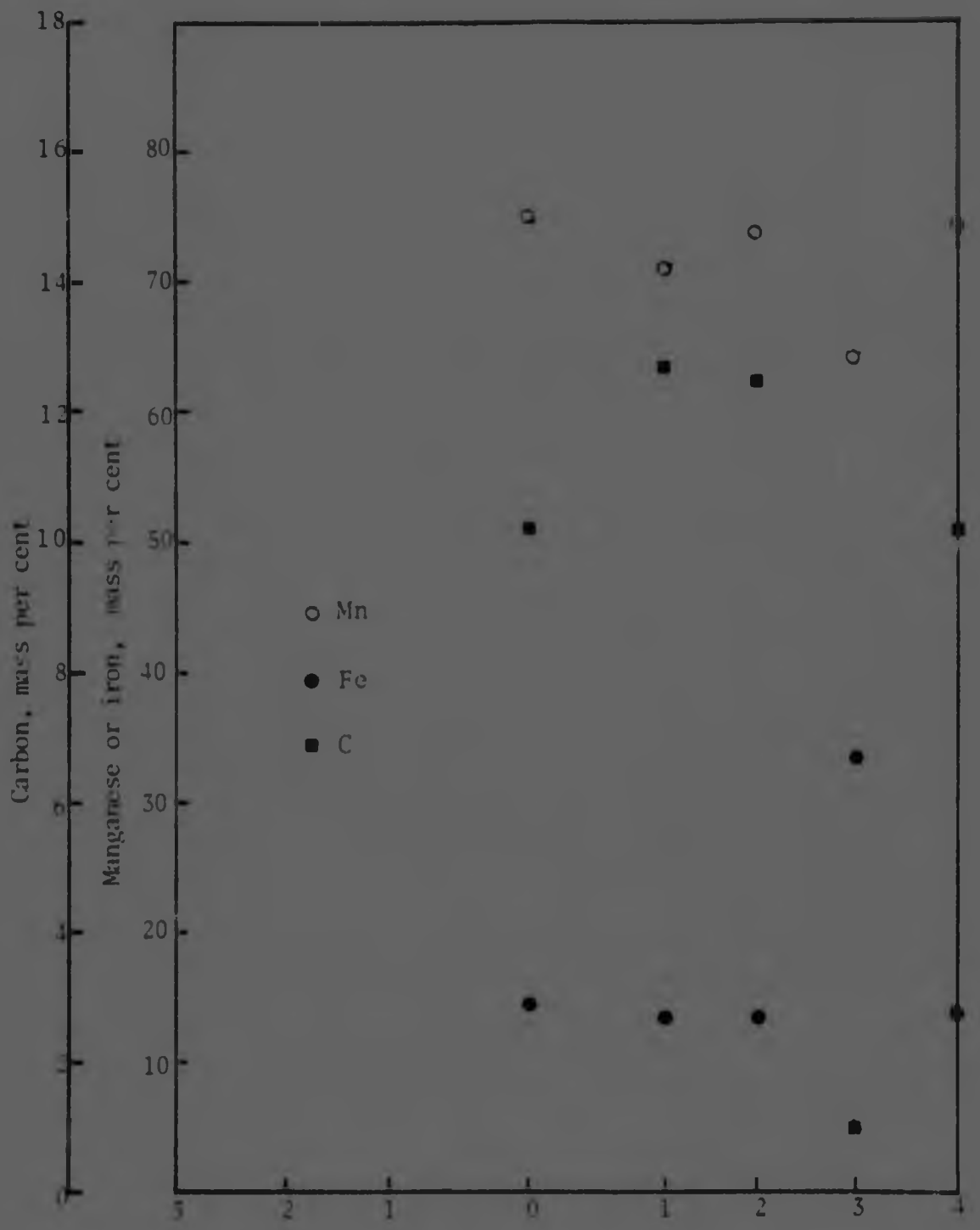


Figure 6.28 The composition of alloys at level F and at various distances from the centre of the furnace hearth.

Figure 6.27 shows the composition of the alloys from level E and at various distances from the centre of the furnace hearth. It can be seen that the composition of the alloys did not show the expected trends. For instance, the manganese content of the alloy might be expected to increase with increased proximity to the electrode. Samples from the central region of the furnace showed the opposite behaviour.

Figure 6.28 shows the composition of the alloys from level F and at various distances from the centre of the furnace hearth. The composition of the alloy appeared to be influenced more by local variations in the consistency of the charge rather than by its horizontal distance from the furnace centre.

6.8 X-ray Microanalysis of Metal, Slag and Oxide

X-ray microanalyses were carried out on the oxide grains, the slag network and the alloy globules in mounted and polished samples to determine the distribution of elements in the three constituents. The equipment and the method used were the same as for the SCICE samples (2.3.4). The results obtained are indicated in Table 6.6 which shows the mean values of at least 5 determinations on each constituent. It should be borne in mind that these values are not quantitative although comparison between Tables 6.5 and 6.6 will show that the compsotion of the metallic constituent in samples 1/E/1 and 1/F/3, determined by conventional chemical analysis and by the EDS method, showed good agreement. The comparison is justified because these furnace samples had a consistent composition throughout and therefore the alloy globules might be expected to have a constant composition.

The analyses of the oxide show that this phase contained mainly MnO with MgO as the main impurity.

The slag network contained mainly CaO, SiO_2 and MnO. The SiO_2 content of the slag was reasonably constant while the proportions of the CaO and MnO varied widely.

TABLE 6.6 The distribution of elements in the oxide, the slag and the alloy in samples from face CE_1W_1

Sample code	CONSTITUENT, MASS PER CENT											
	Analyses of Oxide					Analyses of Slag					Analyses of Alloy	
	Mn	Mg	Ca	Si	Fe	Mn	Mg	Ca	Si	Al	Mn	Fe
1/C/1	85,4	-	-	0,5	14,2	52,7	2,5	12,5	33,6	-	1,9	98,0
1/D/1	88,2	10,2	1,1	-	-	30,6	6,1	29,7	34,4	-	20,3	79,7
C/1/E/3	81,8	13,4	3,0	1,8	-	1,5	10,3	46,7	30,4	15,1	31,6	68,1
C/1/E/2	92,3	6,6	0,6	0,5	-	29,2	6,8	29,2	34,6	-	6,7	92,2
C/1/E/1	93,6	3,5	2,0	-	-	30,1	6,9	48,0	17,9	-	6,7	92,9
1/E/1	55,6	41,8	2,4	0,2	-	0,8	-	64,8	34,4	-	76,5	23,5
1/E/2	83,9	12,8	2,9	0,5	-	0,9	-	67,4	31,8	-	71,6	28,4
1/F/0	82,5	14,8	2,6	-	-	0,9	-	66,9	32,3	-	74,9	24,8
1/F/1	85,8	12,7	1,5	-	-	9,0	1,9	55,1	34,0	-	47,6	52,3
1/F/2	71,0	22,5	6,4	-	-	0,7	-	65,9	33,4	-	86,2	13,4
1/F/3	74,2	19,6	6,2	-	-	1,2	-	65,5	33,3	-	66,6	33,4

The variations in the analyses of the oxide and the slag were investigated by carrying out duplicate tests and by microanalysis traverses which indicated that the variations observed actually existed. A microanalysis traverse from the centre of an oxide grain through the slag to the next oxide grain in a particle from sample 1/E/2, is shown in Figure 6.29. It can be seen that the analyses of both the oxide and the slag are highly consistent and that they are in good agreement with the average values shown in Table 6.6.

The alloy globules contained mainly Mn and Fe with small proportions of Si.

The ratio of Mn to Fe increased with an increase in the size of the alloy globules. Figure 6.30 shows a plot of percent Mn and Fe against globule size for samples from face CE_1W_1 and CE_2W_2. The analyses show appreciable scatter as might be expected from the nature of the reduction process. However, the trend of increasing Mn to Fe ratio with increasing globule size is evident. As in the case of SCICE samples all the globules analysed contained manganese. The total manganese plus iron analysed was equal to or greater than 98,6 per cent in all cases indicating that globules as small as 1 µm in diameter could be analysed without significant interference from the matrix. Interference from the matrix would be indicated mainly as Ca and Si since the globules were surrounded by slag in the main. This was in fact observed when attempts were made to analyse globules of about 0,5 µm in diameter or less.

6.9 Examination of Samples from Face CE_2W_2

The examination of samples from face CE_2W_2 (Figure 6.31) was carried out by use of procedures similar to those described for samples from face CE_1W_1.

6.9.1 Visual Examination

The location of samples that were successfully taken from face CE_2W_2 is indicated in Figure 6.31. The samples were examined visually to assess the condition of the charge at the different levels and positions within the furnace. A consise description of the components in the samples is given in Table 6.7.

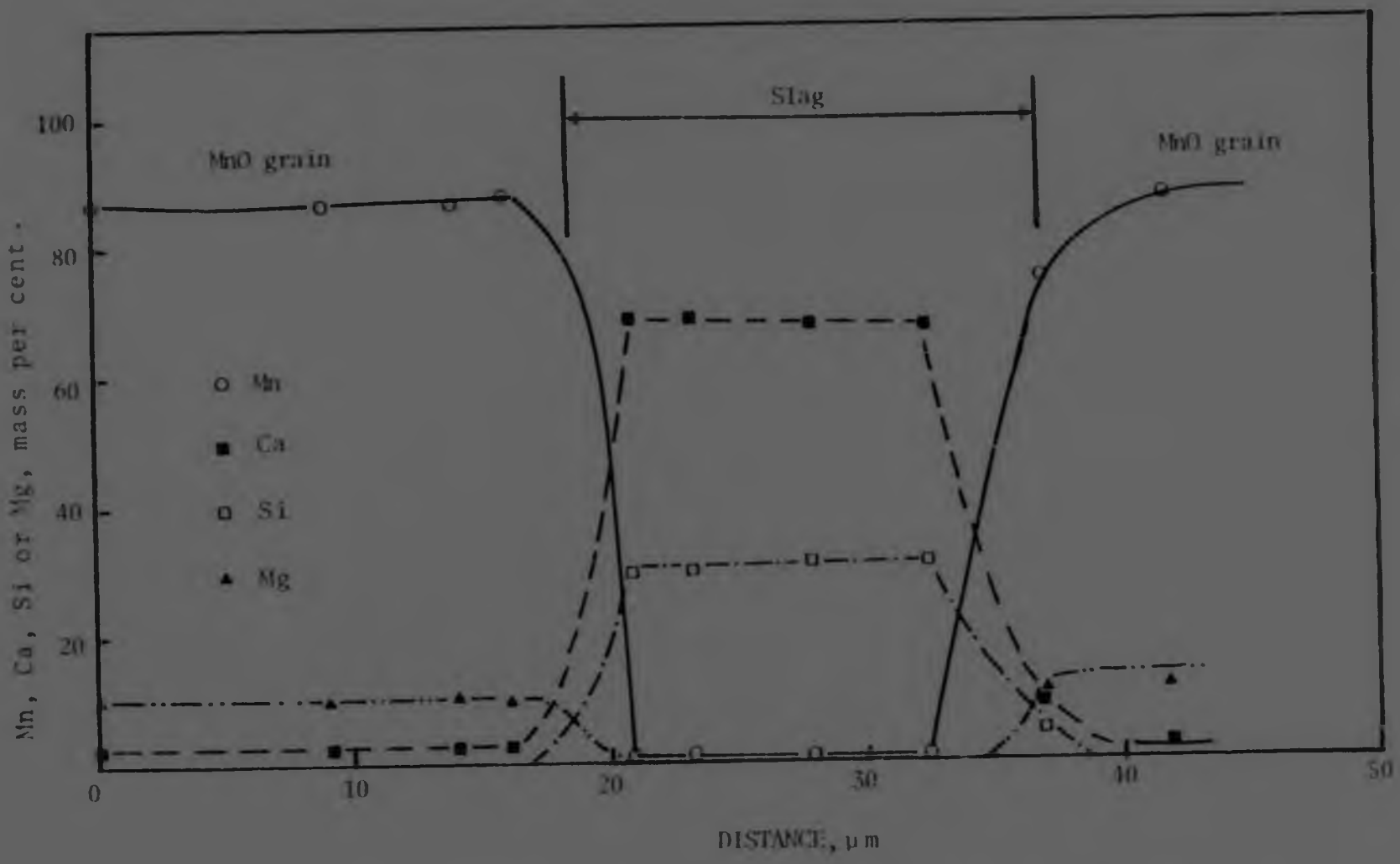


Figure 6.29 A microanalysis traverse from the centre of a grain of MnO across the slag to a neighbouring oxide grain.

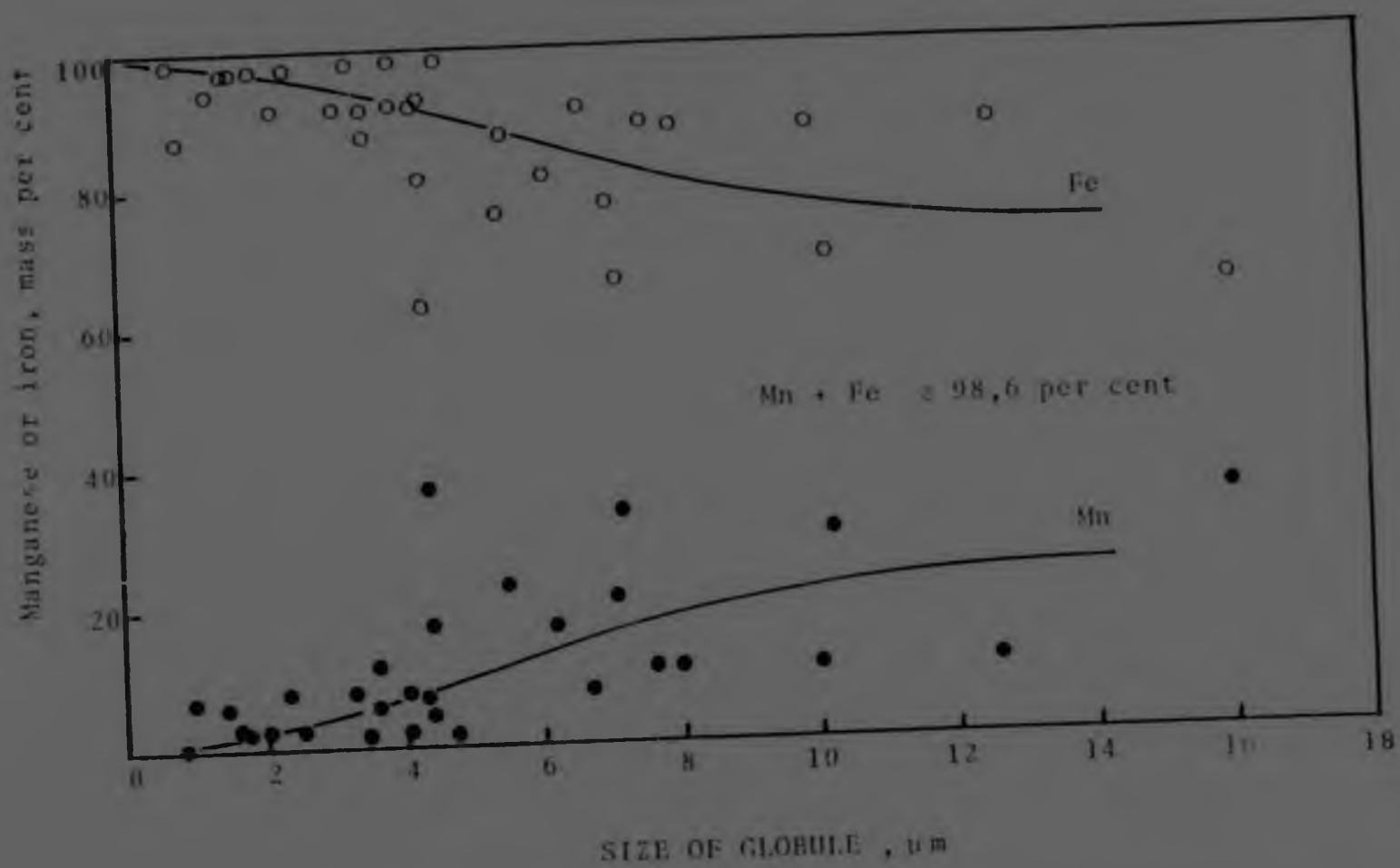


Figure 6.30 The variation in the composition of alloy globules with increasing size.

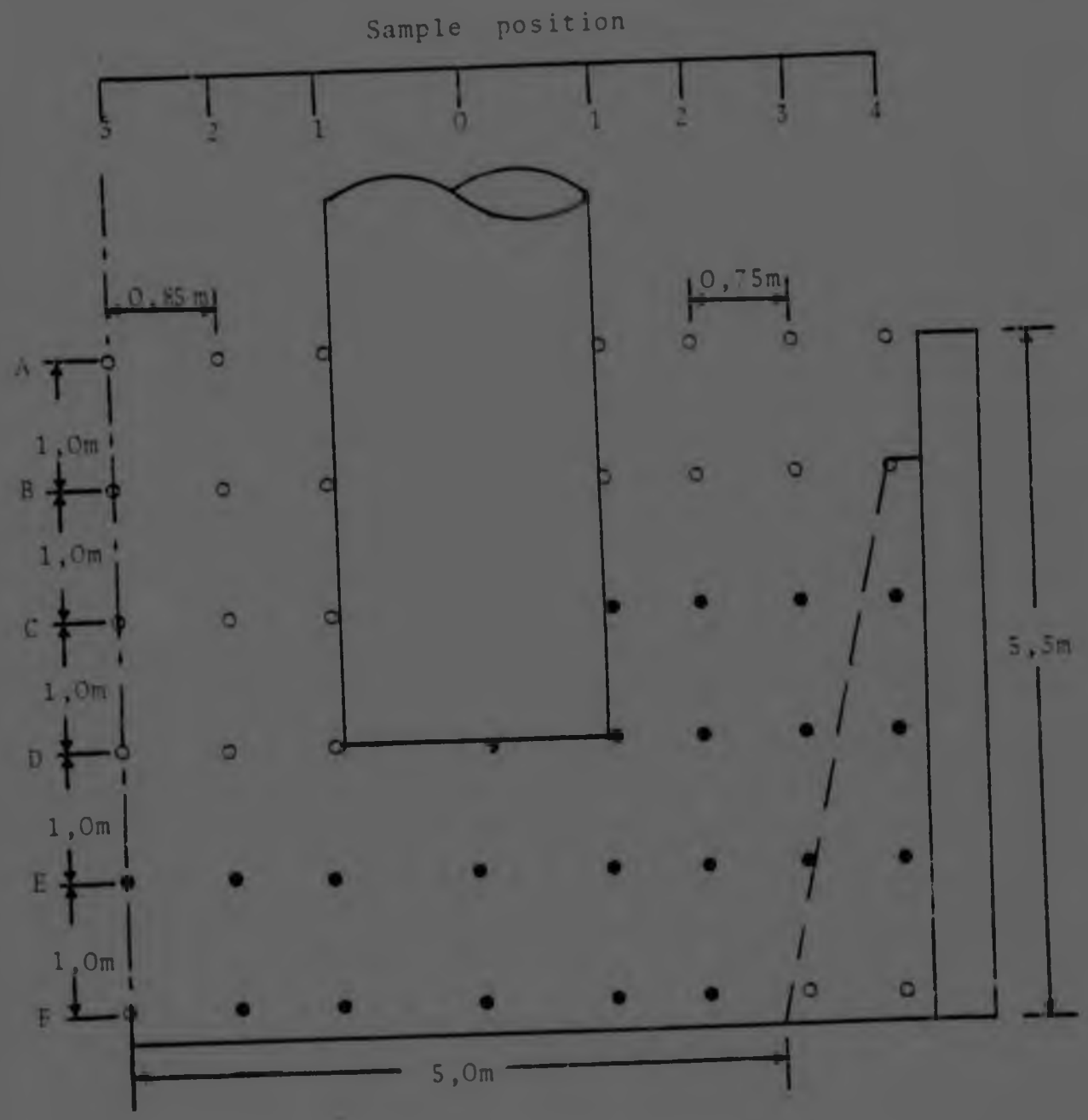


Figure 6.31 The location of samples that were successfully taken (full circles) in plane CE_2W_2 (Figure 6.1).

TABLE 6.7 Summary of the visual examination of samples from face CE_2W_2

Sample level	SAMPLE POSITION							
	3	2	1	0	1	2	3	4
C	X	X	X	Electrode No.2	B	B+S	R	R
D	X	X	X	B+R	B+R	B+R	R	R
E	SL+S+A+R	S+R+A	S+R+A	S+A	B+S+R	R	R+SL	R
F	X	SL+A	R+A+SL	A	R+SL	R+SL	X	X

KEY

B = burden - mixture of unreacted or partially reacted ore and reducing agent

S = sinter - mixture of any number of constituents held together by slag

R = reducing agent - any carbonaceous material

A = alloy - any metallic phase

SL = slag - a homogeneous constituent (macroscopically) formed by fusion and fluxing

X = samples not taken from these positions

The appearance of the samples indicated that reactions in plane CE_2W_2 had not progressed to the same extent as in plane CE_1W_1. Ore samples taken from levels C and D showed little sintering and metallisation.

Appreciable sintering had occurred in samples from the central region of plane CE_2W_2 although the original ore lumps could still be distinguished. The alloy in samples C/2/E/2 and C/2/E/1 occurred as spongy lumps that contained appreciable quantities of non-metallic material.

Complete fluxing of the ore had occurred at level F where slag of a sandstone consistency formed. The hard crystalline type of slag that was found in samples from plane CE_1W_1 was not observed in samples from plane CE_2W_2.

The samples taken directly underneath the electrode indicated that complete fluxing and fusion of the ore had not occurred.

The presence of a coke bed, such as was observed underneath electrode No. 1, was not indicated by the samples taken near electrode No. 2.

Lumps of alloy showing precipitation of graphite were not found. Screen analyses were carried out to determine the proportion of fine material (<3,33 mm) in the samples and to facilitate separation of the lumpy reducing agent from the charge. The proportions of fine material and reducing agent in the coarse fraction of the samples are shown in Table 6.8. The fine fraction of the samples contained varying amounts of reducing agent.

6.9.2 Microscopic Examination

The ore and sinter in samples from face CE_2W_2 were re-sampled and examined microscopically after mounting and polishing. The phases identified are indicated in Table 6.9.

TABLE 6.8 The proportions of fine material and reducing agent in the coarse fraction of samples from face CE_2W_1

Sample code	Material <3,33 mm mass %	Reducing agent in material >3,33 mm mass %
2/C/1	7	12
2/C/2	14	23
2/C/3	0	100
2/C/4	0	100
2/D/0	29	19
2/D/1	19	14
2/D/2	5	95
2/D/3	25	100
2/D/4	31	100
C/2/E/2	0	8
C/2/E/1	0	5
2/E/0	0	-
2/E/1	0	5
2/E/2	0	100
2/E/3	54	46
2/E/4	22	78
C/2/F/2	0	-
C/2/F/1	28	32
2/F/0	-	-
2/F/1	37	63
2/F/2	31	69

TABLE 6.9 The phases in samples from face CE_2W_2

Sample level	SAMPLE POSITION							
	3	2	1	0	1	2	3	4
C	X	X	X	Electrode No.2	S+C	S+C+MnO	-	-
D	X	X	X		A+MnO+SL	A+MnO+SL	-	-
E	SL+MnO+A	SL+MnO+A	SL+MnO+A	SL+A+MnO	SL+A+MnO	-	-	-
F	X	SL+A+MnO	SL+MnO+A	-	-	-	X	X

KEY

S = silicate
C = carbonate
MnO = impure manganous oxide
SL = slag
A = alloy
X = no samples taken from these furnace localities
- = samples unsuitable for microscopic examination

The degree of reaction in these samples was significantly lower than that of samples at the same level in face CE_1W_1. It can be seen from Table 6.9 that the original phases in the ore, namely silicate and carbonates, were present in samples taken from level C. These phases were completely reacted to manganous oxide and slag at level B in plane CE_1W_1 (Table 6.2). Complete reaction of the silicate and carbonates to form slag and grains of MnO occurred at level D or lower.

The microstructures observed in partially reduced particles of ore were similar to those presented in section 6.6.2. (Figures 6.19 to 6.21).

6.9.3 X-ray Diffraction Analysis

X-ray diffraction analyses were carried out on the different constituents of the samples. The phases identified are shown in Table 6.10 in decreasing order of abundance.

It can be seen that the analyses confirm the presence of the original minerals in sample 2/C/1. However, comparison between Tables 6.10 and 3.2 shows that the order of abundance of the different minerals in sample 2/C/1 changed from what it was in the raw ore. It is evident from Table 6.10 that some of the braunite in sample 2/C/1 had decomposed to form hausmannite (Mn_3O_4) which was the second mineral in order of abundance.

The phases in the alloy in samples from plane CE_2W_2 were not identified precisely. The chemical composition of the alloys (Table 6.11) shows that these belong to the $(Fe, Mn)_7C_3$+$(Fe,Mn)_5C_2$ or the $(Fe, Mn)_{23}C_6$+$(Fe, Mn)_5C_2$ phase fields (Figure 4.1). Crystallographic data on the carbide $(Fe, Mn)_{23}C_6$ do not appear to have been published.

6.9.4 The Chemical Composition of Alloys

The chemical composition of the alloy in samples from face CE_2W_2 is shown in Table 6.11.

TABLE 6.10 Phases in the different constituents of samples from plane CE_2W_2.

Sample code	Constituent	Phases
2/C/1	Ore	Braunite, Mn_3O_4, Ca $Mg(CO_3)_2$, $CaCO_3$, Fe_2O_3
	material <3,33 mm	Braunite, C, $CaMg(CO_3)_2$, $CaCO_3$, Mn_3O_4, Fe_2O_3
2/C/2	Ore	MnO, C, x*
	material <3,33 mm	MnO, C, Ca_2SiO_4, x
2/D/O	ore	MnO, Ca_2SiO_4, x
	material <3,33 mm	MnO, C, x
2/D/1	ore	MnO, Ca_2SiO_4, x
	material <3,33 mm	MnO, x, C
2/D/2	ore	MnO, Ca_2SiO_4, C
2/D/3	material <3,33 mm	C, MnO, $(Ca,Mn)_2SiO_4$
C/2/E/2	ore	MnO, $(Ca,Mn)_2SiO_4$
	quartzite	glass, tridymite
C/2/E/1	ore	MnO, $(Ca,Mn)_2SiO_4$
	quartzite	tridymite
2/E/O	ore	MnO, Fe
2/E/1	ore	MnO, $(Ca,Mn)_2SiO_4$)
	quartzite	α-quartz, low α-cristobalite, tridymite
2/E/3	material <3,33 mm	C, MnO, x
	slag	MnO, $(Ca,Mn)_2SiO_4$, C, x
C/2/F/2	slag	MnO, $(Ca,Mn)_2SiO_4$
C/2/F/1	material <3,33 mm	$(Ca,Mn)_2SiO_4$
2/F/1	material <3,33 mm	C, $(Ca,Mn)_2SiO_4$, MnO
2/F/2	material <3,33 mm	C, $(Ca,Mn)_2SiO_4$

* One ore more unidentified phases in appreciable proportions.

TABLE 6.11 The chemical composition of alloys in samples from face CE_2W_2

Sample code	Constituent, mass per cent				
	Fe	Mn	C	Si	Ca
C/2/E/2	57,2	36,4	5,14	0,21	-
C/2/E/1	87,3	3,7	1,43	1,75	1,7
2/E/0	17,0	71,7	6,29	0,19	-
2/E/3	3,6	83,3	6,68	0,30	-
C/2/F/2	18,1	74,0	5,6	0,28	-
C/2/F/1	11,2	78,7	7,2	0,26	-

The alloy in sample C/2/E/1 was low in carbon and contained a significant amount of slag as indicated by the high silicon content of the alloy and by the presence of calcium. The manganese content of the alloys from level F was significantly higher than that of samples from level E.

6.9.5 X-ray Microanalysis of Metal, Slag and Oxide

The results of X-ray microanalyses on samples from face CE_2W_2 are indicated in Table 6.12 which shows the mean values of a minimum of 5 determinations on each constituent.

The concentrations of the major elements in the three constituents, metal, slag and oxide were in good agreement with those obtained from samples of face CE_1W_1. Variations in the analyses of different samples could be expected due to sample inhomogeneities and to variations in the composition of the ore lumps. For instance, the low Mn and high Mg contents of the oxide in sample 2/D/2 were due to the presence of ore lumps that were depleted in manganese minerals. Upon partial reduction the oxide grains that formed were enriched in Mg content. The appearance and the mode of occurrence of these grains was similar to those of other samples as indicated in Figure 6.32. It is evident from the amount of slag, metal and oxide in Figure 6.32 that the ore lump was originally depleted in manganese minerals. The oxide grains analysed about 70 per cent Mg, 27 per cent Mn and 3 per cent Ca. The composition of the grains illustrates clearly the tendency for magnesium oxide to form a solid solution with manganous oxide rather than to dissolve in the slag. The slag matrix in which the oxide grains occurred contained mainly lime and silica with smaller amounts of MnO, K_2O and Na_2O.

TABLE 6.12 The distribution of elements in the oxide, the slag and the alloy in samples from face CE_2W_2

Sample code	CONSTITUENT, MASS PER CENT													
	Analyses of Oxide						Analyses of Slag						Analyses of Alloy	
	Mn	Mg	Ca	Si	Fe	Mn	Mg	Ca	Si	Al	K	S	Mn	Fe
2/C/2	93,9	1,0	4,6	0,4		7,4	1,3	77,0	10,9	1,2	2,1			
2/D/0	93,2	3,6	0,7	1,3	1,0	47,0	5,6	15,4	30,8	-	-	0,2	2,4	96,1
2/D/1	88,7	2,4	3,4	0,7	4,6	26,3		20,6	29,5	8,0	7,6	1,5	2,5	96,1
2/D/2	63,2	24,8	11,4	0,4		7,0	13,1	37,2	20,2	14,6	5,2	-	5,3	93,2
C/2/E/2	83,3	14,9	3,6	0,2	-	15,7	4,2	45,0	32,0	-	-	-	17,4	81,4
C/2/E/1	92,8	5,8	1,0	0,3	-	28,5	-	37,2	29,9	-	-	-	11,1	87,9
2/E/0	74,3	24,2	1,4	-	-	12,2	6,6	42,2	35,1	-	-	-	31,7	67,5
2/E/1	79,8	12,4	6,1	0,5	-	19,0	-	44,2	34,1	-		-	4,0	95,9
C/2/F/2	89,6	9,4	0,9	-	-	25,3	4,4	44,9	33,0	-	-	-	53,3	45,9
C/2/F/1	75,6	23,1	1,1	0,3	-	18,9	6,9	39,5	34,6	-	-	-	25,7	73,8

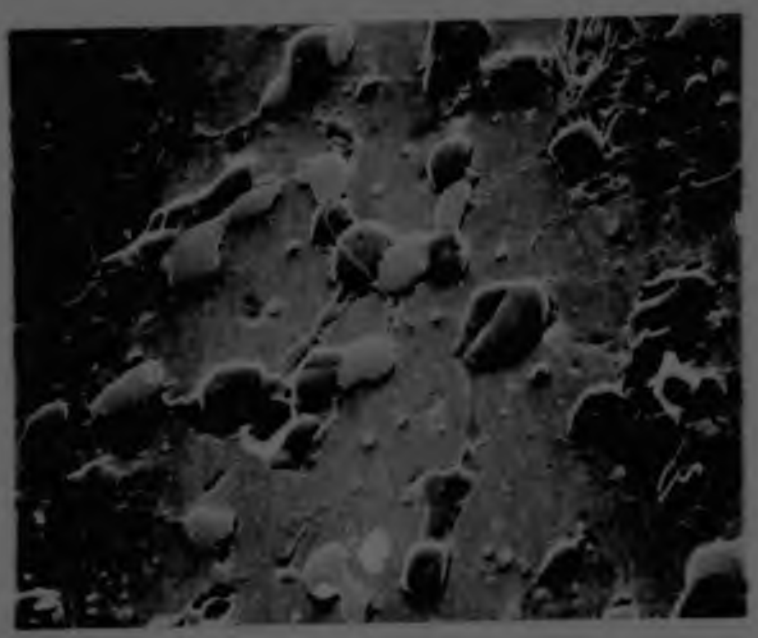


Figure 6.32 Grains of a solid solution of MnO and MgO (dark grey) with adhering metallic particles (light grey) in a matrix of slag.
SEM 500X.

CHAPTER 7

7.0 DISCUSSION

7.1 Some Practical Aspects of Submerged-arc Furnace Operation

The problems associated with the excavation of and the taking of samples from furnace M10 have already been pointed out. One of the major problems associated with the entire project was the fact that only the zones around electrode No. 1 were observed and studied in some detail. The zones around electrode Nos. 2 and 3 could not be reconstructed with a sufficient degree of certainty because the number of samples taken from planes CE_2W_2 and CE_3W_3 was insufficient. In spite of these problems useful information may be obtained by analysing the entire furnace volume on the basis of the observations and measurements made in the vicinity of electrode No. 1 (Figure 6.3). It is obvious that some assumptions have to be made in this respect.

7.1.1. Burden Movement and Distribution of Zones in Furnace M10

Since the furnace cooled down extremely [illegible]ly significant changes could be expected to take place [illegible] the hotter furnace regions where solid and liquid phases coexisted. However, the slow cooling rate would have little effect on several of the zones shown in Figure 6.3. It has been seen from the results of the SCICE experiments that retaining the charge at 1400°C for periods of between 0 and 4 hours did not have a profound effect on its physical or chemical nature. The appearance of the furnace samples suggested that the temperature in a significant proportion of the zones observed was well below 1400°C.

The material around the electrodes (zone 1, Figure 6.3) descends rapidly into the high temperature region underneath the electrodes where melting and smelting take place. If it is assumed that zone 1 (Figure 6.3) will tend to attain a circular shape of equal diameter around the three electrodes then the area of rapidly descending material at stockline level can be traced as in Figure 7.1. It can be seen that the burden over a substantial proportion of the cross-sectional area of the furnace

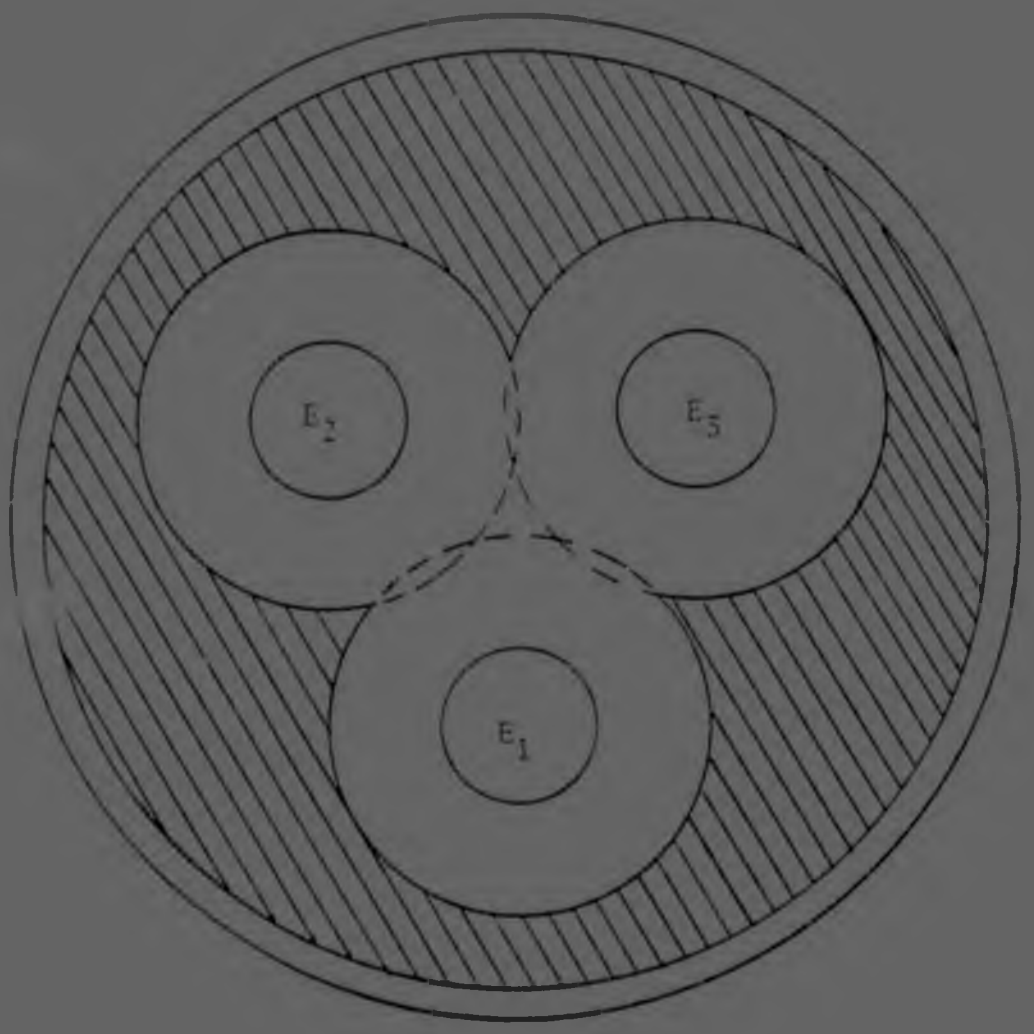


Figure 7.1 The area occupied by partially or completely stagnant burden (shaded) at stockline level.

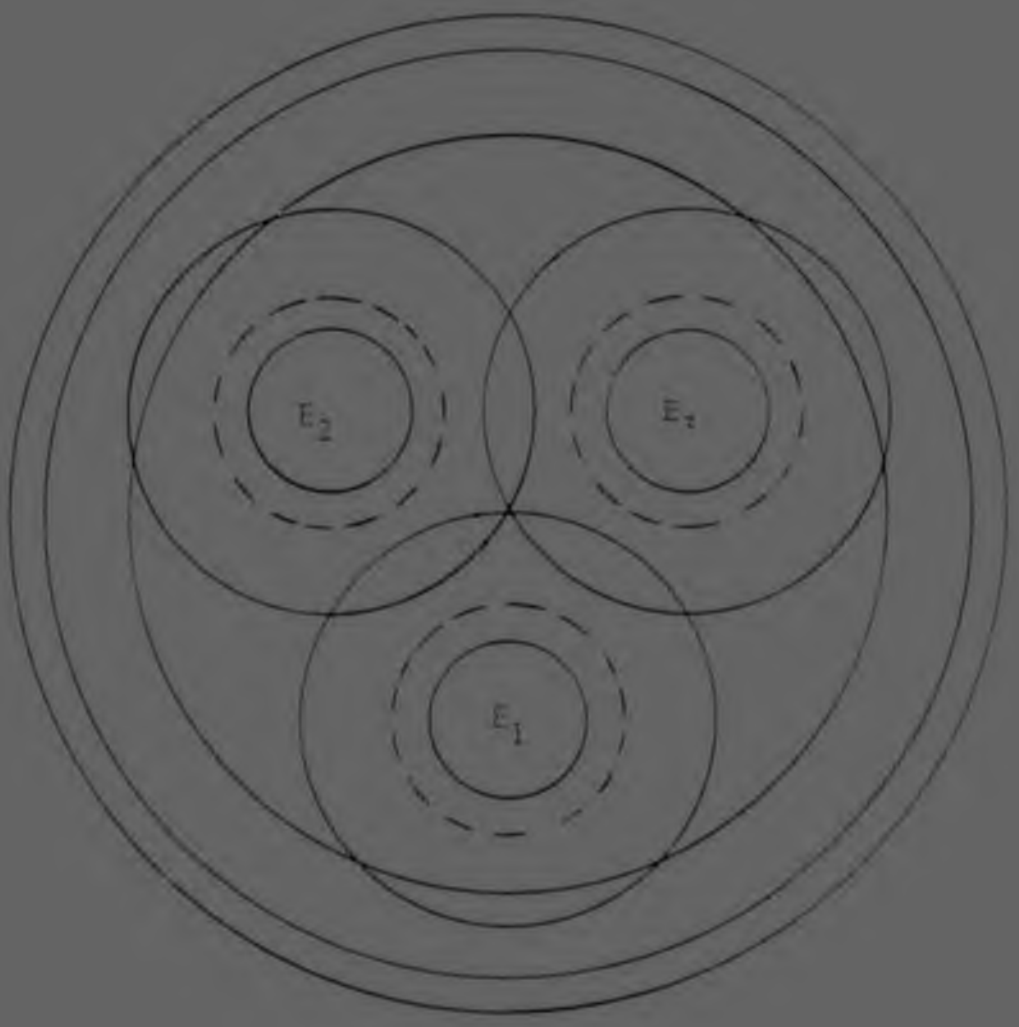
is partially or completely stagnant. Calculation will show that, to a first approximation, only 45 per cent of the cross-sectional area, at stockline level, is active. As can be seen from Figure 6.3 the proportion of the cross-sectional area of the furnace occupied by partially or completely stagnant material increased with increasing depth in the furnace. It is evident, therefore, that the active volume of the furnace was significantly less than 45 per cent of the entire volume. It could be expected however, that the active furnace volume would increase with an increase in furnace load. Andreae,[127] Kelly[58] and Koetzee[128] consider that the reaction zone around the electrode is circular in cross-section with an area proportional to the power imput. Thus if the size of zones 8 and 9 in Figure 6.3 increased, the size of zone 1 can also be expected to increase.

If it is assumed that the zones beneath all three electrodes will tend to attain a circular configuration of equal size then Figure 7.2 may be constructed from the dimensions of zones 8 and 9 shown in Figure 6.3. Figure 7.2 shows the extent of the slag layer and of the mixed slag/oxide layer.

Zones 8 and 9 as well as zone 7 probably comprised a single zone during furnace operation as might be expected from the enormous quantities of the gaseous reaction products generated which would keep the reaction zone in a state of intense agitation. If it is assumed that the reduction of manganous oxide by carbon takes place according to the reaction:

$$MnO + C = Mn + CO \quad . \quad . \quad . \quad 7.1$$

it can easily be shown that the reduction of 1 kg of MnO by 0,17 kg of carbon will produce 0,77 kg of manganese and 0,39 kg of carbon monoxide. At an estimated reaction



Scale 10 mm = 1m

Figure 7.2 Horizontal section through furnace M10 showing the diameter of the furnace at roof and floor levels and the extent of the reaction zone around the three electrodes.

temperature of 1600°C this quantity of gas, at standard pressure will occupy about 2140 l. Since the production rate of the furnace is 8,56 tph (Appendix 3) of about 80 per cent ferromanganese the reduction of 1 kg of MnO takes approximately 0,4 sec. It is evident that under these conditions the separation of zones according to specific gravity is unlikely.

As shown in Figure 7.2 the reaction zones overlapped in the central region of the furnace, touched in the centre and tended to penetrate the furnace lining. The last condition is undesirable since it could result in reactions between the charge and the lining. This was probably one of the reasons why the furnace shell had been penetrated in places as can be seen from Figure 6.5. The extent of the reaction zones in Figure 7.2 related to the spacing of the electrodes has been termed by Kelly [58] "the optimum furnace reaction zone" since these do not leave a dead or an overactive area in the centre. It is evident however, that the diameter of the furnace at floor level was about 1,0 m smaller than that determined by Kelly [58] who assumed that power is dissipated over a fixed area of reaction zone and that the kilowat input is proportional to the square of the reaction zone diameter. Kelly further assumed that the electrode spacing determined by experience was the proper one and concluded that the diameter of a furnace should be 1,15 times greater than that determined from a consideration of the optimum reaction zone diameter. If Kelly's [58] criteria are used in the case of furnace M10 it may be shown that the diameter of the furnace at floor level should have been 12,54m. It may be noted that the diameter at floor level, of the rebuilt furnace was increased from 9,9 m to 12,6 m [129].

7.1.2 Decrepitation and Segregation of Burden Components

The geometry of the furnace, the mode of burden movement and the differences in density of burden components make segregation of the reducing agents towards the outer parts of the furnace unavoidable.

Since the density of the ore is considerably higher than that of coal or coke it can be expected to flow faster in the active furnace volume forcing the reducing agents to segregate towards the upper and outer furnace regions. This was evident from the observations made during the excavation and from the results of sample examination (6.6.1 and 6.9.1). The segregation of burden components in a furnace is a subject that appears not to have been treated by previous investigators. Studies on this subject could prove to be of significant importance due to the similar resistivities of coke and molten slag [69]. Thus, if a continuous layer of coke formed between the electrode tip and the furnace wall current could be conducted from the electrode to the wall rather than from the electrode to the furnace floor through the slag layer.

In plane CE_2W_2 the segregation of reducing agent was extremely high (Table 6.8), especially in samples taken in positions 3 and 4 between the electrode and the furnace wall. From Table A3.2 of Appendix 3 the proportion of reducing agents in the charge may be calculated at 17,10 per cent by mass. Thus, the segregation of reducing agents at the level of the electrode tip (between levels D and E) could cause conduction of current between the electrode tip and the furnace wall. This would be likely if "cold" burden of high resistivity collapsed into the reaction zone or if an electrode were raised too far causing an excessive increase in electrode to hearth resistance. The conduction of current between an electrode and the furnace wall would induce smelting reactions in the current path and generation of slag which could react with the furnace lining and eventually penetrate the furnace shell.

The adverse effects of conduction between an electrode and the furnace wall may be self-rectifying. The smelting processes that occur in the current path will generate a reaction zone and cause the flow of burden into it.

This would increase the resistance to the flow of current and conduction from the electrode tip to the hearth could be re-established.

The high proportions of fine material in samples taken at some distance from the active zone indicated that decrepitation of the ore was caused by long retention periods at relatively high temperatures (600 to 900°C). The structure and mineralogical constitution of Namatwan ore (Figure 3.1) suggests that the finer the ore lumps in the burden (i.e. the greater the surface area), the greater will be the apparent amount of fine material due to the dissociation of the different minerals. As the amount of fine material increases the permeability of the burden to gaseous reaction products decreases. This aggravates the situation further since low burden permeability results in low heating and reaction rates and complete stagnation of some zones may follow.

The appearance of zones 2 and 4 in Figure 6.3 indicated that the material in these zones moved slowly while zones 3 and 5 were completely stagnant.

Decrepitation and stagnation of burden in a furnace is highly undesirable, because they limit the area through which the reaction gases can escape. Figure 6.3 indicates that the gases generated in the reaction zone escaped mostly through zone 1. This is also evident from the shape of the electrode tip (Figure 6.9) which showed severe erosion by solid particles carried in the gases.

The pattern of the electrode tip suggested that electrode wear was mainly due to erosion and not to vaporization by arcing as suggested by Muller [97]. Arcing would tend to occur preferentially from the protuberances at the electrode tip and a smooth rounded tip might be expected to result [97]. The observations made during resistance measurements (5.2.3) and measurements made by Urquhart[53] support this view since the tendency for arcing decreases with increasing temperature.

A narrow passage for the gaseous reaction products increases the probability of a pressure build-up in the reaction zone and of furnace 'blow-outs', especially under conditions of reduced load. It would appear that the risk of 'blow-outs' could be reduced by increasing the size of the reaction zone. This could be achieved by overcoking the furnace and raising the electrodes to maintain the same resistance or by increasing the electrode to hearth voltage [128]. If the voltage is increased the electrode must be raised in order to increase the resistance which reduces the current and makes it possible for the power to be kept constant. An increase in the size of the burden components could also be beneficial. However, when the nature of Mamatwan ore and Figure 6.3 are considered it can be seen that an increase in the size of the reaction zone offers the better solution.

7.2. Reduction of the Ore in the Submerged-arc Furnace

The examination of samples from planes CE_1W_1 and CE_2W_2 showed that the degree of reduction at a given depth in the furnace varied in the two planes. However, the sequence of the reactions that occurred with increasing depth in the furnace remained the same.

The major proportion of the ore was reduced in the cone of fast descending material around the electrodes and in the molten regions underneath the electrode tips. The processes taking place during the descent of the burden will be discussed mainly with reference to the observations and measurements made on samples from position 1 in plane CE_1W_1 where it appeared that at the time of the shut down the burden was descending in a steady manner.

The main reactions that occurred between the different levels in the furnace are summarised in Table 7.1. Consideration of Table 7.1 and of the reactions that took place in the SCICE charges (sections 4.2 to 4.4.3) will show that the same reduction mechanisms were operative in the two cases. Thus the SCICE technique can be used to simulate conditions in an industrial furnace.

TABLE 7.1 Summary of the main reactions that occurred at different levels in the furnace.

Sample level	Depth in furnace m	Reaction number	Reaction
A to B	0 to 1	1	$3(MnO.3Mn_2O_3.SiO_2) = 21Mn_3O_4 + 2O_2 + 3SiO_2$
		2	$CaCO_3 = CaO + CO_2$
		3	$CaMg(CO_3)_2 = CaO + MgO + 2CO_2$
		4	$Mn_3O_4 + CO = 3MnO + CO_2$
		5	$Fe_2O_3 + CO = 2FeO + CO_2$
		6	$FeO + CO = Fe + CO_2$
		7	$CaO + SiO_2 = CaO.SiO_2$
B to C	1 to 2	8	$FeO + CO = Fe + CO_2$
		9	$2CO = [C]_{alloy} + CO_2$
		10	$[C]_{alloy} + MnO = [Mn]_{alloy} + CO$
C to D	2 to 3	11	$(MnO)_{slag} + C = [Mn]_{alloy} + CO$
			$\Delta G^{o}_{11} = 287441 - 170,07T\ J\cdot mol^{-1}$
			$K_{11}\ (1600^{o}C) = 7,41$
		12	$(MnO)_{slag} + CO = [Mn]_{alloy} + CO_2$
			$\Delta G^{o}_{12} = 16734 + 169,3T\ J\cdot mol^{-1}$
			$K_{12}\ (1600^{o}C) = 7,94 \times 10^{-12}$
D to F	3 to 5	13	$(MnO)_{slag} + C = [Mn]_{alloy} + CO$
		14	$(MnO)_{slag} + [C]_{alloy} = [Mn]_{alloy} + CO.$

Braunite and the gangue minerals dissociated between levels A and B and the higher oxides of manganese and iron were reduced to their lowest oxidation state by carbon monoxide. This was evident from the fact that reduction had taken place throughout the cross-section of ore lumps of substantial size. Some of the wustite was reduced to metallic iron and reaction between lime and silica took place to a limited extent to form slag.

Further reduction of wustite to metallic iron occurred between levels B and C. The amount of slag increased and formed a continuous network through the ore lumps and a film on the surface which resulted in appreciable sintering of the burden. The formation of slag reduced the permeability of the ore to carbon monoxide and carburization of the metallic particles in the interior of ore particles did not occur. The metallic particles on the surface of ore lumps or sinter were readily carburized by carbon monoxide and reduction of manganous oxide by carbon dissolved in the alloy took place leading to a subtantial increase in the size of the particles. The manganous oxide could be in the form of solid grains or as dissolved oxide. Reduction of these two forms of oxide would be equally favourable if it is assumed that the solid oxide was pure MnO and that the slag was saturated in the oxide. It has been seen (2.3.4) that the concentration of magnesium oxide in solid solution with the manganous oxide was very low during the early stages of reduction. Therefore the activity of the oxide in the solid and in solution would be close to unity. It can be seen from Table 6.5 that alloy globules from the surface of ore lumps in sample 1/C/1 contained 54 per cent manganese while the metallic particles in the interior of ore particles contained of the order of 2 per cent manganese (Table 6.6). The fact that the amount of metal in the immediate vicinity of lumps of reducing agent was not greater than elsewhere indicated that reduction down to level C occurred mainly by carbon monoxide as an intermediate product.

Between levels C and D the proportion of slag increased drastically and the partially reduced ore lumps became completely covered by a thick layer of slag. This facilitated the draining of the larger metallic particles to the furnace

hearth while smaller particles adhered to the partially reduced ore lumps. The formation of a substantial volume of slag reduced the amount of contact between lumps of ore and reducing agent and improved contact between slag and reducing agent was attained. Under these conditions the reduction of manganous oxide appeared to occur by dissolution of the oxide into the slag and transfer to the slag/reductant interface. Carbon monoxide passing through the charge could also reduce manganous oxide from the slag. However, when the reactions 11 and 12 in Table 7.1 are considered it becomes apparent that reduction by solid carbon is thermodynamically more favourable.

As the burden descended from level D to E and F it entered a region of much higher termperature and vigorous stirring due to the rapid evolution of gaseous reaction products. These conditions caused the complete disintegration of partially reduced ore lumps and the formation of a suspension that consisted of liquid slag, solid reducing agent and solid grains of manganous oxide. The proportion of manganous oxide in samples from level E (Figure 6.22) was significantly higher than that observed in partially reduced ore from other furnace regions or from SCICE samples. This indicated that the structures observed were a result of the settling and coalescence of oxide grains and of the displacement of slag rather than of the settling of ore lumps.

The processes that took place between levels D and F are not certain. It appeared however that reduction occurred, in the main, by reaction between solid reducing agent and manganous oxide dissolved in the slag since these two constituents were permanently in contact. Reduction by carbon monoxide would be possible although less favourable.

The reduction of dissolved manganous oxide by the carbon dissolved in the alloy layer on the bottom of the furnace would be equally favourable to reduction by solid carbon since the alloy would be saturated in carbon. However, the area of contact between the alloy and the slag could be expected to have been much smaller than that between the

slag and the solid reducing agent (Figure 6.7). If, as considered by Daines and Pehlke,[36] the rate of reduction of manganous oxide from a slag, by carbon dissolved in the alloy, is controlled by the rate of the chemical reaction, then, the amount of reduction carried out by carbon in the alloy ca.. be expected to be small relative to that carried out by the solid reducing agent, since the area of contact between slag and metal is relatively small.

Any reduction of manganous oxide by carbon dissolved in the alloy would reduce the carbon content of the alloy and dissolution of carbon would occur from the furnace lining or from the reducing agent in t burden. The fact that the carbon lining at the bottc submerged-arc furnaces can last for as many as 20 years[128] indicates that dissolution of the lining by the alloy layer is normally very low. It would appe therefore that the alloy dissolved carbon mainly from the stagnant zones of the furnace which were rich in reducing agents.

The appearance of samples from the central region of the furnace indicated clearly that reduction of manganous oxide could also take place by a mechanism somewhat different to the mechanisms proposed above. The sequence of carbon/alloy/slag plus oxide interfaces (Figure 6.10) showed that under certain conditions the metal reduced by the solid reducing agent can remain in contact with it and eventually form an envelope around the lumps of reducing agent. Further reduction would then occur by dissolution of carbon into the alloy and transfer to the alloy/slag plus oxide interface. This reduction mechanism is not dissimilar to that proposed by Grimsley[3] for temperatures greater than 1200°C.

The conditions that would favour this mechanism would appear to be relatively low temperatures giving a charge in a mushy state. Under these conditions the fluidity of the slag would be low and the alloy being formed would not drain to lower levels very easily. The appearance of the large quantity of sintered material in the central region

of the furnace indicated that the above conditions actually prevailed. It is also evident from the reduced rate of burden consumption by the central feed chute that the central region of the furnace was one of relative inactivity.

7.3. Temperature Gradients in Submerged-arc Furnaces

Temperature gradients in blast furnaces producing pig iron have been determined by probing techniques [130, 131]. Techniques for the determination of temperature gradients in submerged-arc furnaces appear not to have been developed. Some of the measurements made on samples from furnace M10 can be used to determine the approximate temperature in the region from where the sample was taken. For instance, the phases identified in lumps of quartzite give a reasonably accurate indication of the range of temperatures that prevailed in a particular region.

The phase transformations of silica with increasing temperature are shown in Figure 7.3. The interconversion of quartz, tridymite and cristobalite requires the breaking and reforming of bonds; consequently these transformations tend to occur very slowly. At a given temperature, though only one form is stable, the other two may also exist metastably without appreciable change. At room temperature all three forms may coexist although the stable form is quartz only. Thus, in ordinary heating and cooling the behaviour does not follow the relationships of Figure 7.3. except for the α to β quartz transition and the changes from high to low temperature modifications.

During heating, quartz may remain stable above 870°C and transform directly to cristobalite at 1250°C or higher. Tridymite transforms to cristobalite at 1470°C and cristobalite fuses at 1728°C. Tridymite may remain stable up to temperatures close to 1728°C when it transforms to vitreous silica directly.

Once liquid silica, cristobalite or tridymite are formed each phase tends to be retained on cooling so that when a furnace structure is cooled from the operating temperature the phases existing at that temperature are largely retained.

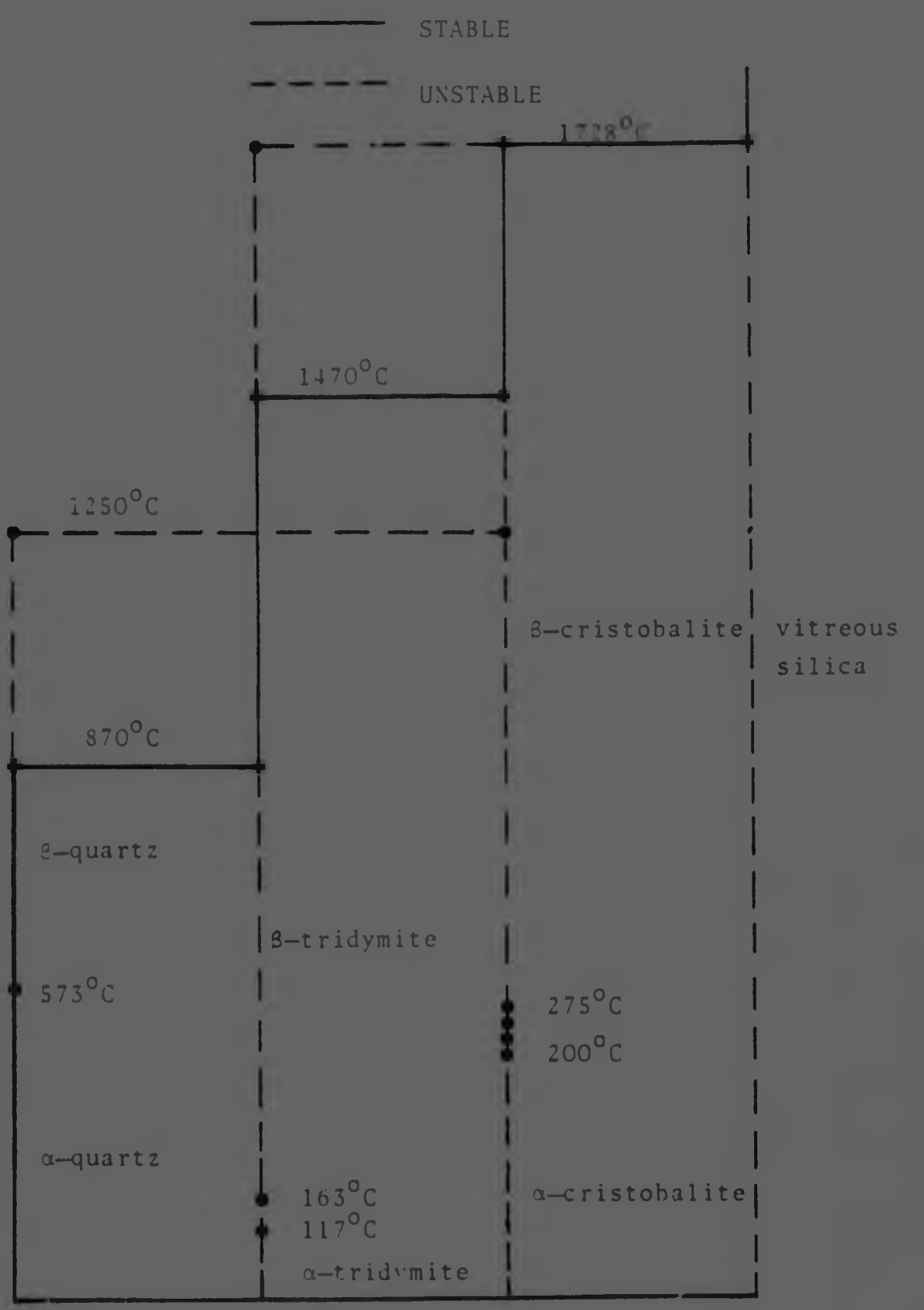
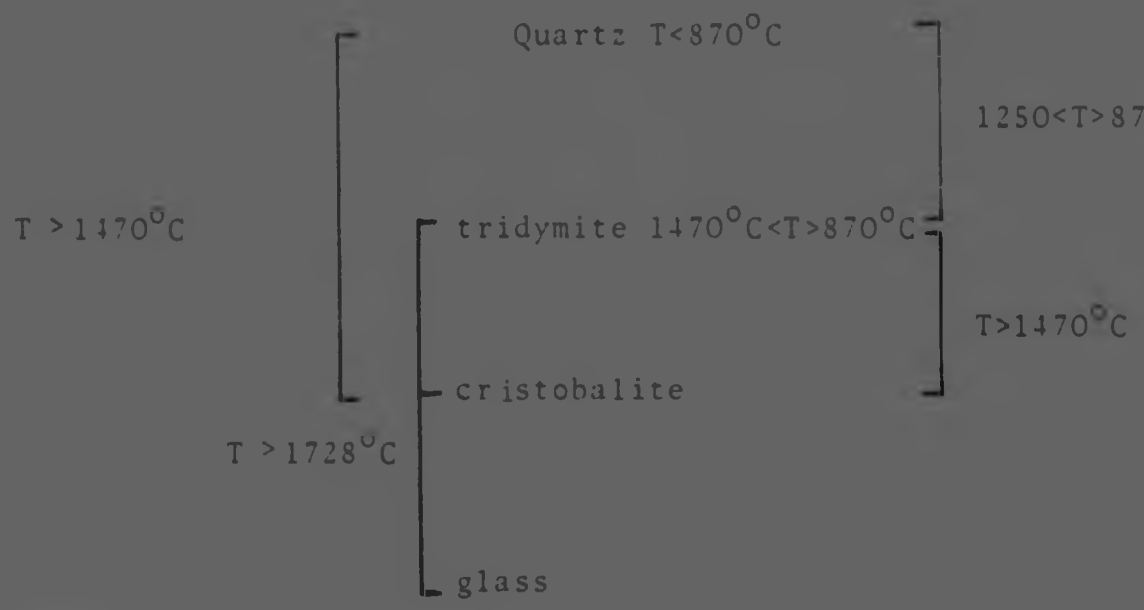


Figure 7.3. The phase transformations of silica as a function of temperature (Ref. 130).

It can be seen from Tables 6.3 and 6.10 that quartz and crystobalite or cristobalite on its own were not detected in any of the samples. Therefore it may be said that the direct conversion of quartz to crystobalite did not occur. The presence of glass and tridymite in sample C/2/E/2 (Table 6.10) indicated that the direct conversion of tridymite to glass occurred. In general however, it appeared that the quartz, tridymite, cristobalite conversion sequence was followed. Thus from the phases present in the different samples the following temperature ranges may be derived.



The phases in quartzite samples (Tables 6.3 and 6.10) indicated that the temperature at level E in planes CE_1W_1 and CE_2W_2 was generally greater than 1470°C. It appeared that the temperature in the region of sample C/2/E/2was greater than 1728°C while that in the region of sample C/2/E/1 could have been between 870 and 1470°C.

7.4. The Carbon Content of Alloy Samples from Furnace M10

The solubility of carbon in alloys of manganese and iron has been investigated by several authors [115,116,133] and Turkdogan et al [134] determined the solubility of carbon in melts of pure manganese. From the results of Chipman et al [115], and Turkdogan et al [116, 134] the curves shown in Figure 7.' may be plotted. The results of Petrushevskii and Geld [133] were in good agreement with those of Chipman et al [115]. From Figure 7.4 it can be seen that the equilibrium carbon content of alloys of iron and manganese is a linear function of the manganese content for temperatures between 1290 and 1690°C. The curves indicate that it would be safe to assume that all alloys at 1400 and 1600°C will show carbon solubilities intermediate to those exhibited by alloys at temperatures between 1290 and 1690°C. If the assumed solubility lines are drawn as indicated in Figure 7.4 and the carbon contents of the alloys produced in the SCICE experiments are plotted it will be seen that the carbon content of the alloys was generally lower than that predicted from the solubility curves especially for alloys produced at 1400°C. This indicates that the alloys in general did not attain equilibrium. The alloys produced at 1600°C showed much better agreement the maximum deviation from the assumed curve being about 0,4 per cent carbon.

If the overall carbon content of furnace samples is considered (Figure 7.4) it will be seen that, in general, alloys which showed graphite precipitation had carbon contents far in excess of those predicted by the equilibrium curves. Alloys that did not show graphite precipitation had carbon contents significantly lower than those predicted by the curves.

A thorough discussion of the reasons for the vast discrepancies in carbon content of laboratory and furnace samples is not possible due to the limited extent to which the Fe-Mn-C system has been investigated [125, 126]. In fact the phases present in this system at temperatures greater than 1100°C do not appear to have been investigated.

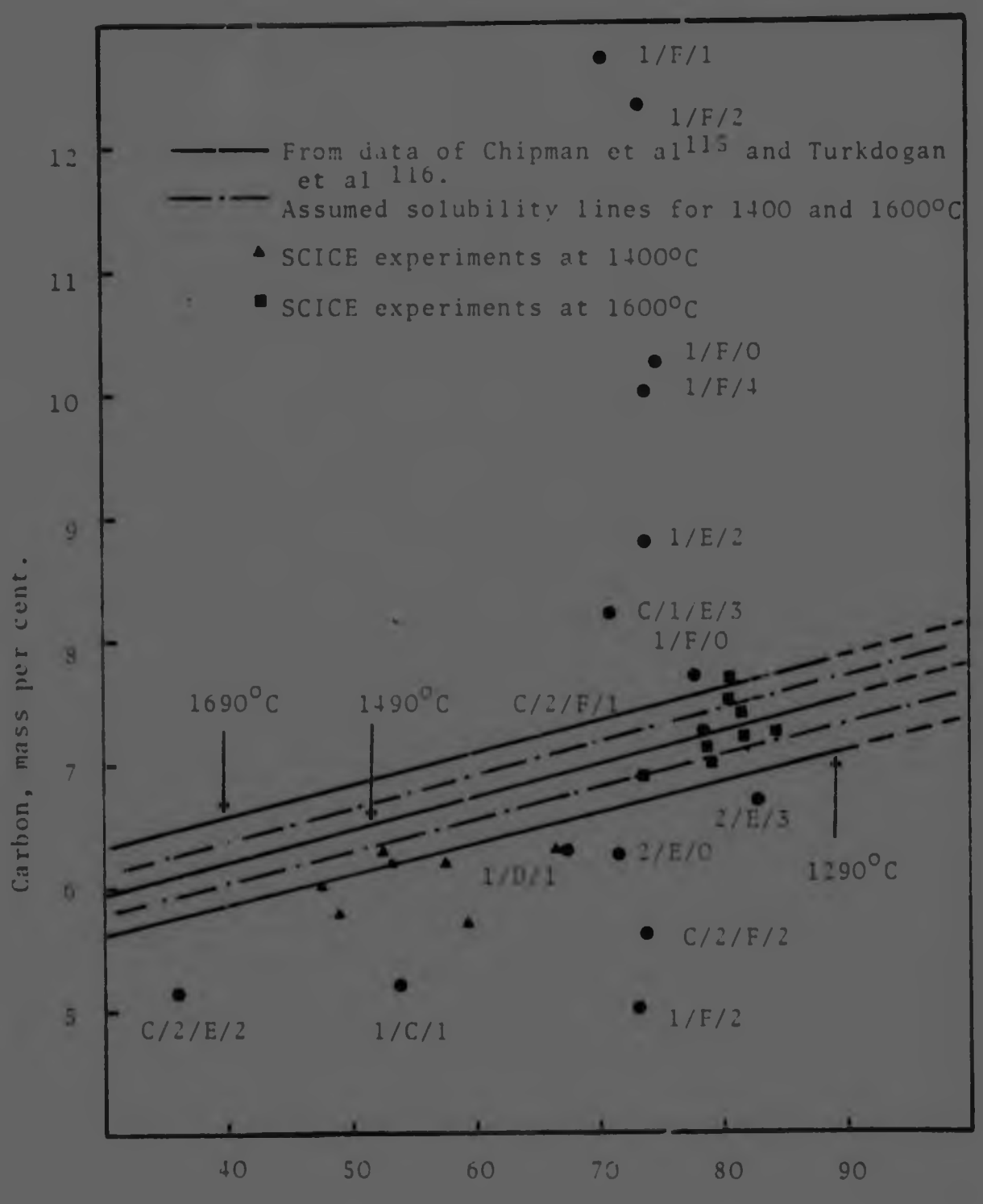


Figure 7.4 The solubility of carbon in alloys of iron and manganese.

Carbon contents below the equilibrium values indicate that equilibrium conditions were not attained. Overall carbon contents greater than the equilibrium values are more difficult to explain.

The intimate mixture of carbide grains and graphite flakes (Figure 6.24) indicated that the carbon was in solution in the liquid alloy and was exsolved during cooling and solidification. Simple extrapolation from the equilibrium curves will show that for a carbon solubility of 12 per cent the temperature would have to be in the region of 6000°C. Temperatures of this order of magnitude are not likely in a ferromanganese furnace although temperatures in excess of 1690°C are. It is possible that the solubility of carbon in alloys of manganese and iron at temperature greater than 1690°C deviates considerably from the established trends.

7.5 CONCLUSIONS

The problems associated with the operation of the furnace during the 10 days prior to close down and the cooling conditions of the burden have already been discussed (6.1 and 7.1.1). The conclusions that follow must therefore be considered in the light of the conditions of furnace operation prior to close-down and the rate of cooling of the burden.

1. There are some 10 zones in a 75 MVA submerged-arc furnace for the production of high-carbon ferromanganese.

   The active furnace volume was, to a first approximation, less than 45 per cent of the entire volume.

2. The decrepitation and segregation of components in the furnace are extremely high particularly in areas remote from the active zones.

3. The mineralogical changes that took place in the ore with increasing depth in the furnace were similar to those that took place in the SCICE charges with increasing severity of reducing conditions.

4. The reduction mechanisms between stockline level and the level of the electrode tip were similar to those operative in the SCICE charges for temperatures between 1300 and 1600°C. Reduction of manganous oxide in the molten regions below the electrode tip took place, in the main, by reaction between manganous oxide dissolved in the slag and solid reducing agent.

5. Evidence was found that electrode wear could be mainly due to erosion by particles in the gaseous reaction products.

6. The carbon content of alloy samples was found to deviate significantly from established laboratory data.

CHAPTER 8

8.0 SUMMARY OF CONCLUSIONS

1. The reduction of Mamatwan ore by coal or coke involved the following three basic steps :

   a) The dissociation of gangue minerals and the gaseous reduction of hematite to metal and of the higher manganese oxides to manganous oxide.

   b) The growth of metallic particles on the surface of ore particles due to reduction of manganous oxide by carbon dissolved in the alloy and the formation of a slag layer on the surface of ore particles.

   c) The reduction of manganous oxide dissolved in the slag by solid reducing agent or by carbon dissolved in the alloy.

2. Reduction of manganous oxide occurred mainly from the slag.

3. The rates of reduction of Mamatwan ore by coal or coke were similar for comparable experimental conditions.

4. The mineralogical changes that took place in the ore with increasing depth in the furnace were similar to those that took place in the SCICE charges with increasing severity of reducing conditions.

5. The reduction mechanisms between stockline level and the level of the electrode tip were similar to those operative in the SCICE charges for temperatures between 1300 and 1600^{o}C. Reduction of manganous oxide in the

molten regions below the electrode tip took place, in the main, by reaction between manganous oxide dissolved in the slag and solid reducing agent.

6. The resistivities of ore-coal and ore-coke mixtures are vastly different at low temperatures, decrease by several orders of magnitude during heating and attain the same value at about 1200°C.

7. The higher resistance of furnaces operating on coal compared to the resistance obtained with coke of the same initial size, appears to be the result of the physical disintegration of the coal and the attendant changes in the internal structure of the furnace rather than to the higher resistance of the coal at low temperatures.

A P P E N D I C E S

A.1.0 Determination of Percent[illegible]e [illegible]tallization

A.1.1 Chemical Tec[illegible]niques

A.1.2 Quantitative X-ray Analysis

A.1.3 Point Counting

A.2.0 Determinat[illegible]n of the Cell Constant of the SCICE Apparatus

A.2.1 The Influence of Temperature on the Resistance of the System

A.2.2 The Influence of the Depth of Solution on the Resistance of theSystem

A.2.3 The Influence of Small Variations in the Position of the Electrode on the Resistance

A.2.4 The Influence of the Distance of the Electrode from the Cell Bottom on the Resistance of the System

A.2.5 Calculation of the Cell Constant

A.2.6 Error in the Cell Constant

A.2.7 The Resistivity with Increasing Temperature of Different SCICE Charges

A.3.0 Furnace Parameters and Feed Material Data.

APPENDIX 1.

A.1.0 Determination of Percentage Metallization

Reports of established analytical methods for the determination of the proportion of metallic material in mixtures such as those examined in this investigation could not be found in the literature. However, a number of methods are described in the literature for the determination of metallic iron in the presence of its oxides.

The two chemical methods that appeared to be the most promising were based on mixtures of industrial ferromanganese and slag. The choice of these materials is justified by the fact that their composition was similar to that of the alloy and slag produced from the SCICE charges. Both analytical methods involved the preferential dissolution of metallic material from mixtures of metallic material and oxides.

The first method [135] used bromine in methanol as the solvent, and the second used copper sulphate [136]. Habashy [136] considers that his method should also be applicable to the determination of the metallic form of any of the elements that have a higher oxidation potential than that of copper.

Other methods considered were quantitative X-ray-diffraction analysis and point counting.

A.1.1 Chemical Techniques

The chemical composition of the alloy and slag were determined, and mixtures of known proportions were made. The proportion of metallic material in the mixtures was varied between 0 and 100 per cent in steps of 25 per cent. The materials examined by the bromine-methanol method were dried in nitrogen at 780°C.

Preliminary tests showed that ferromanganese dissolved rapidly in bromine-methanol, leaving a small quantity of a black, finely divided substance as residue. This was assumed to be

the carbon that was contained in the alloy. The slag was more resistant to dissolution.

The results obtained with the bromine-methanol method showed that, in all the tests, the amount of manganese in solution was higher than that present in the ferromanganese used to make up the sample. The error increased as the proportion of slag in the sample was increased.

For iron, the relationship between error and proportion of slag was reversed, although the trend was not consistent. An approximate mass balance on six mixtures reacted with bromine-methanol showed that the slag was attacked and that the proportion of the slag that dissolved increased with an increase in the proportion of slag in the mixture.

Subsequent to this investigation Josephson et el [137] used various solvents to determine the dissolution behaviour of synthetic mixtures of metallic iron and manganese and their lower oxides, and attempted to apply the process to ferromanganese samples. They found that it was difficult to obtain selective dissolution of metallic iron and manganese in the presence of their oxides and concluded that the methods used are not suitable for ferromanganese alloys and slags because of the complexity and insufficient knowledge of the phases present.

For copper sulphate, the amounts of iron and manganese were calculated on the assumption that the copper sulphate reacted with iron and manganese only in the alloy. However, the results showed that reaction between the copper sulphate and the slag also took place. The nature of this reaction is not well understood, but it was noticed during the experiments that cementation of copper was not involved.

The results showed that the addition of slag to alloy caused a sudden increase in the amounts of dissolved iron and manganese, the calculated amounts of dissolved iron and manganese exceeding the amount initially present in the alloy and the slag.

A.1.2 Quantitative X-ray Analysis

As the chemical methods used for the determination of percentage metallization did not show promise of success, quantitative X-ray diffraction analysis was considered.

The theory of quantitative X-ray diffraction analysis has been reviewed by Herbstein et al [138]. On the assumption that all the requirements relating to the preparation of the powder sample are met [106, 138] it can be shown that, for any two components A and B of a multicomponent mixture,

$$\frac{I_A\ (hkl)}{I_B\ (HKL)} = G_{AB}\ \frac{X_A}{X_B} \quad . \quad . \quad \text{A.1.1}$$

where I_A is the integrated intensity of the hkl reflection from component A, and X_A is the mass fraction of A in the mixture. The symbols with B subscripts have analogous meanings for component B, reflection HKL. The constant G_{AB} can be calculated if the crystal structures of A and B are known. Alternatively, it can be measured if mixtures containing known concentrations of A and B can be obtained.

Equation A.1.1 forms the basis for quantitative X-ray diffraction analysis by the direct-comparison, internal-standard, and dilution methods [138].

For the mixtures considered here, the constant G_{AB} could not be calculated since the crystal structures of the materials in their phase states are not known. A second factor making measurement of G_{AB} impossible was that mixtures in known proportions could not be prepared owing to the nature of the charges.

The intensity-fraction method [138] for quantitative analysis also requires pure samples of the phases to be determined, as well as the mass absorption coefficients of the pure phase and the matrix. These requirements could not be met.

Because of the above considerations, quantitative X-ray diffraction analysis was abandoned.

A.1.3 Point Counting

Preliminary work showed that the density of the non-metallic constituents varied between 4,6g.ml^{-1} for a percentage metallization of 0, and 3,4g.ml^{-1} for a metallization of about 50 per cent. The uncertainty of the values for density meant that the mass fraction could not be determined accurately from the volume fraction found from point counting. Intermediate cases could not be investigated owing to the presence of metallic material that could not be eliminated.

The error introduced by the differences in density of the non-metallic materials increased as their volume fraction decreased. For high values of percentage metallization (e.g. 50 per cent), the error reached a value of about 7,5 per cent. Use could be made of a mean density, but it is believed that the error would still be high enough to obscure the possible influence of the reducing agent on the speed of reduction.

APPENDIX 2.

A.2.0 Determination of the Cell Constant of the SCICE Apparatus

For a conductor of regular geometry the resistance R is given by:

$$R = \rho \frac{L}{A} \qquad A.2.1$$

where R is the resistance of the conductor over a length L

ρ is the resistivity of the conductor, and

A is its cross-sectional area.

The geometry of the SCICE charges was not regular. Hence the cell constant of the system ($\frac{L}{A}$) was determined by measurement of the resistance of a solution of known resistivity in order to convert resistance to resistivity.

The measurements were made with the apparatus shown in Figure A 2.1 using a 0,1 molar solution of sodium chloride. The geometry of the apparatus was the same as that used for the SCICE experiments. The depth of solution in the cell was the same as the depth of the SCICE charge at the start of an experiment. The lower edge of the conducting part of the electrode was 40 mm above the cell bottom. Experiments were also carried out with the electrode at 30 and 50 mm above the cell bottom to establish whether appreciable differences in resistance resulted from small variations in the vertical position of the electrode.

A.2.1 The Influence of Temperature on the Resistance of the System

The cell constant was determined for a temperature of 20°C. A relationship between the temperature of the solution and the resistance of the system was established so that a resistance value obtained at a somewhat higher or lower temperature could be corrected to a value at 20°C.

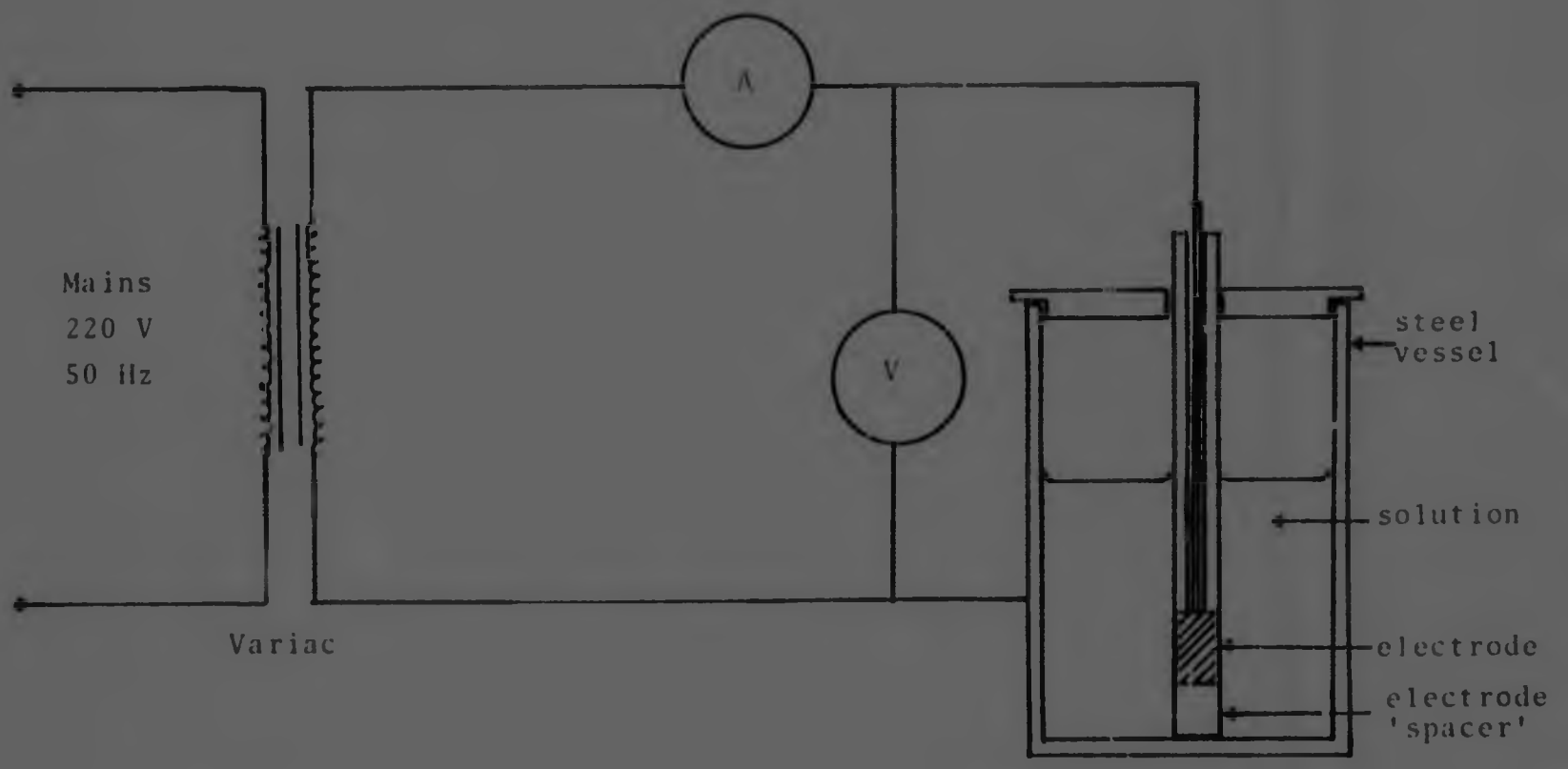


Figure A2.1 Apparatus for the determination of the cell constant of the SCICL system.

The temperature of the electrolyte was raised gradually by passing a small current through it. Measurements of temperature, current and voltage were taken every 15 minutes. Measurements were made between 17 and 23°C. A plot of resistance against temperature is shown in Figure A2.1.

The relationship between temperature and resistance, established by linear regression analysis by the method of least squares was:

$$R = 4{,}055 - 0{,}067T \quad . \quad . \quad . \quad . \quad . \quad . \quad A.2.2$$

$$r^2 = 0{,}99$$

where: R is the resistance in ohms
T is the temperature in °C, and
r^2 is the coefficient of determination
$r^2 = 1$ for a perfect fit.

From equation A.2.2 the resistance at 20°C is 2,72 ohms.

A.2.2 The Influence of the Depth of Solution on the Resistance of the System

From equation A.2.1 it can be seen that the magnitude of the cell constant $(\frac{l}{A})$ is a function of the resistance (R).

Variations in resistance were determined with increasing depth of solution in order to establish whether a significant change in resistance could be expected as the volume of the SCICE charge diminished with reaction temperature and time.

From Figure A2.3 it can be seen that the resistance of the system changes slightly when the depth of the solution is increased from 90 to 110 mm. Further increase in the depth of solution causes no appreciable change in resistance.

From Figure A2.3 it can be established that an increase in the depth of the solution from 130 to 160 mm decreases the resistance from 2,75 ohms to 2,70 ohms, a change of 1,9 per cent.

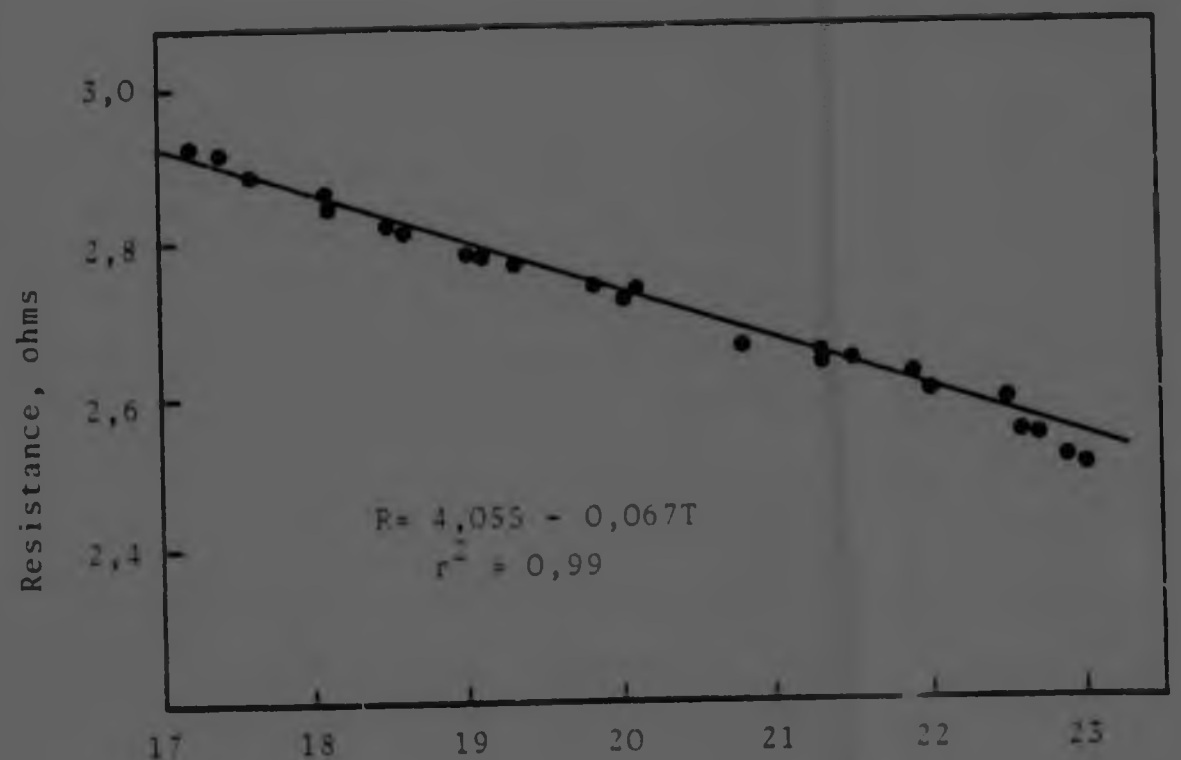


Figure A2.2 The influence of temperature on the resistance of the system.

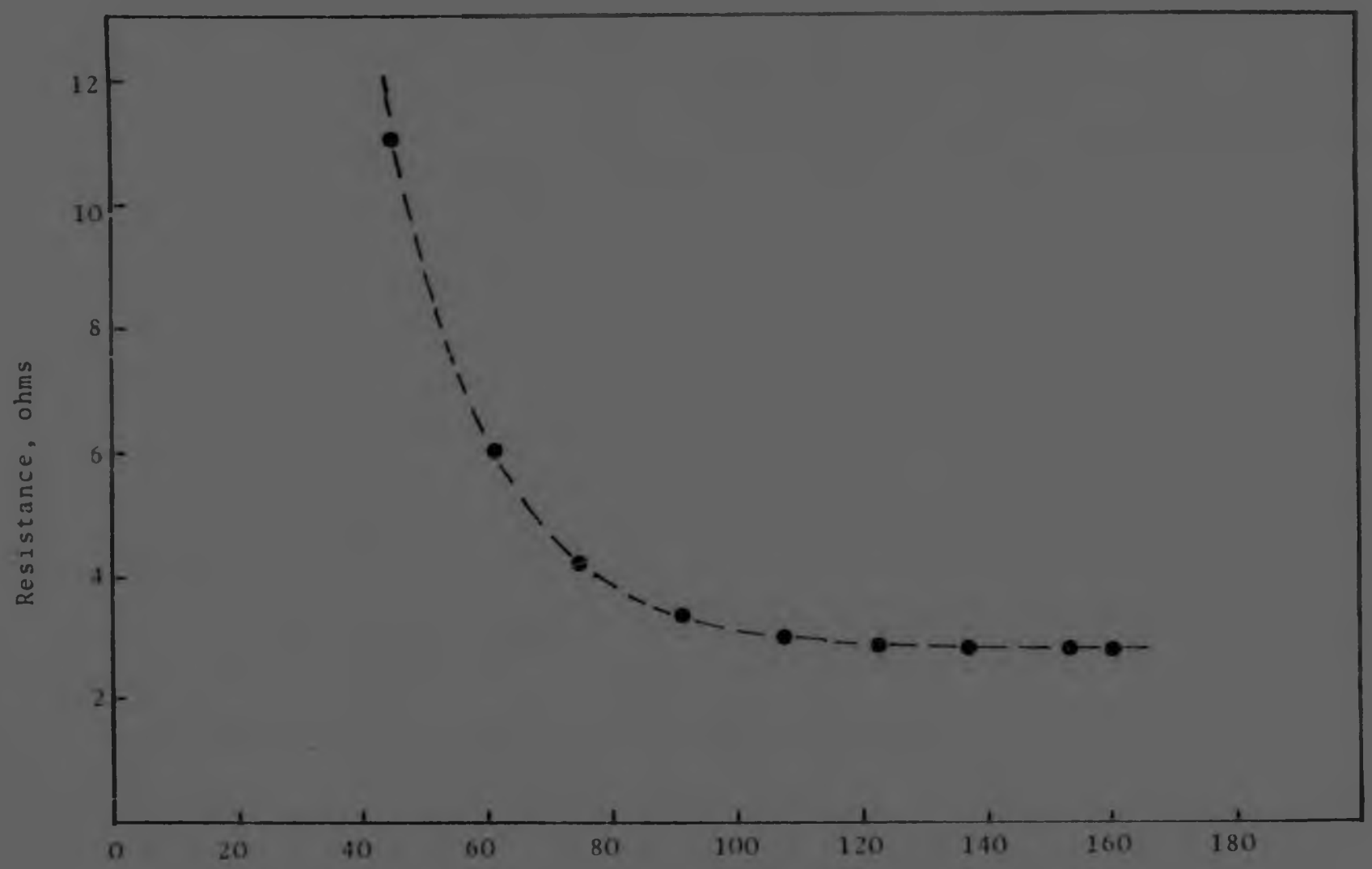


Figure A2.3 The influence of the depth of the solution on the resistance of the system.

During resistance measurements on SCICE charges the level of the charge was 40 mm or more above the upper edge of the electrode. Therefore the maximum variation in resistance due to a decreasing charge level was 1,9 per cent.

A.2.3 The Influence of Small Variations in the Position of the Electrode on the Resistance

As can be seen from Figure A2.1 the electrode had no fixed position on the bottom of the cell. Therefore, the vertical position of the electrode was found to vary slightly when it was withdrawn and replaced.

The influence of small variations in the vertical position of the electrode on the resistance of the system was investigated by raising the electrode out of the solution and re-positioning it.

A mean resistance of 2,70 ohms with a standard deviation of 0,02 ohms was obtained from 10 determinations, at a constant temperature of 20,81°C. From equation A.2.2 the resistance at 20°C is 2,71 ohms. This is 0,4 per cent lower than the resistance determined in A.2.1.

A.2.4 The Influence of the Distance of the Electrode from the Cell Bottom on the Resistance of the System

The influence of the distance of the electrode from the cell bottom on the resistance was investigated by using 'spacers' (Figure A2.1) of 30 and 50 mm height in addition to the usual 40 mm 'spacer'.

A mean resistance of 2,64 ohms with a standard deviation of 0,02 ohms was obtained with the 30 mm 'spacer' at a constant temperature of 21,10°C. From equation A.2.2 the resistance of this system at 20°C is 2,71 ohms.

The mean resistance obtained with the 50 mm 'spacer' was 2,71 ohms with a standard deviation of 0,02 ohms at a constant temperature of 21,10°C. The resistance at 20°C is 2,78 ohms.

The resistance at 20°C is plotted against the distance of the electrode from the cell bottom in Figure A2.4 The estimated maximum error in the vertical position of the electrode during SCICE experiments is indicated. This error corresponds to a change in the resistance of the system of 0,7 per cent.

A.2.5 Calculation of the Cell Constant

The cell constant may be calculated as follows:

From equation A.2.1 $\frac{L}{A} = \frac{R}{\rho}$

Specific conductivity [112] of 0,1 molar solution of NaCl at 20°C =

$$9,7 \text{ m mho cm}^{-1} = 0,0097 \text{ mho cm}^{-1}$$

Resistivity of solution $\rho = \frac{1}{0,0097} = 103,1$ ohm cm

$= 1,031$ ohm m

Therefore:

$$\frac{L}{A} = \frac{2,72}{1,031} = 2,638 \text{ m}^{-1}$$

A.2.6 Error in the Cell Constant

The estimated maximum error in resistance introduced by reduction in the charge volume and by variations in the horizontal and vertical positions of the electrode is $[1,9 + 0,4 + 0,7]^{\frac{1}{2}} = 1,7$ per cent. This corresponds to an error in the value of the cell constant of 2.1 per cent.

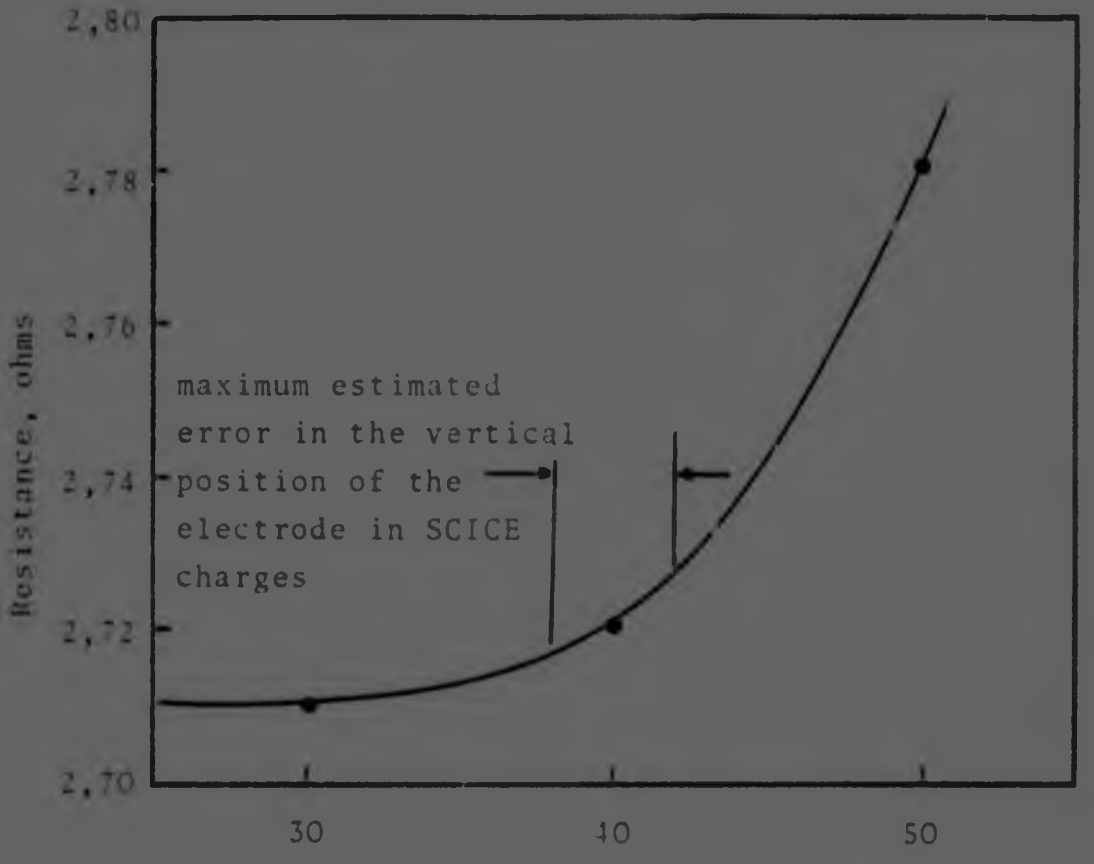


Figure A2.4 Variation in resistance with distance of the electrode from the cell bottom.

A.2.7 The Resistivity with Increasing Temperature of Different SCICE Charges

The resistivity with increasing temperature of different SCICE charges is shown in Tables A2.1 to A2.9 Table A2.10 shows the resistivity of SCICE charges at constant temperature.

TABLE A2.1

The resistivity of a charge of ore of size range 2,83-12,7 mm .

Temperature °C	Resistance Ω	Restivity Ω m
25	7700	2917
150	7700	2917
220	7150	2708
269	6760	2561
318	6660	2523
357	4350	1648
408	3640	1379
477	1940	735
540	765	290
629	182	68,94
719	52	19,69
796	23,8	9,02
845	16,7	6,33
880	11,5	4,36
922	6,25	2,37
964	4,35	1,65
1013	4,36	1,65
1066	5,74	2,17
1172	13,6	5,15
1285	20,2	7,65
1400	13,5	5,11

TABLE A2.2

The resistivity of a charge of coal of size range 2,83-6,35 mm .

Temperature °C	Resistance Ω	Resistivity Ωm
25	2 200 000	833 333
84	880 000	333 333
120	354 000	134 091
162	182 000	68 939
220	80 800	30 606
290	109 000	41 288
325	218 000	82 576
354	455 000	172 348
370	678 000	256 818
418	730 000	276 515
456	730 000	276 515
492	595 000	225 379
519	406 000	153 788
550	167 500	63 447
608	25 150	9 527
660	14 170	5 367
720	3 480	1 318
769	2 270	860
816	19,5	7,39
874	1,75	0,66
934	1,19	0,45
1005	0,92	0,35
1062	0,72	0,27
1118	0,59	0,22
1177	0,48	0,18
1230	0,40	0,15
1.85	0,33	0,13
1 500	0,31	0,12

TABLE A2.3

The resistivity of a charge of coke of size range 2,83-0,35 mm .

Temperature °C	Resistance Ω	Resistivity Ω m
25	0,346	0,131
83	0,376	0,142
162	0,34	0,129
250	0,31	0,117
300	0,246	0,093
340	0,205	0,078
373	0,183	0,069
403	0,175	0,066
445	0,175	0,066
504	0,174	0,066
567	0,176	0,067
660	0,160	0,061
744	0,137	0,052
796	0,125	0,047
836	0,123	0,047
887	0,137	0,052
957	0,143	0,054
1031	0,160	0,061
1094	0,172	0,065
1124	0,182	0,069
1148	0,194	0,074
1220	0,204	0,077
1290	0,200	0,076
1340	0,196	0,074
1398	0,190	0,072

TABLE A2.4

The resistivity of a coke-ore mixture.
Size range of coke 2,83-6,35 mm.
Size range of ore 2,83-12,7 mm.

Temperature °C	Resistance Ω	Resistivity Ωm
360	1380	522,7
450	316	119,7
540	175	66,3
590	65,5	24,8
620	44,3	16,8
650	28,4	10,8
680	21,2	8,03
705	16,4	6,21
740	15,4	5,83
770	14,5	5,49
800	14,0	5,30
830	11,9	4,51
860	11,5	4,36
890	8,6	3.26
920	8,4	3,18
950	10,4	3,94
980	10,7	4,05
1010	11,6	4,39
1040	14,4	5,45
1070	19,5	7,39
1100	25,9	9,81
1140	25,5	9,66
1170	32,0	12,12
1200	23,4	8,86
1230	10,7	4,05
1260	6,8	2,58
1280	3,6	1,36
1310	2,4	0,91
1340	1,5	0,57
1370	0,93	0,35
1400	0,37	0,14

TABLE A2.5

The resistivity of a co[illegible]ore mixture.
Size range of coke 6,35-[illegible],5 mm.
Size range of ore 2,83-12,7 mm.

Temperature °C	Resistance Ω	Resistivity Ωm
25	6450	2443
116	5900	2235
200	4080	1545
272	3080	1167
331	950	360
375	1330	504
410	665	252
452	232	87,9
488	133	[illegible]0,4
525	77	29,2
580	48	1[illegible],2
644	27,4	10,4
704	20,0	7,58
774	16,7	6,33
863	12,8	4,85
972	10,0	3,79
1068	10,0	3,79
1142	14,3	5,42
1205	14,3	5,42
1247	7,75	2,93
1263	2,66	1,01
1277	1,27	0,48
1286	1,30	0,49
1305	0,87	0,33
1380	0,56	0,21
1400	0,38	0,14

TABLE A2.1

The resistivity of a coke-ore mixture.
Size range of coke 9,5-12,7 mm.
Size range of ore 2,83-12,7 mm.

Temperature °C	Resistance Ω	Resistivity Ωm
25	6200	2348
100	9600	3636
190	3520	1333
271	1170	443
309	1640	621
350	880	333
376	615	233
413	473	179
452	334	127
510	191	72,3
585	62,6	23,7
644	28,8	10,9
692	19,6	7,42
770	19,9	7,54
870	13,8	5,22
915	8,1	3,07
964	6,8	2,58
1012	6,8	2,58
1072	8,7	3,30
1130	16,8	6,36
1192	20,2	7,65
1250	7,1	2,69
1322	0,95	0,36
1375	0,50	0,19
1425	0,32	0,12

TABLE A2.7

The resistivity of a coal-ore mixture.
Size range of coal 2,83-0,35 mm.
Size range of ore 2,83-12,7 mm.

Temperature °C	Resistance Ω	Resistivity Ω m
25	1 160 000	439 393
96	696 000	263 636
143	138 000	52 273
206	120 800	45 758
233	170 800	64 697
269	260 000	98 485
283	330 400	125 152
300	430 100	162 917
325	590 100	223 523
346	620 700	235 114
368	590 100	223 523
399	515 000	195 076
465	158 500	60 038
529	41 100	15 568
608	3 040	1 152
686	568	215
750	408	155
806	137	51,9
857	155	58,7
900	145	54,9
944	153	57,9
1004	170	64,4
1066	107	40,5
1144	20,2	7,65
1209	6,9	2,61
1260	1,9	0,72
1300	1,64	0,62

TABLE A2.8

The resistivity of a coal-ore mixture.
Size range of coal 6,35-9,5 mm.
Size range of ore 2,83-12,7 mm.

Temperature °C	Resistance Ω	Resistivity Ω m
25	1 890 000	715 909
107	755 000	285 985
180	190 000	71 970
246	303 000	114 773
304	802 500	303 977
357	401 750	158 178
396	178 300	67 538
438	116 000	43 939
488	85 500	32 386
542	40 500	15 341
598	14 240	5 394
653	3 720	1 409
713	910	345
780	288	110
857	142	53,8
922	202	76,5
965	288	110
1015	341	129
1063	354	134
1120	156	59,1
1192	25	9,47
1262	7,6	2,88
1300	3,4	1,29

TABLE A2.9

The resistivity of a coal-ore mixture.
Size range of coal 9,5-12,7 mm.
Size range of ore 2,83-12,7 mm.

Temperature °C	Resistance Ω	Resistivity Ω m
25	1 060 000	401 515
101	580 000	219 697
180	87 400	33 106
245	128 000	48 485
280	238 700	107 462
297	380 200	144 015
315	470 800	178 333
328	380 200	144 015
348	137 200	51 970
380	64 000	24 242
434	54 900	20 795
492	25 120	9 515
564	2 760	1 045
633	1 270	481
714	316	120
790	63,1	23,9
862	195	73,9
911	260	98,5
971	236	89,4
1020	252	95,5
1081	224	84,8
1200	15,8	5,99
1235	7,9	2,99
1288	5,0	1,89
1300	3,0	1,14

TABLE A2.10 The variations in resistivity of different SCICE charges at constant temperature

	Charges of ore and coke				
Temperature °C	1200	1500	1300	1400	1400
Size range of coke mm	2,83 - 6,35	2,83 - 6,35	9,5 - 12,7	2,83 - 6,35	6,35 - 9,5
Time at temperature mins.	Resistivity Ωm				
0	13,80	0,18	0,74	0,14	0,14
10	4,55	0,15	0,50	0,11	0,11
20	1,29	0,11	0,42	0,10	0,10
30	0,99	0,11	0,37	0,10	0,10
40	0,83	0,11	0,34	0,10	0,08
50	0,83	0,08	0,27	0,08	0,08
60	0,72	0,08	0,27	0,08	0,07
70	0,63	0,07	0,27	0,07	0,07
80	0,58	0,07	0,27	0,07	0,05
90	0,55	0,07	0,28	0,07	0,06
100	0,55	0,07	0,26	0,08	0,06
110	0,52	0,06	0,27	0,07	0,06
120	0,50	0,06	0,33	0,08	0,05
130	0,50	-	0,31	-	0,05
140	0,49	-	0,26	-	-

TABLE A2.10 continued

	Charges of ore and coal		
Temperature ^{o}C	1300	1300	1300
Size range of coke mm	2,83 - 6,35	6,35 - 9,5	9,5 - 12,7
Time at temperature mins.	Resistivity Ωm		
0	0,62	1,9	1,14
10	0,58	0,51	0,57
20	0,55	0,46	0,49
30	0,47	0,51	0,49
40	0,46	0,35	0,48
50	0,42	0,34	0,47
60	0,39	0,33	0,42
70	0,38	0,31	0,42
80	0,36	0,28	0,39
90	0,35	0,27	0,38
100	0,33	0,26	0,36
110	0,32	0,26	0,36
120	0,32	0,26	0,35

APPENDIX 3.

A.3.0 Furnace Parameters and Feed Material Data

The important furnace parameters [1] are shown in Table A3.1.

Tables A3.2 and A3.3 show the raw material type and quantity charged to the furnace over the period 11 September 1977 to 20 September 1977 and their size analysis respectively.

TABLE A3.1

Values of some parameters of Furnace M10

A. DESIGN PARAMETERS	
Inside shell diameter	13,2 m
Inside shell depth	7,04 m
Inside hearth diameter (Floor level)	9,9 m
Inside depth	5,27 m
B. ELECTRODE PARAMETERS	
Diameter	1,9 m
Spacing - P.C.D.	5,43 m
Average length	3,57 m
Average tip to hearth distance	2,75 m
C. ELECTRICAL PARAMETERS	
i) Design Values	
Transformer rating *	48,0MVA
Primary voltage	33,0KV
Primary current	840,0A
Number of transformer taps	22
Secondary voltage range	176-300V
Maximum secondary current	111,3kA
ii) Typical Operating Values	
Furnace load	23,1MW
Secondary current	92,9kA
Secondary voltage (phase to phase)	287 V
Power factor	0,50
Resistance	0,90 mΩ
Reactance	1,56 mΩ
Power consumption per ton hot metal	2700kWH
Electrode current density	3,28A/cm^2
Production rate	8,56tph
k factor	0,42

*The 48 MVA transformer was replaced by a 75 MVA transformer about 18 months before the excavation of the furnace.

TABLE A3.2

Raw material type and quantity charged to Furnace M10

Date	Hotazel ore	Mamatwan ore	TONS PER DAY Return slag	Quartz	Coke	Large nuts (Delmas coal)
11.9.77	17,22	117,18	5,7	3,67	15,67	15,66
12.9.77	24,92	247,08	12,6	7,69	29,26	29,36
13.9.77	20,16	181,44	21,6	6,24	23,25	22,92
14.9.77	24,36	224,28	19,8	9,00	26,67	28,62
15.9.77	20,44	194,04	10,8	6,90	24,14	17,41
16.9.77	36,96	332,64	21,0	8,46	42,57	37,36
17.9.77	22,96	206,64	6,0	5,29	26,18	26,85
18.9.77	25,20	226,80	13,8	5,75	27,61	28,45
19.9.77	70,00	310,80	20,1	6,64	46,46	45,82
20.9.77	25,20	58,80	4,8	2,10	10,00	9,10
TOTALS	287,42	2099,70	136,20	61,74	271,81	261,55

TABLE A3.3

The size analyses of the raw materials fed to Furnace M10 over the period 10 to 20 September 1977

Material	Size range mm
Mamatwan ore	38 to 62
Hotazel ore	25 to 90
Quartz	38 to 60
Rest	15 to 40

REFERENCES

1. VAN DER WALT, I. and GERICKE, W.A. The effect of magnitude of scale on various operating characteristics in the production of high-carbon ferromanganese in electric smelting furnaces. Paper presented at the American Seminar on Ferroalloys, Salvador de Bahia (Brazil), June 22-27. 1975.

2. PENTZ, R.D. An investigation of the beneficiation of low grade manganese ore with special reference to its reducibility. M.Sc. Thesis, University for Higher Cristian Education, Potchefstroom, March 1970.

3. GRIMSLEY, W.D. A study of the reduction characteristics and mechanisms of reduction of manganese ore by solid carbon. M.Sc. Thesis, University of the Witwatersrand, Johannesburg, 1977.

4. ANON. It's all here with more to spare. Base Minerals Survey, Supplement to Financial Mail, May 20. 1977. pp. 9 - 10.

5. ELYUTIN, V.P., PAVLOV, HU.A., LEVIN, B.E. and ALEKSEEV, E.M. Production of ferroalloys. Electrometallurgy. 2nd edition. Israel. Program for Scientific Translation 1957.

6. Manganese ores, alloys, metal and compounds. World survey of production, consumption and prices with special reference to future trends. Roskill Information Services Ltd. August 1972.

7. FEATHERSTONE, R.A. Applications of Mamatwan manganese ore. Infacon '74, Johannesburg, April 1974.

8. DE VILLIERS, P.R. The geology and mineralogy of the Kalahari manganese field north of Sishen, Cape Province. Pretoria, Geological Survey, Memoir 59, 1971.

9. SELMER-OLSEN, S.S. Trends in ferroalloy production. J.S.A. Inst. Min. Metall. Vol. 71, No. 11, 1971. pp 210-214.

10. DUKE, V.W.A. Manganese, Nat. Inst. For Metallurgy, Randburg, Technical Memorandum, Nov. 1974.

11. HOWAT, D.D. The electric smelting revolution. J.S.A. Inst. Min. Metall., Oct. 1971. pp. 74-84.

12. KING, S.G. Electric smelting furnaces in Southern Africa. Infacon '74, Johannesburg, April. 1974.

13. BARCZA, N.A., GERICKE, W.A., and KOURSARIS, A. The "digout" of a 75 MVA high-carbon ferromanganese furnace. Nat. Inst. for Metallurgy, Report No. 1983, August 1978.

14. DYASON, G.J. A study of burden movement in submerged-arc furnaces. M.Sc. Thesis, University of the Witwatersrand, Johannesburg, 1977.

15. SELMER-OLSEN, S.S. Private communication Apr. 1979 National Institute for Metallurgy, Randubrg, Transvaal, South Africa.

16. MAH, A.D. Thermodynamic properties of manganese and its compounds. Washington, U.S. Dept. of the Interior, Bureau of Mines, 1960.

17 KLINGSBERG, C. and ROY, R. Solid-solid and solid vapour reactions and a new phase in the system Mn-O J. Am. Ceram. Soc., vol. 43, No. 12. 1960. pp 620-626.

18. HAHN, W.C. Jr. and MUAN, A. Studies in the system Mn-O; The Mn_2O_3 - Mn_3O_4 and Mn_3O_4 - MnO equilibria. J. Am. Ceram. Soc., vol. 258. Jan. 1960. pp. 66-78.

19. MANILIN, G.V. and TOLMACHEV, Yu.M. Irreversibility of the reaction in the thermal decomposition of certain oxides. Russian J. Inorg. Chem., vol. 14, 1969. p 159.

20 MUAN A. Oxides of transition elements. High Temperature Oxides. Part I. Magnesia, Lime and Chrome Refractories. Alper. M. ed. Academic press. N.Y. 1970. pp. 315 - 346.

21. ABDUL AZIM, A.A., KOLTA, G.A. and ASKAR, M.H. Thermal Behaviour of some artificial manganese dioxides. Electrochim. Acta. vol. 17. 1972. pp 291-302.

22. DRESSEL, W.M. and KENWORTHY, H. Thermal behaviour of manganese minerals in controlled atmospheres. U.S. Dept of the Interior. Bureau of Mines Report of Investigations. 5761. 1961. 35 pp.

23. PILTER, P. The reduction in the solid state of manganese ores with carbon monoxide and hydrogen. Kohaszati Lapok 1967, vol. 11, pp 492-500.

24. KOR, G.J.W. The thermal decomposition of Mn_2O_3 and the reduction of Mn_3O_4 by carbon and carbon monoxide. Met. Trans., vol 9B, 1978. pp 307-311.

25. ASHIN, A.K., and ROSTOVCHEV, S.T. Kinetics and mechanisms of reduction of manganese oxides with carbon. Izv. Vysshikh. Zavedenii. Chem. Met., vol 7, 1964. pp 10-18.

26. MISRA, V.N., SINVHAL, R.C., and KHANGAONKAR, P.R. Pre-reduction of manganese ore pellets with carbon monoxide. Trans. Indian Inst. of Metals, vol 28, No. 3, June 1975, pp. 268-369.

27. DAVIES, M.W. and RICHARDSON, F.D. The non-stoichiometry of manganous oxide. Trans. Faraday Soc. vol. 55, 1959 pp 604 - 610.

28. OATES, W.A. and TODD, D.D. Kinetics of the reduction of oxides. J. Aust. Inst. Met., vol. 7 1962. pp 109 - 114.

29. TOLSTOGUZOV, N.V. The sintering and preheating of a charge for the melting of ferromanganese from oxide and carbonate ores. British Ind. and Scientific Intern. Transl. Service. Nov. 1974.

30 COETZEE, J.P. Modern trends in the design of ferro-alloy furnaces and the future of this smelting industry in the Republic of South Africa. J.S.A. Inst. Min. and Metall., July 1962, pp 649 - 672.

31. RANKIN, W.J. Solid state reduction of chromite spinel of the Bushveld Igneous Complex by graphite and carbon monoxide. Nat. Inst. for Metallurgy. Report No. 1957. May, 1978.

32. KURPKOWSKI, A., and KOPERSKI, S. Reduction of metal oxides by carbon and carbon monoxide. Rudy i Metale Niezelanze, vol. 7, No. 3. 1962, pp 101 - 106.

33. HOOPER, R.T. The production of ferromanganese. Electric Furnace Proceedings. Met. Soc. AIME. vol 25, 1967. pp 141 - 145.

34. ANTONOV, V.K., and CHYFAROV, G.I. Reduction of MnO with solid carbon. Akad. Nauk. SSSR Ural'skii Vilial. Trudy Instituta Metallurgii, No. 7, 1961. pp 101 - 105.

35. TARBY, S.K. and PHILBROOK, W.O. The rate and mechanisms of the reduction of FeO and MnO from silicate and aluminate slags by carbon-saturated iron. Trans. Met. Soc. AIME, vol. 239, July 1967. pp 1005 - 1017.

36. DAINES, W.L., and PEHLKE, R.D. Kinetics of manganese oxide reduction from basic slags by silicon dissolved in liquid iron. Trans. Met. Soc. AIME, vol 242, No. 4. 1968. pp 565 - 575.

37. POMFRET, R.J. and GRIEVESON, P. Kinetics of fast initial stage of reduction of MnO from silicate slags by carbon in molten iron. Ironmaking and Steelmaking, No. 5, 1978. pp 191 - 197.

38. YAGI, T., and ONO, Y. On the rate of reduction of MnO from molten slag by carbon-saturated iron. Iron and Steel Inst. Japan. Trans. vol. 10, No. 1, 1970. pp 30 - 37.

39. KUKHTIN, B.A., BORONENKOV, V.N., ESIN, O.A., and TOPORISHCHEV, F.A. Kinetics of the reduction of manganese from molten slags by solid carbon. Izvestiya Akad. Nauk SSSR Metallii No. 1, 1969. pp 119 - 124.

40. KOLCHIN, O.P. The mechanism of reduction of metals from their oxides by carbon. Mekh. Kinet. Vosstanov. Metal. Mater. Simp., 1968. pp 40 - 48.

41 WAGNER, C. Mechanism of the reduction of oxides and sulphides to metals. Trans. AIME, vol 194, 1952. pp 214 - 216.

42 RICHARDSON, F.D. and DANCY, E. Disc. Far. Soc., No. 4 1948. pp 229 - 230.

43. GELLNER, O.H. and RICHARDSON, F.D. Reduction of ferrous oxide. Nature, vol 168, 1951. pp 23 - 24.

44. RAO, Y.K. The kinetics of reduction of hematite by carbon. Met. Trans. vol 2, May 1971. pp 1439 - 1447.

45. BALDWIN, B.G. The mechanism of the reduction of iron oxides by solid coke. J. Iron Steel Inst., vol 179, 1955. pp 30 - 36.

46. FRANKLIN, R.E., DOUGLAS, R.W., "Summarised proceedings of a conference on the structures of semi-crystalline materials". Brit. Jour. Applied Physics 7 (1956), 389.

47. FRUEHAN, R.J. The rate of reduction of iron oxides by carbon. Met. Trans. B, vol 8B, 1977. pp 279 - 286.

48. TIEN, R.H. and TURKDOGAN, E.T. Mathematical analysis of reactions in metal oxide-carbon mixtures. Met. Trans. vol. 8B, 1977 pp 305 - 313.

49. EDSTROM, J.O. and BITSIANES, G. Solid state diffusion in the reduction of magnetite. Trans. AIME. J. Metals, vol 203, 1955. pp 760 - 765.

50 THEMELIS, N.J. and GAUVIN, W.H. Mechanism of reduction of iron oxides Can. Mining Met. Bull., 1962, vol 55. p 444 - 451.

51 EDSTROM, J.O. The mechanism of reduction of iron oxides. J. Iron Steel Inst. vol 175. 1953 pp 289 - 304.

52. TURKDOGAN, E. T. Blast furnace reactions. Met. Trans., vol. 9B 1978. pp 163 - 179.

53. URQUHART, R.C. A study of the production of high-carbon ferrochromium in the submerged-arc furnace. Ph.D, Thesis, University of the Witwatersrand, Johannesubrg. 1972.

54. BARCZA, N.A. Incipient fusion studies in the system chromite- CaO-MgO-Al_2O_3-SiO_2-C. M.Sc. Thesis, University of the Witwatersrand, 1972.

55 KUCUKKARAGOZ, S. Private communication, Apr. 1979. Department of Metallurgy, University of the Witwatersrand Johannesburg

56. DE VILLIERS, J.P.R. A Mineralogical investigation of natural and heated Mamatwan manganese ore. Nat. Inst. for Metallurgy, Technical Memorandum No. 1. May 1973.

57. OLTROGGE, A.R. Fundamental criteria for large arc furnace power supply systems. J. Metals, Jan. 1971. pp 53 - 64.

58. KELLY, W.M. Design and construction of the submerged-arc furnace. Carbon and Graphite News, vol 5 No. 1.

59. WESTLY, J. Resistance and heat distribution in a submerged arc furnace. Infacon '74, Johannesburg 1974.

60. MULLER, M.B. The crater characteristics for the el ctrical smelting process for pig iron production. Trondheim, Technical University of Norway, Jan. 1970. 21pp.

61. ANDERSEN, H. Chr. Some significant metallurgical aspects of the smelting of pig iron in electric furnaces. Trans. Can. Min. Metall. Bull., Jul. 1963. pp 509 - 516.

62. ANON. Electrical conduction in coals and cokes. Coal Research in C.S.I.R.O., Australia, Aug. 1962. pp 2 - 6.

63. STRAKOV, V.M., ARHIPOV, V.S., and MIZIN, V.G. The reactivity and resistivity of coke from gas coals. Coke and Chemistry U.S.S.R. No. 5, 1966 pp 34 - 37.

64. DIJS, H.M. A laboratory investigation of reducing agents for use in the electric - smelting industry. Nat. Inst. for Metallurgy, Report No. 1997, Dec. 1978.

65. MAZUMDAR, S.K., and MITRA, B. A study of the electrical resistivity of chemical coke and other heat-treated carbonaceous materials. Indian Journal of Technology. Vol. 10. Nov. 1972, pp 404 - 407.

66. UKANAKOV, P.M., MIZIN, V.G., and SEROV, G.V. Electrical resistivity of different forms of carbonaceous reducing agents. Coke and Chemistry U.S.S.R., No. 1, 1973, pp 29 - 35.

67. LORENZ, M., and MARINCEK, B. The electric resistance of charge materials in electric smelting furnaces. Schweizer Archiv. vol. 35, Mar. 1969. pp 91 - 105.

68. DA SILVEIRA, R.C. Electrical characteristics of some raw materials and loads for the production of cast iron in electrical reducing furnaces. Metallurgia ABM, vol 23, No. 119, 1967. pp 739 - 744.

69. DOWNING, J.H. and URBAN, L. Electrical conduction in submerged-arc furnaces. J. Metals, N.Y., Mar. 1966. pp 337 - 344.

70. WILLAND, K. Measurement of the electrical resistance of ferrochromium furnace charges. Nat. Inst. for Metallurgy, Report No. 1698, Apr. 1975.

71. RENNIE, M.W. The electrical resistance characteristics of the charge in the electric reduction furnace. Nat. Inst. for Metallurgy, Report No. 1606, Feb. 1974.

72. SCHEIDIG, K., and THIELE, H. On the electric conductivity of coke. Koks, smola, gaz, vol. 4, No. 12, 1969. pp 362 - 367.

73. RASCH, E., and HINRICHSEN, K. "Uber ein Beziehung zwischen Elektrischen Leitfahig Keit und Temperatur". Z. Elektrochem, vol 14, No. 41, 1908.

74. OHUCHI, H. Study of the conductivity of charcoal. Nenryo Kyokai-Shi. Dec. 1968 pp 856 - 863.

75. DA SILVEIRA, R.C. Electrical and metallurgical reasons for some charges employed in electrical reduction furnaces producing ferroalloys. RUM. Metallurgia, BISI 8045, Mar. 1969.

76. GEIGER, G.H. and WAGNER, J.B. Studies of electrical conductivity of hematite containing titanium or calcium and reduction of the doped hematite to magnetite in CO/CO_2 mixtures. J. Trans. AIME vol. 235, 1965, p 2092 - 2100.

77. HENSLER, J.R. and HENRY, E.C. Electrical resistance of some refractory oxides and their mixtures in the temperature range 600 to 1500°C. J. Am. Ceram. Soc., vol 36, 1953 pp 76 - 83.

78. DA SILVEIRA, R.C. The influence of sizing charcoal on the productivity of electric reduction furnaces. Metallurgia A.B.M. vol. 29, No. 189, Aug. 1973. pp 543 - 546.

79. GREKILA, R.B. and TIEN, T.Y. Conductivity discontinuity in a two-phase system. J. Am. Ceram. Soc., vol 48, No. 1. 1965. pp 22 - 25.

80. BUECKE, F. Electrical resistivity of conducting particles in an insulating matrix. J. Appl. Phys., vol 43, No. 11, Nov. 1972. pp 4837 - 4838.

81 CHUBINIDZE, T.A., and KEKELIDZE, M.A. Viscosity and electrical conductivity of melts in the $MnO-CaO-SiO_2$ system at 10% Al_2O_3 Soobshcheniya Akad. Nauk. Gruzinskoi S.S.R. vol. 43, No. 3, 1966. pp 667 - 674.

82. MULLER, M.B. Scaling-up of submerged-arc furnaces by criteria evaluated from water model studies of pilot smelting craters. Scand. J. Metall., vol 4, 1975. pp 161 - 169.

69. DOWNING, J.H. and URBAN, L. Electrical conduction in submerged-arc furnaces. J. Metals, N.Y., Mar. 1966. pp 337 - 344.

70. WILLAND, K. Measurement of the electrical resistance of ferrochromium furnace charges. Nat. Inst. for Metallurgy, Report No. 1698, Apr. 1975.

71. RENNIE, M.W. The electrical resistance characteristics of the charge in the electric reduction furnace. Nat. Inst. for Metallurgy, Report No. 1600, Feb. 1974.

72. SCHEIDIG, K., and THIELE, H. On the electric conductivity of coke. Koks, smola, gaz, vol. 4, No. 12, 1969. pp 362 - 367.

73. RASCH, E., and HINRICHSEN, K. "Uber ein Beziehung zwischen Elektrischen Leitfahig Keit und Temperatur". Z. Elektrochem, vol 14, No. 41, 1908.

74. OHUCHI, H. Study of the conductivity of charcoal. Nenryo Kyoka.-Shi. Dec. 1968 pp 856 - 863.

75. DA SILVEIRA, R.C. Electrical and metallurgical reasons for some charges employed in electrical reduction furnaces producing ferroalloys. RUM. Metallurgia, BISI 8045, Mar. 1969.

76. GEIGER, G.H. and WAGNER, J.B. Studies of electrical conductivity of hematite containing titanium or calcium and reduction of the doped hematite to magnetite in CO/CO_2 mixtures. J. Trans. AIME vol. 233, 1965, p 2092 - 2100.

77. HENSLER, J.R. and HENRY, E.C. Electrical resistance of some refractory oxides and their mixtures in the temperature range 600 to 1500°C. J. Am. Ceram. Soc., vol 36, 1953 pp 76 - 83.

78. DA SILVEIRA, R.C. The influence of sizing charcoal on the productivity of electric reduction furnaces. Metallurgia A.B.M. vol. 29, No. 189, Aug. 1973. pp 543 - 546.

79. GREKILA, R.B. and TIEN, T.Y. Conductivity discontinuity in a two-phase system. J. Am. Ceram. Soc., vol 48, No. 1. 1965. pp 22 - 25.

80. BUECKE, F. Electrical resistivity of conducting particles in an insulating matrix. J. Appl. Phys., vol 43, No. 11, Nov. 1972. pp 4837 - 4838.

81 CHUBINIDZE, T.A., and KEKELIDZE, M.A. Viscosity and electrical conductivity of melts in the $MnO-CaO-SiO_2$ system at 10% Al_2O_3 Soobshcheniya Akad. Nauk. Gruzinskoi S.S.R. vol. 43, No. 3, 1966. pp 667 - 674.

82. MULLER, M.B. Scaling-up of submerged-arc furnaces by criteria evaluated from water model studies of pilot smelting craters. Scand. J. Metall., vol 4, 1975. pp 161 - 169.

83. KJOLSETH, O. Electrotechnical conditions of the Tysland-hole furnace. Kjemi, Bergv., Metallurgi, vol. 21, No. 2, 1961. pp 27 - 33.

84. ANDRYUKHIN, G.S., GUSEV, V.I., BOGUTSKII, Yu. M., ZUBANOV, V.T., and PETLEVANNYI, L.F. Structure of furnace working volume and processing features of a silicomanganese heat. Stal, vol. 6, No. 4. Apr. 1976. pp 327 - 330.

85. ANDO, R., YAMAGISHI, K., FUKUSHIMA,T., and KAWASAKI, K. A study on the silicomanganese process. El. Furnace Conf. Proc. vol. 32, 1971. pp 107 - 115.

86 DANCOISNE, P.L. Optimum manganese ore preparation. El. Furnace Proc., TMS-AIME, vol 28, 1970.

87. VOLKERT, G. Influence of slag composition on the operational characteristics of an electric furnace. Chemie Ingenieur Technik, vol 42, No. 4, 1970. pp 218 - 221.

88. OZEKI, A., UEDA, Y., ISHII, S., HIRAHARA, T., and SUZUKI, S. On an investigation of the inside condition of the Furnace No. 2. Feroalloys (Japan) vol. 23, No. 1, 1974. pp 30 - 39.

89. YAMAGISHI, K., ENDO, K., and SAGA, J. A comprehensive analysis of the furnace interior for high-carbon ferro-chromium. Infacon '74, Johannesburg, Apr. 1974.

90. JOHNSTON, G.H., Physico-chemical properties of slags in the system $MgO-Al_2O_3-SiO_2$. Ph.D. Thesis, University of the Witwatersrand, 1972.

91. KLEMANTASKI, S. A new experimental technique for studying the blast-furnace process. J. Iron and Steel Inst., vol. 185, 1957. pp 237 - 239.

92. JOHNSON, A. Blast-furnace process research by the SCICE technique. J. Iron and Steel Inst., vol. 206, 1968. pp 671 - 688.

93. WOODHOUSE, W.A.V. Stationary charge in controlled environment (SCICE). A technique for blast furnace iron making research. Brighton, Inst. Chem. Engrs. Symposium series No. 27. On the engineering of gas-solid reactions. Apr. 1968. pp 203 - 207.

94. VOLKERT, G., and FRANG, K.D. Ferromanganese and manganese metal. From the Metallurgy of Ferroalloys, by Durrer and Volkert, 2nd Edition. pp 393 - 463.

95. DEWAR, K. and SEE, J.B. The influence of carbonaceous reducing agents on the rate of reduction of representative manganese and chromium ores. Nat. Inst. for Metallurgy, Report No. 1968. May 1978.

96. CANNON, W.P., URQUHART, R.C., and HOWAT, D.D. The mode of current transfer between electrode and slag in the submerged-arc furnace. J.S.A. Inst. Min. Metall. Aug. 1974. pp 4 - 7.

97. MULLER, M.B. and MAGNUSSEN, T. Electrode wear and arc processes in submerged-arc furnaces. Paper No. 404 at the 7th Internat. Congr. of Electroheat, Warsaw, 1972.

98. MYKLEBUST. R.L. and HEINRICH, K.F.J. Rapid quantitative electron probe microanalysis with a nondiffractive detector system. Energy Dispersion X-ray analysis : X-ray and Electron Probe Analysis, ASTM STP 845, Am. Soc. for Testing and Materials, 1971 pp 232 - 242.

99. MARSHALL, A.T. Electron probe X-ray microanalysis. Principles and Techniques of Scanning Electron Microscopy, vol. 4. Hayat, M.A. editor. 1975. pp 104 - 165.

100 RUSS, J.C. Energy dispersion X-ray analysis on the scanning electron microscope. Energy Dispersion X-ray analysis: X-ray and Electron Probe Analysis, ASTM STP 485, Am. Soc. for Testing and Materials, 1971 pp 154 - 179.

101. GOODHEW. P.J. Electron microscopy and analysis. Wykeham Publication, London, 1975 pp 11 - 16.

102 NEEDLEMAN, B. The role of the metallurgist in the production and usage of austenitic manganese steel castings. J.S.A. Inst. Min. Metall, Dec. 1958. pp 229 - 257.

103 DESFORGES, C.D., DUCKWORTH, W.F., and RYAN, T.F.J.N. Manganese in Ferrous Metallurgy. Edited by the Manganese Centre. May 1976.

104. FRANKEL, J.J. The manganese ores from Kuruman District, Cape Province, South Africa. Econ. Geol., vol 53, No. 5, 1958. pp 577 - 597.

105. DE VILLIERS J.P.R. A mineralogical investigation of Mamatwan and Wessels manganese ores. Nat. Inst. for Metallurgy, Report No. 1920, Sept. 19[illegible].

106. KLUG, H.P. and ALEXANDER, L.E. X-ray diffraction procedures. John Wiley and Sons, 1954.

107. HED, A.Z., and TANNHAUSER, D.S. Contribution to the Mn-O phase diagra[illegible] at high temperature. J. Electrochem. Soc. vol. 114 N . 4, 1967. pp 314 - 318.

108. ARANDA-FORNO, S.B. and JEFFES, J.H.E. Gibbs free energies of formation of silicates. Trans. Inst. Min. Metall., vol. 85. Dec. 1976. pp C213 - C215.

109. NARUSE, W. Manganese alloy production by sintering process. Infacon '74 Johannesburg, Apr. 1974.

110 BODSWORTH, C. and BELL, H.B. Physical chemistry of iron and steel manufacture. Longman 2nd ed., 1972.

111 . BURKE, J.E. Grain growth in ceramics. Kinetics of High Temperature Processes. Kingery, W.D. ed. The Technology Press of M I T, John Wiley and Sons N.Y. and Chapman and Hall, London, 1959. pp 109 - 116.

112. WEAST, R.D. ed. Handbook of Chemistry and Physics, 56th edition, 1975 - 1976. C R C Press.

113. LEVIN, E.M., ROBBINS, C.R. and MCMURDIE H.F. Phase diagrams for ceramists The Am. er. Soc., 1969.

114. LYMAN, T. Editor. M ndbook 8th edition, vol. 8. Metallography Structu and Phase Diagrams, Am. Soc. for Metals, 1973.

115. CHIPMAN, J., ALFRED, R.M., GOTT, L.W., SMALL, R.S., WILSON, D.M., THOMSON, C.N., GUERNSEY, D.L., and FULTON J.C. The solubility of carbon in molten iron and iron-silicon and iron-manganese alloys. Trans. Am. Soc. Metals, vol 44, 1952. pp 1215 - 1230.

116. TURKDOGAN, E.G., HANCOCK, R.A., HERLITZ, S.I. and DENTAN, J. Thermodynamics of carbon dissolved in iron alloys. Part V. Solubilities of graphite in iron-manganese, iron-cobalt and iron-nickel melts. J. Iron Steel Inst., vol 183, 1956. pp 69 - 72.

117. OHTANI, M. Activities of manganese and carbon in iron-carbon-manganese melts. Research Inst. Tokoku University, Science Report A.9.1957. pp 426 - 433.

118. RANKIN, W.J. Discussion. J.S.A. Inst. Min. Metall., May 1979. pp 306 - 308.

119 BARMIN, L.N., SHANTARIN, V.D., BORONENKOV, V.N., KUDRIAVTSEV, V.S., and UTOCHKIN, V.V. Kinetics of manganese oxide reduction by the carbon of iron-manganese-carbon melts. Izv. AN. SSR, Metally, No. 2, 1968. pp 71 - 77.

120. BARMIN, L.N., SHANTARIN, V.D., BORONENKOV, V.N., SHURYGIN, P.M., and KUDRYAVTSEV, V.S. Kinetics of the reduction of solid manganese II oxide by iron-manganese-carbon melts. Fiz. Khim. Osn. Proizvod. Stali. 1968. pp 406 - 411.

121. LISNIAK, S.S., and EVSEEV, N.F. Reduction of chromite with solid carbon. Sb. Nauch. Tekhu. tr., Cheliabinsk vol 3, 1961. pp 12 - 20.

122. INOUYE, K., and ROPPONGI, A. Structure of coke II. Physical properties of cokes produced from various blended slacks. Fuel, vol 34, 1955. pp 471 - 479.

23. ALKOCK, C.B. Principles of Pyrometallurgy. Academic Press, 1976.

124. SANDER, W.J. Coal in the metallurgical industry. Coal Gold and Base Minerals of Southern Africa. Jan 1975. pp 84 - 91.

125. KUO, K., and PERRSON, L.E. A contribution to the constitution of the ternary system Fe-Mn-C. Isothermal sections at 1050°, 910° and 690°C. J. Iron Steel Inst., vol 178. Sept. 1954. pp 39 - 44.

126 BENZ, R., ELLIOTT, J.F. and CHIPMAN, J. Thermodynamics of the solid phases in the system Fe-Mn-C. Met. Trans., vol 4., No. 8 Aug. 1973. pp 1975 - 1986.

127 ANDREAE, F.V. Design and control of ferro-alloy furnaces. Trans. A.I.E.E., vol. 69, 1950. pp 557 - 562.

128 COETZEE, J.J. The design of electric reduction furnaces for ferro-alloy production. J.S.A. Inst. Min. Metall. Jul. 1961. pp 541 - 561.

129. BARCZA. N.A., KOURSARIS, A., SEE, J.B., and GERICKE, W.A. The "dig out" of a 75 MVA high-carbon ferromanganese electric smelting furnace. Paper presented at the 37th Electric Furnace Conf. of the ISS. Dec. 1979.

130 SAUNDERS, H.L., and TWEEDY, J.M. Investigations on an experimental blast-furnace. J. Iron Steel Inst. Oct. 1949. pp 173 - 206

131 CAVAGHAN, N.J., and WILSON, A.R. Use of probes in blast furnaces. J. Iron Steel Inst. Mar. 1970. pp 231 - 246.

132 SCHUHMANN, R. Jr. Metallurgical Engineering vol. 1. Engineering Principles. Addison Wesley Press. 1952.

133. PETRUSHEVSKII, M.S., and GELD, P.V. Equilibrium of carbon with liquid alloys of Fe-Mn, Si and C. J. App. Chem. USSR., vol. 32, 1956. pp 86 - 95.

134 TURKDOGAN, E.T., HANCOCK, R.A., and HERLITZ, S.I. The solubility of graphite in manganese cobalt and nickel. J. Iron Steel Inst., vol. 182, 1956. pp 274 - 277.

135 KINSON, K., DICKESON, J.E., and BELCHER, C.B. The determination of metallic iron, nickel and cobalt in reduced ores and oxides. Anal. Chim. Acta, vol. 41, 1968. pp 107 - 112.

136 HABASHY, M.G. Quantitative determination of metallic iron in the presence of iron oxides in treated ores and slags. Anal. Chem., vol 33, 1961. pp 586 - 588.

137 JOSEPHSON, M., and LEE, A.F. The determination of metallised iron and manganese in ferromanganese alloys and slags. Nat. Inst. for Metallurgy, Tech. Memo 10084, June 1978.

138. HERBSTEIN, F.H., SMUTS, J , and VAN NIEKERK, J.N. Quantitative analysis of Fischer-Tropsch catalysts by X-ray diffraction. Anal. Chem., vol. 32, 1960. pp 20 - 24.

139 CULLITY, B.D. Elements of X-ray diffraction. Addison-Wesley, 1967

140 KUBASCHEWSKI, O . EVANS, E., and ALCOCK, C.B. Metallurgical Thermochemistry. N.Y., Pergamon Press, 19(7.

Author Koursaris A
Name of thesis Aspects of ferromanganese production in the submerged-arc furnace 1980

PUBLISHER:
University of the Witwatersrand, Johannesburg
©2013

LEGAL NOTICES:

Copyright Notice: All materials on the University of the Witwatersrand, Johannesburg Library website are protected by South African copyright law and may not be distributed, transmitted, displayed, or otherwise published in any format, without the prior written permission of the copyright owner.

Disclaimer and Terms of Use: Provided that you maintain all copyright and other notices contained therein, you may download material (one machine readable copy and one print copy per page) for your personal and/or educational non-commercial use only.

The University of the Witwatersrand, Johannesburg, is not responsible for any errors or omissions and excludes any and all liability for any errors in or omissions from the information on the Library website.